
Electronic Thesis and Dissertation Repository

7-18-2017 12:00 AM

System reliability analyses and optimal maintenance planning of corroding pipelines

Changqing Gong
The University of Western Ontario

Supervisor
Wenxing Zhou
The University of Western Ontario

Graduate Program in Civil and Environmental Engineering
A thesis submitted in partial fulfillment of the requirements for the degree in Doctor of
Philosophy
© Changqing Gong 2017

Follow this and additional works at: <https://ir.lib.uwo.ca/etd>



Part of the [Civil Engineering Commons](#)

Recommended Citation

Gong, Changqing, "System reliability analyses and optimal maintenance planning of corroding pipelines" (2017). *Electronic Thesis and Dissertation Repository*. 4669.
<https://ir.lib.uwo.ca/etd/4669>

This Dissertation/Thesis is brought to you for free and open access by Scholarship@Western. It has been accepted for inclusion in Electronic Thesis and Dissertation Repository by an authorized administrator of Scholarship@Western. For more information, please contact wlsadmin@uwo.ca.

Abstract

The failure of corroding pipeline joints may induce severe consequences. However, maintenance is expensive due to the cost of excavating and repairing a single joint and typically a significant number of joints that need repair. It is central to develop an optimal cost-effective maintenance strategy that balances cost and safety. A key component of the strategy is the reliability based condition evaluation of pipeline joints. The focus of the research reported in this thesis is therefore developing efficient reliability assessment methods for pipeline individual joints, and developing an optimal maintenance framework for the entire pipeline system.

First, efficient system reliability methods relying on the first-order reliability method (FORM) and importance sampling (IS) are developed for the assessment of the time-dependent probabilities of small leak and burst failure of pipeline joints containing multiple corrosion defects. In addition, a novel method is developed within the FORM to obtain the design points efficiently. An improved equivalent component approach for evaluating multi-normal integrals is also developed to improve the efficiency of the FORM for system reliability analysis.

In addition, a multi-objective optimization-based maintenance framework for corroding pipeline systems is formulated optimizing three objectives, i.e. the conditioned probabilities of burst and small leak, respectively, and repair cost. An improved genetic algorithm with a pre-training population is utilized to investigate the optimal Pareto front. The benefits of this framework enable decision makers to access a series of non-dominated optimal repairing solutions with respect to multiple conflicting objectives.

Keywords: First Order Reliability Method, design point, multi-normal integral, small leak, burst, importance sampling, competing failure modes, multi-objective optimization, genetic algorithm

Co-Authorship Statement

A version of Chapter 2, co-authored by Wenxing Zhou, **Changqing Gong** and Hanping Hong, has been published in *Journal of Engineering Mechanics*, ASCE, 2017, 143(9), DOI: 10.1061/(ASCE)EM.1943-7889.0001280

A version of Chapter 3, co-authored by **Changqing Gong** and Wenxing Zhou, has been published in *Structural Safety*, 2017, 68, 65-72

A version of Chapter 4, co-authored by **Changqing Gong** and Wenxing Zhou has been published in *Structure and Infrastructure Engineering*, 2017, 1-11, DOI: 10.1080/15732479.2017.1285330

A version of Chapter 5, co-authored by **Changqing Gong** and Wenxing Zhou is under review by *Reliability Engineering and System Safety* (revision submitted)

A version of Chapter 6, co-authored by **Changqing Gong** and Wenxing Zhou will be submitted to a journal

Acknowledgments

I have been very fortunate to have Dr. Wenxing Zhou as my supervisor in my entire doctoral studies. I offer sincere thanks to Prof. Zhou, who provided me with valuable instructions throughout my study at Western University, who gave me illuminating inspiration when I was trapped in research dilemma, and who pushed me forward when I slacked off in studies. I am very impressed by his dedication to research work, critical thinking, and excellent technical writing skills. Without the help provided by Prof. Zhou, my thesis would not have been fulfilled.

I would like to thank Prof. Hanping Hong for his selfless advice on research skills and life philosophy. I extend the appreciation to the committee members – Dr. Michael Bartlett, Dr. Ayman M. El Ansary, Dr. Jiandong Ren and Dr. Mahesh Pandey for their critical evaluation. The financial support from TransCanada, Natural Sciences and Engineering Research Council of Canada (NSERC) and the Faculty of Engineering at Western university is much appreciated.

Eventually, I offer my heartfelt gratitude to my parents and grandparents for their full support of my study in the past years. Their long-time unconditional love has been the strongest motivation for me to strive for the best.

Table of Contents

Abstract.....	i
Co-Authorship Statement.....	ii
Acknowledgments.....	iii
Table of Contents	iv
List of Tables.....	vii
List of Figures	viii
List of Appendices	x
List of Symbols.....	xi
1 Introduction.....	1
1.1 Background.....	1
1.2 Objective and Research Significance.....	4
1.3 Scope of Study	4
1.4 Thesis Format.....	6
1.5 References.....	6
2 New Perspective on the Application of the First-order Reliability Method for Estimating System Reliability	10
2.1 Introduction.....	10
2.2 Basics of the First-order Reliability Method	12
2.2.1 Analyses for a Single Limit State Function	12
2.2.2 Observed Deficiency for System Reliability Analyses with Multiple Limit State Functions.....	14
2.3 Efficient Procedure to Carry Out System Reliability Analyses	15
2.4 Application.....	20
2.4.1 Example 1: System Reliability of Pressurized Pipelines Containing Multiple Corrosion Defects	20
2.4.2 Example 2: Degrading Parallel Systems with Multiple Components.....	22
2.4.3 Example 3: Failure Probability of a Transmission Tower-line System Subjected to a Wind Event.....	24
2.5 Conclusions.....	26
2.6 References.....	27
3 Improvement of Equivalent Component Approach for Reliability Analyses of Series Systems	37
3.1 Introduction.....	37
3.2 Improvement of Equivalent Component Approach	39
3.2.1 Unit Normal Vector for Equivalent Component	39
3.2.2 Adaptive Combining Process.....	41
3.3 Numerical Examples.....	42
3.3.1 Equally Correlated Components.....	42
3.3.2 Unequally Correlated Components.....	44
3.3.3 Application to System Reliability of Corroding Pipelines	47
3.4 Conclusions.....	49
3.5 References.....	49
4 First Order Reliability Method-based System Reliability Analyses of Corroding Pipelines Considering Multiple Defects and Failure Modes	63
4.1 Introduction.....	63
4.2 Limit State Functions.....	64

4.3	FORM-based Time-dependent System Reliability Analyses of Corroding Pipelines	66
4.3.1	Equivalent Limit State Functions for Corroding Pipelines.....	66
4.3.2	Formulations for System Failure Probabilities of Corroding Pipelines....	68
4.4	Numerical Examples.....	70
4.4.1	General Information.....	70
4.4.2	Linear Growth Model for Defect Depth	72
4.4.3	Nonlinear Growth Model for Defect Depth.....	73
4.4.4	Gamma Process-based Growth Model for Defect Depth	73
4.5	Conclusions.....	74
4.6	References.....	75
5	Importance Sampling-based System Reliability Analyses of Corroding Pipelines Considering Multiple Failure Modes	89
5.1	Introduction.....	89
5.2	Formulations for Limit State Functions and Failure Probabilities.....	90
5.3	IS-based System Reliability Analyses of Corroding Pipelines	91
5.3.1	Overview of IS Technique	91
5.3.2	IS for Reliability Analyses of Corroding Pipelines.....	94
5.4	Numerical Examples.....	97
5.4.1	General.....	97
5.4.2	Linear Growth Model for Defect Depth	99
5.4.3	Gamma Process-based Growth Model for Defect Depth	100
5.4.4	Computational Efficiency and Variability of the Failure Probability Estimate.....	101
5.5	Conclusions.....	102
5.6	References.....	103
6	Multi-objective Maintenance Strategy for In-service Corroding Pipeline Using Evolutionary Strategy.....	119
6.1	Introduction.....	119
6.2	Multi-objective Optimization of Maintenance of Corroding Pipelines	120
6.2.1	Practical Aspects	120
6.2.2	Merit Measures	121
6.2.3	Formulation for Multi-objective Optimization	122
6.3	Reliability Analyses of Corroding Pipelines.....	123
6.4	Genetic Algorithm for Multi-objective Optimization.....	125
6.4.1	Overview of Genetic Algorithm.....	125
6.4.2	GA Used in this Chapter	127
6.4.3	Constraint Handling	128
6.5	An Illustrative Example	128
6.6	Conclusion	132
6.7	Reference	132
7	Chapter 7 Summary, Conclusions and Recommendations for Future Study	146
7.1	General.....	146
7.2	A New Perspective on the Application of the First-order Reliability Method....	146
7.3	Development of Improved Equivalent Component Approach for Reliability Analyses of Series Systems	147
7.4	First Order Reliability Method-based System Reliability Analyses of Corroding Pipelines Considering Multiple Defects and Failure Modes	148

7.5 Important Sampling-based System Reliability Analyses of Corroding Pipelines Considering Multiple Failure Modes	148
7.6 Multi-objective Optimization Based Maintenance Strategy for In-service Corroding Pipelines Using Genetic Algorithm	149
7.7 Recommendations for Future Study	150
Appendix A Dimension Reduction Method	152
Curriculum Vitae.....	153

List of Tables

Table 2.1 Empirical equations for estimating F_0 in Eq. (2.4) for the numerical examples considered in this chapter.....	31
Table 2.2 Probabilistic characteristics of random variables for Example 1.....	31
Table 2.3 Summary of design points for two corrosion defects	32
Table 2.4 Computational efficiency of the proposed procedure as reflected in the numerical examples	32
Table 3.1 Order of combination involved in the adaptive combining process for system with equally-correlated components ($m = 30$, $\rho = 0.5$ and $\beta_c = 6$)	52
Table 3.2 Order of combination involved in the adaptive combining process for system with components ($m = 30$ and $\beta_c = 6$) correlated according to Eq. (3.12).....	53
Table 3.3 Probabilistic characteristics of parameters for reliability analyses of corroding pipeline joint	54
Table 4.1 Basic attributes of three pipeline examples.....	78
Table 4.2 Probabilistic characteristics of parameters excluding the defect depth growth.	78
Table 5.1 Basic attributes of pipeline examples.....	106
Table 5.2 Probabilistic characteristics of parameters involved in the reliability analyses....	106
Table 5.3 COV values of the failure probabilities obtained from IS-based and simple MC	107
Table 6.1 The probabilistic characteristics of parameters involved in the reliability analysis	136
Table 6.2 Details of solutions SC1, SC2 and SC3	136
Table 6.3 Details of solutions SV1, SV2, SN1 and SN2	137

List of Figures

Figure 1.1 Schematic illustration of the geometry of a typical corrosion defect.....	9
Figure 2.1 Reliability index and failure probability of a single component for a degrading parallel system with five components.....	33
Figure 2.2 Correlation coefficient between linearized safety margins associated with different components for a degrading parallel system with five components.....	33
Figure 2.3 System failure probability for a degrading parallel system with five components.....	34
Figure 2.4. Correlation matrix of the safety margins associated with the eleven transmission towers in the tower-line system	34
Figure 2.5 Sensitivity of $P_{f_{sys}}$ and $P_{f_{1,3}}$ to ρ_R ($m_R/m_W = 1.25$, $v_R = 0.12$ and $v_W = 0.05$).....	35
Figure 2.6 Sensitivity of $P_{f_{sys}}$ to m_R/m_W , v_R and v_W ($\rho_R = 0.2$)	35
Figure 2.7 Sensitivity of $P_{f_{1,3}}$ to m_R/m_W , v_R and v_W ($\rho_0 = 0.2$).....	36
Figure 3.1 Illustration of the equivalent component approach for a series system with m components	55
Figure 3.2 Schematic illustration of effects of the combining sequence	55
Figure 3.3 Accuracy of IECA for series systems with equicorrelated components.....	56
Figure 3.4 Impact of ρ on the accuracy of IECA for series systems with 250 equicorrelated components	57
Figure 3.5 Comparison of EPM, SCM and IECA for series systems with 250 equicorrelated components and $\beta_c = 6$	58
Figure 3.6 Accuracy of equivalent component approach for series systems with unequally correlated components using correlation structure given by Eq. (3.12)	59
Figure 3.7 Accuracy of equivalent component approach for unequally correlated components with the correlation structure given by Eq. (3.15) ($\rho_{min} = 0$ and $\rho_{max} = 0.98$)	59
Figure 3.8 Accuracy of adaptive combining process for series systems with 250 components correlated according to Eq. (3.15) with $\rho_{max} = 0.98$ and ρ_{min} varying from 0 to 0.98	60
Figure 3.9 Comparison of accuracy and efficiency of EPM, SCM and IECA for series system with $\beta_c = 6$ and the component correlation structure defined by Eq. (3.12).....	61
Figure 3.10 Time-dependent system reliability of the corroding pipeline joint	62
Figure 3.11 Sensitivity of the system reliability of the corroding pipeline joint to the correlation between the defect depth and length growth rates	62
Figure 4.1 Geometric descriptions of $\Delta P_s(\tau, \Delta t)$ and $\Delta P_b(\tau, \Delta t)$	79
Figure 4.2 Probabilities of burst and small leak for examples 1, 2 and 3 based on the linear growth model for defect depth.....	82
Figure 4.3 Probabilities of burst and small leak for examples 1, 2 and 3 based on the nonlinear growth model for defect depth.....	85
Figure 4.4 Probabilities of burst and small leak for examples 1, 2 and 3 based on the homogeneous gamma process-based growth model for defect depth	88
Figure 5.1 Geometry descriptions of $\Delta P_s(\tau, \Delta t)$	107
Figure 5.2 Failure probabilities of four pipeline examples considering a single corrosion defect and linear depth growth model	109
Figure 5.3. Failure probabilities of four pipeline examples considering ten corrosion defects and linear depth growth model	111
Figure 5.4 Failure probabilities of Example 1 considering ten corrosion defects and linear depth growth model with different values of ρ_1	112

Figure 5.5 Failure probabilities of four pipeline examples considering a single corrosion defect and gamma process-based depth growth model	114
Figure 5.6 Failure probabilities of four pipeline examples considering ten corrosion defects and gamma process-based depth growth model	116
Figure 5.7 Failure probabilities of Example 1 considering ten corrosion defects and gamma process-based depth growth model with different values of ρ_2	117
Figure 5.8 Range of probabilities of burst obtained from 30 repeated IS-based analyses for Example 1 with ten corrosion defects and linear defect depth growth model	118
Figure 6.1 Illustration of one maintenance solution coded in GA	137
Figure 6.2 Illustration of the initial solution generation by minimizing C subjected to $P_{sa} \leq P_1$	137
Figure 6.3 The ILI-reported defect information	138
Figure 6.4 Annual conditional failure probability for the considered pipe joints	139
Figure 6.5 Pareto front of optimal solutions in terms of C , P_{sa} , and P_{ba} considering the constant budget constraint in years 1 through 4	140
Figure 6.6 The locations of the to-be-repaired pipe joints associated with SC1, SC2 and SC3, respectively	141
Figure 6.7 The maximum annual conditional probabilities of small leak and burst of all 90 pipe joints corresponding to solutions SC1, SC2 and SC3	142
Figure 6.8 Pareto fronts corresponding to three scenarios of annual budget constraint	143
Figure 6.9 Comparison of Pareto fronts of optimal solutions corresponding to the scenario of constant annual budget constraint, obtained from pre-trained and random initial populations, respectively	145

List of Appendices

Appendix A Dimension reduction method.....	152
--	-----

List of Symbols

a, b	= parameters of the gamma process
$\alpha_{i,1} \alpha_{i,2}$	= the i -th elements of the unit normal vector for α_1 and α_2 , respectively
$\alpha_i^{se}(t)$	= the i -th element of $\alpha^{se}(t)$
α	= unit vector normal to $g_U(\mathbf{u}^*)$
α_j	= unit normal vector associated with β_j
α_{12}^e	= the n -dimensional unit normal vector associated with $g_{12}^e(\mathbf{u})$
$\alpha'(j)$	= m -dimensional unit normal vector associated with $\mathbf{v}^*(j)$
$\alpha^{be}(t)$	= equivalent unit normal vector associated with $G^{be}(t)$
$\alpha^{se}(t)$	= equivalent unit normal vector associated with $G^{se}(t)$
β	= reliability index
β_j	= reliability index associated with the j -th limit state function
β_c	= component reliability index value
$\beta^{be}(t)$	= reliability index associated with $G^{be}(t)$
β^e	= equivalent reliability index for equivalent component C^e
$\beta^{se}(t)$	= reliability index associated with $G^{se}(t)$
$\beta_j^b(t)$	= reliability index associated with $\text{Prob}[g_j^b(t) \leq 0]$
$\beta_j^s(t)$	= reliability index associated with $\text{Prob}[g_j^s(t) \leq 0]$
$\beta^s(t)$	= reliability index vector of $\beta_j^s(t)$ ($j=1, 2, \dots, m$)
β	= reliability index vector
C	= present-value cost of excavation and repairing joints
C_0	= mobilization cost
$C_{a,t}$	= annual budget in terms of the present value allocated for corrosion repair at time t
C_m	= the m -th component of a series system
C_s	= cost of repairing a single joint
$C_{r,t}$	= present-value cost of repairs conducted at time t
C^e	= equivalent component
COV	= coefficient of variation
d	= corrosion defect depth
d_0	= initial corrosion defect depth
d_{0j}	= initial depth of the j -th defect
$d_j(t)$	= depth of the j -th corrosion defect at a given time t
$d_{gj}(t)$	= homogeneous gamma process at the j -th defect at a given time t
$d_{gj}(\Delta t)$	= gamma-distributed increment of the defect depth within Δt
d_{0j}	= initial depth of the j -th corrosion defect
D	= actual outside pipe diameter
e_p	= error associated with estimated system failure probability
EPM	= Equivalent plane method
$\Gamma(\bullet)$	= gamma function
$f_U(\mathbf{u})$	= joint standard normal probability density function of U
$f_X(\mathbf{x})$	= the joint probability density function of X
F ($F < 1$)	= design factor

F_0	= ratio of $\rho_{Zi,k}$ relative to $\rho_{Xi,k}$
$F(\bullet \bullet, \bullet)$	= gamma distribution
$F_R(\bullet, \bullet, \dots, \bullet)$	= joint probability distribution of R_j
$F_{R_j}(\bullet)$	= cumulative distribution function of R_j
$F_X(\bullet, \bullet, \dots, \bullet)$	= joint probability distribution of X
$F_{X_j}(\bullet)$	= cumulative distribution function of $X_j(t)$
$F_{W_j}(\bullet)$	= cumulative distribution function of W_j
FORM	= First order reliability method
FPR	= failure pressure ratio
$g_{12}^e(\mathbf{u})$	= equivalent linearized safety margin for C_1 and C_2 in terms of \mathbf{u}
g_d	= depth growth rate
g_{dj}	= depth growth rate of the j -th corrosion defect
g_l	= length growth rate
g_{lj}	= length growth rate of the j -th corrosion defect
$g(\bullet)$	= limit state function
$g_j(\bullet)$	= the j -th limit state function
$g_j(t)$	= the j -th limit state function at a given time t
$g_j^b(t)$	= limit state function for plastic collapse of the remaining ligament at the j -th defect at time t
$g_j^s(t)$	= limit state function, $g_j^s(t)$, for the j -th defect penetrating the pipe wall at a given time t
$g_U(\bullet)$	= limit state function in standard normal space U
$g_{j,U}(\bullet)$	= the j -th limit state function in terms of random variable vector U
$g_{j,U_j}(\bullet)$	= the j -th limit state function in terms of random variable vector U_j
$g_Z(\bullet)$	= limit state function in the correlated normal space Z
$g_{j,Z}(\bullet)$	= the j -th limit state function in the correlated normal space Z
$g^b(t)$	= limit state function for plastic collapse of the remaining ligament at one single defect at time t
$g^s(t)$	= limit state function for plastic collapse of the remaining ligament at one single defect at time t
$G(\mathbf{u})$	= mapping of $g(\mathbf{x})$ in the standard normal (i.e. U) space
$G_j(\mathbf{u})$	= mapping of $g_j(\mathbf{x})$ in the standard normal (i.e. U) space
$G^b(t)$	= mapping of $g^b(t)$ in the standard normal space
$G^s(t)$	= mapping of $g^s(t)$ in the standard normal space
$G_j^b(t)$	= mapping of $g_j^b(t)$ in the standard normal space
$G_j^s(t)$	= mapping of $g_j^s(t)$ in the standard normal space
$G^{be}(t)$	= linearized equivalent limit state function at time t representing the plastic collapse
$G^{se}(t)$	= linearized equivalent limit state function at time t representing the wall thickness penetration
GA	= Genetic algorithm
$h_U(\bullet)$	= IS density function in the standard normal space
$h_U^b(\mathbf{u}; \tau, \Delta t)$	= weighted average of the IS density functions for $\Delta P_{b,j}(\tau, \Delta t)$

$h_U^S(\mathbf{u}; \tau, \Delta t)$	= weighted average of the IS density functions for $\Delta P_{s,j}(\tau, \Delta t)$
$I(\bullet)$	= failure indicator function
$I_{(\tau, \Delta t)}^S(\bullet)$	= index functions associated with $\Delta P_s(\tau, \Delta t)$
$I_{(\tau, \Delta t)}^b(\bullet)$	= index functions associated with $\Delta P_b(\tau, \Delta t)$
$I_r(n_{r,t})$	= an indicator function that equals unity for $n_{r,t} > 0$ and zero for $n_{r,t} = 0$
IECA	= Improved equivalent component approach
ILI	= In-line inspection
IS	= Important sampling
k_j	= parameters of the power-law growth model for the j -th defect
l	= corrosion defect length
l_0	= initial depth of corrosion defect
l_{0j}	= initial length of the j -th corrosion defect
$l_j(t)$	= length of the j -th corrosion defect at a given time t
$\mathbf{L}, \mathbf{L}(j)$	= lower-triangular matrix of Cholesky decomposition of \mathbf{R}_{ZZ} , $\mathbf{R}_{ZZ}(j)$
\mathbf{L}_Y	= lower-triangular matrix obtained from Cholesky decomposition of \mathbf{R}
$\mathbf{L}_{j,j}, \mathbf{L}_{c,j}$ and $\mathbf{L}_{c,j,cj}$	= submatrices of dimensions of $n_j \times n_j$, $(n-n_j) \times n_j$, and $(n-n_j) \times (n-n_j)$ of $\mathbf{L}(j)$, respectively
m	= number of limit state functions, components or defects
m_p	= number of repaired pipe joints
m_R	= mean value of $F_{Rj}(\bullet)$
m_W	= mean value of $F_{Wj}(\bullet)$
M	= Folias factor
M_j	= Folias factor at the j -th defect
MC	= Monte Carlo simulation
MFL	= magnetic flux leakage
MOP	= Maximum operating pressure
n	= number of random variable in the system
n_j	= number of random variables only involving $g_j(\bullet)$
n_p	= number of inspected pipe joints
$n_{r,t}$	= number of joints repaired at time t
N	= total number of IS trials
ρ	= correlation coefficient value between two linearized safety margin
$\rho_0 \rho_1 \rho_2 \rho_R$	= specified correlation coefficient value between random variables
$\rho_{min} \rho_{max}$	= pre-determined lower and upper bound values of correlation matrix
$\rho_w(\bullet)$	= correlation coefficient between W_j and W_k
$\rho_{Z_i,k}$	= correlation coefficient between Z_i and Z_k
$\rho_{X_i,k}$	= correlation coefficient between X_i and X_k
ρ_{jk}	= correlation coefficient between the linearized safety margins of the j -th and k -th components
p	= internal pressure

p_j	= internal pressure at the j -th defect
p_b	= burst capacity
$p_{bj}(t)$	= burst capacity at at the j -th defect at a given time t
P_0	= nominal maximum operating pressure
$P_1 P_2$	= allowable annual probabilities of maximum small leak and burst, respectively
$P_b(t) P_s(t)$	= cumulative probabilities of burst and small leak of a pipeline joint, respectively, at a given time t
$P_{b,q}(t) P_{s,q}(t)$	= the cumulative probabilities of burst and small leak , respectively, of the q -th joint up to t
$P_{ba} P_{sa}$	= maximum value of $P_{ba,q}(t)$ and $P_{sa,q}(t)$ ($t = 1, 2, \dots, T; q = 1, 2, \dots, n_p$), respectively
$P_{ba,q}(t) P_{sa,q}(t)$	= conditioned annual failure probabilities of burst and small small leak of the q -th joint, respectively, at a given time t
P_f	= system failure probability
$P_{f,q}(t)$	= cumulative failure probability of the q -th joint
P_{f12}	= series system failure probability of two components
$P_{f1,3}$	= probability of simultaneous collapse of towers 1 and 3
P_{fs}	= estimated failure probability of a series system
P_{fse}	= exact system failure probability
P_{fsys}	= probability of collapse of at least one tower
$P_{s,q}(t) P_{b,q}(t)$	= cumulative probabilities of small leak and burst, respectively up to t
$P^s(t)$	= cumulative probability of any of defects penetrating the pipe wall within $[0, t]$
r_j	= value of random variable R_j
$r^{sb}(\tau)$	= correlation coefficient between $G^{se}(\tau)$ and $G^{be}(\tau)$.
R_j	= ultimate capacity of the j -th tower
\mathbf{R}	= correlation matrix of the linearized safety margins
$\mathbf{R}^s(t)$	= correlation matrix of the linearized safety margins associated with $g_j^s(t)$ ($j = 1, 2, \dots, m$) in standard normal space
$\mathbf{R}^{sb}(\tau, \Delta t)$	= correlation matrix of three linearized equivalent limit state functions $G^{se}(\tau + \Delta t)$, $G^{se}(\tau)$ and $G^{be}(\tau)$
$\mathbf{R}^{bs}(\tau, \Delta t)$	= correlation matrix of three linearized equivalent limit state functions $G^{be}(\tau + \Delta t)$, $G^{be}(\tau)$ and $G^{se}(\tau)$
\mathbf{R}_{ZZ}	= correlation matrix of the elements in \mathbf{Z}
$\mathbf{R}_{ZZ}(j)$	= correlation matrix of the elements in $\mathbf{Z}_D(j)$
$\mathbf{R}_{Z_j j}$	= correlation matrix of the elements in \mathbf{Z}_j
$\mathbf{R}_{Z_{cj}, cj}$	= correlation matrix of the elements in \mathbf{Z}_{cj}
$\mathbf{R}_{Z_j, cj}$	= correlation between the elements in \mathbf{Z}_j and \mathbf{Z}_{cj}
SCM	= sequential compounding method
SMTS	= specified minimum tensile strength
SMYS	= specified minimum yield strength
t	= forecasting time
$t_{r,q}$	= the time of repair for the q -th pipe joint
t_j^s	= time at which the j -th defect just penetrates the pipe wall
t_j^b	= time at which plastic collapse takes place at the j -th defect

T	= inspection time horizon
u	= the mean of the depth increment within one year
\mathbf{u}	= value of the vector \mathbf{U}
u_i	= the i -th element of the vector \mathbf{u}
\mathbf{u}_{cj}	= value of the vector \mathbf{U}_{cj}
\mathbf{u}_j	= value of the vector \mathbf{U}_j
\mathbf{u}^*	= design point vector in the standard normal space
\mathbf{u}_{cj}^*	= vector of $(n-n_j)$ design point values that are not in \mathbf{u}_j^*
\mathbf{u}'_i	= i -th random sample generated from $h_U(\mathbf{u})$
$\mathbf{u}^*(j)$	= design point involving the whole system associated with β_j
$\mathbf{u}_D^*(j)$	= vector of re-ordered elements of $\mathbf{u}^*(j)$
\mathbf{u}_j^*	= design point value of \mathbf{U}_j
$\mathbf{u}^{c*}(\tau)$	= design point associated with $G^b(\tau)=0$
$\mathbf{u}^{l*}(\tau)$	= design point associated with $G^s(\tau)=0$
$\mathbf{u}^{b*}(\tau, \Delta t)$	= design point associated with $\Delta P_b(\tau, \Delta t)$
$\mathbf{u}^{s*}(\tau, \Delta t)$	= design point associated with $\Delta P_s(\tau, \Delta t)$
$\mathbf{u}_j^{b*}(\tau, \Delta t)$	= design points associated with $\Delta P_{b,j}(\tau, \Delta t)$
$\mathbf{u}_j^{s*}(\tau, \Delta t)$	= design points associated with $\Delta P_{s,j}(\tau, \Delta t)$
U_i	= the i -th element of the vector \mathbf{U}
\mathbf{U}	= random variable vector in the standard normal space
$\mathbf{U}_D(j)$	= a collection of \mathbf{U}_j and \mathbf{U}_{cj} , i.e., $[\mathbf{U}_j^T, \mathbf{U}_{cj}^T]^T$
\mathbf{U}_j	= vector of n_j independent standard normal variates involving $g_j(\bullet)$ itself
\mathbf{U}_{cj}	= vector of $(n-n_j)$ random variables that are not in \mathbf{U}_j
UT	= ultrasonic technology
v	= coefficient of variation
v_r	= discount rate of the maintenance cost
v_W	= coefficient of variation of $F_{Wj}(\bullet)$
v_R	= coefficient of variation of $F_{Rj}(\bullet)$
$\mathbf{v}^*(j)$	= m -dimensional design point associated with $\mathbf{y}^*(j)$ in the standard normal space
\mathbf{V}	= m -dimensional vector in the independent standard normal space
w_j	= weighting factor assigned to the IS density function associated with the j -th component
wt_j	= wall thickness random variable at the j -th defect
wt_n	= nominal value of wall thickness
$w_j^b(\tau, t)$	= weighting factor for $h_U^b(\mathbf{u}; \tau, \Delta t)$
$w_j^s(\tau, \Delta t)$	= weighting factors for $h_U^s(\mathbf{u}; \tau, \Delta t)$
W_j, W_k	= wind speed at the the j -th and the k -th tower, respectively
x_{cj}	= value of X_{cj}
$x_j(t)$	= value of $X_j(t)$
\mathbf{x}	= value of the vector \mathbf{X}
\mathbf{x}_j	= value of the vector \mathbf{X}_j
$\mathbf{x}^*(j)$	= design point in original space involving the whole system associated with β_j

$\mathbf{x}_D^*(j)$	= design point in the $\mathbf{X}_D(j)$ space
$\mathbf{x}_j(\mathbf{u}_j)$	= function \mathbf{x}_j is defined in terms of \mathbf{u}_j
$\mathbf{x}(\mathbf{z})$	= function \mathbf{x} defined in terms of \mathbf{z}
X_{cj}	= random variable of the critical threshold associated with the j -th component
X_i	= the i -th element of the vector \mathbf{X}
$X_j(t)$	= random variable vector of the cumulative degradation within the interval $[0, t]$ of the j -th component
\mathbf{X}	= random variable vector in the original space
\mathbf{X}_{cj}	= vector of $(n-n_j)$ random variables that are not in \mathbf{X}_j
$\mathbf{X}_D(j)$	= a collection of \mathbf{X}_j and \mathbf{X}_{cj} , i.e., $[\mathbf{X}_j^T, \mathbf{X}_{cj}^T]^T$
\mathbf{X}_j	= vector of n_j random variables involving $g_j(\bullet)$
$\mathbf{y}^*(j)$	= m -dimensional design point associated with the j -th component in the correlated normal space
$\mathbf{y}_D^*(j)$	= re-ordered vector of design point $\mathbf{y}^*(j)$
y_j^*	= one-dimensional design point associated with the j -th component
\mathbf{y}_{cj}^*	= the values of Y_k ($k= 1, 2, \dots, m; k \neq j$) at the design point $\mathbf{y}^*(j)$
y_j	= value of a standard normal variate Y_j
Y_j	= the j -th element of the vector \mathbf{Y}
\mathbf{Y}	= an m -dimensional correlated standard normal variates with the correlation matrix \mathbf{R}
\mathbf{z}	= value of the vector \mathbf{Z}
z_j	= value of normal variate Z_j
\mathbf{z}_j^*	= design point only involving the j -th limit state function in the correlated space
\mathbf{z}_i^S	= the i -th m -dimensional random sample generated from $h(\bullet)$
\mathbf{z}_{ij}^S	= the j -th ($j = 1, 2, \dots, m$) element of the vector \mathbf{z}_i^S
\mathbf{z}_{cj}^*	= $(n-n_j)$ elements of design point that are not in \mathbf{z}_j^* in the correlated space
$\mathbf{z}^*(j)$	= design point involving the whole system in the correlated normal space associated with β_j
$\mathbf{z}_D^*(j)$	= design point in the space $\mathbf{Z}_D(j)$
$\mathbf{z}(\mathbf{u})$	= function \mathbf{z} defined in terms of \mathbf{u}
Z_j, Z_k	= the j -th, k -th element of the vector \mathbf{Z}
\mathbf{Z}	= random variable vector in the correlated normal space
\mathbf{Z}_j	= vector of n_j random variables in the correlated normal space
\mathbf{Z}_{cj}	= vector of $(n-n_j)$ random variables associated with \mathbf{X}_{cj} in the correlated normal space
$\mathbf{Z}_D(j)$	= a collection of \mathbf{Z}_j and \mathbf{Z}_{cj} , i.e., $[\mathbf{Z}_j^T, \mathbf{Z}_{cj}^T]^T$
SC1, SC2 SC3	= solutions selected from the Pareto front with the constant budget constraint
SN1, SN2	= solutions selected from the Pareto front with no budget constraint
SV1, SV2	= solutions selected from the Pareto front with the variable budget constraint
λ	= penalty factor modulating the relative amplitude of the budget

	Constraint
φ_0	= reduction factor
$\varphi(\bullet)$	= standard normal density function
$\phi_2(\bullet, \bullet, \bullet)$	= probability density function of the bivariate normal distribution
$\varphi_m(\bullet, \bullet)$	= m -dimensional normal probability density function
$\Phi(\bullet)$	= standard normal cumulative distribution function
$\Phi^{-1}(\bullet)$	= the inverse of the standard normal cumulative distribution function
$\Phi_m(\bullet, \bullet)$	= m -variate standard normal distribution function
$\Phi_2(\beta_1, \beta_2, \rho_{12})$	= bivariate cumulative normal function evaluated at $[\beta_1 \beta_2]^T$ with correlation coefficient of ρ_{12}
δ_i, δ_k	= coefficients of variation of X_i and X_k , respectively
ϕ_{n-n_j}	= $(n-n_j)$ -dimensional vector of zeros
$\psi_1(\cdot)$	= inverse normal transformation operator
σ	= standard deviation of the depth increment within one year
σ_u	= ultimate tensile strength
σ_{uj}	= ultimate tensile strength at the j -th defect
σ_{yj}	= yield strength at the j -th defect
ξ_j	= model error associated with burst capacity model at the j -th defect
Δ_{jk}	= distance between the j -th and k -th tower sites
$\Delta d_j(t) \Delta l_j(t)$	= growths of the depth and length of the j -th defect, respectively, by time t
$\Delta P_{b,j}(\tau, \Delta t)$	= incremental probability of burst between τ and $\tau + \Delta t$ for the j -th defect
$\Delta P_{s,j}(\tau, \Delta t)$	= incremental probability of small leak between τ and $\tau + \Delta t$ for the j -th defect
$\Delta P_s(\tau, \Delta t) \Delta P_b(\tau, \Delta t)$	= incremental probabilities of small leak and burst, respectively, within a short time interval between τ and $\tau + \Delta t$.
Δt	= incremental time interval
$\ \bullet\ $	= norm of a vector
$\Omega(\mathbf{x})$	= failure domain with \mathbf{x} being the value of \mathbf{X}
$\Omega(\mathbf{u})$	= failure domain with \mathbf{u} being the value of \mathbf{U}
$\Omega^b(\tau, \Delta t)$	= failure domain associated with $\Delta P_b(\tau, \Delta t)$
$\Omega^s(\tau, \Delta t)$	= failure domain associated with $\Delta P_s(\tau, \Delta t)$

1 Introduction

1.1 Background

Onshore pipeline systems are generally recognized as the safest and most economical way to transport oil and gas in a long distance. Failures of pipelines do occur occasionally and are associated with severe consequences in terms of the human safety, property damage and environmental impact. Pipelines are required to be well maintained to ensure safe operation throughout the service life. However, pipeline operators are faced with limited financial resources for maintenance. To achieve a desirable solution between pipeline safety and economic viability, the optimal maintenance strategy for in-service pipelines should be explicitly investigated.

Metal loss corrosion is one major failure cause for onshore pipelines (EGIG 2015; Nessim et al. 2009). Corrosion caused 35% of failures on oil and gas transmission pipelines in Canada between 2010 and 2014 (CEPA 2015) and 32% of reportable incidents on gas transmission pipelines in the US between 2002 and 2013 (Lam and Zhou 2016). A typical corrosion defect is three-dimensional and characterized by its length (in the pipeline longitudinal direction), width (in the circumferential direction) and maximum depth (in the through-pipe wall thickness direction). A representative corrosion defect is showed schematically in Fig. 1.1. Corrosion defects grow actively in length and depth over time. In-Line Inspections (ILI), relying on the Magnetic Flux Leakage (MFL) or ultrasonic technology (UT), are now being commonly employed by pipeline operators to detect, locate and size corrosion defects on the surfaces of pipelines at a regular interval varying from a few to ten years (Kariyawasam and Peterson 2010).

In general, a corroding pipe joint (typically 12-20 m long) may fail by small leak when wall thickness is penetrated by corrosion defect or by burst resulting from pipeline steel plastic collapse at the defect subjected to internal pressure prior to the defect penetrating the pipe wall (Zhou 2010). Small leak and burst result in markedly distinct consequences. Small leak failures typically merely involve the cost of repairing pipeline joints, whereby burst failure could result in ignition of the released substance that may damage the environment and the surrounding properties, and induce fatalities (Nessim et al. 2009).

Industry practice is to mitigate corrosion defects on a joint-by-joint basis as opposed to a defect-by-defect basis (Zhang and Zhou 2014); that is, mitigating a critical corrosion defect requires the excavation of the entire pipe joint containing the defect and repairing (or replacing) the joint. Condition assessment of corroding joints based on the defects reported by ILI tool is a critical part of developing excavation and repairing schedules. Integrity engineer carries out the deterministic or probabilistic defect assessment (Kariyawasam and Huyse 2012; Zhou et al. 2016). The deterministic assessment requires evaluating the Failure Pressure Ratio (FPR) between the nominal burst pressure capacity at the defect and the Maximum Operating Pressure (MOP) of the pipeline (Kariyawasam and Huang 2014). Any defect with FPR less than the pre-defined threshold (e.g., 1.1 or 1.25) is considered critical and the joint containing such a defect is excavated and repaired. The probabilistic defect assessment involves calculating the burst failure probability at the defect, and the one with probability of burst exceeding the pre-defined threshold (e.g. 10^{-3}) is deemed critical. The latter is increasingly employed in industry practice for quantifying the pipeline safety (Kariyawasam and Peterson 2010; Huyse and Brown 2012), chiefly for the advantages of managing various relevant uncertainties such as model error, wall thickness, and pressure et al. However, a single pipeline joint, typically with length of 10 - 20 m long (Al-Amin and Zhou 2014), may contain multiple active corrosion defects. The joint with a single defect is less critical than the one containing more defects with the same size. The joint should be considered as a series system in the reliability assessment. The correlation between the defect sizes, operating pressure and pipe properties (e.g. pipe wall thickness and yield strength) at different defects can result in correlated failures at different defects. Such correlations must be dealt with. Small leak and burst are mutually competing against each other. The occurrence of one failure mode, either small or burst, would eliminate the occurrence probability of the other.

The commonly used method for the assessment of the time-dependent small leak and burst failure probabilities of the corroding pipeline system is the simple Monte Carlo simulation (MC) (Zhou 2010; Zhou 2012). However, this method demands significant computational cost if the probabilities of corroding pipelines are very small (e.g. $\leq 10^{-6}$) and/or there are large numbers of pipeline joints to be analyzed. The application of the efficient FORM to approximate the failure probabilities of pipelines with corrosion defects has been

introduced in the literature (Teixeira et al. 2008; Sahraoui et al. 2013; Zhang and Zhou 2014; Miran et al. 2016). However, those methods either ignore the competing characteristics of small leak and burst failures, or fail to consider multiple correlated corrosion defects as a series system. The application of the FORM to the system reliability analyses relies on the design points to calculate the correlation coefficients between the failures at different defects and the multi-normal integral to evaluate the system reliability. The design point is obtained from the constrained optimization while the multi-normal integral is a function of reliability index at different defects and associated correlation coefficients. With an increased number of defects, the dimension of both optimization and multi-normal integral increases (Kang and Song 2010; Roscoe et al. 2015). It follows that the efficiency of the FORM may be therefore hampered.

Defect mitigation is very costly, with the typical spending for excavating and repairing a single pipe joint in Canada reaches up to CAD\$125,000 (Zhang and Zhou 2014), and in general a significant number of (e.g. dozens or more) joints need to be excavated and repaired in a relatively short pipeline (e.g. one or two hundred kilometers long) after the ILI. The non-critical joint at the ILI time may become critical because corrosion defects grow over time. Besides, the critical joints may be not repaired all immediately after the ILI due to the constraints of the budget, labor resources or accessibility. Therefore, a phased defect mitigation strategy is employed in practice; that is, mitigation actions are spread out over the period between two consecutive ILIs. A challenging task faced by pipeline operators is how to schedule defect mitigation actions to achieve an optimal balance between the safe operation of the pipeline and the maintenance expense, subjected to various constraints.

1.2 Objective and Research Significance

The research described in this thesis is financially supported by Natural Sciences and Engineering Research Council (NSERC) of Canada and TransCanada Ltd. The objective of this research is summarized as follows:

- 1) Development of efficient methods to obtain the design points for limit state functions in the system reliability application of the FORM;
- 2) Development of efficient multi-normal integral methods within the FORM for large series systems with significant number of correlated components;
- 3) Development of the FORM and important sampling (IS) based methodology for assessing small leak and burst system failure probabilities incorporating the competing characteristics;
- 4) Development of the optimum cost-effective maintenance strategy for corroding pipeline systems, with the consideration of the conflicting safety and cost objectives. It is expected that the contribution in this thesis will be beneficial for the reliability assessment of large systems in various other disciplines in addition to pipeline systems. Moreover, it will also facilitate the integrity maintenance management of in-service corroding pipeline systems.

1.3 Scope of Study

This study is composed of five main topics that are described from Chapters 2 to Chapters 6. Chapter 2 presents an efficient procedure employing the FORM to evaluate the reliability of engineering systems governed by multiple limit state functions that are correlated due to the correlation among random variables involved in different limit state functions. To estimate the system reliability, the FORM analyses for an individual limit state function included in the system needs to be carried out by only considering the random variables involved in the limit state function itself; the design point hereby obtained from the FORM can be mapped to the design point in the space that corresponds to all the random variables in the system.

Chapter 3 presents an improved equivalent component approach to evaluate the system reliability of series systems by providing an analytical expression to evaluate the unit normal vector, in the context of the FORM, associated with the equivalent component. It is also proposed that the two components with the highest correlation coefficient be combined at each combining step. The accuracy and efficiency of the adaptive equivalent component approach are demonstrated to be excellent for series systems with equi-correlated and unequally correlated components through various examples.

Chapter 4 introduces a methodology that employs the FORM to evaluate the time-dependent system reliability of a joint of a pressurized pipeline containing multiple active corrosion defects. The methodology considers small leak and burst failure modes of the pipeline joint, and accounts for the correlations among limit state functions at different corrosion defects. The methodology involves first constructing two linearized equivalent limit state functions for the pipe joint in the standard normal space and then evaluating the probabilities of small leak and burst of the joint incrementally over time based on the equivalent limit state functions.

In Chapter 5, an IS technique-based method is introduced to evaluate the time-dependent system reliability of corroding pipeline joints containing multiple active corrosion defects by considering two competing failure modes, i.e., small leak and burst. The IS density functions in the standard normal space for incremental probabilities of small leak and burst of the pipeline joint over a short time interval are established as the weighted averages of the IS density functions for small leak and burst, respectively, at individual corrosion defects. The IS density functions for incremental probabilities of small leak and burst at individual defects are centered at the design points associated with corresponding failure domains.

In Chapter 6, a multi-objective optimization based pipeline maintenance strategy is presented. The optimized variables are the location of to-be-repaired pipeline joints and associated time points after an ILI. Three objectives are optimized simultaneously, i.e. minimizing the maximum annual conditional probabilities of small leak and burst, respectively, and the corresponding cost for exaction and repairing. Genetic algorithm with

specified initial population is employed to improve the robustness of obtaining a complete Pareto front.

It is assumed throughout this thesis that sizes of corrosion defects are monotonically increasing with time. Both stochastic process- and random variable-based defect growths are considered in the work reported in the thesis. Once repaired, a corroding pipe joint is restored to the pristine condition. All pipelines are accessible to ILI. The reliability analysis is carried out based on the corrosion defect information provided by a recently-run ILI. Since a future ILI will provide the updated information for corrosion defects, the time-dependent reliability analysis is generally carried out up to the time of the next ILI.

1.4 Thesis Format

This thesis is prepared in an Integrated-Article Format as specified by the School of Graduate and Postdoctoral Studies at Western University, London, Ontario, Canada. In total, seven chapters are included in the thesis. Chapter 1 is the introduction of the whole thesis, describing the research background, objectives and scope. Chapter 2 through Chapter 6 are the main body of the thesis, where each chapter acts as a stand-alone manuscript that is the key part of the published papers and submitted manuscripts. In the last chapter, conclusions of the thesis and recommendations for the future work are summarized.

1.5 References

Al-Amin, M., and Zhou, W. (2014). Evaluating the system reliability of corroding pipelines based on inspection data. *Structure and Infrastructure Engineering*, 10(9), 1161-1175.

Canadian Energy Pipeline Association (CEPA). (2015). Committed to safety, committed to Canadians. 2015 pipeline performance report. Calgary, Alberta: Canadian Energy Pipeline Association.

EGIG. (2015). Gas Pipeline Incidents Report 1970–2013. Fourth Report of the European Gas Pipeline Incident Data Group

Huyse, L., and Brown, K. A. (2012). Why reliability-based approaches need more realistic corrosion growth modeling. 9th International Pipeline Conference (IPC2012), ASME, IPC2012-90319, Calgary, Alberta, Canada

Kang, W. H., and Song, J. (2010). Evaluation of multivariate normal integrals for general systems by sequential compounding. *Structural Safety*, 32(1), 35-41.

Kariyawasam, S., and Huang, T. (2014). How safe failure pressure ratios are related to % SMYS. In 2014 10th International Pipeline Conference (pp. V002T06A019-V002T06A019). American Society of Mechanical Engineers.

Kariyawasam, S., and Huyse, L. (2012). Providing Safety: Using Probabilistic or Deterministic Methods. In 2012 9th International Pipeline Conference (pp. 725-734). American Society of Mechanical Engineers.

Kariyawasam, S., and Peterson, W. (2010). Effective improvements to reliability based corrosion management. 8th International Pipeline Conference (IPC2010), ASME, IPC2010-31425, Calgary, Alberta, Canada

Lam, C., and Zhou, W. (2016). Statistical analyses of incidents on onshore gas transmission pipelines based on PHMSA database. *International Journal of Pressure Vessels and Piping*, 145, 29-40.

Miran, S. A., Huang, Q., and Castaneda, H. (2016). Time-dependent reliability analyses of corroded buried pipelines considering external defects. *Journal of Infrastructure Systems*, 22(3), 04016019.

Nessim, M., Zhou, W., Zhou, J., and Rothwell, B. (2009). Target reliability levels for design and assessment of onshore natural gas pipelines. *Journal of Pressure Vessel Technology*, 131(6), 061701.

Roscoe, K., Diermanse, F., and Vrouwenvelder, T. (2015). System reliability with correlated components: Accuracy of the Equivalent Planes method. *Structural Safety*, 57, 53-64.

Sahraoui, Y., Khelif, R. and Chateauneuf, A. (2013). Maintenance planning under imperfect inspections of corroded pipelines. *International Journal of Pressure Vessels and Piping*, 104, 76-82.

Teixeira, A. P., Soares, C. G., Netto, T. A. and Estefen, S. F. (2008). Reliability of pipelines with corrosion defects. *International Journal of Pressure Vessels and Piping*, 85(4), 228-237.

Zhang, S. and Zhou, W. (2014). Cost-based optimal maintenance decisions for corroding natural gas pipelines based on stochastic degradation models. *Engineering Structures*, 74, 74-85.

Zhang, S. and Zhou, W. (2014). An Efficient Methodology for the Reliability Analyses of Corroding Pipelines. *Journal of Pressure Vessel Technology*, 136(4), 041701.

Zhou, W. (2010). System reliability of corroding pipelines. *International Journal of Pressure Vessels and Piping*, 87(10), 587-595.

Zhou, W., Gong, C., and Kariyawasam, S. (2016). Failure Pressure Ratios and Implied Reliability Levels for Corrosion Anomalies on Gas Transmission Pipelines. In 2016 11th International Pipeline Conference (pp. V001T03A017-V001T03A017). American Society of Mechanical Engineers.

Zhou, W., Hong, H. P. and Zhang, S. (2012). Impact of dependent stochastic defect growth on system reliability of corroding pipelines. *International Journal of Pressure Vessels and Piping*, 96, 68-77.

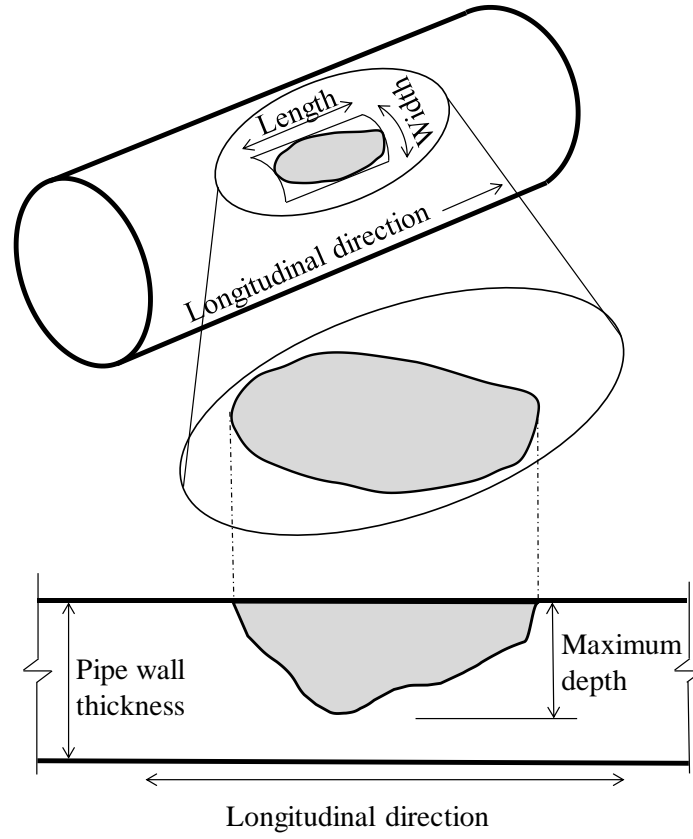


Figure 1.1 Schematic illustration of the geometry of a typical corrosion defect

2 New Perspective on the Application of the First-order Reliability Method for Estimating System Reliability

2.1 Introduction

The reliability of a system governed by a single limit state function can be calculated efficiently using the well-known first-order reliability method (FORM) (Hasofer and Lind 1974; Veneziano 1974; Rackwitz and Fiessler 1978). The calculation involves transforming the random variables involved in the limit state function into the standard normal space and evaluating the reliability index, which equals the minimum distance from the origin to the limit state surface in the standard normal space. The application of the FORM also provides a vector of sensitivity factors at the solution point (i.e., design point) on the limit state surface in the standard normal space (Madsen et al. 2006). Moreover, the FORM assumes that the limit state function is approximated by a linearized safety margin, resulting in the limit state surface being approximated by a tangential hyperplane passing the design point.

If the performance of a system is governed by many limit state functions, the system reliability analyses must consider all the limit state functions and correlations between the corresponding safety margins (Straub and Faber 2005; Der Kiureghian 2005; Madsen et al. 2006; Kang et al. 2012). To take the correlation into account, the application of the FORM to each limit state function is carried out by mapping the random variables in the entire system into the normal space, and the correlation coefficients between the linearized safety margins for any two limit state functions are calculated using the vectors of sensitivity factors at the respective design points (Melchers 1999; Madsen et al. 2006; Ang and Tang 2007). In such a case, the number of random variables involved in the FORM analyses for each limit state function in the transformed normal space may be much greater than that is required for the limit state function in the original space. This increase in the dimensions of the analyses space reduces the computational efficiency and robustness of the FORM.

The above-observed deficiency in using the FORM to calculate the system reliability is relevant to many practical problems. For example, a corroding pipeline may contain many corrosion defects (Hong 1999; Zhou et al. 2012), and the safety margins at different

corrosion defects are correlated if, for example, the sizes of different defects are correlated. This correlation increases the number of random variables involved in the FORM analyses for each individual defect in the standard normal space if the system reliability aspect is considered. Another example is a tower-line system with several transmission towers that are subjected to spatially correlated wind loads (or ice loads or earthquake loads) (Hong et al. 2006, Zhang and Li 2007; Chen and Booth 2011). As a first order approximation, assume that the wind load on each tower can be characterized by the time averaged mean wind speed at the tower site and that the tower capacity can be presented by the nonlinear static pushover curve (Mara and Hong 2013). To evaluate the system reliability of the tower-line systems, the wind load in the FORM analyses for each individual tower needs to be expressed as a combination of standard independent normal variates due to the spatial correlation of the wind loads. This increase in the number of random variables reduces the computational efficiency and robustness of using the FORM to calculate the failure probability of each tower.

In short, the use of the FORM to calculate the reliability of engineering systems could be inefficient if there are many limit state functions involved in the system and each limit state function is a function of only a few random variables in the original space but a large number of random variables for the system in the transformed normal space. A new efficient procedure for calculating the correlation coefficients between the safety margins associated with different limit state functions in the system reliability analyses is proposed in this chapter. The basic steps of the procedure are to 1) apply the FORM to each limit state function by considering only the random variables involved in the limit state function (as opposed to the entire system); 2) identify the design point for each limit state function by considering all random variables for the system based on the results obtained in Step 1); and 3) find the correlation coefficients among the linearized safety margins. Steps 1) - 3) involve the application of a new theorem put forward in this chapter. In the following sections, the basic concept of the FORM is summarized, and the new theorem is presented. The application of the procedure to several practical system reliability analyses problems is shown.

2.2 Basics of the First-order Reliability Method

2.2.1 Analyses for a Single Limit State Function

The basic concept of the FORM is explained in several well-known references, including Melchers (1999), Madsen et al. (2006), and Ang and Tang (2007). It is used to evaluate approximately the failure probability, P_f , represented by the following multidimensional integral

$$P_f = \int_{g(\mathbf{x}) \leq 0} f_{\mathbf{X}}(\mathbf{x}) d\mathbf{x} \quad (2.1)$$

where \mathbf{x} denotes values of a vector of random variables $\mathbf{X} = [X_1, X_2, \dots, X_n]^T$; $g(\mathbf{x})$ is the limit state function with $g(\mathbf{x}) > 0$ and $g(\mathbf{x}) < 0$ defining the safe and failure domains, respectively; $g(\mathbf{x}) = 0$ is known as the limit state surface, and $f_{\mathbf{X}}(\mathbf{x})$ is the joint probability density function of \mathbf{X} . The FORM is carried out by transforming \mathbf{X} into $\mathbf{Z} = [Z_1, Z_2, \dots, Z_n]^T$, and \mathbf{Z} to $\mathbf{U} = [U_1, U_2, \dots, U_n]^T$, where Z_i ($i = 1, \dots, n$) are correlated normal variates with zero means and unity variances, and U_i are independent and standard normal variates. The reliability index β is then given by

$$\beta = \min_{g_{\mathbf{Z}}(\mathbf{z})=0} \sqrt{\mathbf{z}^T \mathbf{R}_{\mathbf{ZZ}}^{-1} \mathbf{z}} \quad (2.2)$$

or,

$$\beta = \min_{g_{\mathbf{U}}(\mathbf{u})=0} \sqrt{\mathbf{u}^T \mathbf{u}} \quad (2.3)$$

where \mathbf{z} denotes the value of \mathbf{Z} ; \mathbf{u} denotes the value of \mathbf{U} ; $\mathbf{R}_{\mathbf{ZZ}}$ is the correlation matrix of \mathbf{Z} , $g_{\mathbf{Z}}(\mathbf{z}) = g(\mathbf{x}(\mathbf{z}))$ is the limit state function in terms of \mathbf{z} ; $\mathbf{x}(\mathbf{z})$ denotes that \mathbf{x} is a function of \mathbf{z} ; $g_{\mathbf{U}}(\mathbf{u}) = g(\mathbf{x}(\mathbf{z}(\mathbf{u})))$ is the limit state function in terms of \mathbf{u} , and $\mathbf{z}(\mathbf{u})$ denotes that \mathbf{z} is a function of \mathbf{u} . The equivalence of Eqs. (2.2) and (2.3) is well established in the context of the first-order second-moment reliability method (Veneziano 1974; Hasofer and Lind 1974). The meaning of Eq. (2.2) in the context of the FORM is explained by Low and Tang (2007); that is, β is the axis ratio of a multi-normal dispersion ellipsoid that just touches the limit state surface $g_{\mathbf{Z}}(\mathbf{z}) = 0$ and the ellipsoid corresponding to $\mathbf{z}^T \mathbf{R}_{\mathbf{ZZ}}^{-1} \mathbf{z} = 1$.

The spreadsheet-based implementation of Eq. (2.2) for simple practical applications is also described in Low and Tang (2007).

The transformation from \mathbf{X} to \mathbf{Z} for dependent or correlated X_i using the Nataf transformation is extensively discussed in Der Kiureghian and Liu (1986) and Der Kiureghian (2005). The use of the (unidimensional) inverse normal distribution and Nataf transformation provides a one-to-one mapping from X_i to Z_i . Let $\rho_{Z_i,k}$ ($i, k = 1, 2, \dots, n; i \neq k$) denote the correlation coefficient between Z_i and Z_k , and $\rho_{X_i,k}$ denote the correlation coefficient between X_i and X_k . Then $\rho_{Z_i,k}$ can be evaluated from $\rho_{X_i,k}$ as (Der Kiureghian and Liu 1986)

$$\rho_{Z_i,k} = F_0 \cdot \rho_{X_i,k} \quad (2.4)$$

where $F_0 (\geq 1)$ is in general a function of $\rho_{X_i,k}$ and parameters of the marginal distributions of X_i and X_k , and can be estimated using the empirical equations for various marginal distributions given in Der Kiureghian and Liu (1986). The empirical equations that are employed for the numerical examples considered in this chapter are summarized in Table 2.1. The transformation from \mathbf{Z} to \mathbf{U} can be carried out by employing $\mathbf{U} = \mathbf{L}^{-1}\mathbf{Z}$, where \mathbf{L} is the lower-triangular matrix obtained from the Cholesky decomposition of \mathbf{R}_{ZZ} (Der Kiureghian 2005).

The failure probability, P_f , is then approximated by

$$P_f = \Phi(-\beta) \quad (2.5)$$

where $\Phi(\bullet)$ is the standard normal cumulative distribution function. One of the assumptions of the FORM is that the limit state surface $g_U(\mathbf{u}) = 0$ is approximated by a hyperplane that is defined by $\beta - \boldsymbol{\alpha}^T \mathbf{u} = 0$ and passes the solution point \mathbf{u}^* , where $\boldsymbol{\alpha}$ is a unit vector normal to $g_U(\mathbf{u}^*)$ and pointing toward the failure domain, and $\boldsymbol{\alpha}$ equals \mathbf{u}^*/β (Madsen et al. 2006).

2.2.2 Observed Deficiency for System Reliability Analyses with Multiple Limit State Functions

Consider a system reliability problem that is defined by m limit state functions, $g_j(\mathbf{x}_j)$ ($j = 1, 2, \dots, m$), where \mathbf{x}_j is the value of \mathbf{X}_j representing a vector of n_j random variables that need to be considered for $g_j(\mathbf{x}_j)$. Let \mathbf{X} denote the union of all \mathbf{X}_j , representing a vector of n random variables that needs to be considered for the system, whereby n can be much greater than n_j .

If the reliability analyses for a single limit state $g_j(\mathbf{x}_j)$ is of interest, the FORM procedure is the same as that shown in the previous section (see Eqs. (2.2) and (2.3)). However, since the safety margins could be correlated and their correlations must be evaluated for estimating the system reliability (Madsen et al. 2006; Der Kiureghian 2005), the most direct application of the FORM in the context of the system reliability is to first transform \mathbf{X} into \mathbf{Z} and/or \mathbf{U} , where the symbols \mathbf{Z} and \mathbf{U} are already defined in the previous section. In the transformed spaces, the reliability index β_j for the j -th limit state function mentioned in the previous paragraph is then given by

$$\beta_j = \min_{g_{j,z}(\mathbf{z})=0} \sqrt{\mathbf{z}^T \mathbf{R}_{zz}^{-1} \mathbf{z}} \quad (2.6)$$

or,

$$\beta_j = \min_{g_{j,u}(\mathbf{u})=0} \sqrt{\mathbf{u}^T \mathbf{u}} \quad (2.7)$$

where $g_{j,z}(\mathbf{z}) = g_j(\mathbf{x}_j(\mathbf{z}))$ is the limit state function in terms of \mathbf{z} , and $g_{j,u}(\mathbf{u}) = g_j(\mathbf{x}_j(\mathbf{z}(\mathbf{u})))$ is the limit state function in terms of \mathbf{u} . The design point corresponding to β_j is denoted by $\mathbf{u}^*(j)$. Both Eqs. (2.6) and (2.7) involve n -dimensional vectors of random variables in the transformed spaces, which decreases the computational efficiency and robustness of using the FORM to evaluate β_j , as compared to the case where the FORM is applied to $g_j(\mathbf{x}_j)$ without considering the system reliability aspect. The decrease in the efficiency can be very significant, especially for n much greater than n_j , because the number of calls to the limit state function in the FORM is proportional to the number of random variables in the limit state function (Rackwitz and Fiessler 1978; Madsen et al. 2006).

Because the limit state surface $g_{j,U}(\mathbf{u}) = 0$ is approximated by a hyperplane defined by $\beta_j - \boldsymbol{\alpha}_j^T \mathbf{u} = 0$, where $\boldsymbol{\alpha}_j = \mathbf{u}^*(j)/\beta_j$, the correlation coefficient between the safety margins at the solution points for the j -th and k -th limit states, ρ_{jk} , equals $\boldsymbol{\alpha}_j^T \boldsymbol{\alpha}_k$ (Madsen et al. 2006). In particular, the failure probability of system, P_f , can be expressed as

$$P_f = 1 - \int_{-\infty}^{\beta_1} \cdots \int_{-\infty}^{\beta_m} \frac{1}{\sqrt{(2\pi)^m |\boldsymbol{\Sigma}|}} \exp\left(-\frac{1}{2} \boldsymbol{\theta}^T \mathbf{R}^{-1} \boldsymbol{\theta}\right) d\theta_1 \cdots d\theta_m \quad (2.8a)$$

if the system is a series system, and

$$P_f = \int_{\beta_1}^{\infty} \cdots \int_{\beta_m}^{\infty} \frac{1}{\sqrt{(2\pi)^m |\boldsymbol{\Sigma}|}} \exp\left(-\frac{1}{2} \boldsymbol{\theta}^T \mathbf{R}^{-1} \boldsymbol{\theta}\right) d\theta_1 \cdots d\theta_m \quad (2.8b)$$

if the system is a parallel system, where \mathbf{R} denotes the correlation matrix of standard normal variates with diagonal elements equal to one and off-diagonal elements defined by ρ_{jk} ; and $\boldsymbol{\theta} = [\theta_1, \theta_2, \dots, \theta_m]^T$ denotes an m -dimensional vector of standard normal variates with zero mean and unity variance. Many approaches for evaluating the integrals in Eqs. (2.8a) and (2.8b) have been proposed in the literature, for example, the Ditlevsen bounds (Ditlevsen 1979); equivalent component method (Gollwitzer and Rackwitz 1983; Estes and Frangopol 1998; Roscoe et al. 2015), sequential compounding method (Kang and Song 2010), and quasi-Monte Carlo algorithms developed by Genz (1992, 1993), which have been implemented in commonly used software packages such as Matlab and R (the corresponding commands in Matlab and R are `mvncdf(x, mu, sigma)` and `pmvnorm(upper = c, corr = R)`), respectively. Moreover, Eqs. (2.8a) and (2.8b) can be further simplified for particular forms of the correlation matrix (Genz 1992, 1993). Discussions on evaluating P_f for systems involving both series and parallel subsystems can be found in Der Kiureghian (2005), Madsen et al. (2006) and Kang et al. (2012).

2.3 Efficient Procedure to Carry Out System Reliability Analyses

The inefficiency in using Eq. (2.6) or Eq. (2.7) to calculate β_j and find the linearized safety margin at the design point in the context of the system reliability can be overcome by using the theorem presented below.

Theorem: Consider that the vector \mathbf{X} of all the n random variables that need to be considered for a system can be divided into two sub-vectors of random variables \mathbf{X}_j and \mathbf{X}_{cj} , where \mathbf{X}_j is a vector of n_j random variables that need to be considered for $g_j(\mathbf{x}_j)$, and \mathbf{X}_{cj} is a vector of $(n-n_j)$ random variables that are not in \mathbf{X}_j . Within the context of the Nataf transformation and FORM, the design point in the n -dimensional standard normal space is

given by $\begin{pmatrix} \mathbf{u}_j^* \\ \boldsymbol{\phi}_{n-n_j} \end{pmatrix}$ and the reliability index β_j , is given by,

$$\beta_j = \min_{g_j, \mathbf{u}_j(\mathbf{u}_j)=0} \sqrt{\mathbf{u}_j^T \mathbf{u}_j} \quad (2.9)$$

where $\boldsymbol{\phi}_{n-n_j}$ denotes an $(n-n_j)$ -dimensional vector of zeros; \mathbf{u}_j^* is the design point obtained by solving Eq. (2.9); $g_j, \mathbf{u}_j(\mathbf{u}_j) = g_j(\mathbf{x}_j(\mathbf{u}_j))$ is the limit state function in terms of \mathbf{u}_j ; \mathbf{u}_j denotes the value of \mathbf{U}_j that represents a vector of n_j independent standard normal variates transformed from \mathbf{X}_j ; and $\mathbf{x}_j(\mathbf{u}_j)$ emphasizes that \mathbf{x}_j is a function of \mathbf{u}_j .

To show that the above holds, consider $\mathbf{X}_D(j) = [\mathbf{X}_j^T, \mathbf{X}_{cj}^T]^T$. Note that $\mathbf{X}_D(j)$ is not necessarily equal to \mathbf{X} because the orders of the random variables in $\mathbf{X}_D(j)$ and in \mathbf{X} could differ. By applying the (unidimensional) inverse normal transformation to each of the random variables in $\mathbf{X}_D(j)$, denoted as $\psi_1(\mathbf{X}_D(j))$ (i.e., $\psi_1(\cdot)$ represents an element to element inverse normal transformation operator) a vector of n zero mean and unity variance normal variates, $\mathbf{Z}_D(j) = \psi_1(\mathbf{X}_D(j))$, is obtained. Similar to $\mathbf{X}_D(j)$, $\mathbf{Z}_D(j)$ is divided in two sub-vectors, $\mathbf{Z}_D(j) = [\mathbf{Z}_j^T, \mathbf{Z}_{cj}^T]^T$. The correlation matrix of $\mathbf{Z}_D(j)$, $\mathbf{R}_{ZZ}(j)$ obtained based on the Nataf transformation, can be partitioned as follows:

$$\mathbf{R}_{ZZ}(j) = \begin{bmatrix} \mathbf{R}_{Z_j,j} & \mathbf{R}_{Z_j,cj} \\ \mathbf{R}_{Z_{cj},j} & \mathbf{R}_{Z_{cj},cj} \end{bmatrix} \quad (2.10)$$

where $\mathbf{R}_{Z_j,j}$ represents the correlation matrix of the elements in \mathbf{Z}_j ; $\mathbf{R}_{Z_{cj},cj}$ represents the correlation matrix of the elements in \mathbf{Z}_{cj} ; $\mathbf{R}_{Z_j,cj}$ denotes the correlation between the elements in \mathbf{Z}_j and \mathbf{Z}_{cj} , and $\mathbf{R}_{Z_j,cj}$ equals $\mathbf{R}_{Z_{cj},j}^T$.

It can be shown that the Cholesky decomposition of $\mathbf{R}_{ZZ}(j)$ results in the lower diagonal matrix $\mathbf{L}(j)$ given by

$$\mathbf{L}(j) = \begin{bmatrix} \mathbf{L}_{j,j} & 0 \\ \mathbf{L}_{cj,j} & \mathbf{L}_{cj,cj} \end{bmatrix} \quad (2.11)$$

where $\mathbf{L}_{j,j}$ depends only on $\mathbf{R}_{Zj,j}$, and $\mathbf{L}_{j,j}$, $\mathbf{L}_{cj,j}$ and $\mathbf{L}_{cj,cj}$ are submatrices of dimensions of $n_j \times n_j$, $(n-n_j) \times n_j$, and $(n-n_j) \times (n-n_j)$, respectively (Press et al. 1992). Moreover, $\mathbf{R}_{Zj,j} = \mathbf{L}_{j,j}(\mathbf{L}_{j,j})^T$. As the inverse matrix of an invertible lower triangular matrix is also a lower triangular matrix, the inverse of $\mathbf{L}(j)$, $(\mathbf{L}(j))^{-1}$, can be expressed as

$$(\mathbf{L}(j))^{-1} = \begin{bmatrix} \mathbf{L}_{j,j}^{-1} & 0 \\ -\mathbf{L}_{cj,cj}^{-1}\mathbf{L}_{cj,j}\mathbf{L}_{j,j}^{-1} & \mathbf{L}_{cj,cj}^{-1} \end{bmatrix} \quad (2.12)$$

The application of this rotational transformation defined by $(\mathbf{L}(j))^{-1}$ maps $\mathbf{Z}_D(j)$ into the n -dimensional (independent) normal space $\mathbf{U}_D(j)$. That is, $\mathbf{U}_D(j) = [\mathbf{U}_j^T, \mathbf{U}_{cj}^T]^T = (\mathbf{L}(j))^{-1}\mathbf{Z}_D(j)$, where again, similar to $\mathbf{X}_D(j)$, $\mathbf{U}_D(j)$ is divided in two sub-vectors \mathbf{U}_j and \mathbf{U}_{cj} . More specifically,

$$\begin{pmatrix} \mathbf{U}_j \\ \mathbf{U}_{cj} \end{pmatrix} = \begin{bmatrix} \mathbf{L}_{j,j}^{-1} & 0 \\ -\mathbf{L}_{cj,cj}^{-1}\mathbf{L}_{cj,j}\mathbf{L}_{j,j}^{-1} & \mathbf{L}_{cj,cj}^{-1} \end{bmatrix} \begin{pmatrix} \mathbf{Z}_j \\ \mathbf{Z}_{cj} \end{pmatrix} \quad (2.13)$$

This indicates that \mathbf{U}_j only depends on \mathbf{Z}_j , which depends only on \mathbf{X}_j . Based on this, the limit state function $g_j(\mathbf{x}_j)$ depends only on the value of \mathbf{U}_j , \mathbf{u}_j , (i.e., $g_{j,U}(\mathbf{u}) = g_{j,U_j}(\mathbf{u}_j)$) and β_j is given by

$$\beta_j = \min_{g_{j,U_j}(\mathbf{u}_j)=0} \sqrt{\mathbf{u}_j^T \mathbf{u}_j + \mathbf{u}_{cj}^T \mathbf{u}_{cj}} \quad (2.14)$$

As $g_{j,U_j}(\mathbf{u}_j)$ is independent of \mathbf{u}_{cj} , the minimum of $\mathbf{u}_j^T \mathbf{u}_j$ subjected to $g_{j,U_j}(\mathbf{u}_j) = 0$ that occurs at the design point $\mathbf{u}_j = \mathbf{u}_j^*$, is independent of the values of \mathbf{u}_{cj} . Since for β_j to be minimum, both $\mathbf{u}_j^T \mathbf{u}_j$ and $\mathbf{u}_{cj}^T \mathbf{u}_{cj}$ must be minimum, and the minimum of $\mathbf{u}_{cj}^T \mathbf{u}_{cj}$ occurs at $\mathbf{u}_{cj}^* = \phi_{n-n_j}$, it follows that Eq. (2.14) becomes Eq. (2.9), which completes the proof.

The above theorem indicates that the reliability analyses needs only to be carried out for n_j random variables involved in the considered limit state function rather than for the n random variables for the system. The design point in the $X_{D(j)}$ space for the j -th limit state function, $\mathbf{x}_{D^*}(j)$, is obtained from

$$\mathbf{x}_{D^*}(j) = \Psi_1^{-1}\left(\begin{pmatrix} \mathbf{z}_j^* \\ \mathbf{z}_{cj}^* \end{pmatrix}\right) = \Psi_1^{-1}\left(\mathbf{L}(j) \begin{pmatrix} \mathbf{u}_j^* \\ \boldsymbol{\phi}_{n-n_j} \end{pmatrix}\right) \quad (2.15)$$

where according to Eq. (2.13), $\begin{pmatrix} \mathbf{z}_j^* \\ \mathbf{z}_{cj}^* \end{pmatrix} = \mathbf{L}(j) \begin{pmatrix} \mathbf{u}_j^* \\ \boldsymbol{\phi}_{n-n_j} \end{pmatrix}$ represents the design point in the $\mathbf{Z}_{D(j)}$ space.

This indicates that at the design point the values of the random variables in X_{cj} may not necessarily be equal to zero although $\mathbf{u}_{cj}^* = \boldsymbol{\phi}_{n-n_j}$. This can be explained by noting that the probability density function of X_j depends on the value of X_{cj} , and the likelihood of the failure may not necessarily be the greatest for X_{cj} equal to zero. Because the orders of the random variables in $X_{D(j)}$ and \mathbf{X} may differ, the elements of the design point $\mathbf{x}_{D^*}(j)$ must be re-ordered so it represents the design point for the j -th limit state function, denoted as $\mathbf{x}^*(j)$, in the \mathbf{X} space.

Note that the above can also be expressed in the $\mathbf{Z}_{D(j)}$ space rather than in the $\mathbf{U}_{D(j)}$ space.

To see this, note that from Eq. (2.13), $\mathbf{u}_j = \mathbf{L}_{j,j}^{-1} \mathbf{z}_j$. This leads to

$$\mathbf{u}_j^T \mathbf{u}_j = \mathbf{z}_j^T (\mathbf{L}_{j,j}^{-1})^T \mathbf{L}_{j,j}^{-1} \mathbf{z}_j = \mathbf{z}_j^T (\mathbf{L}_{j,j} \mathbf{L}_{j,j}^T)^{-1} \mathbf{z}_j. \text{ Substituting this relation and } \mathbf{R}_{Z_j,j} = \mathbf{L}_{j,j} \mathbf{L}_{j,j}^T$$

into Eq. (2.9) results in

$$\beta_j = \min_{g_{j,z_j}(\mathbf{z}_j)=0} \sqrt{\mathbf{z}_j^T \mathbf{R}_{Z_j,j}^{-1} \mathbf{z}_j} \quad (2.16)$$

The solution of Eq. (2.16) denoted as \mathbf{z}_j^* is equal to $\mathbf{L}_{j,j} \mathbf{u}_j^*$. Since $\begin{pmatrix} \mathbf{z}_j^* \\ \mathbf{z}_{cj}^* \end{pmatrix} = \mathbf{L}(j) \begin{pmatrix} \mathbf{u}_j^* \\ \boldsymbol{\phi}_{n-n_j} \end{pmatrix}$,

it follows that $\mathbf{z}_{cj}^* = \mathbf{L}_{cj,j} \mathbf{L}_{j,j}^{-1} \mathbf{z}_j^*$. By considering $\mathbf{R}_{Z_j,j} = \mathbf{L}_{j,j} \mathbf{L}_{j,j}^T$ and $\mathbf{R}_{Z_{cj},j} = \mathbf{L}_{cj,j} \mathbf{L}_{j,j}^T$, as

well as writing $\mathbf{z}_{cj}^* = \mathbf{L}_{cj,j} \mathbf{L}_{j,j}^T (\mathbf{L}_{j,j}^T)^{-1} \mathbf{L}_{j,j}^{-1} \mathbf{z}_j^*$, a more convenient equation for calculating \mathbf{z}_{cj}^* is given by

$$\mathbf{z}_{cj}^* = \mathbf{R}_{\mathbf{z}_{cj,j}} \mathbf{R}_{\mathbf{z}_{j,j}}^{-1} \mathbf{z}_j^* \quad (2.17)$$

In other words, the theorem shown in the above can be restated as that the reliability analyses problem is equivalent to solving Eq. (2.16), and the solution point in the $\mathbf{Z}_D(j)$ space, denoted as $\mathbf{z}_D^*(j)$, is given by

$$\mathbf{z}_D^*(j) = \begin{pmatrix} \mathbf{z}_j^* \\ \mathbf{z}_{cj}^* \end{pmatrix} = \begin{pmatrix} \mathbf{z}_j^* \\ \mathbf{R}_{\mathbf{z}_{cj,j}} \mathbf{R}_{\mathbf{z}_{j,j}}^{-1} \mathbf{z}_j^* \end{pmatrix} \quad (2.18)$$

Note that the advantage of solving the reliability problem for the j -th limit state function in the $\mathbf{Z}_D(j)$ space shown in Eq. (2.16) is that it avoids the need to transform $\mathbf{Z}_D(j)$ to $\mathbf{U}_D(j)$, and the design point is obtained from Eq. (2.18) once solution to Eq. (2.16) is found. The design point for the j -th limit state function, $\mathbf{z}^*(j)$ in the \mathbf{Z} space can be obtained by re-ordering $\mathbf{z}_D^*(j)$. The elements of \mathbf{R} , ρ_{jk} ($j, k = 1, 2, \dots, m$), are computed as: $\rho_{jk} =$

$$\frac{1}{\beta_j \beta_k} (\mathbf{u}^*(j))^T \mathbf{u}^*(k) = \frac{1}{\beta_j \beta_k} (\mathbf{L}^{-1} \mathbf{z}^*(j))^T (\mathbf{L}^{-1} \mathbf{z}^*(k)) = \frac{1}{\beta_j \beta_k} (\mathbf{z}^*(j))^T (\mathbf{L}^{-1})^T \mathbf{L}^{-1} \mathbf{z}^*(k) \quad .$$

Considering $\mathbf{R}_{\mathbf{z}\mathbf{z}}^{-1} = (\mathbf{L}^{-1})^T \mathbf{L}^{-1}$, we can derive the following: $\rho_{jk} =$

$$\frac{1}{\beta_j \beta_k} (\mathbf{z}^*(j))^T \mathbf{R}_{\mathbf{z}\mathbf{z}}^{-1} \mathbf{z}^*(k). \text{ This derivation allows obtaining } \rho_{jk} \text{ without calculating } \mathbf{L}, \text{ which}$$

would improve the efficiency when number of variables is very large and Cholesky decomposition of $\mathbf{R}_{\mathbf{z}\mathbf{z}}$ is computationally expensive.

Based on the above, the system reliability analyses problem can be carried out according to the following steps:

- 1) applying the FORM to the j -th limit state function by solving Eq. (2.16) and evaluating the design point $\mathbf{z}_D^*(j)$ given in Eq. (2.18) in the $\mathbf{Z}_D(j)$ space for $j = 1, 2, \dots, m$;
- 2) re-ordering $\mathbf{z}_D^*(j)$ into the \mathbf{Z} space represented by $\mathbf{z}^*(j)$;

3) calculating ρ_{jk} to define \mathbf{R} , and evaluating the integrals in Eq. (2.8) to estimate P_j .

Ensuring the positive definiteness of \mathbf{R}_{ZZ} is, however, a more challenging issue, especially for high-dimensional systems for which the proposed procedure is most advantageous. Although in this chapter, the derivation for elements of \mathbf{R} , ρ_{jk} ($j, k = 1, 2, \dots, m; j \neq k$), among linearized safety margins, does not require Cholesky decomposition of \mathbf{R}_{ZZ} , \mathbf{R} can be non-positive definite if positive definiteness of \mathbf{R}_{ZZ} is not guaranteed. In such a case, it makes no sense to evaluate Eqs. (2.8a) and (2.8b) since a positive definite \mathbf{R} is a prerequisite for the multi-normal integral. One solution to deal with this problem is to calculate the nearest positive definite matrix of \mathbf{R} using the methodology proposed by Higham (2002), which has been implemented in nearPD function of the *R* package.

2.4 Application

2.4.1 Example 1: System Reliability of Pressurized Pipelines Containing Multiple Corrosion Defects

A joint of pressurized natural gas pipeline contains two corrosion defects. The pipeline joint has a diameter (D) of 610 mm, a nominal wall thickness (wt_n) of 7.16 mm, a nominal maximum operating pressure (P_o) of 6.0 MPa, and a specified minimum tensile strength (SMTS) of 517 MPa. The joint may fail by burst under the internal pressure at either or both of the two corrosion defects; it is a series system consisting of two components. It should be noted that although the proposed procedure is most advantageous for systems consisting of a large number of components, only two corrosion defects are considered in this example for the sake of illustrating the application of the procedure. The limit state function at the j -th ($j = 1, 2$) defect at a given time t , g_j^b , is given by (Zhou et al. 2012)

$$g_j^b = p_{bj} - p_j \quad (2.19)$$

$$p_{bj} = \xi_j \frac{1.8wt_j\sigma_{uj}}{D} \left[\frac{1 - \frac{d_j}{wt_j}}{1 - \frac{d_j}{M_jwt_j}} \right] \quad (2.20)$$

and,

$$M_j = \begin{cases} \sqrt{1 + 0.6275 \frac{l_j^2}{D_j w t_j} - 0.003375 \frac{l_j^4}{(D_j w t_j)^2}} & \frac{l_j^2}{D_j w t_j} \leq 50 \\ 3.3 + 0.032 \frac{l_j^2}{D_j w t_j} & \frac{l_j^2}{D_j w t_j} > 50 \end{cases} \quad (2.21)$$

where the symbol with the subscript j in the above equations indicates the value of a variable at the j -th defect; p_b and p denote the burst capacity and internal pressure, respectively, of the pipeline; ξ is the model error associated with the burst capacity model (Zhou and Huang 2012); D and σ_u are the actual (as opposed to nominal) pipe diameter and tensile strength, respectively; d and l are the depth (i.e. in the through-pipe wall thickness direction) and length (i.e. in the pipe longitudinal direction) of the corrosion defect, respectively, and M is the so-called Folias factor.

The probabilistic characteristics of the random variables included in the limit state functions are summarized in Table 2.2. There are four independent random variables (σ_u , p , d , ξ) (i.e. $n_j = 4$) for each limit state function, whereas the total number of random variables included in the system is eight (i.e. $n = 8$). Therefore, $\mathbf{R}_{\mathbf{Z}_{j,j}}$ ($j = 1, 2$) is a 4×4 identity matrix. However, random variables representing the same physical parameter (i.e., σ_u , p , d , or ξ) at different defects are correlated, with the corresponding correlation coefficients summarized in Table 2.2. The reliability indices obtained by carrying out the FORM in the n_j -dimensional space based on Eq. (2.16) equal 3.25 and 3.19 for the first and second defects, respectively. The corresponding design points in the $\mathbf{Z}_{D(j)}$ ($j = 1, 2$) space are shown in Table 2.3, where \mathbf{z}_j^* is obtained directly from the FORM analyses, and $\mathbf{z}_{c j}^*$ is obtained from $\mathbf{z}_{c j}^* = \mathbf{R}_{\mathbf{Z}_{c j,j}} \mathbf{R}_{\mathbf{Z}_{j,j}}^{-1} \mathbf{z}_j^*$. For this example, $\mathbf{R}_{\mathbf{Z}_{j,j}}^{-1}$ is a 4×4 identity matrix for both g_1 and g_2 , whereas $\mathbf{R}_{\mathbf{Z}_{c j,j}}$ for both g_1 and g_2 is a 4×4 diagonal matrix with (diagonal elements) $\text{diag}(\mathbf{R}_{\mathbf{Z}_{c j,j}}) = (0.300, 0.810, 0.504, 0.504)$. The design points in the \mathbf{Z} and \mathbf{U} spaces for g_1 and g_2 are also shown in Table 2.3. Note that $\mathbf{z}^*(1)$ ($\mathbf{z}^*(2)$) is obtained by re-ordering the elements of \mathbf{z}_1^* and \mathbf{z}_{c1}^* (\mathbf{z}_2^* and \mathbf{z}_{c2}^*) based on the order of random variables Z_1, Z_2, \dots, Z_8 . Finally, $\mathbf{u}^*(1) = \mathbf{L}^{-1} \mathbf{z}^*(1)$ and $\mathbf{u}^*(2) = \mathbf{L}^{-1} \mathbf{z}^*(2)$, where \mathbf{L} is obtained from the Cholesky decomposition of the correlation matrix of Z_1, Z_2, \dots, Z_8 . The correlation coefficient between the two linearized limit state functions is subsequently computed as

0.64. By substituting $\beta_1 = 3.25$, $\beta_2 = 3.19$ and $\rho_{12} = 0.64$ into Eq. (2.8a), the failure probability of the pipeline joint is evaluated to be 8.2×10^{-4} . To demonstrate the computational efficiency of the proposed procedure for this example, the numbers of evaluations of the limit state function and relative CPU times required for solving Eq. (2.6) (i.e. without using the proposed procedure) and Eq. (2.16) (i.e. using the proposed procedure) are compared in Table 2.4. As indicated in the table, the proposed procedure leads to an approximately 40% reduction in the computational cost of searching for the design points associated with the corrosion defects.

2.4.2 Example 2: Degrading Parallel Systems with Multiple Components

This example involves the evaluation of the reliability of a system consisting of five components that are connected in parallel and subjected to dependent stochastic degradation over time (Hong et al. 2014). The limit state function at time t (year) for the j -th component, $g_j(t)$ ($j = 1, 2, \dots, 5$), is given by,

$$g_j(t) = x_{cj} - x_j(t) \quad (2.22)$$

where x_{cj} (mm) denotes the value of the critical threshold, X_{cj} , for degradation of the j -th component beyond which failure occurs; X_{cj} is a lognormal variate with a mean of 2.7 mm and a COV of 25%; $x_j(t)$ (mm) denotes the value of the cumulative degradation within the interval $[0, t]$ of the j -th component, $X_j(t)$, and assumed to be characterized by a homogeneous gamma process (van Noortwijk 2009). The probability density function of $X_j(t)$, $F(x_j(t)|at, b)$, is,

$$F(x_j(t)|at, b) = b^{at} (x_j(t))^{at-1} \exp(-bx_j(t)) / \Gamma(at) \quad (2.23)$$

where a and b are parameters of the gamma process and assigned values of 10/9 (/year) and 100/9 (mm), respectively, and $\Gamma(\bullet)$ is the gamma function. It follows that the mean and variance of $X_j(t)$ equal $0.1t$ (mm) and $0.009t$ (mm²), respectively. It is assumed that X_{cj} of different components are identically distributed and correlated with a correlation coefficient of 0.5, whereas $X_j(t)$ of different components are identically distributed and

statistically dependent, with the joint probability distribution function, $F_X(x_1, x_2, \dots, x_m)$, characterized by the Gaussian copula (Nelsen 2006),

$$F_X(x_1, x_2, \dots, x_m) = \Phi_m(\Phi^{-1}(F_{X_1}(x_1)), \Phi^{-1}(F_{X_2}(x_2)), \dots, \Phi^{-1}(F_{X_m}(x_m)), \mathbf{R}) \quad (2.24)$$

where $m = 5$; $F_{X_j}(x_j)$ denotes the cumulative distribution function of $X_j(t)$; $\Phi^{-1}(\bullet)$ denotes the inverse of the standard normal distribution function, and $\Phi_m(\bullet, \bullet)$ is the m -variate standard normal distribution function with the correlation matrix \mathbf{R} . For simplicity, equal correlation coefficient ρ_0 for this example is assumed in the Gaussian copula among $\Phi^{-1}(F_{X_j}(x_j))$.

Because X_{c_j} and $X_j(t)$ of different components are identically distributed and because equal correlation is assumed in the normal copula, the reliability indices for different components are identical and the linearized safety margins of different components are also equicorrelated. Therefore, the FORM analyses only needs to be carried out for a single component, say the first component, in the n_1 -dimensional space ($n_1 = 2$) to evaluate β_1 . Figure 2.1 depicts β_1 and the corresponding failure probability as a function of time.

The design point for the first component in the n -dimensional \mathbf{Z} space ($n = 10$), $\mathbf{z}^*(1)$, is obtained from the proposed procedure: the 2-dimensional \mathbf{z}_1^* is obtained from the FORM; the 8-dimensional \mathbf{z}_{c1}^* is obtained from $\mathbf{z}_{c1}^* = \mathbf{R}_{\mathbf{z}_{c1,1}} \mathbf{R}_{\mathbf{z}_1,1}^{-1} \mathbf{z}_1^*$ with $\mathbf{R}_{\mathbf{z}_1,1}^{-1}$ being a 2×2 identity matrix and $\mathbf{R}_{\mathbf{z}_{c1,1}}$ being an 8×2 matrix, and finally $\mathbf{z}^*(1)$ is obtained by reordering the elements of $\begin{pmatrix} \mathbf{z}_1^* \\ \mathbf{z}_{c1}^* \end{pmatrix}$ based on the predefined unique order of the n random variables (physical parameters) in the \mathbf{Z} space. To obtain the design points for the other four components, note that $\mathbf{z}_j^* = \mathbf{z}_1^*$ and $\mathbf{z}_{c_j}^* = \mathbf{z}_{c1}^*$ for $j = 2, 3, 4, 5$. Reordering the elements of $\begin{pmatrix} \mathbf{z}_j^* \\ \mathbf{z}_{c_j}^* \end{pmatrix}$ based on the order of the n random variables in the \mathbf{Z} space then generates $\mathbf{z}^*(j)$. It must be emphasized that $\mathbf{z}^*(j) \neq \mathbf{z}^*(1)$ ($j = 2, 3, 4, 5$) because the physical parameters corresponding to \mathbf{z}_j^* ($\mathbf{z}_{c_j}^*$) are different from those corresponding to \mathbf{z}_1^* (\mathbf{z}_{c1}^*), i.e. \mathbf{z}_j^* corresponding to X_{c_j} and $X_j(t)$ whereas \mathbf{z}_1^* corresponding to X_{c1} and $X_1(t)$.

Let ρ_{jk} denote the correlation coefficient between the linearized safety margins of the j -th and k -th components ($j, k = 1, 2, \dots, 5; j \neq k$) and it is assumed that $\rho_{jk} = \rho$. Since the design point for the component depends on time and the value of ρ_0 , it follows that ρ is also a function of time and ρ_0 . Figure 2.2 depicts the values of ρ at different times and for three different values of ρ_0 (i.e. 0.1, 0.5 and 0.9). The failure probability of a parallel system consisting of five components with equicorrelated safety margins can be obtained from the following integral (Genz 1993):

$$P_f = \frac{1}{\sqrt{2\pi}} \int_{-\infty}^{\infty} e^{-\frac{s^2}{2}} \prod_{j=1}^5 \Phi\left(\frac{-\beta_j + \sqrt{\rho} s}{\sqrt{1-\rho}}\right) ds \quad (2.25)$$

The failure probabilities as a function of time are depicted in Figure 2.3 for ρ_0 equal to 0.1, 0.5 and 0.9, respectively. Because the system in Example 2 includes more components than that in Example 1, the improvement in the computational efficiency achieved by the proposed procedure for Example 2 is more significant than that achieved for Example 1 (Table 2.4).

2.4.3 Example 3: Failure Probability of a Transmission Tower-line System Subjected to a Wind Event

The reliability analyses of the electrical transmission tower-line system under wind hazard is a complex task and involves the consideration of uncertainties in the material and geometric variables in tower-line systems, the variability in the pressure coefficients and spatially varying wind speed (Zhang and Li 2007). The nonlinear inelastic static and dynamic analyses of a tower for estimating the tower-capacity curve as well as its ultimate capacity is computationally intensive by considering the mentioned variabilities (Mara and Hong 2013, Mara et al. 2016). Consider a joint of straight tower-line system with 11 towers and a separation between two adjacent towers equal to 500 m. The tower-line system is subjected to transversal wind loading. For simplicity and illustrative purpose, it is considered that the ultimate capacity, R_j (m/s), of the j -th tower in terms of sustaining the 3-second gust mean wind speed at 10 m height at the tower site is lognormally distributed with the cumulative distribution function $F_{R_j}(r_j)$, mean m_R and COV v_R . It is further assumed that R_j ($j = 1, \dots, 11$) are identically distributed and equally correlated with a

correlation coefficient ρ_R . The joint probability distribution of R_j ($j = 1, \dots, 11$), denoted by $F_R(r_1, r_2, \dots, r_{11})$, can be represented by the Gaussian copula as given by Eq. (2.24) with $m = 11$, x_j replaced by r_j , and $F_{X_j}(x_j)$ by $F_{R_j}(r_j)$ for $j = 1, \dots, 11$.

Furthermore, it is considered that for a rare scenario wind event, the 3-second gust mean wind speed at 10 m height at the j -th tower site, W_j ($j = 1, \dots, 11$) (m/s), is Gumbel distributed with the cumulative distribution function $F_{W_j}(w_j)$, mean m_W and COV v_W . For illustration purpose, the correlation coefficient between W_j and W_k ($j, k = 1, \dots, 11$), $\rho_w(\Delta_{jk})$, is assumed to be given by (Hong et al. 2006)

$$\rho_w(\Delta_{jk}) = \exp(-0.02\Delta_{jk}^{0.65}) \quad (2.26)$$

where Δ_{jk} (km) denotes the distance between the j -th and k -th tower sites. The joint probability distribution of W_j ($j = 1, \dots, 11$) is assumed to be modeled by the Gaussian copula. The elements of the correlation matrix in the Gaussian copula are obtained from $\rho_w(\Delta_{jk})$ and the empirical equation given in Der Kiureghian and Liu (1986) for the Nataf transformation of the Gumbel distribution.

The reliability index β_j for the j -th ($j = 1, \dots, 11$) tower can be evaluated by applying the FORM in the n_j -dimensional space ($n_j = 2$) with $R_j - W_j \leq 0$ indicating collapse of the tower. In particular, for $m_R/m_W = 1.25$, $v_R = 0.12$ and $v_W = 0.05$, the calculated reliability indices β_j ($j = 1, \dots, 11$) are identical and equal to 1.73. The design point in the n -dimensional space ($n = 22$) for each tower is obtained for $\rho_R = 0.2$ using the procedure given in the previous sections, and the obtained 11×11 correlation matrix \mathbf{R} (see Eq. (2.8)) for the eleven linearized safety margins is shown in Figure 2.4. Because n is much greater than n_j for this example, the proposed procedure results in a substantial reduction in the computational cost in computing β_j and the corresponding design point compared with the conventional FORM analyses (Table 2.4).

Based on the above-indicated β_j and \mathbf{R} , the probability of collapse of at least one tower, $P_{f_{sys}}$, evaluated from Eq. (2.8a) (with $m = 11$) equals 0.27. The probability of simultaneous failure of a number of specific towers can also be estimated. For example, the probability

of simultaneous collapse of towers 1 and 3 only, $P_{f1,3}$, is estimated to be 1.1×10^{-3} by using the following integral:

$$P_{f1,3} = \int_{\beta_1}^{\infty} \int_{\beta_3}^{\infty} \int_{-\infty}^{\beta_2} \int_{-\infty}^{\beta_4} \cdots \int_{-\infty}^{\beta_{11}} \frac{1}{\sqrt{(2\pi)^{11}|\Sigma|}} \exp\left(-\frac{1}{2}\boldsymbol{\theta}^T \mathbf{R}^{-1}\boldsymbol{\theta}\right) d\theta_1 \cdots d\theta_{11} \quad (2.27)$$

The computation of \mathbf{R} , $P_{f\text{sys}}$ and $P_{f1,3}$ is repeated for ρ_R varying from 0.3 to 0.7. The corresponding values of $P_{f\text{sys}}$ and $P_{f1,3}$ are depicted in Figure 2.5. The figure indicates that both $P_{f\text{sys}}$ and $P_{f1,3}$ decrease slightly as ρ_R increases from 0.3 to 0.7.

The effects of m_R/m_W , ν_R and ν_W on $P_{f\text{sys}}$ and $P_{f1,3}$ are examined by fixing ρ_R at 0.2 but varying m_R/m_W from 1.3 to 1.5, ν_R from 0.10 to 0.14, and ν_W from 0.04 to 0.08. The computation of β_j , Σ , $P_{f\text{sys}}$ and $P_{f1,3}$ is then repeated with the corresponding values of $P_{f\text{sys}}$ and $P_{f1,3}$ shown in Figure 2.6 and 2.7, respectively. The results suggest that both $P_{f\text{sys}}$ and $P_{f1,3}$ become less sensitive to the increase in ν_W as m_R/m_W decreases from 1.5 to 1.3 and ν_R increases from 0.10 to 0.14. At $m_R/m_W = 1.3$ and $\nu_R = 0.14$, $P_{f\text{sys}}$ ($P_{f1,3}$) remains practically the same as ν_W varies from 0.04 to 0.08.

2.5 Conclusions

The present chapter is focused on the application of the FORM to evaluate the reliability of systems whose performance is governed by multiple limit state functions that are correlated as a result of correlations among random variables involved in different limit state functions. A theorem is put forward, which basically states that the reliability index for the j -th limit state function within a multi-limit-state-function system obtained by using the FORM and only the n_j random variables included in the j -th limit state function is identical to the reliability index for the same limit state function obtained by involving all n random variables in the system and using the FORM analyses. Moreover, the design point obtained from the FORM for the j -th limit state function in the n_j -dimension space can be directly used to evaluate its corresponding design point in the n -dimension space by considering all the random variables involved in the system. The design points in the n -dimension space for different limit state functions are used as the basis to compute the correlation coefficients among the linearized safety margins required for the system reliability evaluation. Based on the theorem, a procedure is proposed to evaluate the

system reliability by using the FORM. The procedure is particularly efficient for systems involving many limit state functions with n much greater than n_j . The efficiency is illustrated through system reliability analyses of three examples: a pressurized pipeline joint containing two corrosion defects, a parallel system consisting of five components subjected to dependent stochastic degradation over time, and a group of 11 transmission towers in a tower-line system subjected to spatially correlated wind loads for a scenario wind event.

2.6 References

Ang, A. H-S., and Tang, W. H. (2007). Probability concepts in engineering: emphasis on application to civil and environmental engineering, 2nd Ed., John Wiley and Sons, Inc., New York.

Chen, Y., and Booth, D. C. (2011). The Wenchuan earthquake of 2008: anatomy of a disaster. Springer Science and Business Media.

Der Kiureghian, A. (2005). First- and second-order reliability methods. In: Singhal S, Ghiocel DM, Nikolaidis E, editors. Engineering design reliability handbook. CRC Press.

Der Kiureghian, A., and Liu, P. L. (1986). Structural reliability under incomplete probability information. Journal of Engineering Mechanics, 112(1), 85-104.

Ditlevsen, O. (1979). Narrow reliability bounds for structural systems. Journal of structural mechanics, 7(4): 453-472.

Estes, A. C., and Frangopol, D. M. (1998). RELSYS: A computer program for structural system reliability. Structural Engineering and Mechanics, 6(8): 901-919.

Genz, A. (1992). Numerical computation of multivariate normal probabilities. Journal of Computational and Graphical statistics, 1(2): 141-149.

Genz, A. (1993). Comparison of methods for the computation of multivariate normal probabilities. Computing Science and Statistics, 25: 400-405.

- Gollwitzer, S., and Rackwitz, R. (1983). Equivalent components in first-order system reliability. *Reliability Engineering*, 5(2), 99-115.
- Hasofer, A. M., and Lind, N. C. (1974). Exact and invariant second-moment code format. *Journal of the Engineering Mechanics division*, 100(1), 111-121.
- Higham, N. (2002). Computing the nearest correlation matrix - a problem from finance; *IMA Journal of Numerical Analyses* 22, 329–343.
- Hong, H. P. (1999). Inspection and maintenance planning of pipeline under external corrosion considering generation of new defects. *Structural Safety*, 21(3): 203–222.
- Hong, H.P., Miller, C. Mikitiuk, M., Ho, T.C.E., and Xu, Z. (2006). Weather risk assessment of the existing interlake transmission corridor and potential mitigation strategies for Manitoba Hydro's HVDC transmission, The boundary Layer Wind Tunnel Laboratory, Report BLWT-SS15-2006, London, ON
- Hong, H. P., Zhou, W., Zhang, S., and Ye, W. (2014). Optimal condition-based maintenance decisions for systems with dependent stochastic degradation of components. *Reliability Engineering and System Safety*, 121: 276-288.
- Kang, W. H., and Song, J. (2010). Evaluation of multivariate normal integrals for general systems by sequential compounding. *Structural Safety*,32(1): 35-41.
- Kang, W.H., Lee, Y.J., Song, J., and Gencturk, B. (2012). Further development of matrix-based system reliability method and applications to structural systems. *Structure and Infrastructure Engineering*, 8(5): 441-457.
- Low, B. K., and Tang, W. H. (2007). Efficient spreadsheet algorithm for first-order reliability method. *Journal of Engineering Mechanics*, 133(12): 1378-1387.
- Madsen, H. O., Krenk, S., and Lind, N. C. (2006). *Methods of structural safety*. Dover Publications, Inc., N. Y.
- Mara, T.G., and Hong, H. P. (2013). Effect of wind direction on the response and capacity

surface of a transmission tower. *Engineering Structures*, 57: 493-501.

Mara, T.G., Hong, H.P., Lee, C.-S., and Ho, T.C.E. (2016). Capacity of a transmission tower under downburst wind loading, *Wind and Structures*, 22(1): 65-87.

Melchers, R. E. (1999). *Structural reliability analyses and prediction*, 2nd Ed., Wiley, New York.

Nelsen, R. B. (2006). *An introduction to copulas*, 2nd Ed. Springer, New York.

Press, W. H., Teukolsky, S.A., Vetterling, W. T., and Flannery, B. P. (1992). *Numerical recipes in C, the art of scientific computing*, 2nd Ed., Cambridge University Press, Cambridge, U.K.

Rackwitz, R., and Fiessler, B. (1978). Structural reliability under combined load sequences. *Computers and Structures*, 9: 489–494.

Roscoe, K., Diermanse, F., and Vrouwenvelder, T. (2015). System reliability with correlated components: accuracy of the Equivalent Planes method. *Structural Safety*, 57: 53-64.

Straub, D., and Faber, M.H. (2005). Risk based inspection planning for structural systems. *Structural Safety*, 27(4): 335-355.

Van Noortwijk, J. M. (2009). A Survey of the application of gamma process in maintenance. *Reliability Engineering and System Safety*, 94(1): 2–21.

Veneziano, D. (1974). Contributions to second moment reliability. Research Rep. No. R74-33, Dept. of Civil Engineering, MIT, Cambridge, Mass.

Zhang, L., and Li, J. (2007). Probability density evolution analyses on dynamic response and reliability estimation of wind-excited transmission towers. *Wind and Structure*, 10(1): 45-60.

Zhou, W., Hong, H. P., and Zhang, S. (2012). Impact of dependent stochastic defect growth on system reliability of corroding pipelines. *International Journal of Pressure Vessels and Piping*, 96: 68-77.

Zhou, W., and Huang, G. X. (2012). Model error assessments of burst capacity models for corroded pipelines. *International Journal of Pressure Vessels and Piping*, 99: 1-8.

Table 2.1 Empirical equations for estimating F_0 in Eq. (2.4) for the numerical examples considered in this chapter

Marginals of X_i and X_k	Equation for F_0
Lognormal	$\frac{\ln(1+\rho_{X_i,k}\delta_i\delta_k)}{\rho_{X_i,k}\sqrt{\ln(1+\delta_i^2)\ln(1+\delta_k^2)}}{}^{a, b}$
Gumbel	$1.064-0.069\rho_{X_i,k}+0.005\rho_{X_i,k}^2$
Weibull	$1.063-0.004\rho_{X_i,k}-0.200(\delta_i+\delta_k)-0.001\rho_{X_i,k}^2+0.337(\delta_i^2+\delta_k^2)+0.007\rho_{X_i,k}(\delta_i+\delta_k)-0.007\delta_i\delta_k{}^b$

^aThe F_0 equation for the lognormal marginals is exact.

^b δ_i and δ_k denote the coefficients of variation (COV) of X_i and X_k , respectively.

Table 2.2 Probabilistic characteristics of random variables for Example 1

Parameter	Distribution	Mean	COV (%)	Corr. coef. at different defects
D	Deterministic	D	-	-
wt	Deterministic	wt_n	-	-
σ_u	Lognormal	1.09SMTS	3.0	0.3 (0.300) ^b
p	Gumbel	1.05 P_o	10.0	0.8 (0.810) ^b
l	Deterministic	50 (mm)	-	-
d	Weibull	0.25/0.30 wt_n ^a	20	0.5 (0.504) ^b
ξ	Lognormal	1.10	17.2	0.5 (0.504) ^b

^aThe mean defect depth equals 0.25 wt_n and 0.30 wt_n for defects #1 and #2, respectively.

^bThe first value is the correlation coefficient in the original space, and the bracketed value is the corresponding correlation coefficient in the normal space obtained by using the empirical equation developed by Der Kiureghian and Liu (1986) and shown in Table 2.1.

Table 2.3 Summary of design points for two corrosion defects

Random variables in the Z space	Physical para.	g_1				g_2			
		z_1^*	z_{c1}^*	$z^*(1)$	$u^*(1)$	z_2^*	z_{c2}^*	$z^*(2)$	$u^*(2)$
Z_1	σ_{u1}	-0.42		-0.42	-0.42		-0.12	-0.12	-0.12
Z_2	p_1	2.16		2.16	2.16		1.71	1.71	1.71
Z_3	d_1	0.17		0.17	0.17		0.12	0.12	0.12
Z_4	ξ_1	-2.39		-2.39	-2.39		1.19	1.19	1.19
Z_5	σ_{u2}		-0.13	-0.13	0	-0.41		-0.41	-0.39
Z_6	p_2		1.75	1.75	0	2.11		2.11	1.24
Z_7	d_2		0.09	0.09	0	0.23		0.23	0.20
Z_8	ξ_2		-1.20	-1.20	0	-2.35		-2.35	-2.03

Table 2.4 Computational efficiency of the proposed procedure as reflected in the numerical examples

Numerical Example	Number of evaluations for solving Eq. (2.6)	of limit state Eq. (2.16)	function	Ratio of CPU time for solving Eq. (2.16) to that for solving Eq. (2.6)
1	158 ^a	94 ^a		0.59 ^a
2	1340 ^b	435 ^b		0.35 ^b
3	143 ^c	23 ^c		0.125 ^c

^aComparison based on the computational costs for finding the design points for the two corrosion defects.

^bComparison based on the computational costs for finding the design points for one degrading component over a span of 20 years (with a time step of one year), corresponding to the scenario of $\rho_0 = 0.5$.

^cComparison based on the computational cost for finding the design point for one transmission tower corresponding to the scenario of $\rho_R = 0.2$, $m_R/m_W = 1.25$, $v_R = 0.12$ and $v_W = 0.05$.

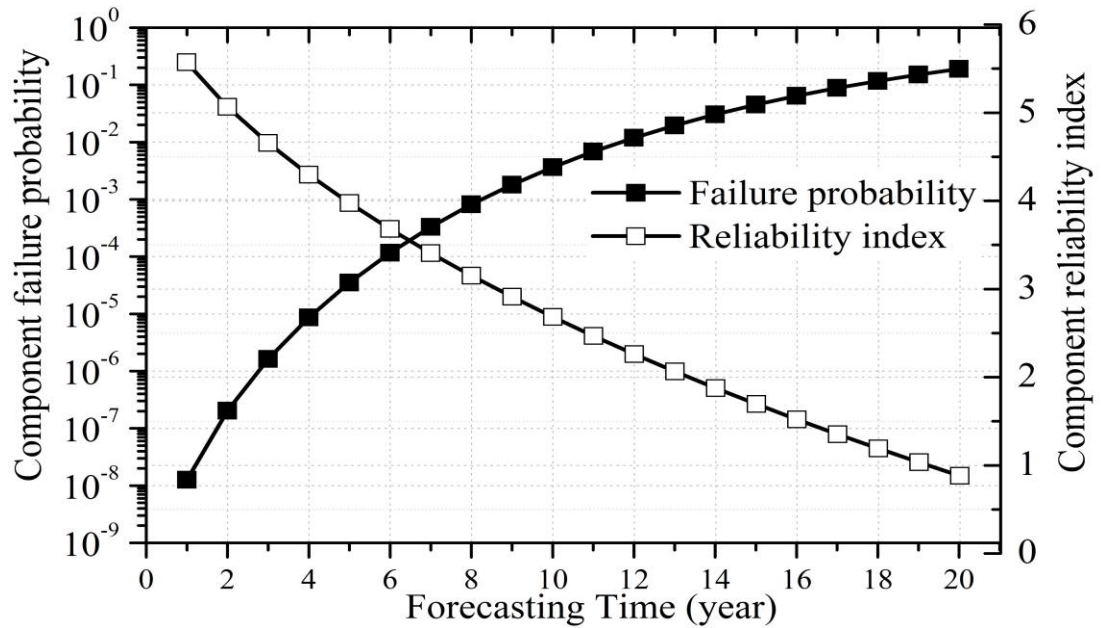


Figure 2.1 Reliability index and failure probability of a single component for a degrading parallel system with five components

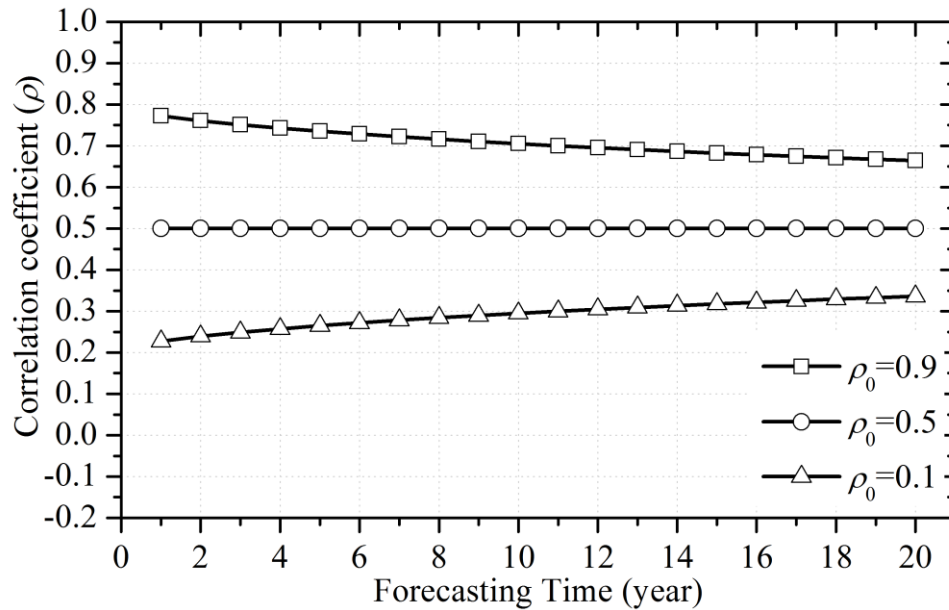


Figure 2.2 Correlation coefficient between linearized safety margins associated with different components for a degrading parallel system with five components

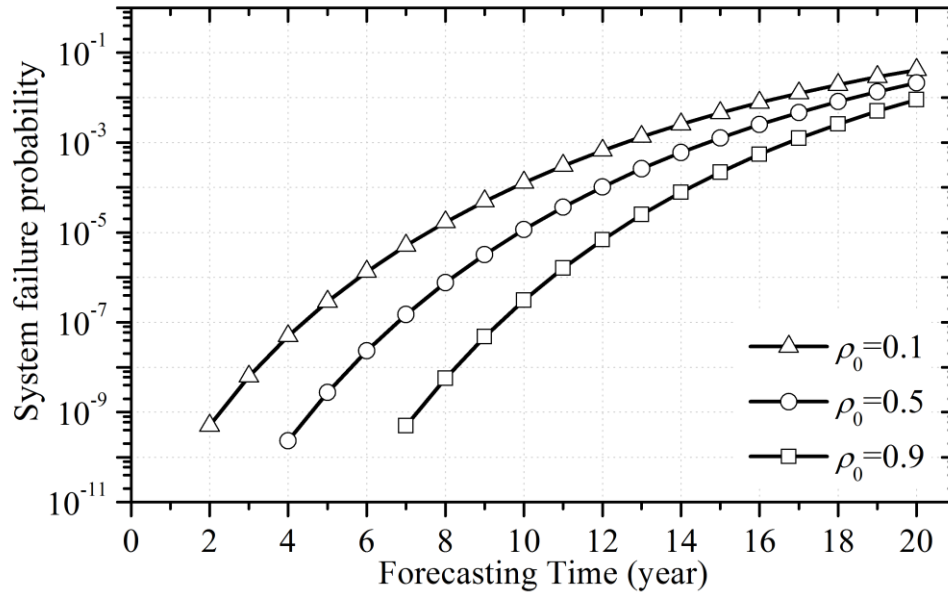


Figure 2.3 System failure probability for a degrading parallel system with five components

	1	2	3	4	5	6	7	8	9	10	11
1	1										
2	0.347	1									
3	0.346	0.347	1								
4	0.345	0.346	0.347	1							
5	0.344	0.345	0.346	0.347	1						
$R =$ 6	0.343	0.344	0.345	0.346	0.347	1					
7	0.342	0.343	0.344	0.345	0.346	0.347	1				
8	0.341	0.342	0.343	0.344	0.345	0.346	0.347	1			
9	0.341	0.341	0.342	0.343	0.344	0.345	0.346	0.347	1		
10	0.340	0.341	0.341	0.342	0.343	0.344	0.345	0.346	0.347	1	
11	0.339	0.340	0.341	0.341	0.342	0.343	0.344	0.345	0.346	0.347	1

Figure 2.4. Correlation matrix of the safety margins associated with the eleven transmission towers in the tower-line system

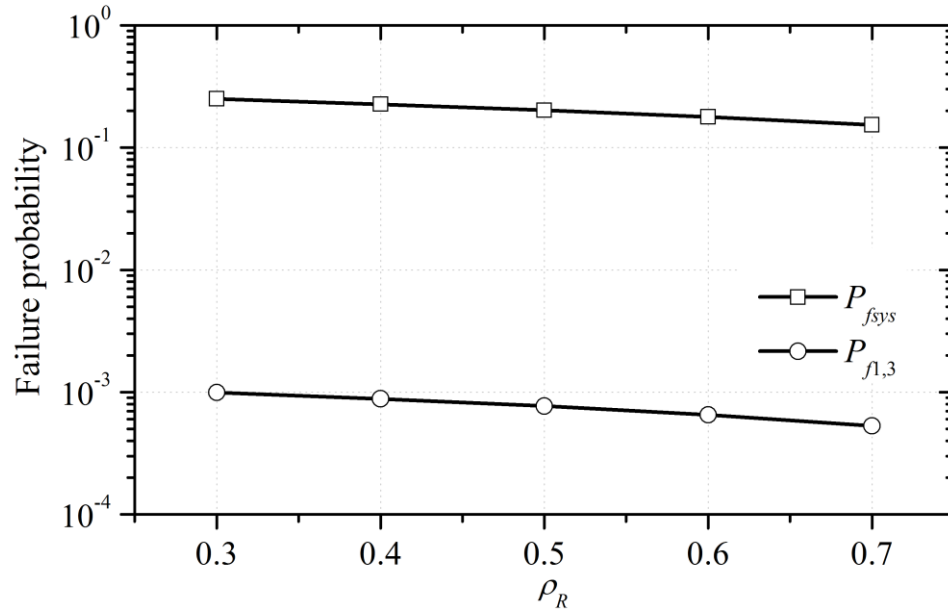


Figure 2.5 Sensitivity of $P_{f_{sys}}$ and $P_{f_{1,3}}$ to ρ_R ($m_R/m_W = 1.25$, $\nu_R = 0.12$ and $\nu_W = 0.05$)

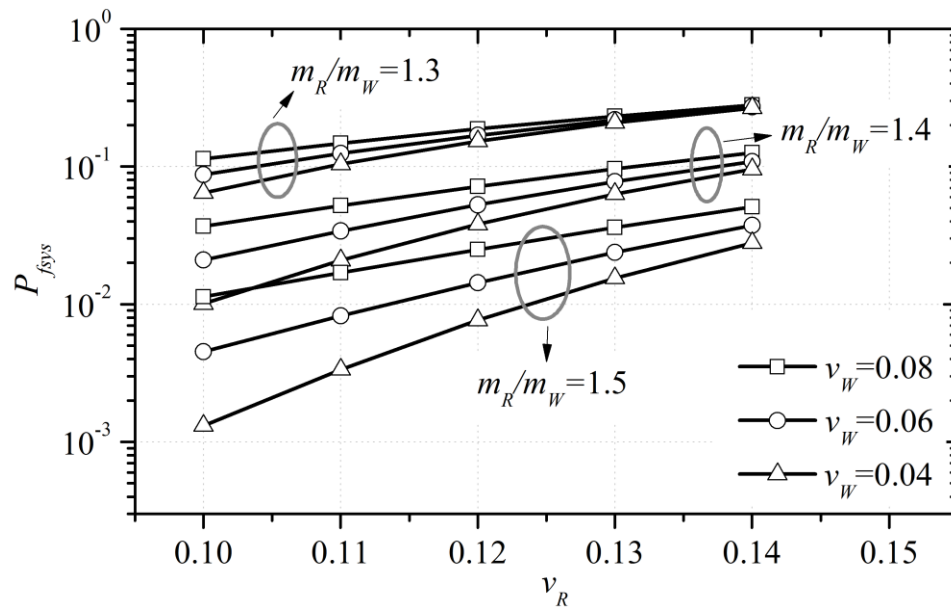


Figure 2.6 Sensitivity of $P_{f_{sys}}$ to m_R/m_W , ν_R and ν_W ($\rho_R = 0.2$)

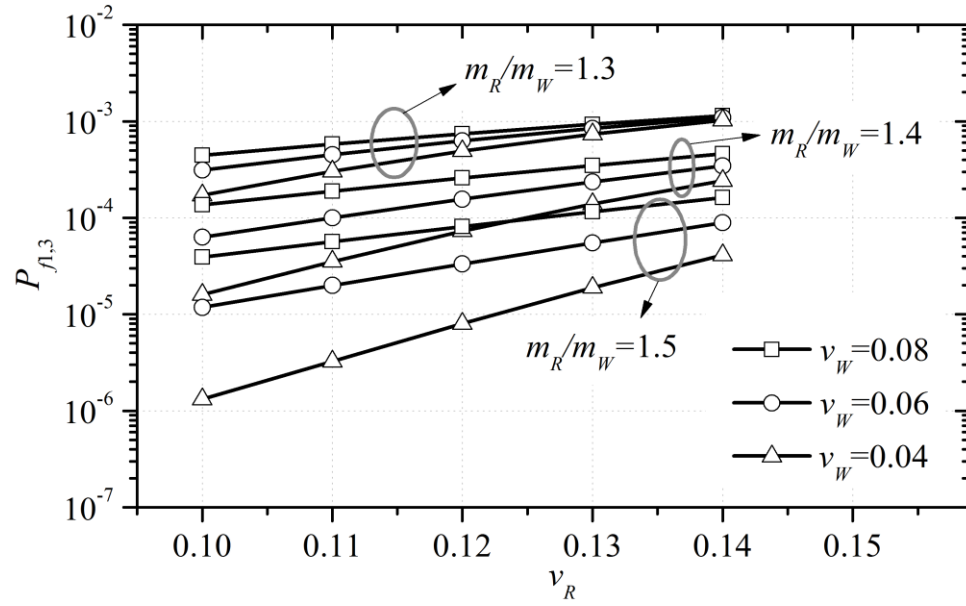


Figure 2.7 Sensitivity of $P_{l,3}$ to m_R/m_W , v_R and v_W ($\rho_0 = 0.2$)

3 Improvement of Equivalent Component Approach for Reliability Analyses of Series Systems

3.1 Introduction

Many engineering structures are characterized as series systems, e.g. pressurized pipelines containing multiple corrosion defects (Zhou 2010; Zhou et al. 2012), bridge girders with different failure modes (Yang et al. 2004) and levee systems for flood defense (Roscoe et al. 2015). Failure of any component of a series system leads to failure of the system. The first-order reliability method (FORM) (Rackwitz and Fiessler 1978; Ditlevsen 1996; Der Kiureghian 2005; Madsen et al. 2006; Low and Tang 2007) can be employed to evaluate the system reliability of series systems. Consider a series system consisting of m components. The application of the FORM to the j -th ($j = 1, 2, \dots, m$) component results in a linearized safety margin (i.e. a hyperplane to approximate the limit state surface) in the standard normal space and the corresponding reliability index β_j . The failure probability of the system, P_{fs} , is evaluated as $P_{fs} = 1 - \Phi_m(\boldsymbol{\beta}, \mathbf{R})$, where $\boldsymbol{\beta} = [\beta_1, \beta_2, \dots, \beta_m]^T$; T denotes transposition; \mathbf{R} is the $m \times m$ matrix of the correlation coefficients among the linearized safety margins for different components, and $\Phi_m(\bullet, \bullet)$ is the m -variate standard normal cumulative distribution function. The elements of \mathbf{R} , ρ_{jk} ($j, k = 1, 2, \dots, m$), are computed as the inner product of the unit normal vectors associated with the j -th and k -th components obtained from the FORM (Der Kiureghian 2005; Madsen 2006).

Two key aspects of the FORM-based evaluation of P_{fs} are the computation of \mathbf{R} and m -dimensional normal integral $\Phi_m(\boldsymbol{\beta}, \mathbf{R})$. A direct way to compute \mathbf{R} is to carry out the FORM for each component by including all the random variables involved in the system. This ensures that the unit normal vectors for all components have the same dimension; the evaluation of ρ_{jk} then follows straightforwardly. Approaches for evaluating $\Phi_m(\boldsymbol{\beta}, \mathbf{R})$ are well reported in the literature (Gollwitzer and Rackwitz 1983; Genz 1992; Estes and Frangopol 1998; Yuan and Pandey 2006; Kang and Song 2010; Roscoe et al. 2015). Among them, the equivalent component approach (Roscoe et al. 2015; Gollwitzer and Rackwitz 1983; Estes and Frangopol 1998; Kang and Song 2010) is the focus of the present chapter because of its ability to deal with systems with a large number of components. The

basic idea of the equivalent component approach is to combine two components of the system into an equivalent component, which is then combined with a third component of the system. This process continues until a single equivalent component replaces all the components in the system.

Several variations of the equivalent component approach reported in the literature differ primarily in the way to evaluate the correlation coefficients between the equivalent component and remaining system components. In the approaches proposed by Gollwitzer and Rackwitz (1983) as well as Estes and Frangopol (1998), a linearized safety margin for the equivalent component is constructed in the standard normal space. The corresponding unit normal vector is then estimated from the finite difference method and used to evaluate the correlation coefficients between the equivalent component and remaining system components. The equivalent planes method (EPM) reported by Roscoe et al. (2015) assumes that the same set of physical parameters are involved in different components. This assumption allows efficient evaluation of the unit normal vector of the linearized safety margin for the equivalent component through the finite difference method, but restricts the general applicability of the equivalent planes method. In the sequential compounding method (SCM) proposed by Kang and Song (2010), the correlation coefficient between the equivalent component and a system component is evaluated by solving a nonlinear equation resulting from approximate decomposition of the bi- and tri-variate normal distributions using conditional probabilities.

In this chapter, an analytical expression to evaluate the unit normal vector associated with the equivalent component is derived using the chain rule. The expression facilitates the evaluation of the correlation coefficients between the equivalent component and remaining system components. Moreover, an adaptive combining process for generating the equivalent component is proposed and shown to markedly improve the accuracy of the equivalent component approach for series systems with unequally correlated components. The remainder of the chapter is organized as follows. The improvement of the equivalent component approach is described in Section 3.2, and the illustration and validation of the proposed improvements in terms of numerical examples are presented in Section 3.3 followed by conclusions in Section 3.4.

3.2 Improvement of Equivalent Component Approach

3.2.1 Unit Normal Vector for Equivalent Component

Let C_1, C_2, \dots, C_m denote, respectively, the m components of the series system. The application of the equivalent component approach to the system is illustrated in Fig. 3.1, where C_{\bullet}^e denotes an equivalent component. The first combining step results in the equivalent component C_{12}^e . Given the reliability indices β_1 and β_2 for C_1 and C_2 , respectively, as well as the correlation coefficient between linearized safety margins at C_1 and C_2 , ρ_{12} , the failure probability of C_{12}^e , P_{f12} , equals $1 - \Phi_2(\beta_1, \beta_2, \rho_{12})$ and is represented by an equivalent reliability index $\beta_{12}^e = -\Phi^{-1}(P_{f12})$. To continue the combining process and generate the equivalent component C_{123}^e , the correlation coefficient between C_{12}^e and C_3 , $\rho_{12,3}$, needs to be computed. This can be achieved by developing an equivalent linearized safety margin, $g_{12}^e(\mathbf{u})$, in the standard normal space for C_{12}^e (Roscoe et al. 2015; Gollwitzer and Rackwitz 1983; Estes and Frangopol 1998):

$$g_{12}^e(\mathbf{u}) = \beta_{12}^e - (\boldsymbol{\alpha}_{12}^e)^T \mathbf{u} \quad (3.1)$$

where $\boldsymbol{\alpha}_{12}^e$ is the n -dimensional unit normal vector associated with $g_{12}^e(\mathbf{u})$ and can be obtained as follows based on the sensitivity interpretation of the unit normal vector:

$$\boldsymbol{\alpha}_{12}^e = \frac{\partial \beta_{12}^e}{\partial \mathbf{u}} / \left\| \frac{\partial \beta_{12}^e}{\partial \mathbf{u}} \right\| \quad (3.2)$$

with $\|\bullet\|$ denoting the norm of a vector. The value of $\rho_{12,3}$ then equals $(\boldsymbol{\alpha}_{12}^e)^T \boldsymbol{\alpha}_3$. The finite difference method is generally used to evaluate $\boldsymbol{\alpha}_{12}^e$ in the literature (Roscoe et al. 2015; Gollwitzer and Rackwitz 1983; Estes and Frangopol 1998); however, this method is time consuming for systems involving a large number of random variables and may not be numerically robust.

In this chapter, an analytical expression utilizing the chain rule is developed to evaluate $\boldsymbol{\alpha}_{12}^e$. To this end, the i -th ($i = 1, 2, \dots, n$) element of $\frac{\partial \beta_{12}^e}{\partial \mathbf{u}}$, $\frac{\partial \beta_{12}^e}{\partial u_i}$, is given by

$$\frac{\partial \beta_{12}^e}{\partial u_i} = \frac{\partial \beta_{12}^e}{\partial P_{f12}} \frac{\partial P_{f12}}{\partial \beta_1} \frac{\partial \beta_1}{\partial u_i} + \frac{\partial \beta_{12}^e}{\partial P_{f12}} \frac{\partial P_{f12}}{\partial \beta_2} \frac{\partial \beta_2}{\partial u_i} \quad (3.3)$$

Note that

$$\frac{\partial \beta_{12}^e}{\partial P_{f12}} = -\frac{1}{\varphi(-\beta_{12}^e)} \quad (3.4)$$

where $\varphi(\bullet)$ is the standard normal density function, and that $\frac{\partial P_{f12}}{\partial \beta_1}$ and $\frac{\partial P_{f12}}{\partial \beta_2}$ have analytical expressions as follows (Chun et al. 2015):

$$\frac{\partial P_{f12}}{\partial \beta_1} = -\varphi(\beta_1) \Phi\left(\frac{\beta_2 - \rho_{12}\beta_1}{\sqrt{1 - \rho_{12}^2}}\right) \quad (3.5a)$$

$$\frac{\partial P_{f12}}{\partial \beta_2} = -\varphi(\beta_2) \Phi\left(\frac{\beta_1 - \rho_{12}\beta_2}{\sqrt{1 - \rho_{12}^2}}\right) \quad (3.5b)$$

Note also that $\partial \beta_1 / \partial u_i$ and $\partial \beta_2 / \partial u_i$ can be obtained from the component FORM analyses with respect to C_1 and C_2 ; that is,

$$\partial \beta_1 / \partial u_i = \alpha_{i,1} \quad (3.6a)$$

$$\partial \beta_2 / \partial u_i = \alpha_{i,2} \quad (3.6b)$$

where $\alpha_{i,1}$ and $\alpha_{i,2}$ are the i -th elements of the unit normal vectors for C_1 and C_2 , $\boldsymbol{\alpha}_1$ and $\boldsymbol{\alpha}_2$, respectively.

Substituting Eqs. (3.4), (3.5) and (3.6) into Eq. (3.3) leads to

$$\frac{\partial \beta_{12}^e}{\partial u_i} = e^{\frac{(\beta_{12}^e)^2 - (\beta_1)^2}{2}} \Phi\left(\frac{\beta_2 - \rho_{12}\beta_1}{\sqrt{1 - \rho_{12}^2}}\right) \alpha_{i,1} + e^{\frac{(\beta_{12}^e)^2 - (\beta_2)^2}{2}} \Phi\left(\frac{\beta_1 - \rho_{12}\beta_2}{\sqrt{1 - \rho_{12}^2}}\right) \alpha_{i,2}, \quad (i = 1, 2, \dots, n) \quad (3.7)$$

Equation (3.7) allows the unit normal vector for C_{12}^e to be evaluated analytically as opposed to using the finite difference method. Note that Chen et al. (2012) derived the same equation, albeit by employing the first-order Taylor series expansion of the expression for evaluating β_{12}^e . Equation (3.7) can be repeatedly applied to evaluate the unit normal

vectors associated with the equivalent components generated from subsequent combining steps. For example, let β_{123}^e denote the equivalent reliability index associated with C_{123}^e as shown in Fig. 3.1. It follows from Eq. (3.7) that $\frac{\partial \beta_{123}^e}{\partial u_i}$ is given by

$$\frac{\partial \beta_{123}^e}{\partial u_i} = e^{\frac{(\beta_{123}^e)^2 - (\beta_{12}^e)^2}{2}} \Phi \left(\frac{\beta_3 - \rho_{12,3} \beta_{12}^e}{\sqrt{1 - \rho_{12,3}^2}} \right) \alpha_{i,12}^e + e^{\frac{(\beta_{123}^e)^2 - (\beta_3)^2}{2}} \Phi \left(\frac{\beta_{12}^e - \rho_{12,3} \beta_3}{\sqrt{1 - \rho_{12,3}^2}} \right) \alpha_{i,3}, \quad (i = 1, 2, \dots, n) \quad (3.8)$$

where $\alpha_{i,12}^e$ and $\alpha_{i,3}$ are the i -th elements of α_{12}^e and α_3 (i.e. the unit normal vector for C_3), respectively.

3.2.2 Adaptive Combining Process

The sequence of the combining process can affect the accuracy of the equivalent component method. This is illustrated using a simple example described in the following. Consider a series system consisting of three components C_1 , C_2 and C_3 , with the corresponding linearized limit state surfaces in the standard normal (\mathbf{u}) space and reliability indices schematically shown in Fig. 3.2(a). The limit state surface corresponding to C_1 is perpendicular to those corresponding to C_2 and C_3 . It follows that the exact failure probability of the system equals $1 - \Phi(\beta_1)\Phi(\beta_2)$. The equivalent component approach is now employed to estimate the system failure probability by using two different combining sequences. One sequence involves first combining C_2 and C_3 , i.e. the two components having the highest correlation coefficient, into an equivalent component C_{23}^e , which is then combined with C_1 to generate the equivalent component C_{231}^e . It follows that this combining sequence results in $\beta_{23}^e = \beta_2$, and the exact system failure probability can be subsequently obtained. For the second combining sequence, C_1 , C_2 and C_3 are simply combined in the order of their numerical designations; that is, C_1 and C_2 are first combined into C_{12}^e (see Fig. 3.2(b)), which is then combined with C_3 to generate C_{123}^e . Such a combining sequence however overestimates the system failure probability by the amount corresponding to the shaded area as illustrated in Fig. 3.2(b).

In light of the above example, an adaptive combining process is proposed in this chapter; that is, at each combining step the two components with the highest correlation coefficient be combined. More specifically, the two system components having the highest correlation coefficient are combined into an equivalent component at the first combining step; at the second step, the two components that have the highest correlation and are to be combined could be two components out of the remaining $(m - 2)$ system components, or one system component and the equivalent component obtained from the first step, and at the third step, the two components to be combined could be two system components, two equivalent components obtained from the previous steps or one system component and one equivalent component. Such a process continues until all the system components are replaced by a single equivalent component.

3.3 Numerical Examples

To demonstrate the effectiveness of the improved equivalent component approach (IECA), numerical examples representing series systems with equally and unequally correlated components are investigated. All the numerical examples are implemented in Matlab[®] on a personal computer with an Intel[®] i7 dual-core processor.

3.3.1 Equally Correlated Components

We first consider series systems consisting of m equally correlated components. Without loss of generality, it is assumed that each component includes one random variable; therefore, the system involves a total of m random variables. It should be emphasized that for systems whereby each component involves more than one random variable, a procedure that is based on the methodology proposed in (Zhou et al. 2017) can be used to reduce the total number of random variables to one for each component. This procedure is described in Appendix A. To eliminate the error associated with the linearization of the limit state function in the normal space in the FORM, linear limit state functions are assumed in the correlated standard normal (i.e. \mathbf{Z}) space for all components. The limit state function in the \mathbf{Z} space for the j -th component is given by

$$g_j(z_j) = \beta_j - z_j, (j = 1, 2, \dots, m) \quad (3.9)$$

where z_j is the value of a standard normal variate Z_j . It is assumed that the reliability indices for all components are identical, i.e. $\beta_j = \beta_c$ for $j = 1, 2, \dots, m$. The improved equivalent component approach is then applied to evaluate system failure probability, P_{fs} , with the unit normal vector of the equivalent component evaluated by Eq. (3.7). For series systems with m equally correlated components having the identical reliability index β_c and correlation coefficient ρ , the exact system failure probability, P_{fse} , can be computed from the following unidimensional integral (Grigoriu and Turkstra 1979):

$$P_{fse} = \frac{1}{\sqrt{2\pi}} \int_{-\infty}^{\infty} e^{-\frac{s^2}{2}} \left[1 - \left(\Phi \left(\frac{\beta_c + \sqrt{\rho} s}{\sqrt{1-\rho}} \right) \right)^m \right] ds \quad (3.10)$$

The error, e_p (%), associated with P_{fs} obtained from IECA is quantified as

$$e_p = \frac{P_{fs} - P_{fse}}{P_{fse}} \times 100\% \quad (3.11)$$

Note that positive and negative values of e_p mean overestimation and underestimation, respectively, of the system failure probability. The values of P_{fs} from IECA and e_p corresponding to m ranging from 30 to 250, ρ equal to 0.1 or 0.9, and β_c ranging from 3 to 6 are shown in Fig. 3.3.

Figure 3.3 indicates that P_{fs} from IECA is in excellent agreement with (albeit consistently lower than) P_{fse} for all the cases considered: the largest absolute value of e_p ($|e_p|$) is about 20% corresponding to $m = 250$ and $\beta_c = 6$. Given ρ and β_c , $|e_p|$ increases as m increases. Given m , $|e_p|$ decreases as β_c increases from 3 to 6 for $\rho = 0.1$; however, $|e_p|$ increases as β_c increases from 3 to 6 for $\rho = 0.9$. To further investigate the impact of ρ on e_p , P_{fs} and P_{fse} are evaluated for systems with $m = 250$, ρ ranging from 0.05 to 0.95 and β_c ranging from 3 to 6. The corresponding values of e_p are shown in Fig. 3.4. The figure indicates that for a given β_c , $|e_p|$ increases first as ρ increases until ρ reaches a transition point, after which $|e_p|$ decreases as ρ increases. The transition ρ at which $|e_p|$ peaks increases with β_c : the transition ρ equals 0.40, 0.60, 0.75 and 0.85 corresponding to β_c equal to 3, 4, 5 and 6, respectively. The maximum $|e_p|$ in Fig. 3.4 is slightly over 20%, which again indicates the excellent accuracy of the equivalent component approach. Table 3.1 lists the order of

combinations involved in the adaptive combining process for a system with 30 components and $\rho = 0.5$. The table indicates that for systems with equally correlated components, the adaptive combining process is the same as combining the system components based on the order of their numerical designations.

The accuracy and efficiency of IECA are further compared with those of the equivalent planes method (EPM) (Roscoe et al. 2015) and sequential compounding method (SCM) (Kang and Song 2010) for series systems with 250 equicorrelated components, $\beta_c = 6$ and ρ ranging from 0.05 to 0.95. Figure 3.5(a) compares the accuracies of IECA, EPM and SCM - the accuracy of the latter two methods is quantified using Eq. (3.11), with the values of P_{fs} obtained from the two methods, respectively. Figure 3.5(b) compares the efficiencies of EPM, SCM and IECA in terms of the relative CPU times. Figure 3.5(a) indicates that the accuracy of SCM is the highest compared with EPM and IECA. For $\rho \leq 0.3$, the accuracies of the three methods are essentially the same; for $0.3 < \rho \leq 0.65$, the accuracies of EPM and IECA are comparable and somewhat lower than that of SCM, and for $\rho > 0.65$, the accuracy of IECA is markedly higher than EPM and somewhat lower than that of SCM. It is noted that although IECA is somewhat less accurate than SCM, the computational efficiency of IECA is two orders of magnitude higher than that of SCM for the examples considered as shown in Fig. 3.5(b). IECA is also markedly more efficient than EPM as shown in the same figure.

3.3.2 Unequally Correlated Components

Now consider series systems with m unequally correlated components. Each component involves one random variable, and for simplicity, all components are assumed to have the same reliability index β_c . The limit state function in the \mathbf{Z} space for the j -th component is given by Eq. (3.9). The correlation coefficient between the j -th and k -th components, ρ_{jk} , is defined using the following equation (Kang and Song 2010), which satisfies the positive definite condition for the correlation matrix:

$$\rho_{jk} = 1 - \frac{|k-j|}{m-1}, (k, j = 1, 2, \dots, m; k \neq j) \quad (3.12)$$

Note that the largest value of the correlation coefficients defined using Eq. (3.12) for a given system is a function of m (the smallest correlation coefficient is zero). Since there is no closed-form solution for the failure probability of systems with unequally correlated components, the importance sampling (IS) is employed to evaluate the benchmark system failure probability P_{fse} as follows (Schuëller and Stix 1987):

$$P_{fse} \approx \frac{1}{N} \sum_{i=1}^N I(\mathbf{z}_i^s) \frac{\varphi_m(\mathbf{z}_i^s, \mathbf{R})}{h_U(\mathbf{z}_i^s)} \quad (3.13)$$

where N is the total number of IS trials; \mathbf{z}_i^s denotes the i -th ($i = 1, 2, \dots, N$) m -dimensional random sample generated from the IS density function $h_U(\bullet)$; $\varphi_m(\bullet, \mathbf{R})$ is an m -dimensional normal probability density function with zero means and correlation matrix \mathbf{R} , and $I(\cdot)$ is the failure indicator function, equal to unity if $\beta_c - \max_j z_{ij}^s \leq 0$ and zero otherwise, where z_{ij}^s is the j -th ($j = 1, 2, \dots, m$) element of the vector \mathbf{z}_i^s . The IS density function is constructed to be the weighted average of m probability density functions, each associated with an individual component:

$$h_U(\mathbf{z}_i^s) = \sum_{j=1}^m w_j \varphi_m(\mathbf{z}_i^s - \mathbf{z}^*(j), \mathbf{R}) \quad (3.14)$$

where \mathbf{z}_j^* is the m -dimensional design point for the j -th component in the \mathbf{Z} space; $\varphi_m(\bullet - \mathbf{z}^*(j), \mathbf{R})$ is the IS density function associate with the j -th component, which is an m -dimensional normal probability density function with the mean vector equal to $\mathbf{z}^*(j)$ and correlation matrix \mathbf{R} , and w_j is the weighting factor assigned to the IS density function associated with the j -th component. Since all components are assumed to have the same reliability index, equal weighting for all components is assumed, i.e. $w_j = 1/m$. For each analyses case, P_{fse} is estimated using 10,000 IS simulation trials, with the corresponding coefficient of variation (COV) of the estimated P_{fse} being generally less than 4%.

Figure 3.6 depicts the values of e_p for systems with m ranging from 30 to 250 and β_c ranging from 3 to 6, where e_p is defined by Eq. (3.11) with P_{fs} evaluated with the unit normal vector of the equivalent component evaluated by Eq. (3.7). Two sets of results are plotted in Fig. 3.6: one obtained by combining the system components in the order of their numerical designations (i.e. the sequential combining process) and the other obtained by using the

adaptive combining process as described in Section 3.2. The figure indicates that the sequential combining process consistently overestimates the system failure probability with the corresponding values of e_p ranging from 30 to 270%. In contrast, the adaptive combining process leads to markedly improved accuracy: values of e_p are between 10 and 20% for all the cases considered. The order of combination involved in the adaptive combining process for the system with $m = 30$ and $\beta_c = 6$ is shown in Table 3.2. As indicated in the table, all the system components are combined in the first 15 steps, and remaining steps involve the combination of equivalent components only.

To further illustrate the effectiveness of the adaptive combining process, we investigate systems with the correlation coefficient between the j -th and k -th components defined as follows:

$$\rho_{jk} = \frac{m-1-|k-j|}{m-2} (\rho_{max} - \rho_{min}) + \rho_{min}, (j, k = 1, 2, \dots, m; j \neq k) \quad (3.15)$$

where ρ_{min} and ρ_{max} are pre-determined lower and upper bound values, respectively, of the correlation coefficient. The equivalent component approach is then employed to evaluate the system reliability for systems with $\rho_{min} = 0$, $\rho_{max} = 0.98$ and m ranging from 30 to 250. The accuracy of the evaluation is depicted in Fig. 3.7. Similar to Fig. 3.6, two sets of results are shown in Fig. 3.7, corresponding to the sequential and adaptive combining processes, respectively. The figure clearly shows the significant improvement in the accuracy achieved by using the adaptive combining process compared with the sequential combining process. Figure 3.8 depicts the accuracy of the adaptive combining process for systems with 250 components that are correlated according to Eq. (3.15) with ρ_{max} fixed at 0.98 and ρ_{min} varying from 0 to 0.98. As shown in the figure, the maximum value of $|e_p|$ is about 13%, demonstrating excellent accuracy of the adaptive combining process.

The accuracy and efficiency of EPM, SCM and IECA for systems with $\beta_c = 6$, m varying from 30 to 240 and the component correlation structure defined by Eq. (3.12) are compared in Figs. (3.9a) and (3.9b), respectively. The efficiency of IS in terms of the relative CPU time is also shown in Fig. 3.9(b). Figure 3.9(a) indicates that the accuracies of EPM and IECA are almost identical and somewhat higher than that of SCM, whereas Fig. 3.9(b)

indicates that IECA is two orders of magnitude more efficient than IS, EPM and SCM in most of the cases analyzed.

3.3.3 Application to System Reliability of Corroding Pipelines

The application of IECA is now illustrated through the system reliability analyses of a pressurized steel pipeline joint containing multiple active corrosion defects. The pipeline joint has a diameter (D) of 914 mm, a nominal wall thickness (wt_n) of 13.2 mm, a nominal operating pressure (P_o) of 8.5 MPa, and a specified minimum yield strength (SMYS) of the pipe steel of 483 MPa. It is assumed that the joint contains ten active corrosion defects. The joint may fail by burst under the internal pressure at any of the ten corrosion defects; therefore, it is a series system consisting of ten components. The limit state function at the j -th ($j = 1, 2, \dots, 10$) defect at a given time t , $g_j^b(t)$, is given by (Zhou et al. 2012)

$$g_j^b(t) = p_{bj}(t) - p_j \quad (3.16)$$

where $p_{bj}(t)$ and p_j are the burst pressure capacity in the time of t and internal pressure of the pipe joint at the j -th defect, respectively. The B31G Modified model (Kiefner and Vieth 1989) is adopted to evaluate p_{bj} as follows:

$$p_{bj} = \frac{2wt_j(\sigma_{yj} + 68.95)}{D} \left[\frac{1 - \frac{0.85d_j}{wt_j}}{1 - \frac{0.85d_j}{M_j wt_j}} \right] \quad (3.17)$$

$$M_j = \begin{cases} \sqrt{1 + 0.6275 \frac{l_j^2}{Dwt_j} - 0.003375 \frac{l_j^4}{(Dwt_j)^2}}, & \frac{l_j^2}{Dwt_j} \leq 50 \\ 3.3 + 0.032 \frac{l_j^2}{Dwt_j}, & \frac{l_j^2}{Dwt_j} > 50 \end{cases} \quad (3.18)$$

where the subscript j indicates the value of a variable at the j -th defect; D , wt and σ_y are the actual (as opposed to nominal) pipe diameter, wall thickness and yield strength, respectively; $(\sigma_y + 68.95)$ (MPa) is the pipe flow stress; d and l are the depth (i.e. in the through-pipe wall thickness direction) and length (i.e. in the pipe longitudinal direction) of the corrosion defect, respectively, and M is the so-called Folias factor. For brevity, $p_{bj}(t)$, $M_j(t)$, $d_j(t)$ and $l_j(t)$ are simply written as p_{bj} , M_j , d_j and l_j , respectively, in Eqs. (3.17) and

(3.18). For simplicity, the dependence of d_j and l_j on time is made implicit in Equations (3.17) and (3.18). For illustrative purpose, the following simple linear growth model is adopted to characterize the growth of the defect depth and length over time:

$$d_j(t) = d_{0j} + g_{dj}t \quad (3.19)$$

$$l_j(t) = l_{0j} + g_{lj}t \quad (3.20)$$

where the subscript j refers to the j -th defect; d_0 and l_0 are the initial depth and length, respectively; g_d and g_l are the depth and length growth rates, respectively.

The probabilistic characteristics of the parameters included in the limit state functions are summarized in Table 3.3. All ten defects are assumed to have the same deterministic initial length of 50 mm, whereas defects #1 through #5 are assumed have a deterministic initial depth of $0.25wt_n$, and defects #6 through #10 have a deterministic initial depth of $0.30wt_n$. Different random variables involved at the same defect are mutually independent. Wall thicknesses at different defects are assumed to be fully correlated; the same assumption also applies to the yield strength and internal pressure. Finally, it is assumed that g_d (g_l) for defects #1 through #10 are equicorrelated with a correlation coefficient of ρ_1 . Although empirical equations for the Nataf transformation developed by Der Kiureghian and Liu (1986) can be employed to convert the correlation coefficient in the original (non-normal) space into the equivalent correlation coefficient in the normal space, the correlation coefficient in the original space is used in the analyses for the sake of simplicity.

The system failure probability (P_{fs}) of the pipeline joint is evaluated using the improved equivalent component approach, with the two components having the highest correlation coefficient combined at each combining step. The values of P_{fs} corresponding to ρ_1 equal to 0.2, 0.5 and 0.8, respectively, are depicted in Fig. 3.10 for t ranging from one to ten years. The results indicate that P_{fs} is insensitive to the correlation among growth rates for this example. To investigate the impact of the potential correlation between the depth and length growth rates on the system reliability, it is assumed that g_d and g_l at the same defect are correlated with a correlation coefficient of ρ_2 . For simplicity, the growth rates at different defects are assumed to be mutually independent in this case. The values of P_{fs}

corresponding to ρ_2 equal to 0.2, 0.5 and 0.8, respectively, are depicted in Fig. 3.11. The results indicate that P_{fs} is sensitive to ρ_2 for $t \geq 5$ years: a stronger correlation between g_d and g_l results in a higher system failure probability, as expected. It is also observed from Figs. 3.10 and 3.11 that the failure probabilities increase rapidly after year 5. This is likely caused by the nonlinear relationship between the burst pressure capacity and defect depth as shown in Eq. (3.17): once the defect depth becomes sufficiently large at around year 5, the burst pressure capacity decreases more rapidly as the depth further increases.

3.4 Conclusions

This chapter is aimed at improving the equivalent component approach for evaluating the failure reliability of series systems. An analytical expression is derived using the chain rule to evaluate the unit normal vector for the equivalent component in the context of the FORM. The expression facilitates the evaluation of the correlation coefficient between the equivalent and system components. An adaptive combining process is also proposed such that the two components with the highest correlation be combined at each combining step, whereby the two components could be both system components, both equivalent components, or one system component and one equivalent component. The improved equivalent component approach is shown to be accurate for systems with equicorrelated components and systems with unequally correlated components, and markedly more efficient than the equivalent planes method and sequential compounding method. Finally, the equivalent component approach is applied to evaluate the time-dependent system failure probability of a corroding pressurized pipeline joint containing ten active corrosion defects by considering the spatial correlation among different defects and correlation between the depth and length growth rates at a given defect.

3.5 References

Chen, W. D., Li, J. C., and Zhang, F. (2012). Multiple correlation-equivalent plane method for calculating structural system reliability. In *Quality, Reliability, Risk, Maintenance, and Safety Engineering (ICQR2MSE)*, 2012 International Conference on (pp. 1452-1457). IEEE.

Chun, J., Song, J., and Paulino, G. H. (2015). Parameter sensitivity of system reliability using sequential compounding method. *Structural safety*, 55, 26-36.

Der Kiureghian A (2005). First- and second-order reliability methods. In: Nikolaidis E, Ghiocel DM, Singhal S, editors. *Engineering design reliability handbook*. Boca Raton (FL): CRC Press.

Der Kiureghian, A., and Liu, P. L. (1986). Structural reliability under incomplete probability information. *Journal of Engineering Mechanics*, 112(1), 85-104.

Ditlevsen, O., and Madsen, H. O. (1996). *Structural reliability methods* (Vol. 178). New York: Wiley.

Estes, A. C., and Frangopol, D. M. (1998). RELSYS: A computer program for structural system reliability. *Structural engineering and mechanics*, 6(8), 901-919.

Gollwitzer, S., and Rackwitz, R. (1983). Equivalent components in first-order system reliability. *Reliability Engineering*, 5(2), 99-115.

Genz, A. (1992). Numerical computation of multivariate normal probabilities. *Journal of computational and graphical statistics*, 1(2), 141-149.

Grigoriu, M., and Turkstra, C. (1979). Safety of structural systems with correlated resistances. *Applied Mathematical Modelling*, 3(2), 130-136.

Kang, W. H., and Song, J. (2010). Evaluation of multivariate normal integrals for general systems by sequential compounding. *Structural Safety*, 32(1), 35-41.

Kiefner JF, Vieth PH. (1989.) A modified criterion for evaluating the remaining strength of corroded pipe. Battelle Columbus Div., OH (USA)

Low, B. K., and Tang, W. H. (2007). Efficient spreadsheet algorithm for first-order reliability method. *Journal of engineering mechanics*, 133(12), 1378-1387.

Madsen, H. O., Krenk, S., and Lind, N. C. (2006). *Methods of structural safety*. Courier Corporation.

Rackwitz, R., and Flessler, B. (1978). Structural reliability under combined random load sequences. *Computers & Structures*, 9(5), 489-494.

Roscoe, K., Diermanse, F., and Vrouwenvelder, T. (2015). System reliability with correlated components: Accuracy of the Equivalent Planes method. *Structural Safety*, 57, 53-64.

Schuëller, G. I., and Stix, R. (1987). A critical appraisal of methods to determine failure probabilities. *Structural Safety*, 4(4), 293-309.

Yang, S. I., Frangopol, D. M., and Neves, L. C. (2004). Service life prediction of structural systems using lifetime functions with emphasis on bridges. *Reliability Engineering and System Safety*, 86(1), 39-51.

Yuan, X. X., and Pandey, M. D. (2006). Analyses of approximations for multinormal integration in system reliability computation. *Structural Safety*, 28(4), 361-377.

Zhou, W. (2010). System reliability of corroding pipelines. *International Journal of Pressure Vessels and Piping*, 87(10), 587-595.

Zhou, W., Gong, C., and Hong, H. P. (2017). New Perspective on Application of First-Order Reliability Method for Estimating System Reliability. *Journal of Engineering Mechanics*, 143(9), 04017074.

Zhou, W., Hong, H. P., and Zhang, S. (2012). Impact of dependent stochastic defect growth on system reliability of corroding pipelines. *International Journal of Pressure Vessels and Piping*, 96, 68-77.

Table 3.1 Order of combination involved in the adaptive combining process for system with equally-correlated components ($m = 30$, $\rho = 0.5$ and $\beta_c = 6$)

Combining step	Components combined	
	#1	#2
1	S1	S2
2	E-1	S3
3	E-2	S4
4	E-3	S5
...
14	E-13	S15
15	E-14	S16
16	E-15	S17
17	E-16	S18
...
27	E-26	S-28
28	E-27	S-29
29	E-28	S-30

Note: S# denotes a system component with a numerical designation of #, and E-# denotes an equivalent component generated from the combining step #.

Table 3.2 Order of combination involved in the adaptive combining process for system with components ($m = 30$ and $\beta_c = 6$) correlated according to Eq. (3.12)

Combining step	Components combined	
	#1	#2
1	S1	S2
2	S3	S4
3	S5	S6
4	S7	S8
...
14	S27	S28
15	S29	S30
16	E-1	E-2
17	E-3	E-4
...
27	E-23	E-26
28	E-24	E-25
29	E-27	E-28

Note: S# denotes a system component with a numerical order of #, and E-# denotes an equivalent component generated from the combining step #.

Table 3.3 Probabilistic characteristics of parameters for reliability analyses of corroding pipeline joint

Parameter	Distribution	Mean	COV (%)
D	Deterministic	D_n	-
wt_j	Normal	wt_n	1.5
σ_{yj}	Normal	1.1SMYS	3.5
p_j	Gumbel	$1.05P_o$	3.0
l_{0j}	Deterministic	50 (mm)	-
d_{0j}	Deterministic	$0.25/0.30wt_n$	-
g_{dj}	Weibull	0.3 (mm/year)	50
g_{lj}	Weibull	3.0 (mm/year)	50

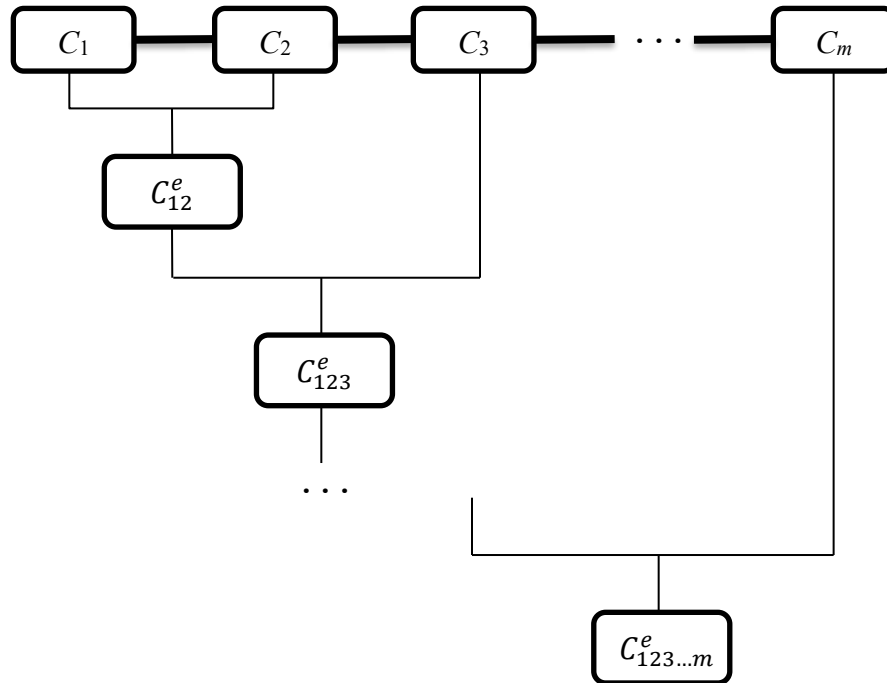


Figure 3.1 Illustration of the equivalent component approach for a series system with m components

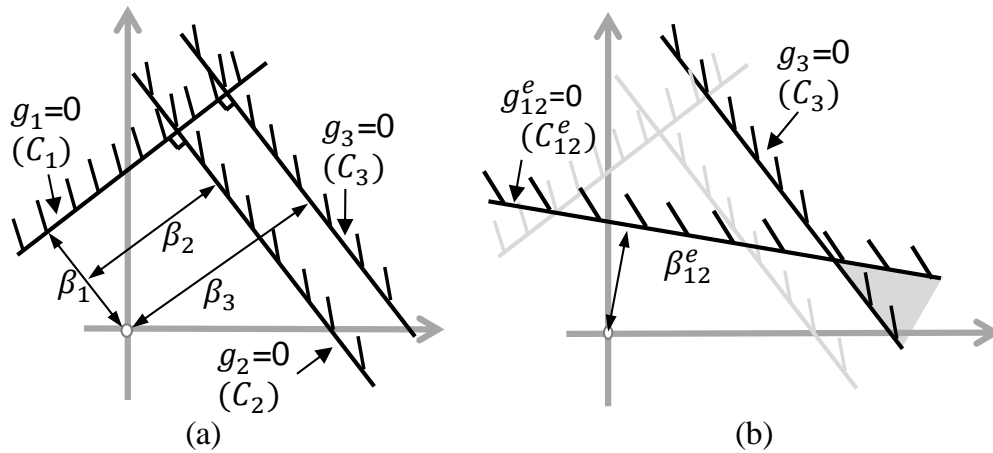
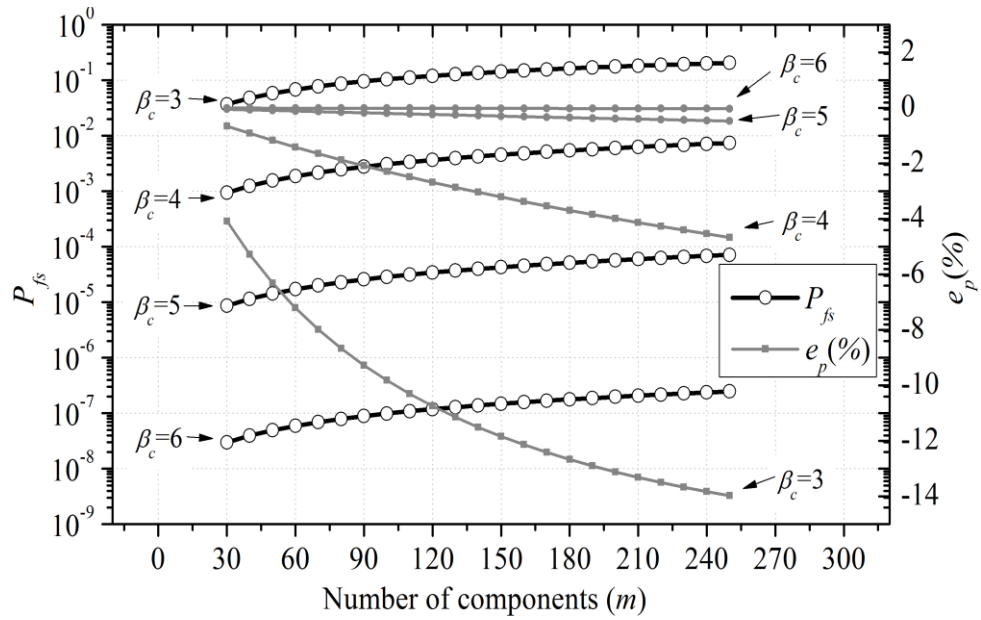
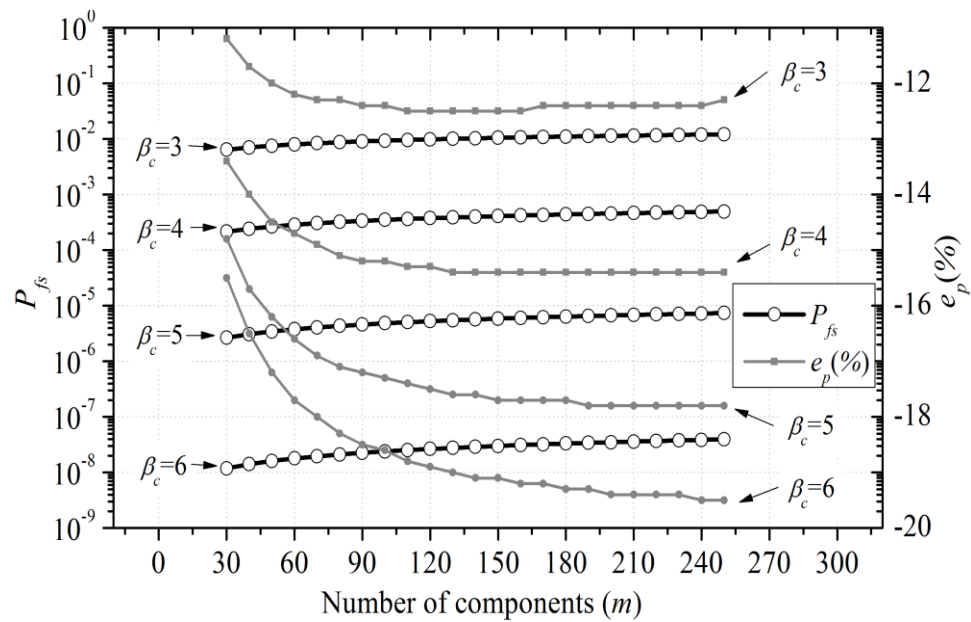


Figure 3.2 Schematic illustration of effects of the combining sequence

(a) $\rho = 0.1$ (b) $\rho = 0.9$ **Figure 3.3 Accuracy of IECA for series systems with equicorrelated components**

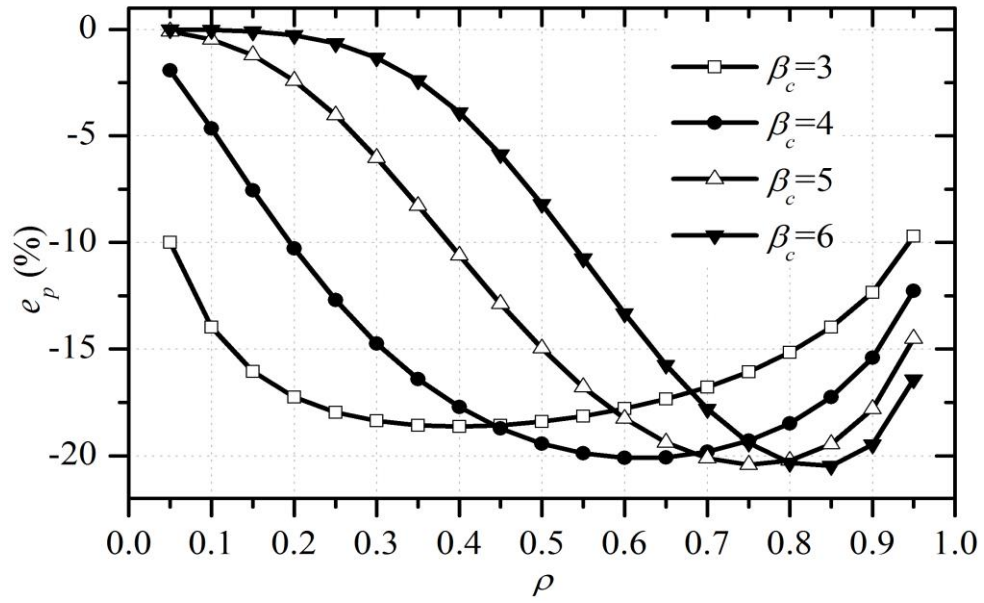
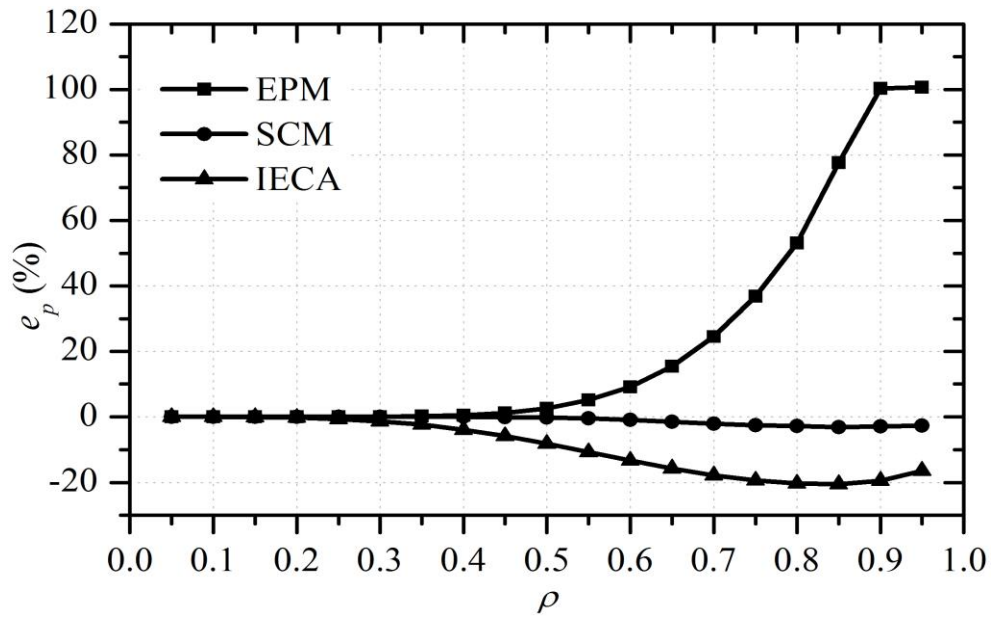
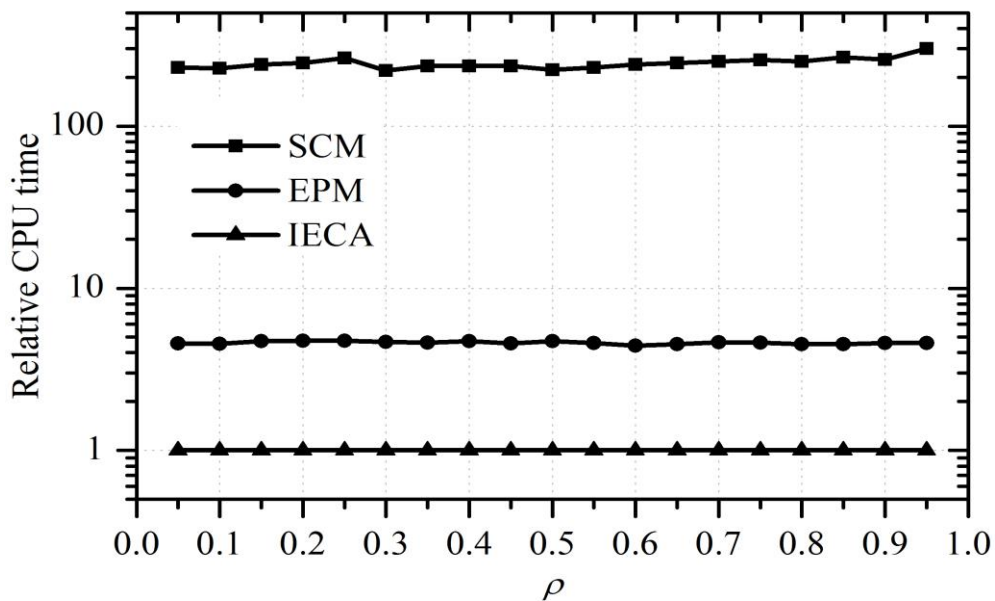


Figure 3.4 Impact of ρ on the accuracy of IECA for series systems with 250 equicorrelated components



(a) Comparison of accuracy



(b) Comparison of efficiency

Figure 3.5 Comparison of EPM, SCM and IECA for series systems with 250 equicorrelated components and $\beta_c = 6$

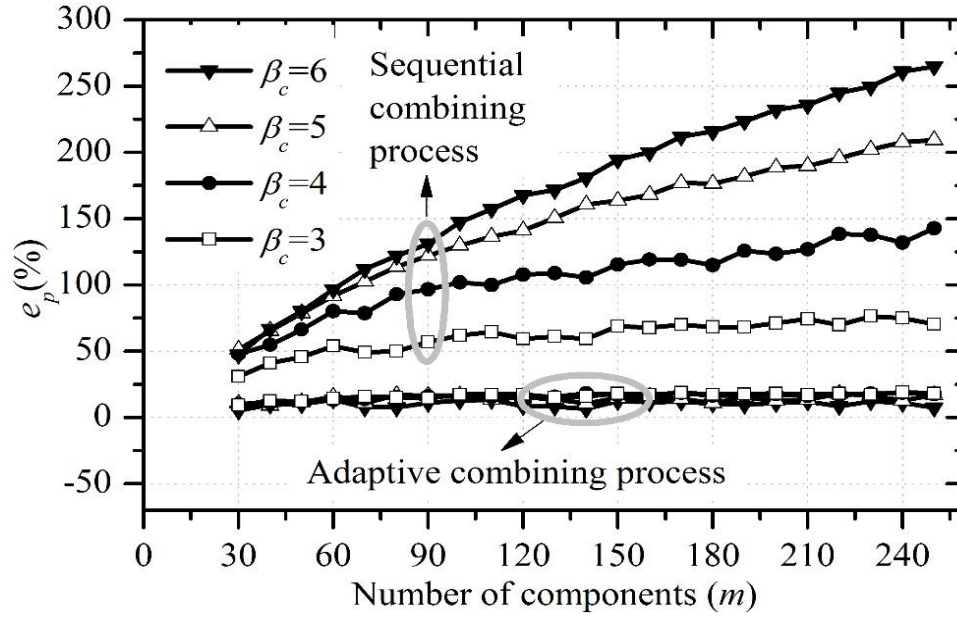


Figure 3.6 Accuracy of equivalent component approach for series systems with unequally correlated components using correlation structure given by Eq. (3.12)

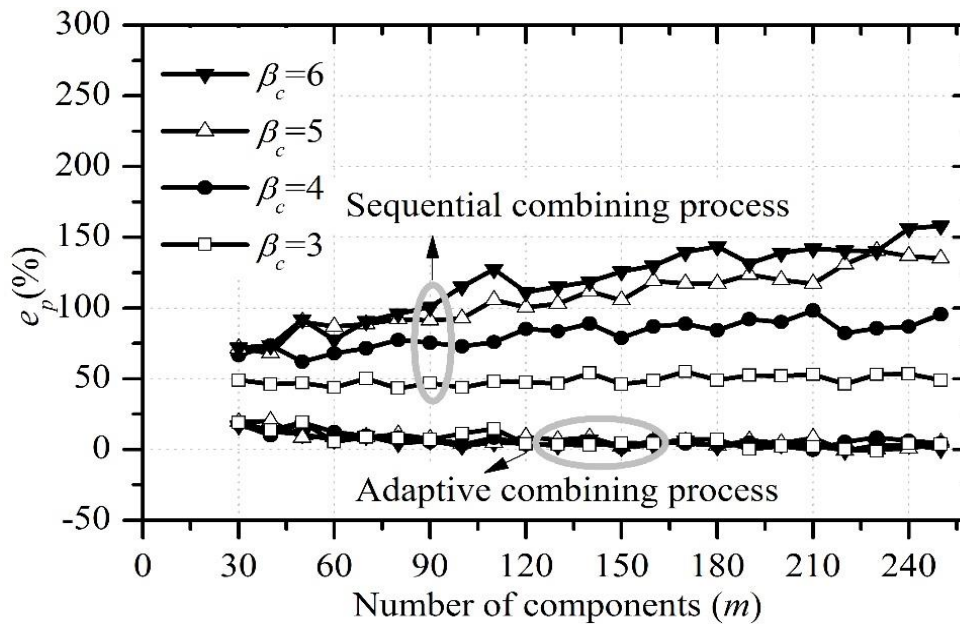


Figure 3.7 Accuracy of equivalent component approach for unequally correlated components with the correlation structure given by Eq. (3.15) ($\rho_{min} = 0$ and $\rho_{max} = 0.98$)

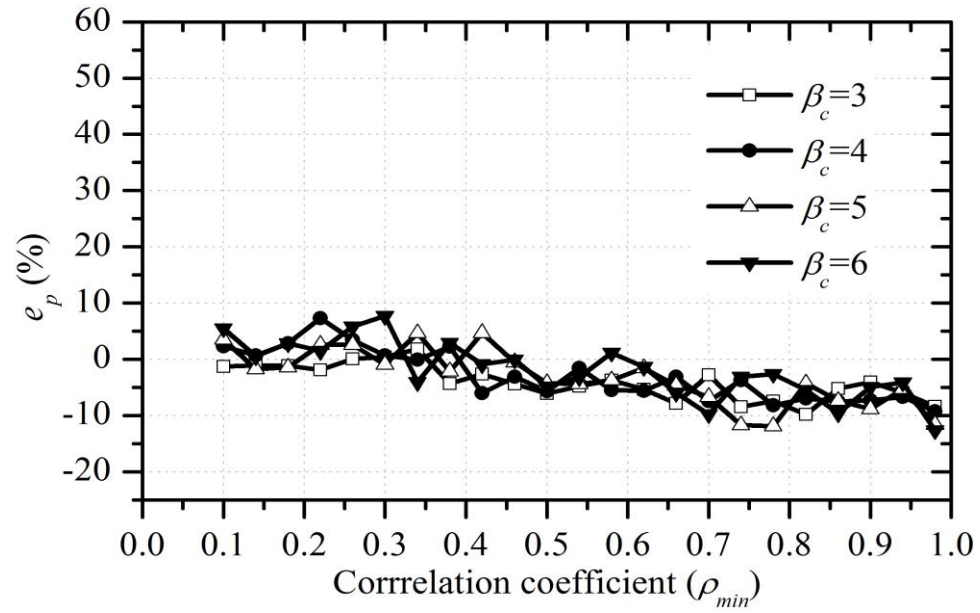
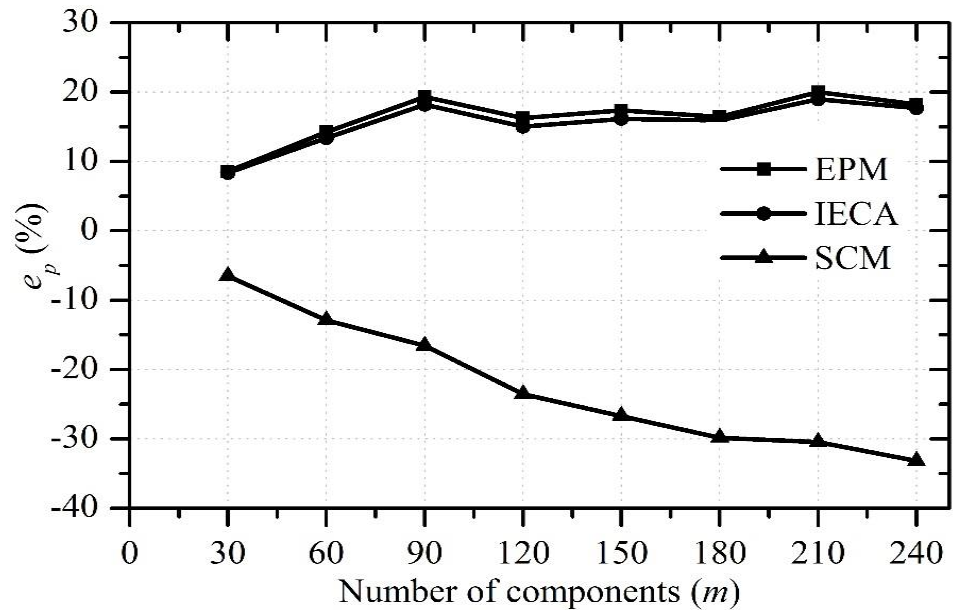
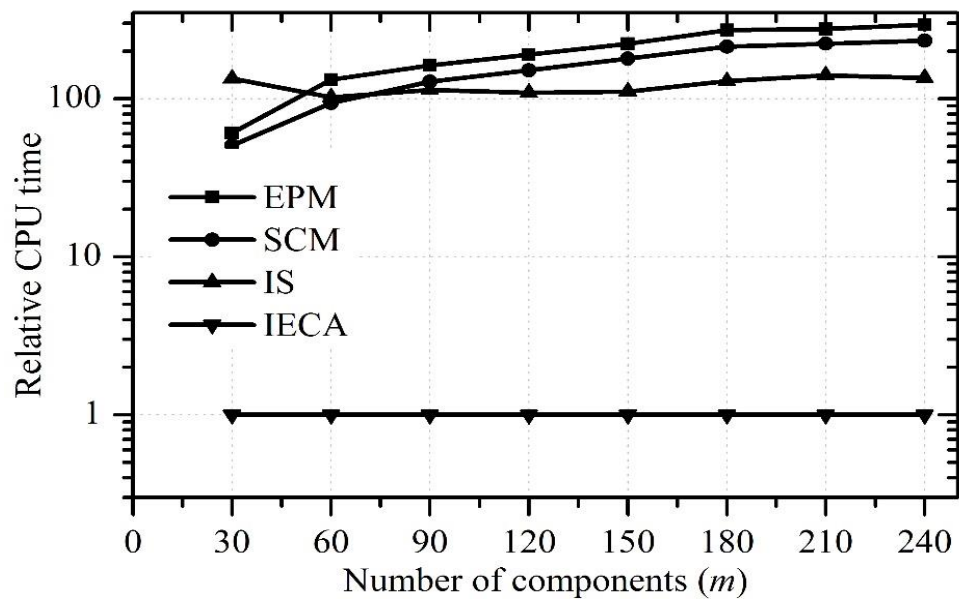


Figure 3.8 Accuracy of adaptive combing process for series systems with 250 components correlated according to Eq. (3.15) with $\rho_{max}=0.98$ and ρ_{min} varying from 0 to 0.98



(a) Comparison of accuracy



(b) Comparison of efficiency

Figure 3.9 Comparison of accuracy and efficiency of EPM, SCM and IECA for series system with $\beta_c=6$ and the component correlation structure defined by Eq. (3.12)

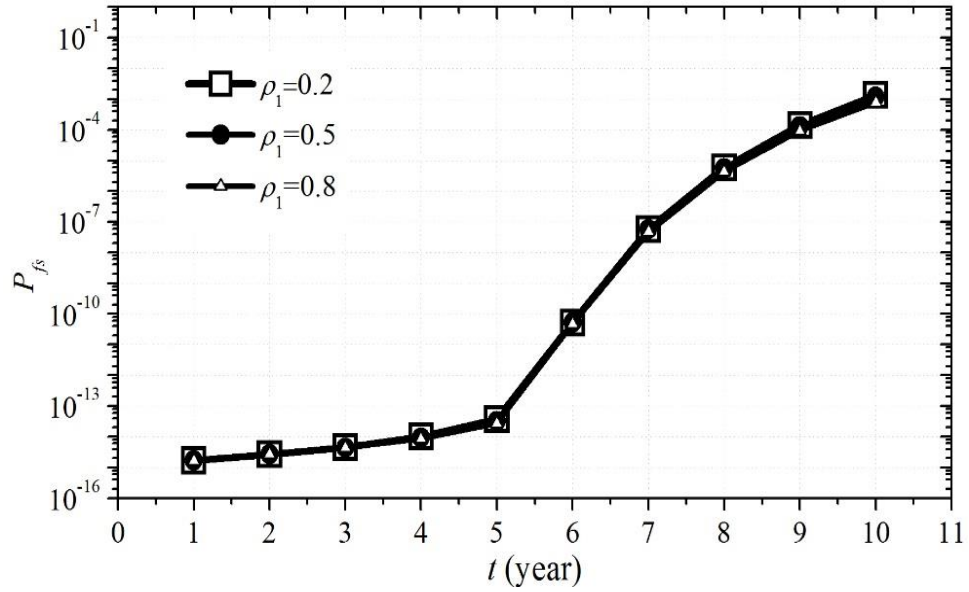


Figure 3.10 Time-dependent system reliability of the corroding pipeline joint

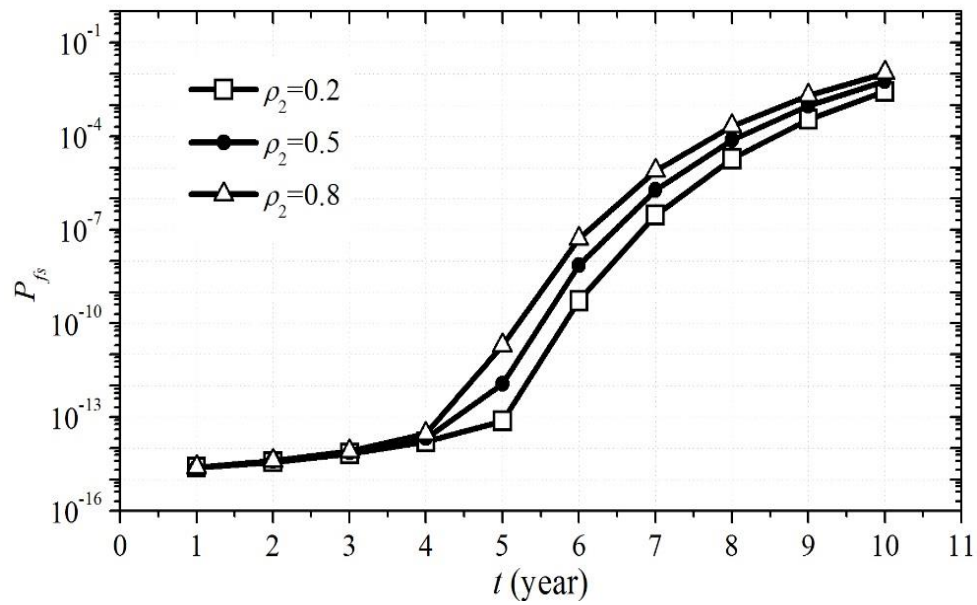


Figure 3.11 Sensitivity of the system reliability of the corroding pipeline joint to the correlation between the defect depth and length growth rates

4 First Order Reliability Method-based System Reliability Analyses of Corroding Pipelines Considering Multiple Defects and Failure Modes

4.1 Introduction

The efficient first-order reliability method (FORM) (Melchers 1999; Der Kiureghian 2005; Low and Tang 2007) is widely used to evaluate the reliability of engineering systems. The application of the FORM to evaluate the failure probabilities of pipelines with corrosion defects has been reported in the literature (Teixeira et al. 2008; Sahraoui et al. 2013; Zhang and Zhou 2014; Miran et al. 2016). Teixeira et al. (2008) and Sahraoui et al. (2013) employed the FORM to evaluate the probability of burst of a pipeline at a given corrosion defect, but did not consider the leak failure mode in the analyses. Zhang and Zhou (2014) developed a FORM-based methodology to evaluate the time-dependent probabilities of small leak and burst at a single active corrosion defect on a pipeline. However, the methodology is not applicable to evaluating the time-dependent probabilities of small leak and burst of a pipe joint containing multiple active corrosion defects. Miran et al. (2016) evaluated the system failure probability of pipe joints considering multiple defects and multiple failure modes (i.e. small leak, large leak and rupture) using the FORM. However, their study did not consider the potential correlations among failures at different defects.

The objective of the work in this chapter is to develop an efficient FORM-based methodology to evaluate the time-dependent probabilities of small leak and burst of a pipeline joint containing multiple active corrosion defects by taking into account the correlations among failures at different defects. The methodology includes two key components. First, two equivalent linearized time-dependent limit state functions, one for leak and the other for burst, are constructed in the standard normal space for the multiple defects on the pipeline joint, based on the FORM results obtained for individual failure modes associated with individual defects. Second, formulations are developed for computing the incremental probabilities of small leak and burst of the pipeline joint over a short time increment based on the equivalent limit state functions. The proposed methodology is illustrated using three numerical examples, in which different models characterizing the growth of corrosion defects are employed. The accuracy of the proposed

methodology is demonstrated by comparing the evaluated probabilities of small leak and burst with the corresponding values obtained from the simple Monte Carlo (MC) analyses.

4.2 Limit State Functions

Consider a pipeline joint with a total of m active corrosion defects. The limit state function, $g_j^s(t)$, for the j -th defect ($j = 1, 2, \dots, n$) penetrating the pipe wall at a given time t is given by

$$g_j^s(t) = \varphi_0 w t_j - d_j(t) \quad (4.1)$$

where $w t_j$ is the pipe wall thickness at the location of the j -th defect; $d_j(t)$ is the maximum depth of the j -th defect at time t ; φ_0 ($\varphi_0 \leq 1$) is a reduction factor to account for the fact that the remaining ligament of the pipe wall is prone to developing cracks that could lead to a small leak once the defect is sufficiently deep (Al-Amin and Zhou 2014). A typical value of φ_0 is 0.8 (Caleyo et al. 2002; Zhou 2010). Note that both random variable- and stochastic process-based models have been reported in the literature to characterize the defect growth (Zhou 2010; Lu et al. 2013; Gomes and Beck 2014).

The limit state function, $g_j^b(t)$, for plastic collapse of the remaining ligament at the j -th defect at time t is given by

$$g_j^b(t) = p_{bj}(t) - p_j \quad (4.2)$$

where $p_{bj}(t)$ is the burst pressure capacity of the pipeline joint at the j -th defect at time t and p_j is the internal pressure at the j -th defect. Although the pipe internal pressure is controlled during operation, there are inevitable random pressure fluctuations over time. Therefore, the internal pressure should ideally be modeled as a time-dependent random process. However, such a model will significantly complicate the proposed methodology. Given that the uncertainty in the internal pressure is in general much less than that in the corrosion growth process (CSA 2015), the internal pressure is characterized by a time-independent random variable instead of a time-dependent random process in this chapter. p_{bj} is evaluated using the well-known ASME B31G Modified model (Kiefner and Vieth 1989) as follows:

$$p_{bj} = \xi_j \frac{2wt_j(\sigma_{yj} + 68.95)}{D} \left[\frac{1 - \frac{0.85d_j}{wt_j}}{1 - \frac{0.85d_j}{M_jwt_j}} \right] \quad (4.3)$$

$$M_j = \begin{cases} \sqrt{1 + 0.6275 \frac{l_j^2}{Dwt_j} - 0.003375 \frac{l_j^4}{(Dwt_j)^2}}, & \frac{l_j^2}{Dwt_j} \leq 50 \\ 3.3 + 0.032 \frac{l_j^2}{Dwt_j}, & \frac{l_j^2}{Dwt_j} > 50 \end{cases} \quad (4.4)$$

where ξ is the model error associated with the B31G Modified model (Zhou and Huang 2012); D is the pipe outside diameter; σ_y and $\sigma_y + 68.95$ (MPa) are the yield strength and empirically-defined flow stress of the pipe steel, respectively; M is the so-called Folias factor; l is the defect length, and the subscript j denotes the value of the variable corresponding to the j -th defect. For brevity, $p_{bj}(t)$, $M_j(t)$, $d_j(t)$ and $l_j(t)$ are simply written as p_{bj} , M_j , d_j and l_j , respectively, in Eqs. (4.3) and (4.4). For simplicity, the dependence of d_j and l_j on time is made implicit in Equations (4.3) and (4.4).

Let $P_s(t)$ and $P_b(t)$ denote the cumulative probabilities of small leak and burst of the pipeline joint, respectively, within a time interval $[0, t]$. Further let t_j^s denote the time at which the j -th defect just penetrates the pipe wall, and t_j^b denote the time at which plastic collapse takes place at the j -th defect due to the internal pressure. Because of the competing nature of the small leak and burst failure modes, $P_s(t)$ and $P_b(t)$ are defined as follows using t_j^s and t_j^b :

$$P_s(t) = \text{Prob} \left[\left(0 \leq \min_j \{t_j^s\} \leq t \right) \cap \left(\min_j \{t_j^s\} < \min_j \{t_j^b\} \right) \right] \quad (4.5a)$$

$$P_b(t) = \text{Prob} \left[\left(0 \leq \min_j \{t_j^b\} \leq t \right) \cap \left(\min_j \{t_j^b\} < \min_j \{t_j^s\} \right) \right] \quad (4.5b)$$

where \cap denotes the intersection of two events.

4.3 FORM-based Time-dependent System Reliability Analyses of Corroding Pipelines

4.3.1 Equivalent Limit State Functions for Corroding Pipelines

The pipeline joint containing m active corrosion defects can be considered to include two series systems, one system with m limit state functions ($g_j^s(t), j = 1, 2, \dots, m$) representing the defect penetrating the pipe wall and the other system with m limit state functions ($g_j^b(t)$) representing the plastic collapse. Let the union of all the random variables (e.g. pipe wall thicknesses, yield strengths, internal pressures and defect sizes) involved in $g_j^s(t)$ and $g_j^b(t)$ ($j = 1, 2, \dots, m$) be represented by an n -dimensional vector \mathbf{X} . The probabilistic characteristics of some of the random variables included in \mathbf{X} may depend on the axial and circumferential locations of the corrosion defect on the pipeline. For example, defects at a certain location on the pipeline may on average grow faster than the defects at other locations.

Consider the series system representing the wall penetration first. At a given time t , the FORM can be used to evaluate $\text{Prob}[g_j^s(t) \leq 0]$ with the corresponding reliability index denoted by $\beta_j^s(t)$. For the detailed introduction of the FORM, please refer to Chapter 2. It is noted that because $g_j^s(t)$ monotonically decreases over time as corrosion defects cannot self-heal, $\beta_j^s(t)$ corresponds to the cumulative probability of the j -th defect penetrating the pipe wall within the time interval $[0, t]$ (Andrieu-Renaud et al. 2004). Define $\boldsymbol{\beta}^s(t) = [\beta_1^s(t), \beta_2^s(t), \dots, \beta_m^s(t)]^T$, and let $\mathbf{R}^s(t)$ denote the correlation matrix of the linearized safety margins associated with $g_1^s(t), g_2^s(t), \dots, g_m^s(t)$ in the standard normal space. The cumulative probability of any of the m defects penetrating the pipe wall within $[0, t]$, $P^s(t)$, then equals $1 - \Phi_m(\boldsymbol{\beta}^s(t), \mathbf{R}^s(t))$. The reliability index, $\beta^e(t)$, corresponding to $P^s(t)$ equals $-\Phi^{-1}(P^s(t))$. If m is small, Genz's method (Genz, 1992) is advised to evaluate $P^s(t)$ for its high accuracy. Otherwise, improved equivalent component approach (see Chapter 3) should be preferred due to the efficiency advantages.

Following Gollwitzer and Rackwitz (1983) as well as Estes and Frangopol (1998), we construct a linearized equivalent limit state function at time t , $G^{se}(t)$, in the standard normal space whose reliability index equals $\beta^{se}(t)$. It follows that

$$G^{se}(t) = \beta^{se}(t) - (\boldsymbol{\alpha}^{se}(t))^T \mathbf{u} \quad (4.6)$$

where \mathbf{u} denotes values of the n -dimensional vector of the standard normal variates transformed from \mathbf{X} , and $\boldsymbol{\alpha}^{se}(t)$ is the equivalent unit normal vector associated with the linearized equivalent limit state function at time t . Given that the unit normal vector represents the sensitivity of the reliability index with respect to the random variables involved, $\boldsymbol{\alpha}^{se}(t)$ can be evaluated as (Gollwitzer and Rackwitz 1983)

$$\alpha_i^{se}(t) = \frac{\frac{\partial \beta^{se}(t)}{\partial u_i}}{\sqrt{\sum_{i=1}^n \left(\frac{\partial \beta^{se}(t)}{\partial u_i}\right)^2}}, \quad (i = 1, 2, \dots, n) \quad (4.7)$$

where $\alpha_i^{se}(t)$ is the i -th element of $\boldsymbol{\alpha}^{se}(t)$. In this chapter, $\frac{\partial \beta^{se}(t)}{\partial u_i}$ is computed by utilizing the chain rule as follows:

$$\frac{\partial \beta^{se}(t)}{\partial u_i} = \sum_{j=1}^m \frac{\partial \beta^{se}(t)}{\partial \beta_j^s(t)} \frac{\partial \beta_j^s(t)}{\partial u_i} \quad (4.8)$$

where $\frac{\partial \beta_j^s(t)}{\partial u_i}$ is already available from the FORM analyses carried out for the individual limit state function $g_j^s(t)$; therefore, only $\frac{\partial \beta^{se}(t)}{\partial \beta_j^s(t)}$ needs to be evaluated. This can be achieved through the finite difference method. The use of Eq. (4.8) to evaluate the equivalent unit normal vector is more efficient and numerically stable than the approach employed by Gollwitzer and Rackwitz (1983), which involves directly calculating $\frac{\partial \beta^{se}(t)}{\partial u_i}$ by perturbing the value of u_i at the design point associated with the individual limit state function.

Now consider the series system for the plastic collapse. The FORM can be used to evaluate $\text{Prob}[g_j^b(t) \leq 0]$ with the corresponding reliability index denoted by $\beta_j^b(t)$. It is noted that $g_j^b(t)$ is a monotonically decreasing function of time because $p_{bj}(t)$ monotonically decreases over time and the pipe internal pressure is assumed to be time-independent in this chapter. Therefore, $\beta_j^b(t)$ represents the cumulative probability of plastic collapse at

the j -th defect within $[0, t]$. The procedure for constructing $G^{se}(t)$ is equally applicable to construct a linearized equivalent limit state function, $G^{be}(t)$, for the series system representing the plastic collapse, with the corresponding reliability index $\beta^{be}(t)$ and equivalent unit normal vector $\alpha^{be}(t)$, where $\beta^{be}(t)$ corresponds to the cumulative probability of plastic collapse at any of the m defects within $[0, t]$. With the equivalent limit state functions for the wall penetration and plastic collapse established, the m active defects on the pipeline are now represented by a single equivalent active defect, which greatly simplifies formulations for $P_s(t)$ and $P_b(t)$ as described in the next section.

4.3.2 Formulations for System Failure Probabilities of Corroding Pipelines

As implied by Eq. (4.5), the evaluation of $P_s(t)$ and $P_b(t)$ is a problem of computing the probability of first excursion into the failure region associated with either small leak or burst within $[0, t]$. It follows that $P_s(t)$ and $P_b(t)$ must be evaluated incrementally; that is,

$$P_s(\tau + \Delta t) = P_s(\tau) + \Delta P_s(\tau, \Delta t) \quad (4.9a)$$

$$P_b(\tau + \Delta t) = P_b(\tau) + \Delta P_b(\tau, \Delta t) \quad (4.9b)$$

where $\Delta P_s(\tau, \Delta t)$ and $\Delta P_b(\tau, \Delta t)$ ($0 \leq \tau < t$) are incremental probabilities of small leak and burst, respectively, within a short time interval between τ and $\tau + \Delta t$. The value of Δt in the range of half to one year is considered a reasonable choice for the reliability analyses of corroding pipelines, considering that the growth of corrosion on pipelines is typically a slow process. The geometric descriptions of $\Delta P_s(\tau, \Delta t)$ and $\Delta P_b(\tau, \Delta t)$ in terms of the equivalent limit state functions $G^{se}(\tau)$ and $G^{be}(\tau)$ are shown in Figs. 4.1(a) and 4.1(b), respectively. Four hyperplanes representing $G^{be}(\tau + \Delta t) = G^{se}(\tau + \Delta t) = G^{be}(\tau) = G^{se}(\tau) = 0$ respectively are shown in Fig. 4.1. The incremental probabilities of small leak and burst as time increases from τ to $\tau + \Delta t$ are depicted as the two shaded areas, in Fig. 4.1(a) and 4.1(b), respectively. The grey arrows in Fig. 4.1 point to the design points associated with limit state functions relevant to the calculations of $\Delta P_s(\tau, \Delta t)$ and $\Delta P_b(\tau, \Delta t)$. It follows from Fig. 4.1 that $\Delta P_s(\tau, \Delta t)$ and $\Delta P_b(\tau, \Delta t)$ are given by

$$\Delta P_s(\tau, \Delta t) = \Phi_3([\beta^{se}(\tau), -\beta^{se}(\tau + \Delta t), \beta^{be}(\tau)]^T, \mathbf{R}^{sb}(\tau, \Delta t)) \quad (4.10a)$$

$$\Delta P_b(\tau, \Delta t) = \Phi_3([\beta^{be}(\tau), -\beta^{be}(\tau + \Delta t), \beta^{se}(\tau)]^T, \mathbf{R}^{bs}(\tau, \Delta t)) \quad (4.10b)$$

where $\mathbf{R}^{sb}(\tau, \Delta t)$ is the 3×3 matrix of correlation coefficients of the three linearized equivalent limit state functions $G^{se}(\tau + \Delta t)$, $G^{se}(\tau)$ and $G^{be}(\tau)$, and $\mathbf{R}^{bs}(\tau, \Delta t)$ is the 3×3 matrix of correlation coefficients of $G^{be}(\tau + \Delta t)$, $G^{be}(\tau)$ and $G^{se}(\tau)$. The correlation coefficient between $G^{se}(\tau + \Delta t)$ and $G^{se}(\tau)$ equals $(\boldsymbol{\alpha}^{se}(\tau + \Delta t))^T \boldsymbol{\alpha}^{se}(\tau)$; the correlation coefficient between $G^{se}(\tau + \Delta t)$ and $G^{be}(\tau)$ equals $(\boldsymbol{\alpha}^{se}(\tau + \Delta t))^T \boldsymbol{\alpha}^{be}(\tau)$, and the other correlation coefficients can be evaluated in a similar fashion.

The area ABCD indicated in Fig. 4.1 corresponds to the probability of the occurrence of both small leak and burst within $[\tau, \tau + \Delta t]$. Because it is not feasible for the proposed methodology to determine which failure mode will occur first within this time interval, the area ABCD is included in both $\Delta P_s(\tau, \Delta t)$ and $\Delta P_b(\tau, \Delta t)$. For reasonably small values of Δt , the error introduced by this approximation is considered insignificant. Note that the growth of corrosion defects on pipelines is generally a gradual process; therefore, it can be assumed that the hyperplanes corresponding to $G^{se}(\tau) = G^{se}(\tau + \Delta t) = 0$ are parallel to each other and that the hyperplanes corresponding to $G^{be}(\tau) = G^{be}(\tau + \Delta t) = 0$ are parallel to each other. In other words, $G^{se}(\tau)$ and $G^{se}(\tau + \Delta t)$ are assumed to be fully correlated, and $G^{be}(\tau)$ and $G^{be}(\tau + \Delta t)$ are assumed to be fully correlated. Based on these assumptions, Eqs. (4.10a) and (4.10b) can be slightly simplified as

$$\Delta P_s(\tau, \Delta t) = \int_{-\infty}^{\beta^{be}(\tau)} \int_{\beta^{se}(\tau+\Delta t)}^{\beta^{se}(\tau)} \Phi_2(\theta_1, \theta_2, r^{sb}(\tau)) d\theta_1 d\theta_2 \quad (4.11a)$$

$$\Delta P_b(\tau, \Delta t) = \int_{-\infty}^{\beta^{se}(\tau)} \int_{\beta^{be}(\tau+\Delta t)}^{\beta^{be}(\tau)} \Phi_2(\theta_1, \theta_2, r^{sb}(\tau)) d\theta_1 d\theta_2 \quad (4.11b)$$

where $\phi_2(\bullet, \bullet, \bullet)$ is the probability density function of the bivariate normal distribution, and $r^{sb}(\tau) = (\boldsymbol{\alpha}^{se}(\tau))^T \boldsymbol{\alpha}^{be}(\tau)$ is the correlation coefficient between $G^{se}(\tau)$ and $G^{be}(\tau)$. Given the formulations for $\Delta P_l(\tau, \Delta t)$ and $\Delta P_b(\tau, \Delta t)$, $P_l(t)$ and $P_b(t)$ can be evaluated recursively from Eqs (4.10a) and (4.10b) starting from $P_s(0)$ and $P_b(0)$, which can be evaluated as $\text{Prob}[G^{se}(0)$

$\leq 0]$ and $\text{Prob}[G^{be}(0) \leq 0]$, respectively.

4.4 Numerical Examples

4.4.1 General Information

Three examples, which are representative of small-, medium- and large-diameter pipeline joints respectively, are used to illustrate the application and accuracy of the above-described methodology for evaluating the system reliability of corroding pipelines. Table 4.1 summarizes the basic attributes of these examples, which includes their nominal outside diameters (D), nominal wall thicknesses (wt_n), specified minimum yield strengths (SMYS) and maximum operating pressures (P_0). For illustrative purpose, it is assumed that ten active corrosion defects have been detected and sized by a recently-run ILI on each of the three pipeline joints although the methodology can easily cope with more defects. The initial lengths (l_{0j}) of all ten defects reported by the ILI tool are assumed to equal 50 mm; the ILI-reported initial depths (d_{0j}) of five defects equal $0.25wt_n$, and the initial depths of the other five defects equal $0.3wt_n$. The burst pressure capacity of the joint at a given defect is evaluated using the B31G Modified model as given by Eqs. (4.3) and (4.4). The reduction factor φ_0 in Eq. (4.1) is set to be 0.8.

For simplicity, the following simple linear growth model is adopted to characterize the growth of the defect length over time t :

$$l_j(t) = l_{0j} + g_{lj}t \quad (4.12)$$

where g_l is the length growth rate; the subscript j denotes the value of the variable corresponding to the j -th defect. In addition, three different defect depth growth models that are widely adopted in the literature are employed, namely the linear, nonlinear and gamma process-based models (Zhou 2010; Al-Amin and Zhou 2014; Zhang and Zhou 2014; Ellingwood and Mori 1997; Valor et al. 2013). Details of these models are described in the following sections. In practice, the growth of corrosion defects is often quantified through the so-called defect matching procedure, i.e. comparing sizes of the same defect reported in successive ILIs. Extensive studies (Achterbosch and Grzelak 2006; Al-Amin et al. 2014; Zhang et al. 2014) have been reported in the literature for quantifying various

growth models based on the defect sizes reported by multiple ILIs, while taking into account the measurement errors associated with the ILI results.

The probabilistic characteristics of all parameters except for the defect depth growth are summarized in Table 4.2. Note that the uncertainties in d_{0j} and l_{0j} are intended to reflect the measurement errors associated with the ILI tools, which can be quantified from typical accuracy specifications of the tool such as the measured depth (length) being within $\pm 5\%wt_n$ (10 mm) of the actual depth (length). Note further that the pipe internal pressure is in general bounded (CSA 2015); however, for simplicity but without affecting the objective of the numerical examples, the internal pressure is assumed to be characterized by an unbounded distribution (Gumbel distribution) based on the findings of the well-known SUPERB project (Jiao et al. 1995).

Also indicated in Table 4.2 is the assumed correlation coefficient (ρ_1) between random variables representing the same physical parameter at different defects. Random variables associated with the same defect may also be correlated (e.g. the growths of the defect depth and length); such correlations can be easily accounted for in the analyses but are ignored for the sake of simplicity. The spatial correlation between the growths of different defects can be quantified based on the results obtained from the defect matching practice; however, the measurement errors of the ILI tools as well as the potential spatial correlation associated with the measurement errors make this a challenging task. In the present chapter, parametric analyses with respect to the spatial correlation between the defect growths are carried out.

The correlation coefficient between non-normally distributed random variables can be modified using the empirical equations provided in (Der Kiureghian and Liu 1986) to estimate the corresponding correlation coefficient in the normal space. For simplicity and without affecting the purpose of the examples, the unmodified correlation coefficients are employed in the analyses. To verify the failure probabilities evaluated by using the proposed methodology, the simple MC with 10^6 simulation trials is performed to evaluate the benchmark failure probability of each example.

4.4.2 Linear Growth Model for Defect Depth

The growth of the defect depth is characterized by

$$d_j(t) = d_{0j} + g_{dj}t \quad (4.13)$$

where d_0 and g_d is the initial defect depth and depth growth rate; the subscript j denotes the value of the variable corresponding to the j -th defect. A Weibull distribution with a COV of 50% is assigned to g_d , with the corresponding mean value assumed to equal 0.1, 0.2 and 0.3 mm/year for examples 1, 2 and 3, respectively. The growth rates at different defects on a given pipeline joint are assumed to be equicorrelated, with the correlation coefficient ρ_2 equal to 0.2 or 0.8.

The results of the time-dependent system reliability analyses are shown in Fig. 4.2. Note that the probabilities of burst and small leak obtained by using Eq. (4.11) (i.e. based on the parallel hyperplane assumption) are shown along with those obtained by using Eq. (4.10) (i.e. without the parallel hyperplane assumption). Moreover, the probabilities of burst and small leak obtained from the simple MC are shown in Fig. 4.2 as the benchmark results. Because the number of simulation trials included in MC equals 10^6 , the lowest failure probability corresponding to MC shown in Fig. 4.2 is 10^{-6} . Fig. 4.2 indicates that the failure probabilities corresponding to Eqs. (4.10) and (4.11) are practically identical, therefore validating the assumption that the hyperplane represented by $G^{se}(\tau) = 0$ ($G^{be}(\tau) = 0$) is parallel to that represented by $G^{se}(\tau + \Delta t) = 0$ ($G^{be}(\tau + \Delta t) = 0$). The probabilities of small leak evaluated by using the proposed methodology are essentially the same as the corresponding failure probabilities obtained from MC for all three examples and the two values (i.e. 0.2 and 0.8) of ρ_1 and ρ_2 considered. The probabilities of burst evaluated by using the proposed methodology also in general agree very well with the corresponding MC results. The proposed methodology tends to slightly underestimate the probabilities of burst for the small- and medium-diameter pipelines as shown in Figs. 4.2(a) through 4.2(d), but slightly overestimate the probabilities of burst for the large-diameter pipeline as shown in Figs. 4.2(e) and 4.2(f).

4.4.3 Nonlinear Growth Model for Defect Depth

A nonlinear power-law growth model (Ellingwood and Mori 1997; Valor et al. 2013) is employed to characterize $d_j(t)$ as follows:

$$d_j(t) = d_{0j} + k_j t^{0.5} \quad (4.14)$$

where k_j is the parameters of the power-law growth model corresponding to the j -th defect (Ellingwood and Mori 1997); k_j is characterized by a Weibull variate with a COV of 50%. The mean value of k_j is assumed to equal 0.332, 0.663 and 0.995 mm/year^{0.5} for examples 1, 2 and 3, respectively. Furthermore, the Weibull variates representing k_j for different defects are assumed to be equicorrelated, with the correlation coefficient ρ_2 equal to 0.2 or 0.8.

The probabilities of burst and small leak obtained from the proposed methodology and simple MC for the nonlinear growth model of the defect depth are depicted in Fig. 4.3. This figure leads to similar observations as those from Fig. 4.2. First, the validity of the parallel hyperplane assumption is further demonstrated in Fig. 4.3 as the results corresponding to Eqs (4.10) and (4.11) are the same. Second, the probabilities of small leak corresponding to the proposed methodology are in excellent agreement with those from MC for all three examples. The proposed methodology somewhat underestimates the probabilities of burst for small- and medium-diameter pipelines, especially the latter case as shown in Figs. 4.3(c) and 4.3(d), but the difference is considered acceptable. Finally, the proposed methodology slightly overestimates the probabilities of burst for the large-diameter pipeline as shown in Figs. 4.3(e) and 4.3(f).

4.4.4 Gamma Process-based Growth Model for Defect Depth

The homogeneous gamma process (Van Noortwijk 2009) is employed to characterize the growth of the defect depth as follows:

$$d_j(t) = d_{0j} + d_{gj}(t) \quad (4.15)$$

where $d_{gj}(t)$ denotes the homogeneous gamma process corresponding to the j -th defect at a given time t . The probability density function of the gamma-distributed $d_{gj}(t)$, $F(d_{gj}(t)|at, b)$, is given by

$$F(d_{gj}(t)|at, b) = b^{at} (d_{gj}(t))^{at-1} \exp(-bd_{gj}(t)) / \Gamma(at) \quad (4.16)$$

where a and b are parameters of the gamma process, and $\Gamma(\bullet)$ is the gamma function. It follows from the properties of the gamma process (Van Noortwijk 2009) that $d_{gj}(\tau + \Delta t) = d_{gj}(\tau) + d_{gj}(\Delta t)$, where $d_{gj}(\Delta t)$ is the gamma-distributed increment of the defect depth within Δt and is independent of $d_{gj}(\tau)$.

Let μ and σ denote, respectively, the mean and standard deviation of the depth increment within one year. The parameters of the gamma process, a and b , are related to μ and σ as $\mu = a/b$ and $\sigma^2 = a/b^2$ (Van Noortwijk 2009). In this chapter, a is assumed to equal 4, whereas b is assumed to equal 40, 20 and 13.33 (mm/year)⁻¹ for examples 1, 2 and 3, respectively. This corresponds to $\mu(\sigma) = 0.1$ (0.05), 0.2 (0.1) and 0.3 (0.15) mm/year for examples 1, 2 and 3, respectively. For simplicity, the gamma processes $d_{gj}(t)$ at different defects are assumed to be mutually independent.

Figure 4.4 depicts the failure probabilities obtained from the proposed methodology and MC for the gamma-process based defect depth growth. The figure indicates that the failure probabilities obtained from the proposed methodology agree very well with those obtained from MC for all three examples and $\rho_1 = 0.2$ and 0.8. Finally, the results shown in Figs. 4.2, 4.3 and 4.4 demonstrate the applicability of the proposed methodology for both random variable- and stochastic process-based defect growth models and accuracy of the methodology.

4.5 Conclusions

A FORM-based methodology is proposed in this chapter to evaluate the time-dependent system reliability of a joint of pressurized steel pipeline containing multiple active corrosion defects. The methodology considers two competing failure modes of the pipe joint, i.e. small leak and burst, and takes into account correlations among limit state

functions at different defects. At a given time, the FORM is applied to the limit state functions corresponding to the defect penetrating the pipe wall and plastic collapse at individual corrosion defects on the pipe joint. Two linearized equivalent limit state functions, corresponding to the defect penetrating the pipe wall and plastic collapse respectively, are then established in the standard normal space for all the defects on the pipe joint. The unit normal vectors associated with the equivalent limit state functions are computed using the chain rule that incorporates the sensitivity factors obtained from the FORM analyses for each individual defect. Based on the equivalent limit state functions, a procedure is developed to incrementally evaluate the probabilities of small leak and burst for the pipe joint over a forecasting time period.

The proposed methodology is applied to three numerical examples that are representative of small-, medium- and large-diameter pipeline joints. Each example is assumed to contain ten active corrosion defects. Furthermore, three widely used models are adopted to characterize the growth of the defect depth, namely the linear, nonlinear and homogeneous gamma process-based growth models. The probabilities of small leak and burst of the examples evaluated by using the proposed methodology are compared with those obtained from the simple Monte Carlo simulation. The comparison indicates that the proposed methodology is accurate for different defect growth models and various levels of correlations among limit state functions at different defects.

4.6 References

- Achterbosch, G. G. J., and Grzelak, L. A. (2006). Determination of the corrosion rate of a MIC influenced pipeline using four consecutive pig runs. Proceedings of the International Pipeline Conference (IPC2006), IPC2006-10142, ASME, Alberta, Canada.
- Al-Amin, M., and Zhou, W. (2014). Evaluating the system reliability of corroding pipelines based on inspection data. *Structure and Infrastructure Engineering*, 10, 1161-1175.
- Andrieu-Renaud, C., Sudret, B., and Lemaire, M. (2004). The PHI2 method: a way to compute time-variant reliability. *Reliability Engineering and System Safety*, 84(1), 75-86.
- Caleyo, F., Gonzalez, J. L., and Hallen, J. M. (2002). A study on the reliability assessment

methodology for pipelines with active corrosion defects. *International Journal of Pressure Vessels and Piping*, 79(1), 77-86.

Canadian Standards Association (CSA). (2015). *CSA Z662: Oil and gas pipeline systems*. Canadian Standards Association, Mississauga, Ontario.

Der Kiureghian, A., and Liu, P. L. (1986). Structural reliability under incomplete probability information. *Journal of Engineering Mechanics*, 112, 85-104.

Der Kiureghian, A. (2005). First- and second-order reliability methods. *Engineering design reliability handbook: Chapter 14*, E. Nikolaidis et al. Eds., CRC Press, Boca Raton, Fla.

Ellingwood, B. R., and Mori, Y. (1997). Reliability-based service life assessment of concrete structures in nuclear power plants: optimum inspection and repair. *Nuclear Engineering and Design*, 175, 247-258.

Estes, A. C., and Frangopol, D. M. (1998). RELSYS: A computer program for structural system reliability. *Structural Engineering and Mechanics*, 6, 901-919.

Gollwitzer, S., and Rackwitz, R. (1983). Equivalent components in first-order system reliability. *Reliability Engineering*, 5, 99-115.

Gomes, W. J., and Beck, A. T. (2014). Optimal inspection and design of onshore pipelines under external corrosion process. *Structural Safety*, 47, 48-58.

Jiao, G., Sotberg, T., and Igland, R. T. (1995). SUPERB 2M statistical data-basic uncertainty measures for reliability analyses of offshore pipelines. SUPERB JIP Report No. STF70-F95212, Norwegian Marine Technology Research Institute, Trondheim, Norway.

Kiefner, J. F., and Vieth, P. H. (1989). A modified criterion for evaluating the remaining strength of corroded pipe (No. PR-3-805). Battelle Columbus Div., OH (USA). Retrieved from <http://www.osti.gov/scitech/biblio/7181509>

Lu, D., Xie, W. C., and Pandey, M. D. (2013). An efficient method for the estimation of parameters of stochastic gamma process from noisy degradation measurements.

Proceedings of the Institution of Mechanical Engineers, Part O: Journal of Risk and Reliability, 227(4), 425-433.

Low, B. K., and Tang, W. H. (2007). Efficient spreadsheet algorithm for first-order reliability method. *Journal of Engineering Mechanics*, 133, 1378-1387.

Melchers, R.E. (1999). *Structural reliability analyses and prediction*. John Wiley and Son Ltd.

Miran, S. A., Huang, Q., and Castaneda, H. (2016). Time-Dependent Reliability Analyses of Corroded Buried Pipelines Considering External Defects. *Journal of Infrastructure Systems*, 22(3), 04016019.

Sahraoui, Y., Khelif, R., and Chateauneuf, A. (2013). Maintenance planning under imperfect inspections of corroded pipelines. *International Journal of Pressure Vessels and Piping*, 104, 76-82.

Teixeira, A. P., Soares, C. G., Netto, T. A., and Estefen, S. F. (2008). Reliability of pipelines with corrosion defects. *International Journal of Pressure Vessels and Piping*, 85, 228-237.

Valor, A., Caleyó, F., Hallen, J. M., and Velázquez, J. C. (2013). Reliability assessment of buried pipelines based on different corrosion rate models. *Corrosion Science*, 66, 78-87.

Van Noortwijk, J. M. (2009). A survey of the application of gamma processes in maintenance. *Reliability Engineering and System Safety*, 94(1), 2-21.

Zhang, S., and Zhou, W. (2014). An efficient methodology for the reliability analyses of corroding pipelines. *Journal of Pressure Vessel Technology*, 136(4), 041701.

Zhang, S., Zhou, W., Al-Amin, M., Kariyawasam, S., and Wang, H. (2014). Time-dependent corrosion growth modeling using multiple in-line inspection data. *Journal of Pressure Vessel Technology*, 136(4), 041202, 1-7.

Zhou, W. (2010). System reliability of corroding pipelines. *International Journal of Pressure Vessels and Piping*, 87, 587-595.

Zhou, W., and Huang, G. X. (2012). Model error assessments of burst capacity models for corroded pipelines. *International Journal of Pressure Vessels and Piping*, 99, 1-8.

Table 4.1 Basic attributes of three pipeline examples.

Example	D (mm)	wt_n (mm)	SMYS (MPa)	P_0 (MPa)
1	324	4.32	359	5
2	610	7.16	414	6
3	914	13.15	483	10

Table 4.2 Probabilistic characteristics of parameters excluding the defect depth growth.

Parameter	Distribution	Mean	Coefficient of variation (COV) (%)	Corr. coef. at different defects (ρ_1)
D	Deterministic	D_n	-	-
wt_j	Normal	wt_n	1.5	
σ_{yj}	Normal	1.1SMYS	3.5	
p_j	Gumbel	1.05 P_0	3.0	
l_{0j}	Normal	50 (mm)	15	0.2 or 0.8
d_{0j}	Normal	0.25/0.3 wt_n	15	
g_{lj}	Weibull	3.0 (mm/year)	15	
ξ_j	Gumbel	1.297	25.8	

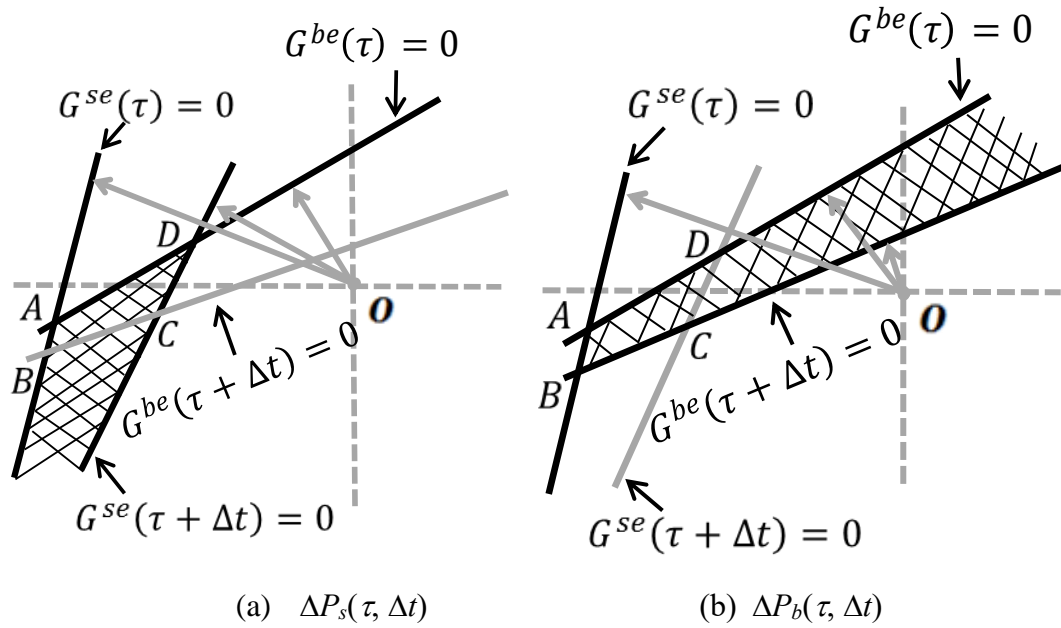
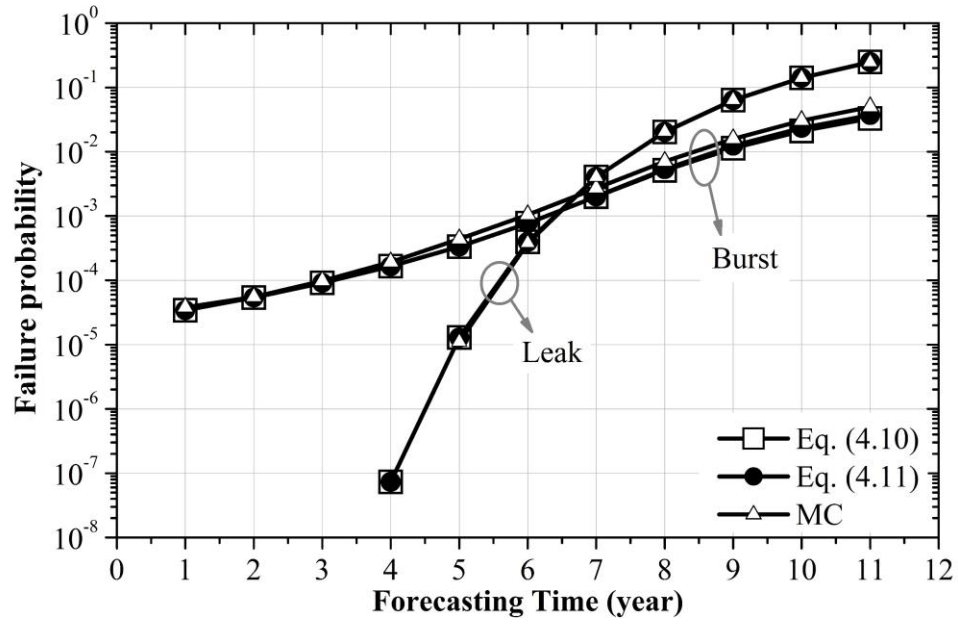
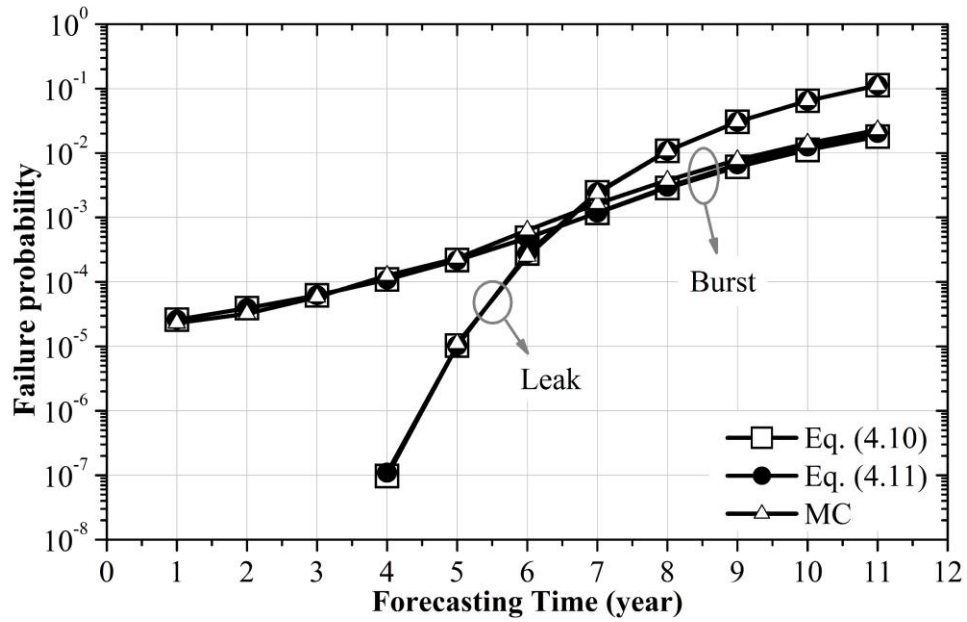
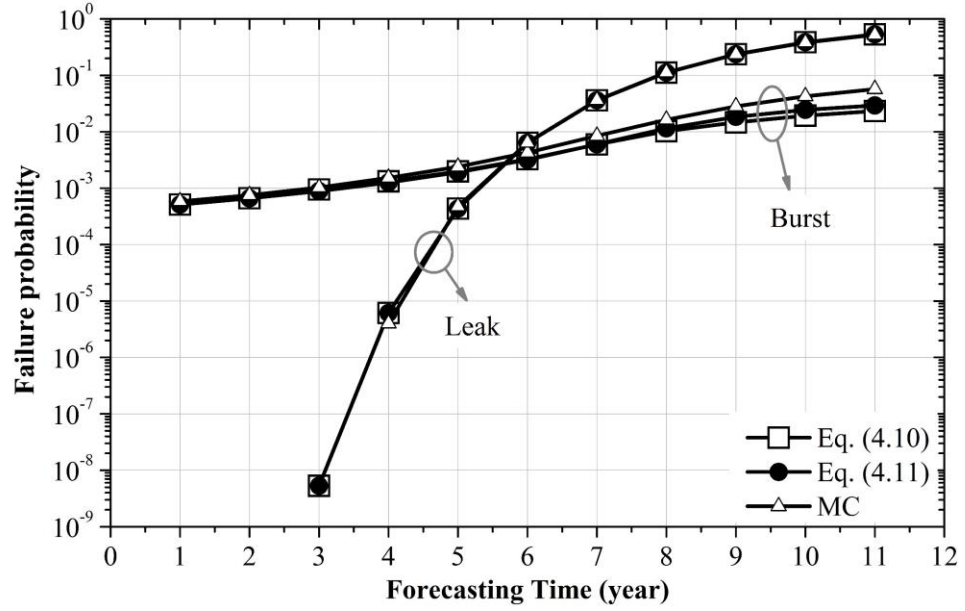
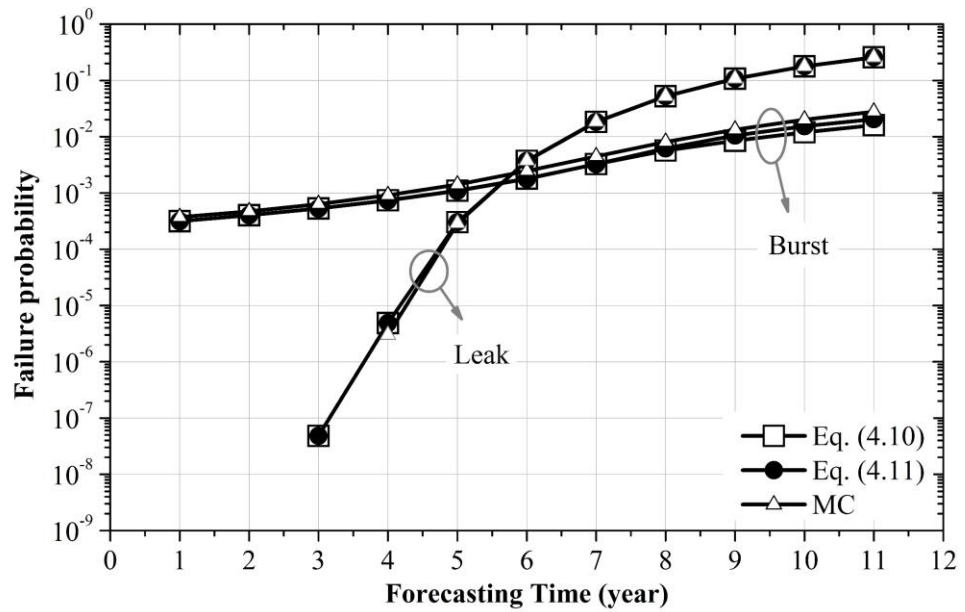


Figure 4.1 Geometric descriptions of $\Delta P_s(\tau, \Delta t)$ and $\Delta P_b(\tau, \Delta t)$

(a) Example 1; Small diameter; $\rho_1=\rho_2=0.2$ (b) Example 1; Small diameter; $\rho_1=\rho_2=0.8$

(c) Example 2; Medium diameter; $\rho_1=\rho_2=0.2$ (d) Example 2; Medium diameter; $\rho_1=\rho_2=0.8$

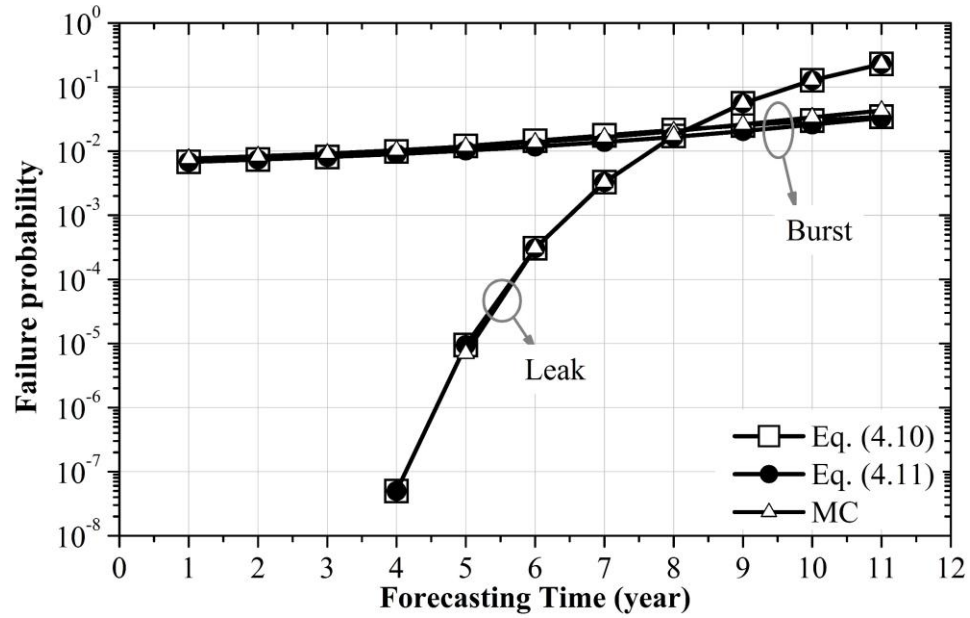
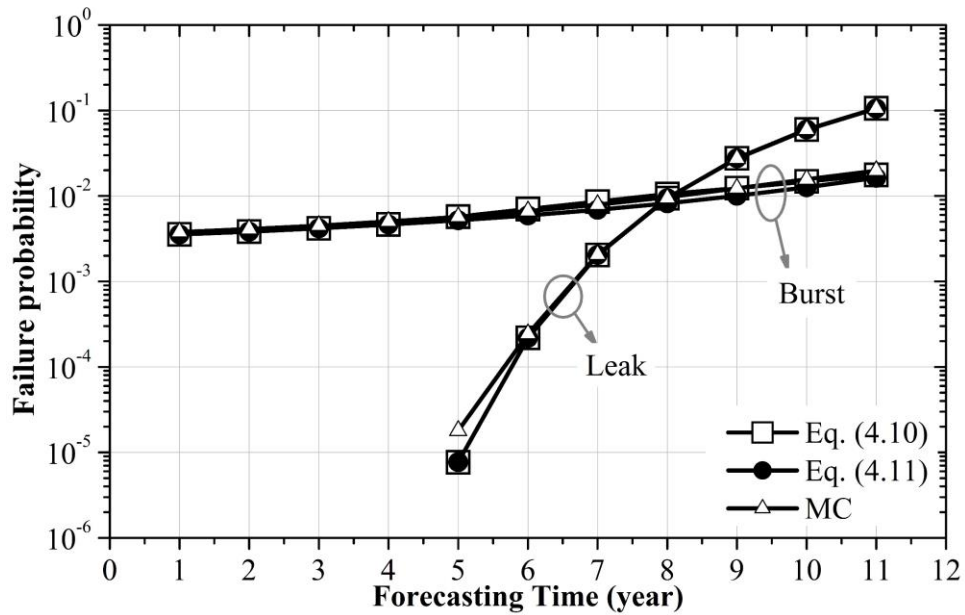
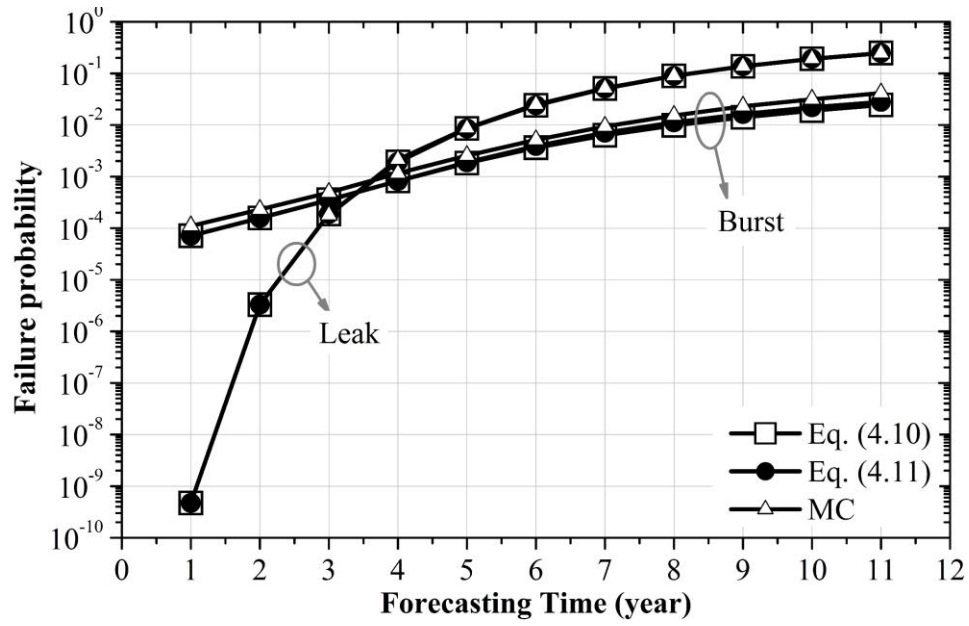
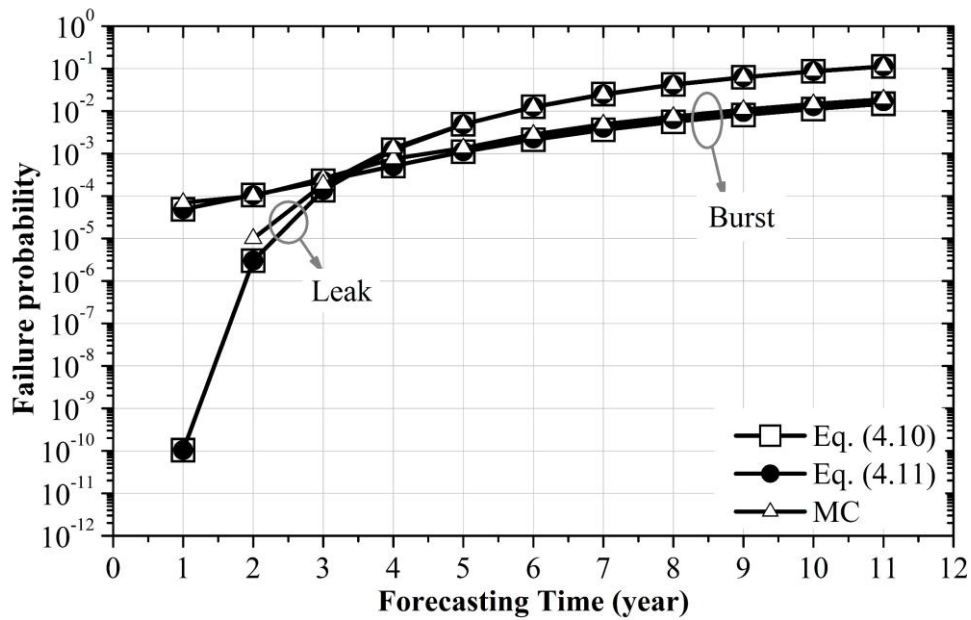
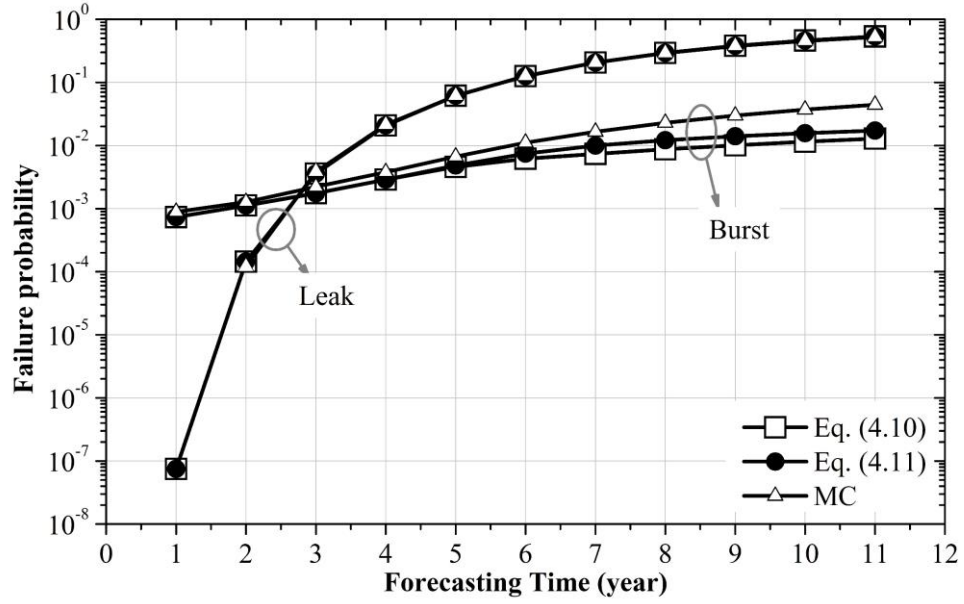
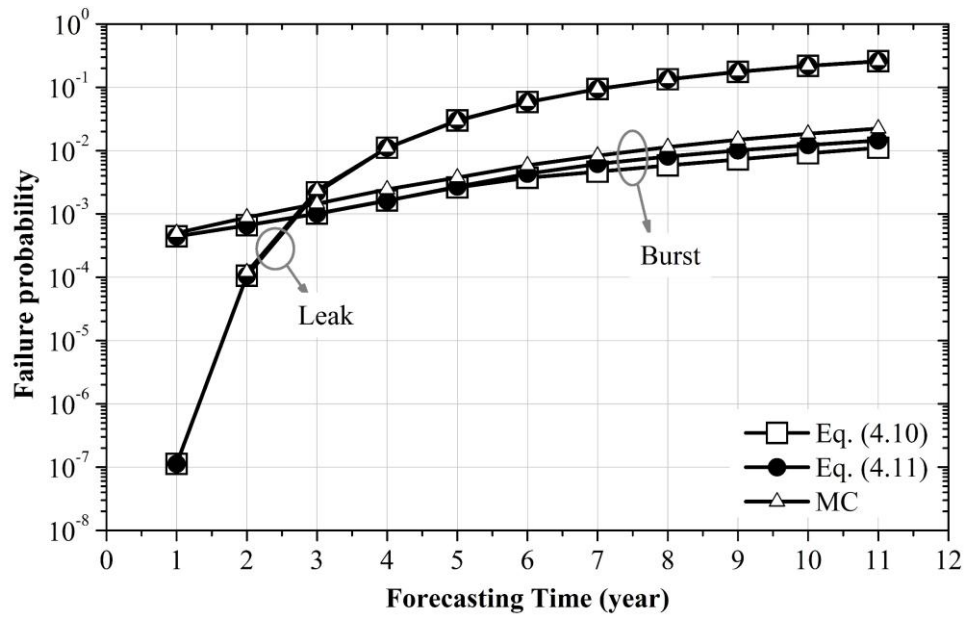
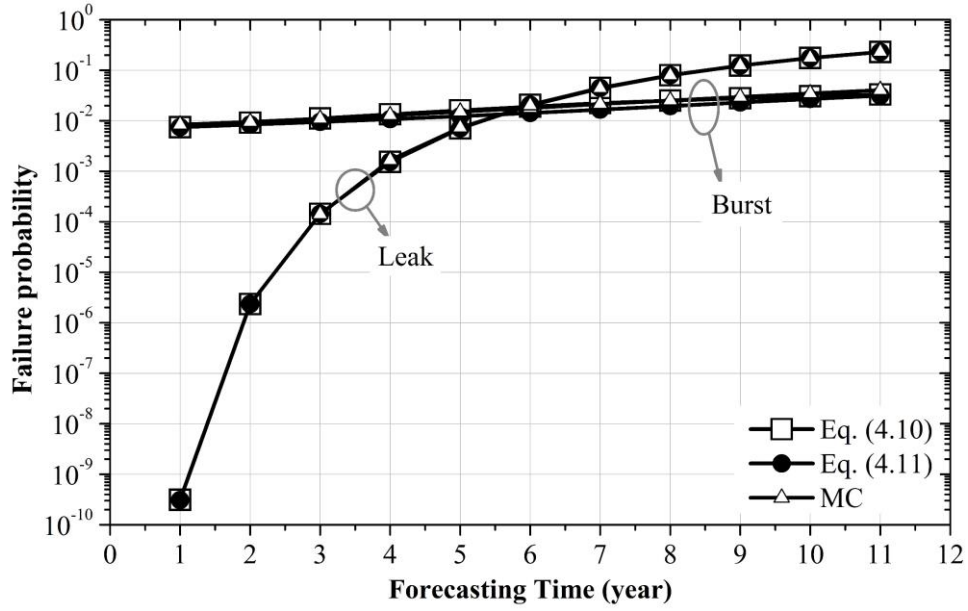
(e) Example 3; Large diameter; $\rho_1=\rho_2=0.2$ (f) Example 3; Large diameter; $\rho_1=\rho_2=0.8$

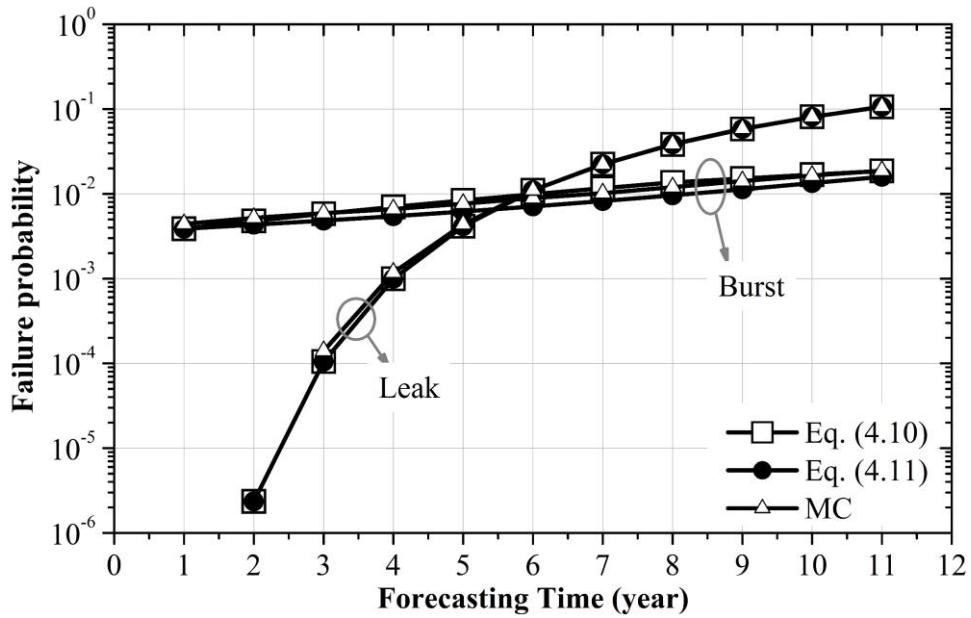
Figure 4.2 Probabilities of burst and small leak for examples 1, 2 and 3 based on the linear growth model for defect depth

(a) Example 1; Small diameter; $\rho_1=\rho_2=0.2$ (b) Example 1; Small diameter; $\rho_1=\rho_2=0.8$

(c) Example 2; Medium diameter; $\rho_1=\rho_2=0.2$ (d) Example 2; Medium diameter; $\rho_1=\rho_2=0.8$

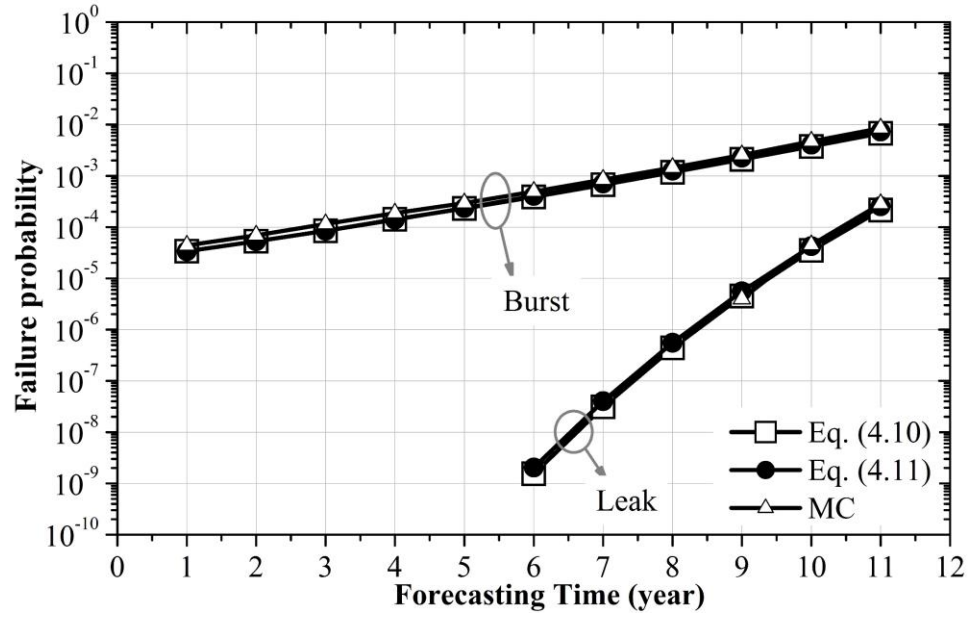
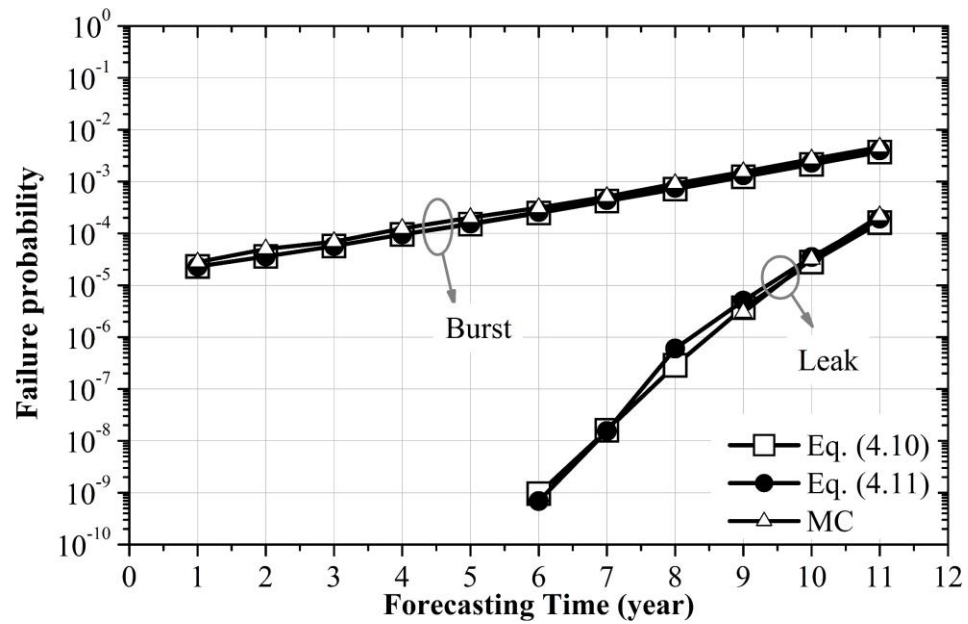


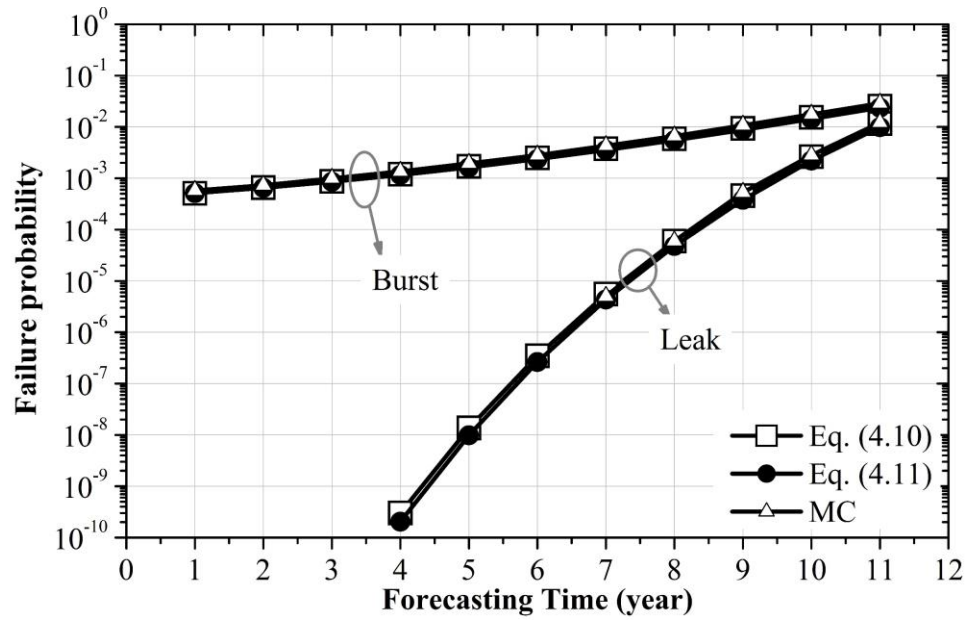
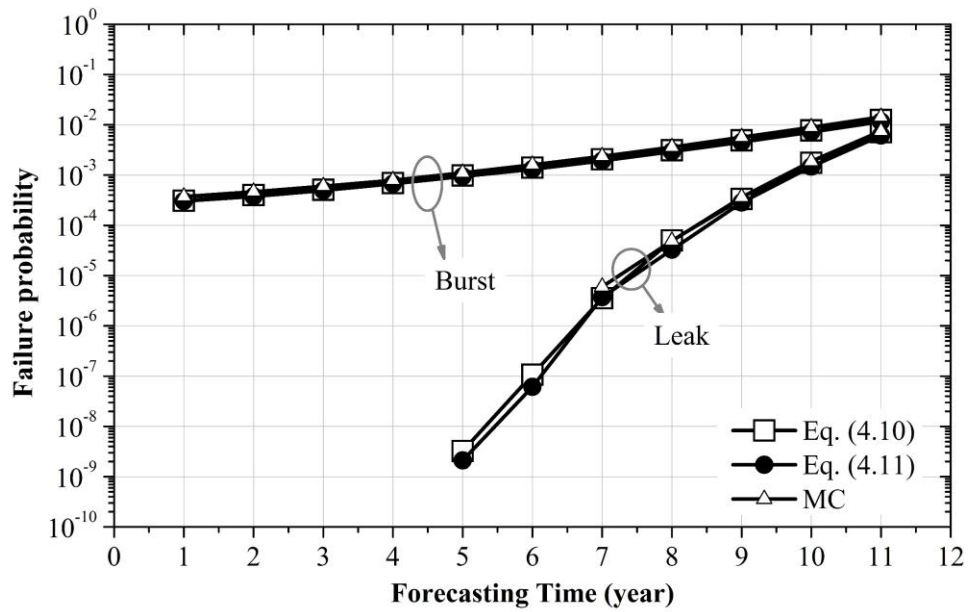
(e) Example 3; Large diameter; $\rho_1=\rho_2=0.2$



(f) Example 3; Large diameter; $\rho_1=\rho_2=0.8$

Figure 4.3 Probabilities of burst and small leak for examples 1, 2 and 3 based on the nonlinear growth model for defect depth

(a) Example 1; Small diameter; $\rho_1=0.2$ (b) Example 1; Small diameter; $\rho_1=0.8$

(c) Example 2; Medium diameter; $\rho_l=0.2$ (d) Example 2; Medium diameter; $\rho_l=0.8$

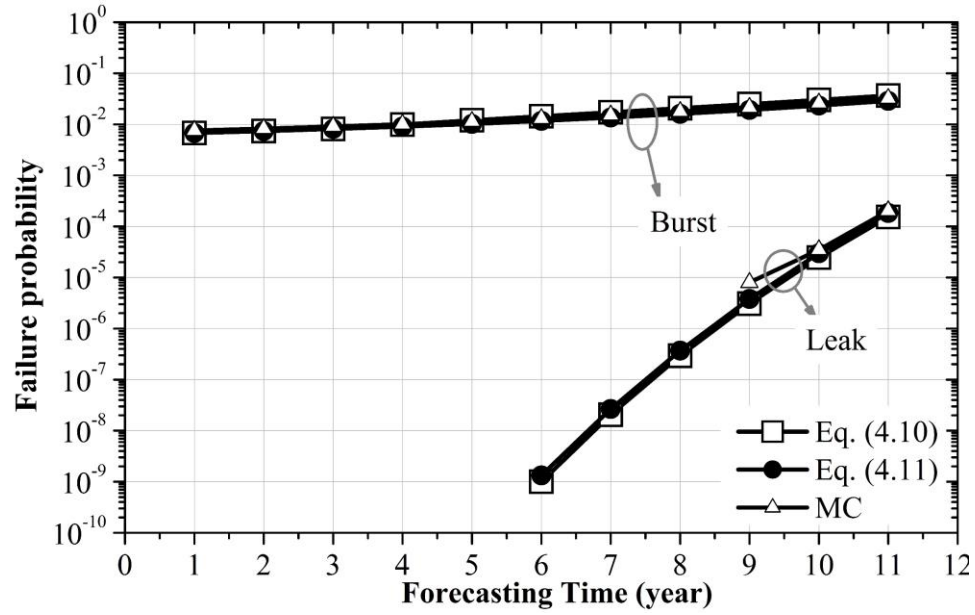
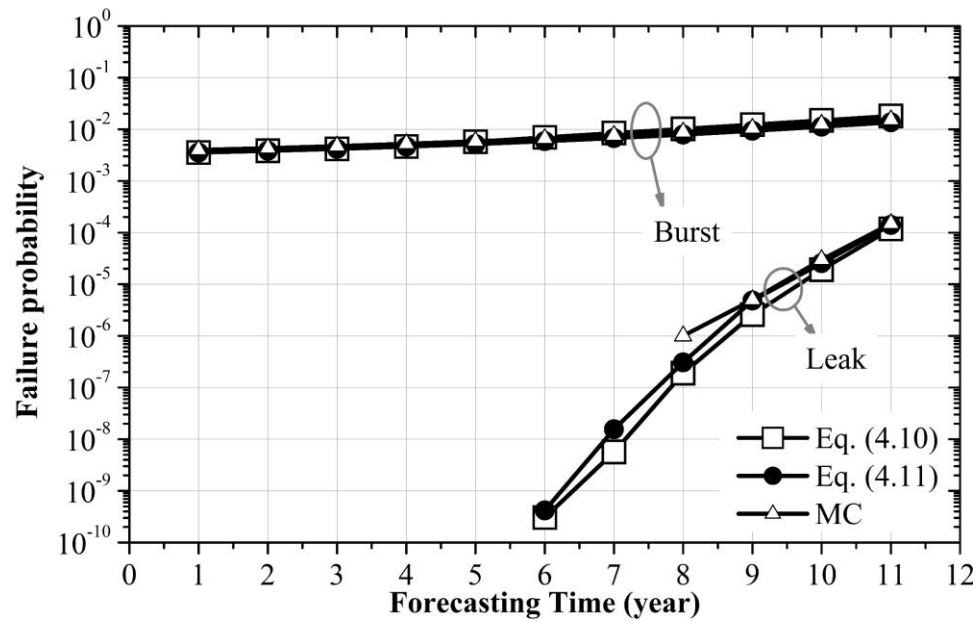
(e) Example 3; Large diameter; $\rho_1=0.2$ (f) Example 3; Large diameter; $\rho_1=0.8$

Figure 4.4 Probabilities of burst and small leak for examples 1, 2 and 3 based on the homogeneous gamma process-based growth model for defect depth

5 Importance Sampling-based System Reliability Analyses of Corroding Pipelines Considering Multiple Failure Modes

5.1 Introduction

The simple Monte Carlo simulation (MC) is the most straightforward approach to evaluate the time-dependent system reliability of corroding pipelines considering the small leak and burst failure modes (Zhou 2010; Zhou et al. 2012). However, this approach is in general time-consuming, especially if the failure probability is small (e.g. $\leq 10^{-6}$) and/or the number of pipelines to be analyzed is large. Leira et al. (2016) proposed an enhanced MC simulation technique to evaluate the probability of burst of a corroding pipeline containing multiple defects. The enhancement results from fitting a parametric probability function at moderately high failure levels and extrapolating the tail probability, thus improving the efficiency of the simulation. However, this approach is potentially subjected to tail sensitivity issues.

The efficiency of the simple MC simulation can be improved by using the importance sampling (IS) technique. The theory of the IS technique is well described in the literature (Schuëller and Stix 1987; Engelund and Rackwitz 1993; Melchers 1989). By using an appropriately selected IS density function, the IS-based simulation samples the failure domain more frequently and therefore achieves a higher efficiency in estimating the failure probability than the simple MC simulation. Studies on selecting the appropriate IS density functions for evaluating the system reliability of series and parallel systems have been reported in the literature (Schuëller and Stix 1987; Melchers 1989; Mori and Kato 2003; Patelli et al. 2011; Wang and Song 2016). Once a corroding pipeline joint fails, by small leak or burst, it is usually detected and repaired within a short time frame such as several days. It follows that the occurrence of small leak eliminates the potential occurrence of burst, and vice versa. Therefore, the small leak and burst should be considered as two competing failure modes in the system reliability analyses of corroding pipelines. However, the application of the IS technique to evaluate the time-dependent system reliability of corroding pipelines by considering the small leak and burst failure modes has, to our best knowledge, not been reported in the literature.

The objective of the work reported in this chapter is to explore the use of the IS technique to evaluate the time-dependent system reliability of corroding pipelines containing multiple active, stochastically dependent corrosion defects by considering the small leak and burst failure modes. The remainder of the chapter is organized as follows. Section 5.2 describes the limit state functions relevant to the small leak and burst failure modes for a corroding pipeline; Section 5.3 presents the methodologies for evaluating the system reliability of corroding pipelines based on the IS technique and selecting the IS density function; numerical examples are given in Section 5.4 to demonstrate the accuracy of the proposed methodology, followed by conclusions.

5.2 Formulations for Limit State Functions and Failure Probabilities

Consider a pipeline joint containing m ($m \geq 1$) active corrosion defects. The limit state function, $g_j^s(t)$, for the j -th ($j = 1, 2, \dots, m$) defect to penetrate the pipe wall as a function of time t is given by Zhou (2010)

$$g_j^s(t) = \varphi_0 w t_j - d_j(t) \quad (5.1)$$

where $w t_j$ denotes the pipe wall thickness at the j -th defect; $d_j(t)$ is the depth (i.e. in the through-pipe wall thickness direction) of the j -th defect at time t ; φ_0 ($\varphi_0 \leq 1$) is a reduction factor to account for that the remaining ligament of the pip wall may develop cracks that result in leaks for relatively deep corrosion defects (Al-Amin and Zhou 2014), and φ_0 is typically assumed to equal 0.8 (Al-Amin and Zhou 2014; Caleyó et al. 2002). The time-dependent limit state function, $g_j^b(t)$, for the severance of the remaining ligament at the j -th defect is given by Zhou (2010)

$$g_j^b(t) = p_{bj}(t) - p_j \quad (5.2)$$

where $p_{bj}(t)$ is the burst capacity pressure at the j -th defect at time t and p_j is the internal pressure at the j -th defect. In this chapter, p_j is considered a random variable as opposed to a stochastic process. Many empirical and semi-empirical models have been developed to evaluate the burst capacity pressure at a corrosion defect; a summary of these models

can be found in Zhou and Huang (2012). In this chapter, the model proposed by Leis and Stephens (1997) is adopted to calculate p_{bj} as follows:

$$p_{bj} = \xi_j \frac{2wt_j\sigma_{uj}}{D} \left[1 - \frac{d_j}{wt_j} \left(1 - \exp \left(\frac{-0.157l_j}{\sqrt{\frac{D(wt_j - d_j)}{2}}} \right) \right) \right] \quad (5.3)$$

where σ_u denotes the pipe ultimate tensile strength; ξ is the associated model error; D is the pipe outside diameter, and l denotes the length (i.e. in the longitudinal direction of the pipeline) of the defect. The subscript j for a given symbol indicates its association with the j -th defect. Similar to the defect depth, the defect length can also grow with time. For brevity, $p_{bj}(t)$, $d_j(t)$ and $l_j(t)$ are simply written as p_{bj} , d_j and l_j , respectively, in Eq. (5.3).

Let $P_s(t)$ and $P_b(t)$ denote the cumulative probabilities of small leak and burst of the pipeline joint, respectively, within a time interval $[0, t]$. Further let t_j^s denote the time at which the j -th defect just penetrates the pipe wall, and t_j^b denote the time at which plastic collapse takes place at the j -th defect due to the internal pressure. Because of the competing characteristics of the small leak and burst failure modes, $P_s(t)$ and $P_b(t)$ can be expressed in terms of t_j^s and t_j^b as follows:

$$P_s(t) = \text{Prob} \left[\left(0 \leq \min_j \{t_j^s\} \leq t \right) \cap \left(\min_j \{t_j^s\} < \min_j \{t_j^b\} \right) \right] \quad (5.4a)$$

$$P_b(t) = \text{Prob} \left[\left(0 \leq \min_j \{t_j^b\} \leq t \right) \cap \left(\min_j \{t_j^b\} < \min_j \{t_j^s\} \right) \right] \quad (5.4b)$$

where $\text{Prob}[\bullet]$ denotes the probability of an event, and the symbol “ \cap ” denotes the intersection of two events.

5.3 IS-based System Reliability Analyses of Corroding Pipelines

5.3.1 Overview of IS Technique

The failure probability, P_f , of an engineering system can be calculated as

$$P_f = \int_{\Omega(\mathbf{x})} f_{\mathbf{X}}(\mathbf{x}) d\mathbf{x} \quad (5.5)$$

where \mathbf{X} is a vector of random variables involved in the system; $f_{\mathbf{X}}(\mathbf{x})$ is the joint probability density function (PDF) of \mathbf{X} , and $\Omega(\mathbf{x})$ denotes the failure domain with \mathbf{x} being the value of \mathbf{X} . It is generally more advantageous to evaluate P_f in the standard normal space than in the original (i.e. \mathbf{X}) space due to the rotational symmetry of the joint standard normal PDF (Der Kiureghian 2005; Madsen 2006). To this end, \mathbf{X} is transformed to a vector of independent standard normal variate \mathbf{U} that has the same dimension as \mathbf{X} , and P_f is then given by

$$P_f = \int_{\Omega'(\mathbf{u})} f_{\mathbf{U}}(\mathbf{u}) d\mathbf{u} \quad (5.6)$$

where \mathbf{u} is the value of \mathbf{U} ; $\Omega'(\mathbf{u})$ is the failure domain in the standard normal space, and $f_{\mathbf{U}}(\mathbf{u})$ is the joint (standard normal) PDF of \mathbf{U} . The techniques for transforming \mathbf{X} to \mathbf{U} are described in many well-known references on the structural reliability theory (Melchers 1989; Der Kiureghian 2005; Madsen 2006). By applying the IS technique, P_f expressed by Eq. (5.6) can be evaluated as (Melchers 1989)

$$P_f \approx \frac{1}{N} \sum_{i=1}^N \frac{I(\mathbf{u}_i) f_{\mathbf{U}}(\mathbf{u}_i)}{h_{\mathbf{U}}(\mathbf{u}_i)} \quad (5.7)$$

where N is the total number of IS simulation trials; $h_{\mathbf{U}}(\mathbf{u})$ is the so-called importance sample density function; \mathbf{u}_i is the i -th random ($i = 1, 2, \dots, N$) sample generated from $h_{\mathbf{U}}(\mathbf{u})$, and $I(\mathbf{u}_i)$ is an index function that equals unity if \mathbf{u}_i falls in the failure domain and zero otherwise.

To define $h_{\mathbf{U}}(\mathbf{u})$, first consider the case where the failure domain of the system is characterized by a single limit state function, $g(\mathbf{x})$, with $g(\mathbf{x}) < 0$ and $g(\mathbf{x}) > 0$ representing the failure and safe domains, respectively. Let $G(\mathbf{u})$ denote the mapping of $g(\mathbf{x})$ in the standard normal (i.e. \mathbf{U}) space, with $G(\mathbf{u}) < 0$ and $G(\mathbf{u}) > 0$ representing the failure and safe domains, respectively in the \mathbf{U} space; $g(\mathbf{x}) = 0$ and $G(\mathbf{u}) = 0$ are known as the limit state surfaces in the \mathbf{X} and \mathbf{U} spaces, respectively. The importance sampling function $h_{\mathbf{U}}(\mathbf{u})$ for the single limit state function case can be determined by simply shifting $f_{\mathbf{U}}(\mathbf{u})$ to the so-

called design point \mathbf{u}^* (Melchers 1989; Schuëller and Stix 1987), i.e. $h_U(\mathbf{u}) = f_U(\mathbf{u} - \mathbf{u}^*)$, where \mathbf{u}^* is located on the limit state surface and has the shortest distance to the origin (Der Kiureghian 2005). Making $h_U(\mathbf{u})$ centred at \mathbf{u}^* is justified by the fact that \mathbf{u}^* is the point in the failure domain that has the highest probability density (Der Kiureghian 2005). The value of \mathbf{u}^* can be determined using the well-known first-order reliability method (FORM) (Der Kiureghian 2005), which is in essence a constrained optimization analyses with the constraint being $G(\mathbf{u}) = 0$, i.e. $\mathbf{u}^* = \arg \min \{\|\mathbf{u}\| \mid G(\mathbf{u}) = 0\}$, where $\|\mathbf{u}\| = \mathbf{u}^T \mathbf{u}$ (all vectors are assumed to be column vectors); T denotes transposition, and “arg min” is the argument of the minimization.

Consider now the case where the failure domain of the system is defined by a union of m ($m > 1$) limit state functions, i.e. $\Omega(\mathbf{x}) = \cup_{j=1}^m (g_j(\mathbf{x}) \leq 0)$, where $g_j(\mathbf{x})$ is the j -th ($j = 1, 2, \dots, m$) limit state function, and \cup denotes the union of events. Let $G_j(\mathbf{u})$ ($j = 1, 2, \dots, m$) denote the mapping of $g_j(\mathbf{x})$ in the \mathbf{U} space. Further let \mathbf{u}_j^* denote the design point associated with $G_j(\mathbf{u})$, i.e. $\mathbf{u}_j^* = \arg \min \{\|\mathbf{u}\| \mid G_j(\mathbf{u}) = 0\}$. The corresponding importance sampling function, $h_U(\mathbf{u})$, can be determined as a weighted average of m importance sampling functions, each of which is generated by shifting $f_U(\mathbf{u})$ to one of m design points \mathbf{u}_j^* ($j = 1, 2, \dots, m$) (Melchers 1989; Schuëller and Stix 1987) that is,

$$h_U(\mathbf{u}) = \sum_{j=1}^m w_j f_U(\mathbf{u} - \mathbf{u}_j^*) \quad (5.8)$$

where w_j is the weighting factor and can be evaluated as (Mori and Kato 2003; Schuëller and Stix 1987)

$$w_j = \Phi(-\|\mathbf{u}_j^*\|) / \sum_{k=1}^m \Phi(-\|\mathbf{u}_k^*\|) \quad (5.9)$$

where $\Phi(\bullet)$ is the standard normal cumulative distribution function. Note that the computational efficiency and robustness of the constrained optimization for determining \mathbf{u}_j^* can be significantly improved by using a methodology recently proposed in Chapter 2 if the number of random variables involved in each of the m limit state functions is much less than that involved in the system.

5.3.2 IS for Reliability Analyses of Corroding Pipelines

5.3.2.1 Single Defect

Consider first the IS-based time-dependent reliability analyses of a pipeline containing a single active corrosion defect. Note that \mathbf{X} in the context of the reliability analyses of corroding pipelines includes random variables representing the pipe properties, defect depth and length, and internal pressure, as reflected in the limit state functions $g^s(t)$ and $g^b(t)$ defined in Section 5.2. Following the descriptions in Section 5.3.1, we apply the IS technique in the standard normal space. To this end, let $G^s(t)$ and $G^b(t)$ denote the mapping of $g^s(t)$ and $g^b(t)$, respectively, in the standard normal space. The fact that both $G^s(t)$ and $G^b(t)$ are functions of \mathbf{u} in addition to t is made implicit to simplify the notation. As implied by Eq. (5.4), the evaluation of $P_s(t)$ and $P_b(t)$ is a problem of computing the probability of first excursion into the failure region associated with either small leak or burst within $[0, t]$. Therefore, the IS technique is employed to compute $P_s(t)$ and $P_b(t)$ incrementally; that is,

$$P_s(\tau + \Delta t) = P_s(\tau) + \Delta P_s(\tau, \Delta t) \quad (5.10a)$$

$$P_b(\tau + \Delta t) = P_b(\tau) + \Delta P_b(\tau, \Delta t) \quad (5.10b)$$

where $\Delta P_s(\tau, \Delta t)$ and $\Delta P_b(\tau, \Delta t)$ ($0 \leq \tau < t$) are incremental probabilities of small leak and burst, respectively, within a short time interval between τ and $\tau + \Delta t$. The evaluation of $P_s(0)$ and $P_b(0)$ can be straightforwardly carried out using, for example, the FORM (Der Kiureghian 2005). The IS technique is used to evaluate $\Delta P_s(\tau, \Delta t)$ and $\Delta P_b(\tau, \Delta t)$, and $P_s(t)$ and $P_b(t)$ can then be evaluated recursively using Eq. (5.10). Typically Δt in the range of half to one year is considered adequate given that the growth of corrosion defects on pipelines is in general a relatively slow process, i.e. on average no more than several percentages of the pipe wall thickness per year.

The evaluation of $\Delta P_s(\tau, \Delta t)$ is schematically illustrated in Fig. 5.1. The figure depicts three limit state surfaces, i.e. $G^s(\tau) = G^s(\tau + \Delta t) = G^b(\tau) = 0$, in the standard normal space, with the corresponding design points denoted by $\mathbf{u}^{l*}(\tau)$, $\mathbf{u}^{l*}(\tau + \Delta t)$ and $\mathbf{u}^{c*}(\tau)$, respectively. The failure region delineated by a given limit state surface is also indicated in Fig. 5.1.

Figures 5.1(a) and 5.1(b) represent two potential scenarios for evaluating $\Delta P_s(\tau, \Delta t)$, which is represented by the shaded area in each of the two figures. The IS density function for $\Delta P_s(\tau, \Delta t)$ can be chosen to be centred at the design point ($\mathbf{u}^{s*}(\tau, \Delta t)$) for $\Delta P_s(\tau, \Delta t)$, defined as point in the shaded area and has the shortest distance to the origin, i.e. the point of the highest probability density in the shaded area. To this end, $\mathbf{u}^{s*}(\tau, \Delta t)$ for the scenario depicted in Fig. 5.1(a) is the intersection between $G^b(\tau) = 0$ and $G^s(\tau + \Delta t) = 0$. On the other hand, $\mathbf{u}^{s*}(\tau, \Delta t)$ for the scenario depicted in Fig. 5.1(b) is the same as the design point for $G^s(\tau + \Delta t) = 0$, $\mathbf{u}^{l*}(\tau + \Delta t)$. For both scenarios, $\mathbf{u}^{s*}(\tau, \Delta t)$ can be obtained by solving the following constrained optimization problem: $\mathbf{u}^{s*}(\tau, \Delta t) = \arg \min\{\|\mathbf{u}\| \mid \Omega^s(\tau, \Delta t)\}$, where $\Omega^s(\tau, \Delta t) = \{G^s(\tau) > 0 \cap G^s(\tau + \Delta t) \leq 0 \cap G^b(\tau) \leq 0\}$.

Similarly, the IS density function for $\Delta P_b(\tau, \Delta t)$ is chosen to be centred at the design point ($\mathbf{u}^{b*}(\tau, \Delta t)$) for $\Delta P_b(\tau, \Delta t)$, where $\mathbf{u}^{b*}(\tau, \Delta t)$ is obtained as $\mathbf{u}^{b*}(\tau, \Delta t) = \arg \min\{\|\mathbf{u}\| \mid \Omega^b(\tau, \Delta t)\}$ with $\Omega^b(\tau, \Delta t) = \{G^b(\tau) > 0 \cap G^b(\tau + \Delta t) \leq 0 \cap G^s(\tau) \leq 0\}$. The values of $\Delta P_s(\tau, \Delta t)$ and $\Delta P_b(\tau, \Delta t)$ are then evaluated as follows:

$$\Delta P_s(\tau, \Delta t) \approx \frac{1}{N} \sum_{i=1}^N \frac{I_{(\tau, \Delta t)}^s(\mathbf{u}_i) f_U(\mathbf{u}_i)}{f_U(\mathbf{u}_i - \mathbf{u}^{s*}(\tau, \Delta t))} \quad (5.11a)$$

$$\Delta P_b(\tau, \Delta t) \approx \frac{1}{N} \sum_{i=1}^N \frac{I_{(\tau, \Delta t)}^b(\mathbf{u}_i) f_U(\mathbf{u}_i)}{f_U(\mathbf{u}_i - \mathbf{u}^{b*}(\tau, \Delta t))} \quad (5.11b)$$

where $I_{(\tau, \Delta t)}^s(\mathbf{u}_i)$ and $I_{(\tau, \Delta t)}^b(\mathbf{u}_i)$ are index functions associated with $\Delta P_s(\tau, \Delta t)$ and $\Delta P_b(\tau, \Delta t)$, respectively; $I_{(\tau, \Delta t)}^s(\mathbf{u}_i)$ equals unity if \mathbf{u}_i is in $\Omega^s(\tau, \Delta t)$ and zero otherwise, and $I_{(\tau, \Delta t)}^b(\mathbf{u}_i)$ equals unity if \mathbf{u}_i is in $\Omega^b(\tau, \Delta t)$ and zero otherwise.

If the growth of the defect is extremely slow such that the failure domains corresponding to the incremental probabilities of small leak and burst become very small for the typical time increment (e.g. one year), a significant number of IS simulation trials may be required to generate adequate number of samples that fall into the incremental failure domains. Alternatively, a larger time increment may be used.

5.3.2.2 Multiple Defects

Now consider the time-dependent reliability analyses of a pipeline containing m ($m > 1$) active corrosion defects, whereby $G_j^s(t)$ and $G_j^b(t)$ denote mapping of $g_j^s(t)$ and $g_j^b(t)$ in the standard normal space. Similar to the approach described in the previous section, the IS technique is employed to evaluate $\Delta P_s(\tau, \Delta t)$ and $\Delta P_b(\tau, \Delta t)$ for the pipeline. Following Eq. (5.8), we define the IS density function for $\Delta P_s(\tau, \Delta t)$, $h_U^s(\mathbf{u}; \tau, \Delta t)$, as the weighted average of the IS density functions for $\Delta P_{s,j}(\tau, \Delta t)$ ($j = 1, 2, \dots, m$), where $\Delta P_{s,j}(\tau, \Delta t)$ is the incremental probability of small leak between τ and $\tau + \Delta t$ for the j -th defect; the IS density function for $\Delta P_b(\tau, \Delta t)$, $h_U^b(\mathbf{u}; \tau, \Delta t)$, is defined as the weighted average of the IS density functions for $\Delta P_{b,j}(\tau, \Delta t)$ ($j = 1, 2, \dots, m$), where $\Delta P_{b,j}(\tau, \Delta t)$ is the incremental probability of burst between τ and $\tau + \Delta t$ for the j -th defect. That is,

$$h_U^s(\mathbf{u}; \tau, \Delta t) = \sum_{j=1}^m w_j^s(\tau, \Delta t) f_U(\mathbf{u} - \mathbf{u}_j^{s*}(\tau, \Delta t)) \quad (5.12a)$$

$$h_U^b(\mathbf{u}; \tau, \Delta t) = \sum_{j=1}^m w_j^b(\tau, \Delta t) f_U(\mathbf{u} - \mathbf{u}_j^{b*}(\tau, \Delta t)) \quad (5.12b)$$

where $w_j^s(\tau, \Delta t)$ and $w_j^b(\tau, \Delta t)$ ($j = 1, 2, \dots, m$) are weighting factors for $h_U^s(\mathbf{u}; \tau, \Delta t)$ and $h_U^b(\mathbf{u}; \tau, \Delta t)$, respectively, and $\mathbf{u}_j^{s*}(\tau, \Delta t)$ and $\mathbf{u}_j^{b*}(\tau, \Delta t)$ are design points for $\Delta P_{s,j}(\tau, \Delta t)$ and $\Delta P_{b,j}(\tau, \Delta t)$, respectively. Note that the weighting factors should reflect the relative contributions of individual defects to the incremental probabilities of small leak or burst. To this end, we propose the following empirical equations to compute the weighting factors:

$$w_j^s(\tau, \Delta t) = \begin{cases} \frac{\Phi(-\|\mathbf{u}_j^{s*}(\tau, \Delta t)\|) - \Phi(-\|\mathbf{u}_j^{s*}(\tau - \Delta t, \Delta t)\|)}{\sum_{k=1}^m (\Phi(-\|\mathbf{u}_k^{s*}(\tau, \Delta t)\|) - \Phi(-\|\mathbf{u}_k^{s*}(\tau - \Delta t, \Delta t)\|))} & \tau > 0 \\ \frac{\Phi(-\|\mathbf{u}_j^{s*}(\tau, \Delta t)\|)}{\sum_{k=1}^m \Phi(-\|\mathbf{u}_k^{s*}(\tau, \Delta t)\|)} & \tau = 0 \end{cases} \quad (5.13a)$$

$$w_j^b(\tau, \Delta t) = \begin{cases} \frac{\Phi(-\|\mathbf{u}_j^{b*}(\tau, \Delta t)\|) - \Phi(-\|\mathbf{u}_j^{b*}(\tau - \Delta t, \Delta t)\|)}{\sum_{k=1}^m (\Phi(-\|\mathbf{u}_k^{b*}(\tau, \Delta t)\|) - \Phi(-\|\mathbf{u}_k^{b*}(\tau - \Delta t, \Delta t)\|))} & \tau > 0 \\ \frac{\Phi(-\|\mathbf{u}_j^{b*}(\tau, \Delta t)\|)}{\sum_{k=1}^m \Phi(-\|\mathbf{u}_k^{b*}(\tau, \Delta t)\|)} & \tau = 0 \end{cases} \quad (5.13b)$$

where $\mathbf{u}_j^{s*}(\tau - \Delta t, \Delta t)$ and $\mathbf{u}_j^{b*}(\tau - \Delta t, \Delta t)$ are the design points for $\Delta P_{s,j}(\tau - \Delta t, \Delta t)$ and $\Delta P_{b,j}(\tau - \Delta t, \Delta t)$ ($j = 1, 2, \dots, m$), respectively. Given $h_{\mathbf{U}}^s(\mathbf{u}; \tau, \Delta t)$ and $h_{\mathbf{U}}^b(\mathbf{u}; \tau, \Delta t)$, the IS formulations for evaluating $\Delta P_s(\tau, \Delta t)$ and $\Delta P_b(\tau, \Delta t)$ are then given by

$$\Delta P_s(\tau, \Delta t) \approx \frac{1}{N} \sum_{i=1}^N \frac{I_{(\tau, \Delta t)}^s(\mathbf{u}_i) f_{\mathbf{U}}(\mathbf{u}_i)}{h_{\mathbf{U}}^s(\mathbf{u}; \tau, \Delta t)} \quad (5.14a)$$

$$\Delta P_b(\tau, \Delta t) \approx \frac{1}{N} \sum_{i=1}^N \frac{I_{(\tau, \Delta t)}^b(\mathbf{u}_i) f_{\mathbf{U}}(\mathbf{u}_i)}{h_{\mathbf{U}}^b(\mathbf{u}; \tau, \Delta t)} \quad (5.14b)$$

where $I_{(\tau, \Delta t)}^s$ equals unity if \mathbf{u}_i is in the domain defined by $\left(\min_j \{G_j^s(\tau)\} \geq 0 \cap \min_j \{G_j^s(\tau + \Delta t)\} \leq 0 \cap \min_j \{G_j^b(\tau)\} \geq 0 \right)$ ($j = 1, 2, \dots, m$) and zero otherwise, and $I_{(\tau, \Delta t)}^b$ equals unity if \mathbf{u}_i is in the domain defined by $\left(\min_j \{G_j^b(\tau)\} \geq 0 \cap \min_j \{G_j^b(\tau + \Delta t)\} \leq 0 \cap \min_j \{G_j^s(\tau)\} \geq 0 \right)$ and zero otherwise.

5.4 Numerical Examples

5.4.1 General

The proposed IS technique is employed to evaluate the reliability of four examples that are representative of natural gas transmission pipelines in the US. The nominal wall thickness, wt_n , of a gas pipeline in the US is in general determined as follows (ASME B31.8 2016):

$$wt_n = \frac{P_0 D}{2 \cdot F \cdot SMYS} \quad (5.15)$$

where P_0 and D are the nominal operating pressure and outside pipe diameter, respectively; SMYS is the specified minimum yield strength, and F ($F < 1$) is the design factor. Depending on the population density in the vicinity of the pipeline, it is categorized as Class 1, 2, 3 or 4, whereby Class 1 is associated with the lowest population density (e.g. farmland and desert) and Class 4 is associated with the highest population density (e.g. city centre). The design factor F equals 0.72, 0.6, 0.5 or 0.4 for Class 1, 2, 3 or 4, respectively (ASME B31.8 2016). The four pipeline examples are selected to be representative of gas

pipelines of four different classes. The basic attributes of the pipelines are summarized in Table 5.1, where SMTS denotes the specified minimum tensile strength.

It is assumed, somewhat arbitrarily, that each pipeline contains ten active corrosion defects that have been detected and sized by a recently run ILI, although the proposed methodology can easily deal with cases with larger numbers of defects. The probabilities of small leak and burst of the pipelines are then evaluated for a period of ten years starting from the time of the recent inspection (i.e. time zero) by taking into account the growth of the corrosion defects. Two different growth models are considered for the defect depth, i.e. the linear and homogeneous gamma process-based models (Zhou 2010; Van Noortwijk 2009). For the linear growth model, the depth of the j -th defect ($j = 1, 2, \dots, 10$) at time t , $d_j(t)$, is given by

$$d_j(t) = d_{0j} + g_{dj}t \quad (5.16)$$

where d_{0j} is the initial depth of the j -th defect and can be inferred from the inspection result, and g_{dj} is the constant but uncertain depth growth rate associated with the j -th defect. For the gamma process-based growth model, $d_j(t)$ ($j = 1, 2, \dots, 10$) is given by

$$d_j(t) = d_{0j} + d_{gj}(t) \quad (5.17)$$

where $d_{gj}(t)$ denotes the gamma process that characterizes the depth growth of the j -th defect. For simplicity, only the linear growth model is considered for the defect length, i.e.

$$l_j(t) = l_{0j} + g_{lj}t \quad (5.18)$$

where l_{0j} is the initial length of the j -th defect can be inferred by the inspection result, and g_{lj} is the length growth rate associated with the j -th defect.

The professional factor φ_0 in the limit state function g_j^S (Eq. (5.1)) is set to be 0.8 in the reliability analyses. The probabilistic characteristics of the parameters involved in the analyses, except for g_{dj} and $d_{gj}(t)$ ($j = 1, 2, \dots, 10$), are summarized in Table 5.2. The probabilistic characteristics of g_{dj} and $d_{gj}(t)$ are described in Sections 5.4.2 and 5.4.3, respectively. Note that the uncertainties in the defect initial depth and length reflect the

measurement errors associated with the inspection tool. The pipe wall thicknesses at different defects are assumed to be identical, i.e. represented by a single random variable. The same assumption also applies to the tensile strength σ_{uj} , internal pressure p_j and model error ξ_j . The initial depths (lengths) of different defects are assumed to be mutually independent. Furthermore, g_{lj} ($j = 1, 2, \dots, 10$) are assumed to be independent identically distributed for a given example.

The time step Δt is taken as one year in the IS analyses, and 1,000 IS simulation trials are used to evaluate each of $\Delta P_{s,j}(\tau, \Delta t)$ and $\Delta P_{b,j}(\tau, \Delta t)$ ($\tau = 0, 1, 2, \dots$ and $j = 1, 2, \dots, 10$), respectively. The sequential quadratic programming (SQP) algorithm, SNOPT (Sparse Nonlinear OPTimizer) (Gill et al. 2005), is employed to evaluate $\mathbf{u}_j^{s*}(\tau, \Delta t)$ and $\mathbf{u}_j^{b*}(\tau, \Delta t)$ ($j = 1, 2, \dots, 10$) for the determination of the corresponding IS density functions. Finally, to demonstrate the accuracy of the proposed IS technique, the simple Monte Carlo (MC) analyses is performed to evaluate benchmark failure probabilities for all the cases analyzed, with the number of simulation trials equal to 10^7 for each case.

5.4.2 Linear Growth Model for Defect Depth

For the linear growth model, it is assumed that g_{dj} ($j = 1, 2, \dots, 10$) are independent identically Weibull distributed for a given pipeline example. The COV of g_{dj} equals 50% for all four pipelines, whereas the mean of g_{dj} equals 0.4, 0.3, 0.2 and 0.2 mm/year for Examples 1, 2, 3 and 4, respectively. It is further assumed that the depth and length growth rates at the same defect are correlated with a correlation coefficient (ρ_1) equal to 0.5. Since both the depth and length growth rates are non-normally distributed, ρ_1 should be modified, e.g. using the empirical equation proposed by Der Kiureghian and Liu (1986) for the Nataf transformation, to estimate the corresponding correlation coefficient in the normal space. Note that the correlation coefficients in the normal and original spaces are in general similar; therefore, $\rho_1 = 0.5$ is used in the normal space for simplicity.

Figure 5.2 depicts the failure probabilities of the four pipeline examples obtained from IS and simple MC analyses by considering a single defect only with the corresponding mean of the initial defect depth equal to $0.2wt_n$. Figure 5.3 depicts the failure probabilities of the

four pipelines by considering all ten defects. Both figures indicate that the failure probabilities obtained from the proposed IS technique are in excellent agreement with those obtained from the simple MC analyses. To investigate the sensitivity of the failure probabilities to the value of ρ_1 , failure probabilities of Example 1 are evaluated using the IS technique and simple MC simulation for $\rho_1 = 0.2, 0.4, 0.7$ and 0.9 , respectively. The results (Fig. 5.4) again demonstrate the excellent accuracy of the proposed IS technique. Figure 5.4 indicates that the probability of small leak is practically independent of the value of ρ_1 , which is not unexpected given that the limit state function for small leak is independent of the defect length. On the other hand, the probability of burst increases markedly as ρ_1 increases from 0.2 to 0.9.

5.4.3 Gamma Process-based Growth Model for Defect Depth

The homogenous gamma process $d_{gj}(t)$ is defined by its shape parameter a and rate parameter b (Van Noortwijk 2009). At a given time t , $d_{gj}(t)$ is gamma distributed with the corresponding PDF, $F(d_{gj}(t)|at, b)$, given by

$$F(d_{gj}(t)|at, b) = b^{at} (d_{gj}(t))^{\alpha t - 1} \exp(-bd_{gj}(t)) / \Gamma(at) \quad (5.19)$$

where a and b are the parameters of the gamma process; $\Gamma(\bullet)$ denotes the gamma function. An important property of the gamma process is that it has independent gamma distributed increments over disjoint time intervals (Van Noortwijk 2009). For each of the four examples, $d_{gj}(t)$ ($j = 1, 2, \dots, 10$) at different defects are assumed to be identical and correlated. Let μ and ν denote, respectively, the mean and COV of the depth growth within one year. It follows from the properties of the gamma process that $\alpha = 1/\nu^2$ and $b = 1/(\mu\nu^2)$ (Van Noortwijk 2009). The values of μ are assumed to be 0.4, 0.3, 0.2 and 0.2 mm/year for Examples 1, 2, 3 and 4, respectively, whereas ν is assumed to equal 50% for all four examples (i.e. the same as the means and COVs of the growth rates assumed in the linear growth model). This leads to $a = 4$ for all four examples, and $b = 10, 13.33, 20$ and 20 (mm/year)⁻¹ for Examples 1, 2, 3 and 4, respectively.

The correlation between $d_{gj}(t)$ and $d_{gk}(t)$ ($j, k = 1, 2, \dots, 10; j \neq k$) for a given example is established by assuming that the annual increments of $d_{gj}(t)$ and $d_{gk}(t)$, denoted by $d_{gj}(1)$ and $d_{gk}(1)$ respectively, are coupled by the Gaussian copula (Nelsen 2006) characterized by a correlation coefficient (ρ_2) equal to 0.5. For simplicity, the depth and length growths for a given defect are assumed to be independent in the analyses. The analyses results are shown in Fig. 5.5 for the single defect case (with the mean of the initial defect depth equal to $0.2wt_n$) and in Fig. 5.6 by considering all ten defects. Due to the limited number (10^7) of simulation trials, failure probabilities obtained from the MC analyses for Examples 3 and 4 are available at year 10 only as shown in Fig. 5.5. Figures 5.5 and 5.6 indicate the excellent accuracy of the proposed IS technique compared with the MC analyses. The sensitivity of the failure probability to the value of ρ_2 is depicted in Fig. 5.7 for Example 1 with ρ_2 equal to 0.2, 0.4, 0.7 and 0.9, respectively. These results indicate that the failure probability is insensitive to the correlation among the depth growths of different defects.

5.4.4 Computational Efficiency and Variability of the Failure Probability Estimate

To illustrate the efficiency of the proposed IS-based methodology, the computational costs of the proposed methodology and simple MC analysis are compared. It is noted that the dominant component of the computational cost in both analyses is the cost of repeated evaluations of the limit state functions, i.e. function calls (Dubourg et al. 2013; Echard et al. 2013; Zhao et al. 2015). The numbers of function calls associated with the IS-based and simple MC analyses are therefore compared for the analysis case of Example 1 with ten corrosion defects and linear defect depth growth (the corresponding failure probabilities are shown in Fig. 5.3(a)). The fact that failure probabilities for this example are relatively high ($> 10^{-4}$) after year four implies that the number of simulation trials (10^7) used in the simple MC analysis is unnecessarily large for evaluating the failure probabilities after year four. To avoid unfairly penalizing the efficiency of the simple MC analysis, the comparison is based on the total number of function calls up to year four for the IS-based and simple MC analyses. The IS-based analysis involves a total of 312,655 function calls, which include 72,655 calls involved in the constrained optimization for finding the design points and 2.4×10^5 calls involved in the IS-based simulation. In contrast, the simple MC analysis

involves a total of 8×10^8 function calls. Therefore, the number of function calls associated with the IS-based analysis is approximately 0.04% of that involved in the simple MC analysis. This demonstrates the excellent efficiency of the IS-based methodology.

The variability of the failure probabilities evaluated using the IS-based methodology and simple MC analysis is also compared for the same example as described above. To this end, the IS-based analysis is repeated 30 times (each time with a different random seed in the simulation) for the example. This process generates an ensemble of time-dependent failure probabilities (i.e. 30 sets of probabilities of small leak and 30 sets of probabilities of burst), which allow the estimation of COV values associated with the failure probabilities evaluated. The COV values associated with the failure probabilities evaluated from the simple MC analysis are estimated in the same fashion. The COV values corresponding to these two analyses are compared (up to year 6) in Table 5.3. The table shows that the variability of the probabilities of small leak obtained from the IS-based analysis is in most case markedly lower than that from the simple MC analysis. The variability of the probabilities of burst obtained from the IS-based analysis is comparable to that of the probabilities of burst obtained from the simple MC analysis except for year four, at which the former is markedly higher than the latter. Figure 5.8 depicts the minimum, mean and maximum values of the set of 30 probabilities of burst obtained from the repeated IS-based analyses. Although the range of the probability of burst at year four is relatively large as shown in Fig. 5.8, it is well acceptable from practical perspective.

5.5 Conclusions

An IS-based methodology is proposed in this chapter to evaluate the time-dependent system reliability of pressurized steel pipelines containing multiple active corrosion defects. The methodology considers the pipe joint as a series system with two competing failure modes, i.e. small leak and burst, and takes into account potential correlations among failures at different defects. The IS technique is applied in the standard normal space to evaluate the probabilities of small leak and burst of the pipe joint incrementally over time. The IS density functions for small leak and burst, respectively, are constructed as the weighted averages of the corresponding IS density functions for individual defects. Simple empirical equations for evaluating the weighting factors are proposed. The IS density

function for small leak (burst) of a given defect is centred at the corresponding design point, i.e. the point that is in the incremental domain for small leak (burst) and closest to the origin of the standard normal space.

The application of the proposed methodology is illustrated using four pipeline examples that are representative of onshore natural gas transmission pipelines in the US. Two models are employed to characterize the growth of the defect depth in the numerical examples: the constant growth rate model and homogeneous gamma process model. The probabilities of small leak and burst are evaluated using the proposed methodology over a time period of 10 years and compared with those evaluated using the simple Monte Carlo analyses. The comparison demonstrates the excellent accuracy and efficiency of the proposed methodology for all four examples. Analyses are further carried out to investigate the sensitivity of the system reliability with respect to the correlation between the growths of defect depth and length and correlations among the depth growths of different defects on the same pipe joint. Finally, a comparison study regarding the calls to limit state functions are conducted with the results showing that the usage of IS significantly reduces the number of calls.

5.6 References

Al-Amin, M., and Zhou, W. (2014). Evaluating the system reliability of corroding pipelines based on inspection data. *Structure and Infrastructure Engineering*, 10(9), 1161-1175.

ASME B31.8 (2016): Gas transmission and distribution piping systems. Three Park Avenue, New York, USA: American Society of Mechanical Engineers (ASME)

Der Kiureghian, A. (2005). First- and second-order reliability methods. *Engineering design reliability handbook: Chapter 14*, E. Nikolaidis et al. Eds., CRC Press, Boca Raton, Fla.

Der Kiureghian, A., and Liu, P. L. (1986). Structural reliability under incomplete probability information. *Journal of Engineering Mechanics*, 112(1), 85-104.

Dubourg, V., Sudret, B., and Deheeger, F. (2013). Metamodel-based importance sampling for structural reliability analysis. *Probabilistic Engineering Mechanics*, 33, 47-57.

Echard, B., Gayton, N., Lemaire, M., and Relun, N. (2013). A combined importance sampling and kriging reliability method for small failure probabilities with time-demanding numerical models. *Reliability Engineering and System Safety*, 111, 232-240.

Engelund, S., and Rackwitz, R. (1993). A benchmark study on importance sampling techniques in structural reliability. *Structural safety*, 12(4), 255-276.

Gill, P. E., Murray, W., and Saunders, M. A. (2005). SNOPT: An SQP algorithm for large-scale constrained optimization. *SIAM review*, 47(1), 99-131.

Leira, B. J., Næss, A., and Næss, O. E. B. (2016). Reliability analyses of corroding pipelines by enhanced Monte Carlo simulation. *International Journal of Pressure Vessels and Piping*, 144, 11-17.

Leis, B. N., and Stephens, D. R. (1997). An alternative approach to assess the integrity of corroded line pipe-part I: current status. In the Seventh International Offshore and Polar Engineering Conference. International Society of Offshore and Polar Engineers.

Madsen, H. O., Krenk, S., and Lind, N. C. (2006). *Methods of structural safety*. Courier Corporation.

Melchers, R. E. (1989). Importance sampling in structural systems. *Structural safety*, 6(1), 3-10.

Mori, Y., and Kato, T. (2003). Multinormal integrals by importance sampling for series system reliability. *Structural Safety*, 25(4), 363-378.

Nelsen, R. B. (2006). *An introduction to copulas*, 2nd. New York: SpringerScience Business Media.

Patelli, E., Pradlwarter, H. J., and Schuëller, G. I. (2011). On multinormal integrals by importance sampling for parallel system reliability. *Structural Safety*, 33(1), 1-7.

Schuëller, G. I., and Stix, R. (1987). A critical appraisal of methods to determine failure probabilities. *Structural Safety*, 4(4), 293-309.

Van Noortwijk, J. M. (2009). A survey of the application of gamma processes in maintenance. *Reliability Engineering and System Safety*, 94(1), 2-21.

Wang, Z., and Song, J. (2016). Cross-entropy-based adaptive importance sampling using von Mises-Fisher mixture for high dimensional reliability analyses. *Structural Safety*, 59, 42-52.

Zhao, H., Yue, Z., Liu, Y., Gao, Z., and Zhang, Y. (2015). An efficient reliability method combining adaptive importance sampling and Kriging metamodel. *Applied Mathematical Modelling*, 39(7), 1853-1866.

Zhou, W. (2010). System reliability of corroding pipelines. *International Journal of Pressure Vessels and Piping*, 87(10), 587-595.

Zhou, W., Hong, H. P., and Zhang, S. (2012). Impact of dependent stochastic defect growth on system reliability of corroding pipelines. *International Journal of Pressure Vessels and Piping*, 96, 68-77.

Zhou, W., and Huang, G. X. (2012). Model error assessments of burst capacity models for corroded pipelines. *International Journal of Pressure Vessels and Piping*, 99, 1-8.

Table 5.1 Basic attributes of pipeline examples

Example	Class	F	D (mm)	wt_n (mm)	SMTS (MPa)	SMYS (MPa)	P_0 (MPa)
1	1	0.72	914	13.14	565	483	10
2	2	0.6	610	8.62	517	413	7
3	3	0.5	508	7.38	517	413	6
4	4	0.4	406	7.07	455	359	5

Table 5.2 Probabilistic characteristics of parameters involved in the reliability analyses

Parameter	Distribution	Mean	Coefficient of Variation (COV) (%)
D/D_n	Deterministic	1.0	-
wt_j/wt_n	Normal	1.0	1.5
σ_{uj}/SMTS	Lognormal	1.09	3.0
p_j/p_0	Gumbel	1.0	3.0
d_{0j}/wt_n ($j = 1 - 5$)	Normal	0.2	20.0
($j = 6 - 10$)		0.3	
l_{0j} (mm) ($j = 1 - 10$)	Normal	50.0	20.0
g_{lj} (mm/year) ($j = 1 - 10$)	Lognormal	5.0	50.0
ξ_j	Lognormal	1.0	10.0

Table 5.3 COV values of the failure probabilities obtained from IS-based and simple MC

Forecasting time (year)	Burst		Small leak	
	IS	MC	IS	MC
1	0.13	0.12	0.09	-
2	0.13	0.09	0.06	4.47
3	0.12	0.05	0.05	0.28
4	0.23	0.03	0.08	0.02
5	0.09	0.01	0.07	0.01
6	0.07	0.003	0.06	0.001

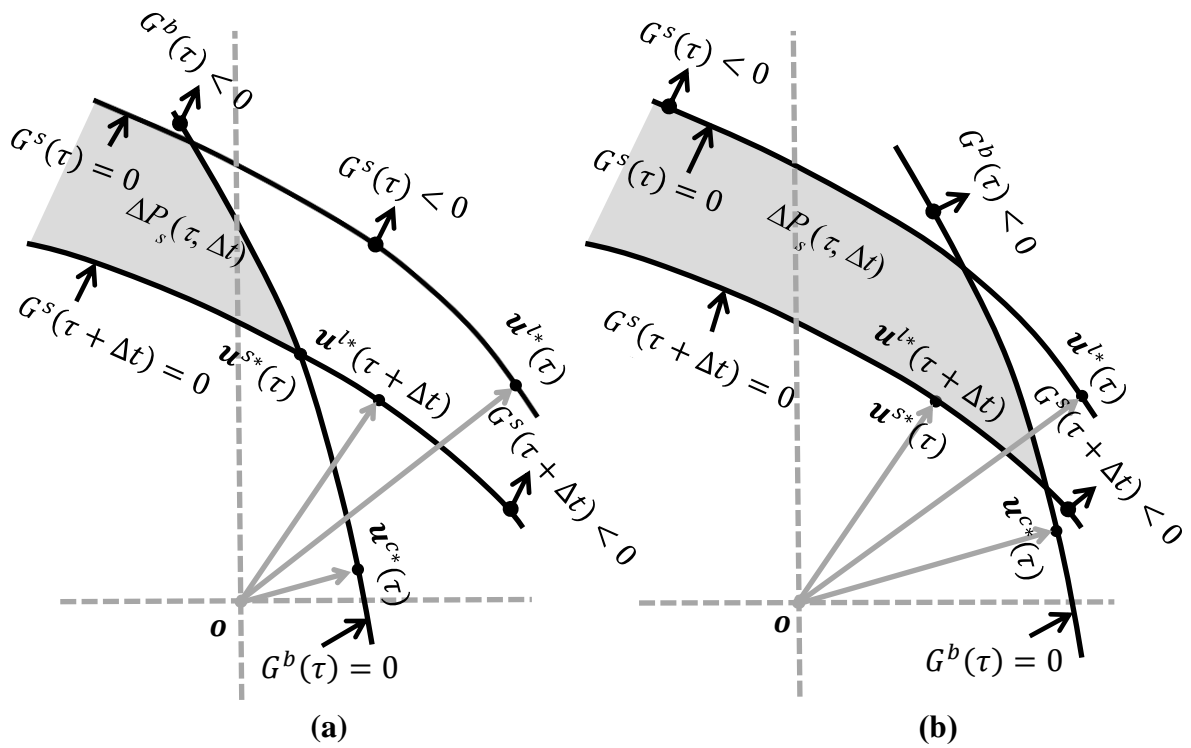
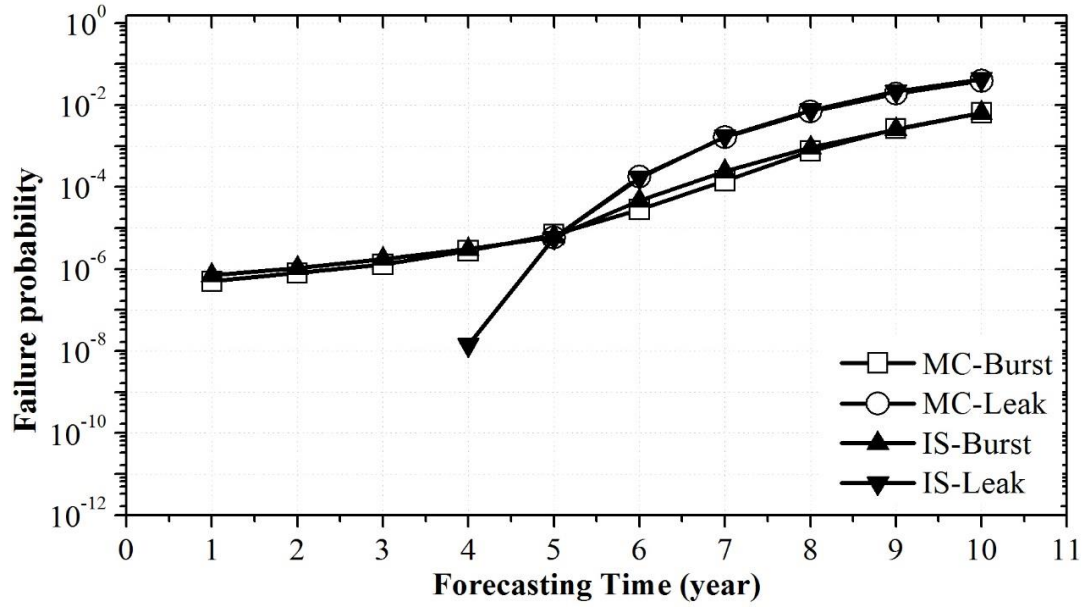
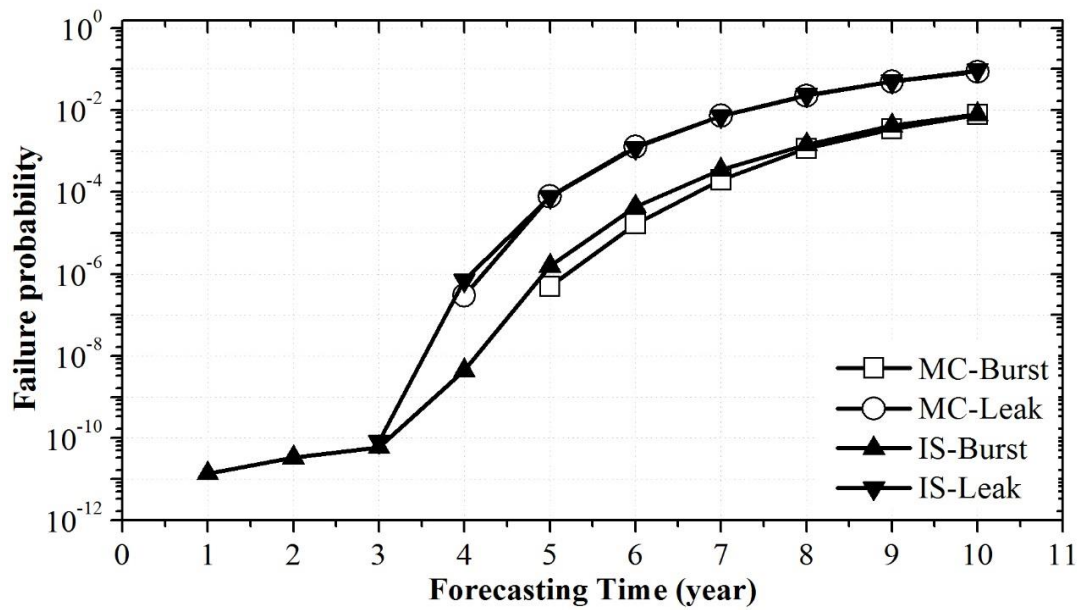


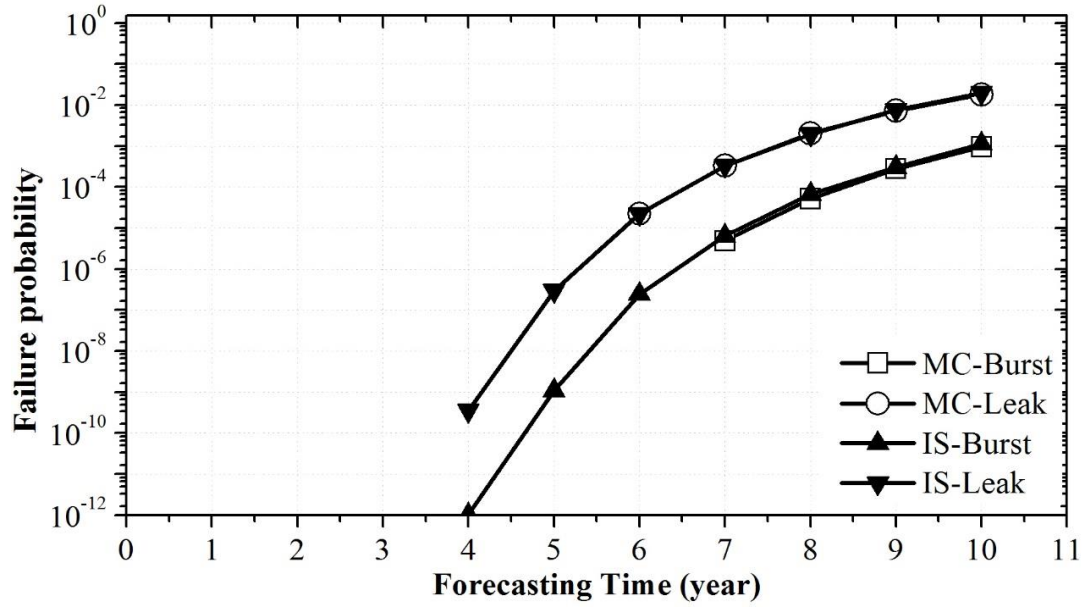
Figure 5.1 Geometry descriptions of $\Delta P_s(\tau, \Delta t)$



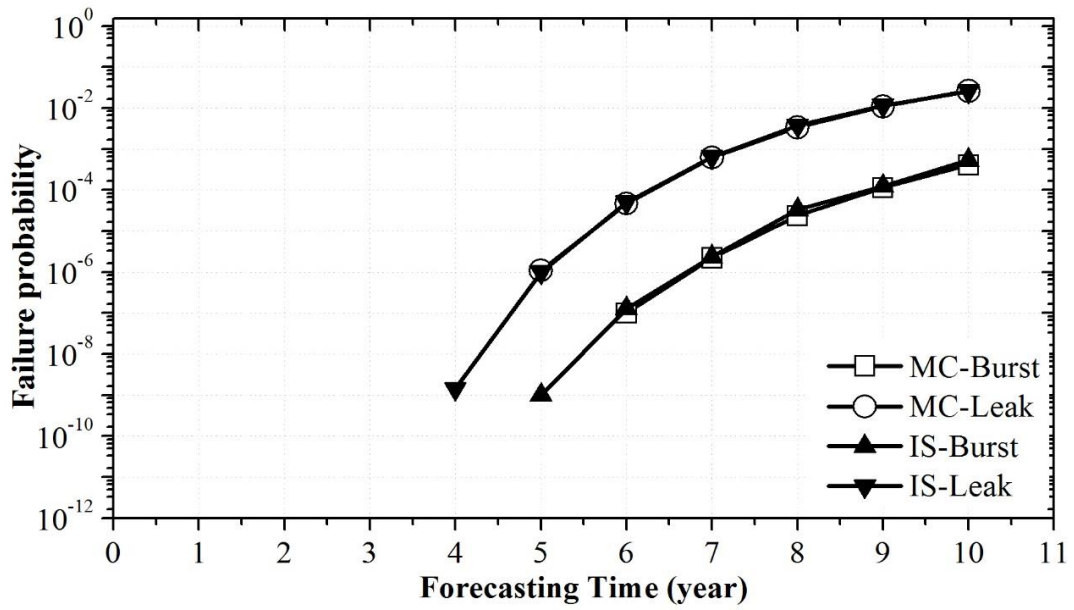
(a) Example 1



(b) Example 2

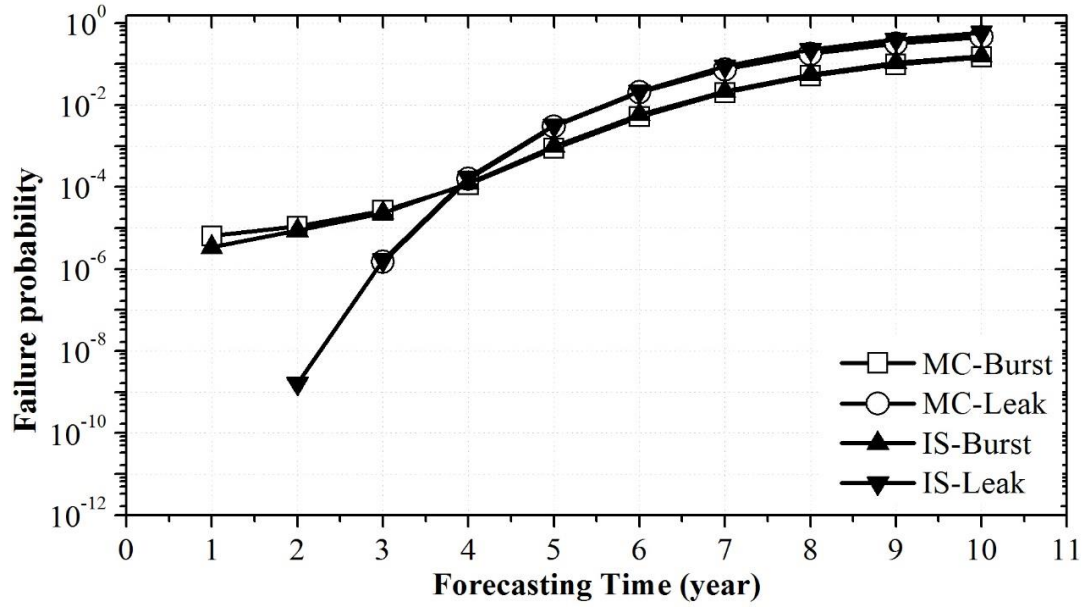


(b) Example 3

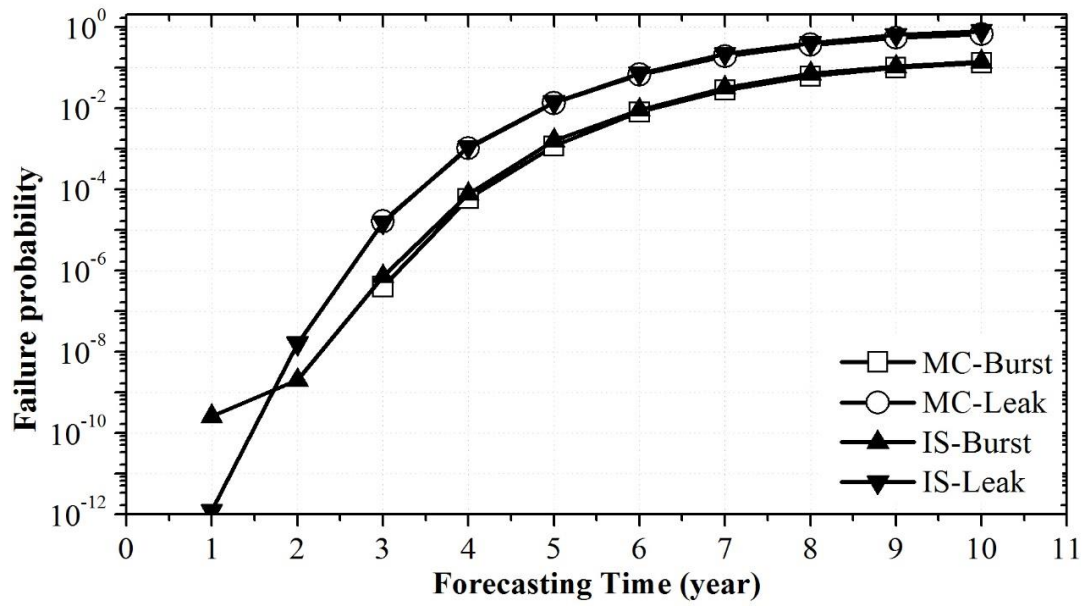


(c) Example 4

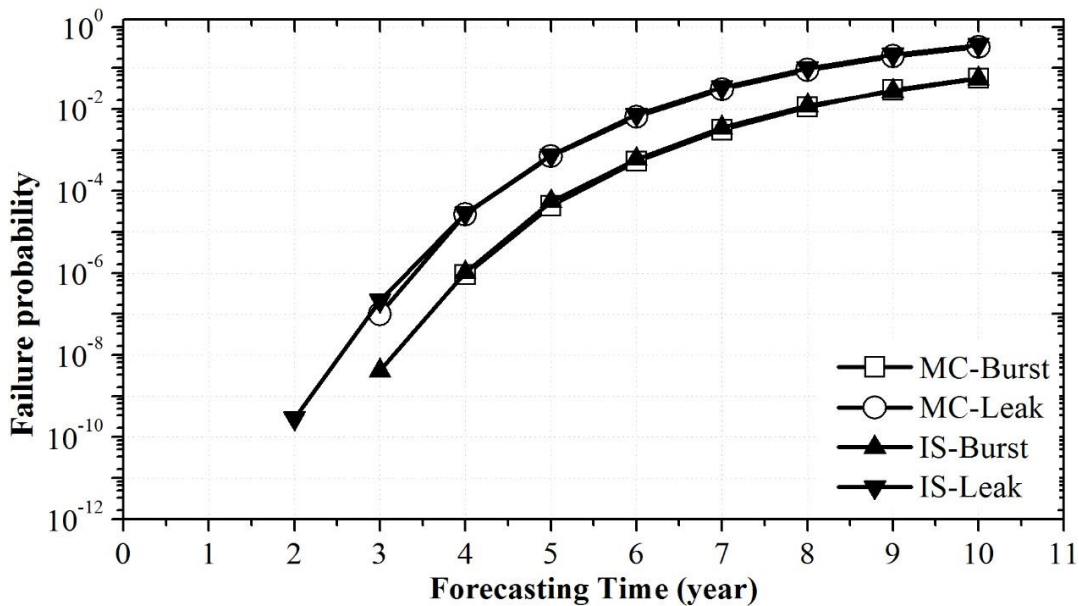
Figure 5.2 Failure probabilities of four pipeline examples considering a single corrosion defect and linear depth growth model



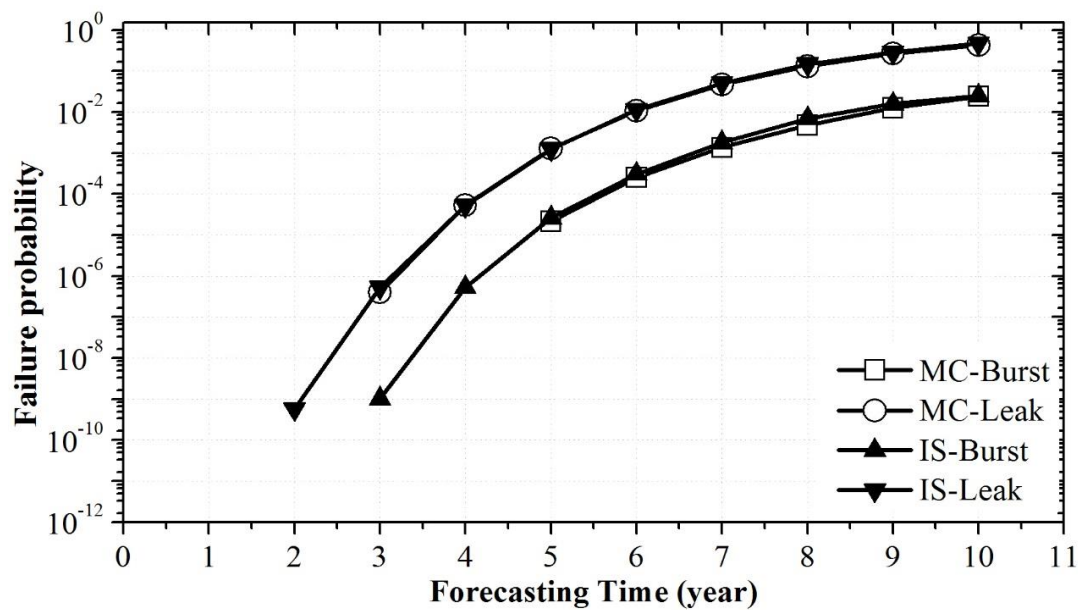
(a) Example 1



(b) Example 2

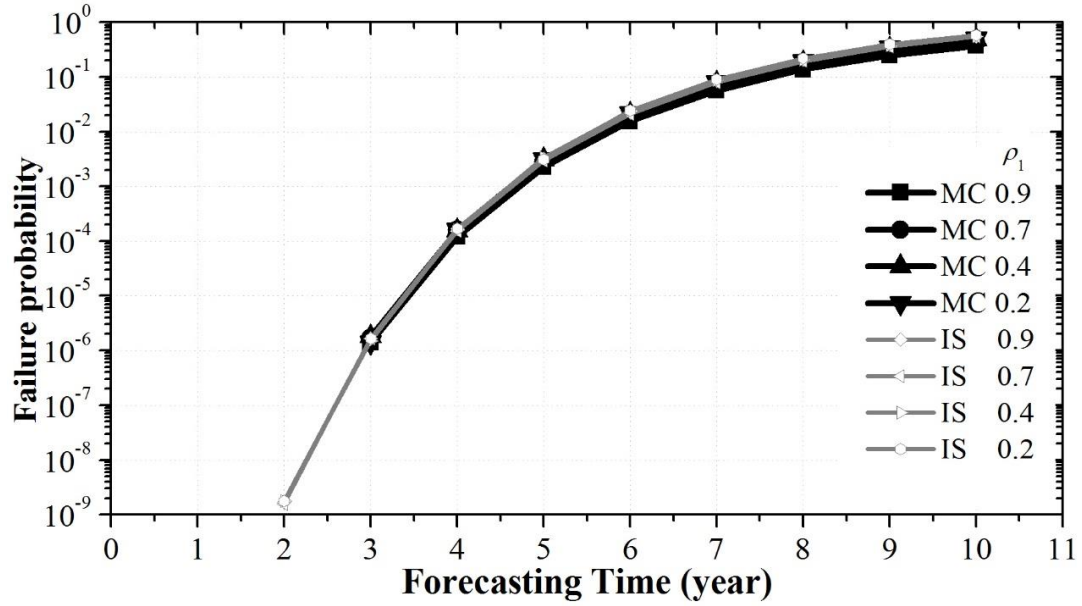


(c) Example 3

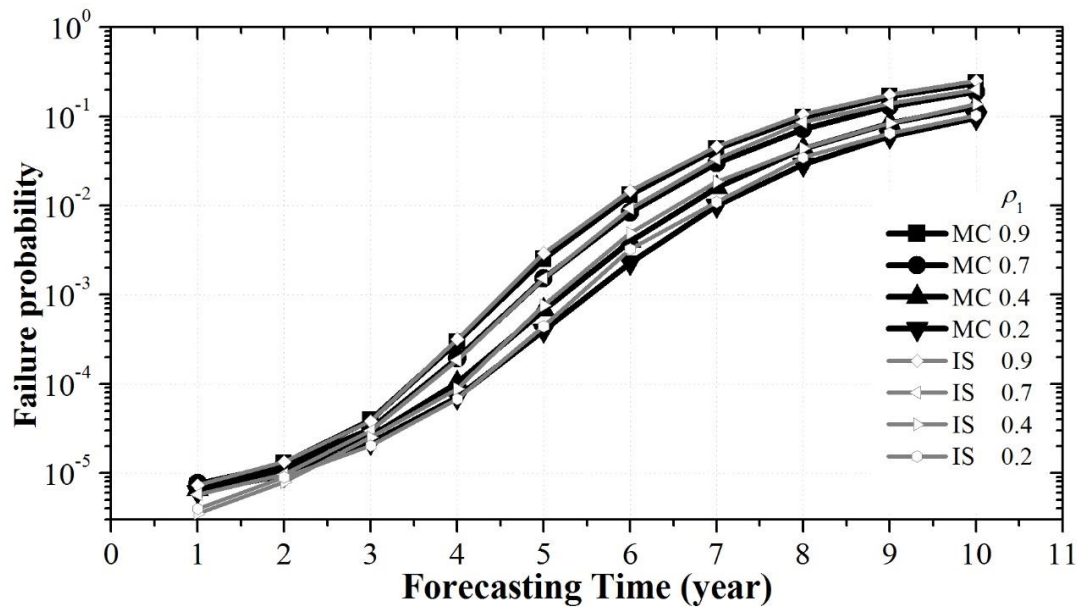


(d) Example 4

Figure 5.3. Failure probabilities of four pipeline examples considering ten corrosion defects and linear depth growth model

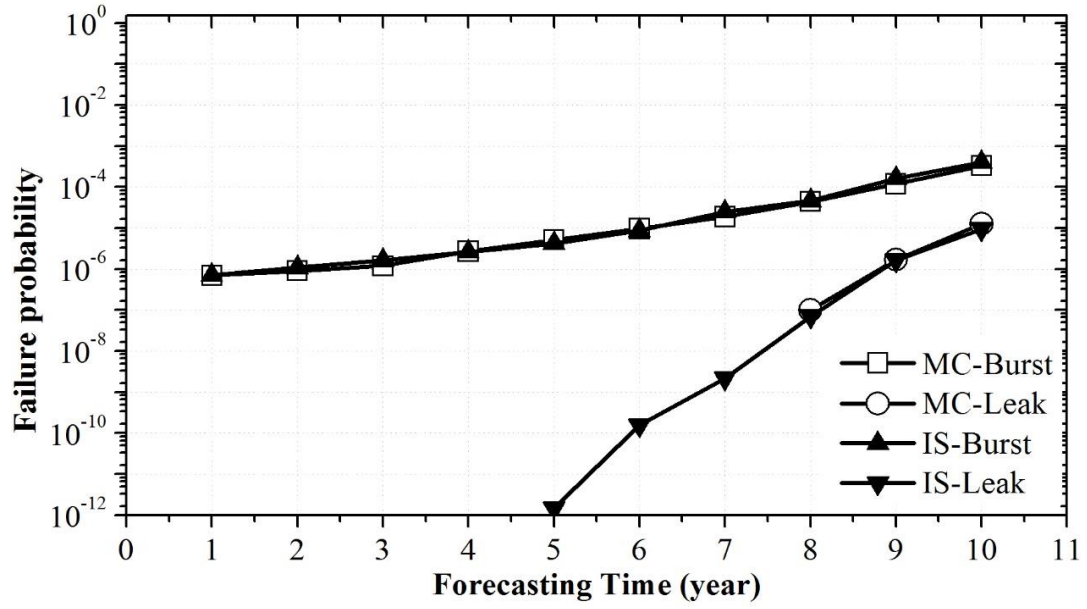


(a) Small leak

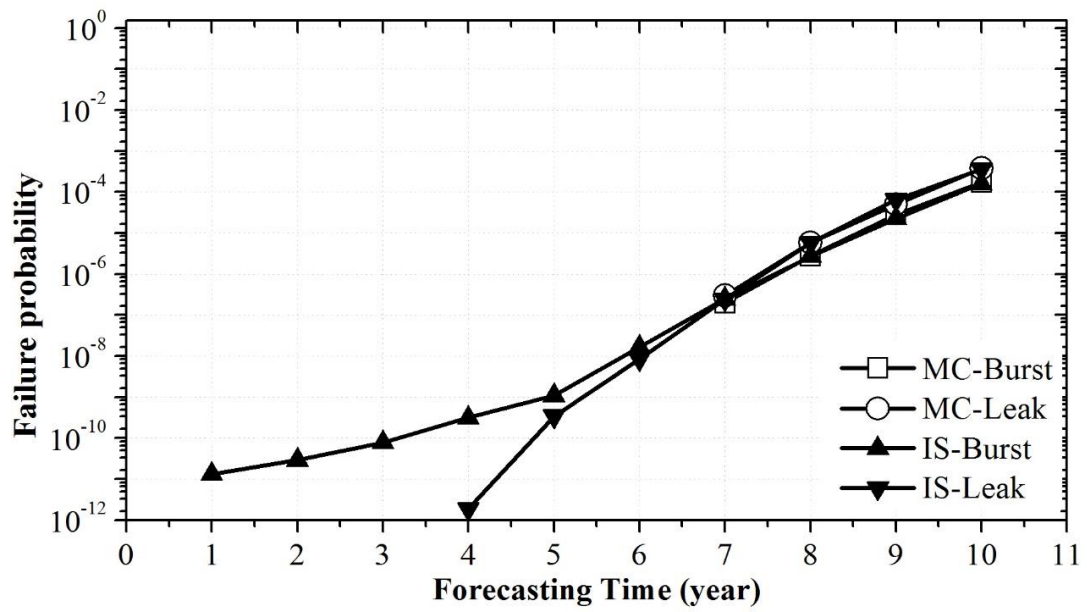


(b) Burst

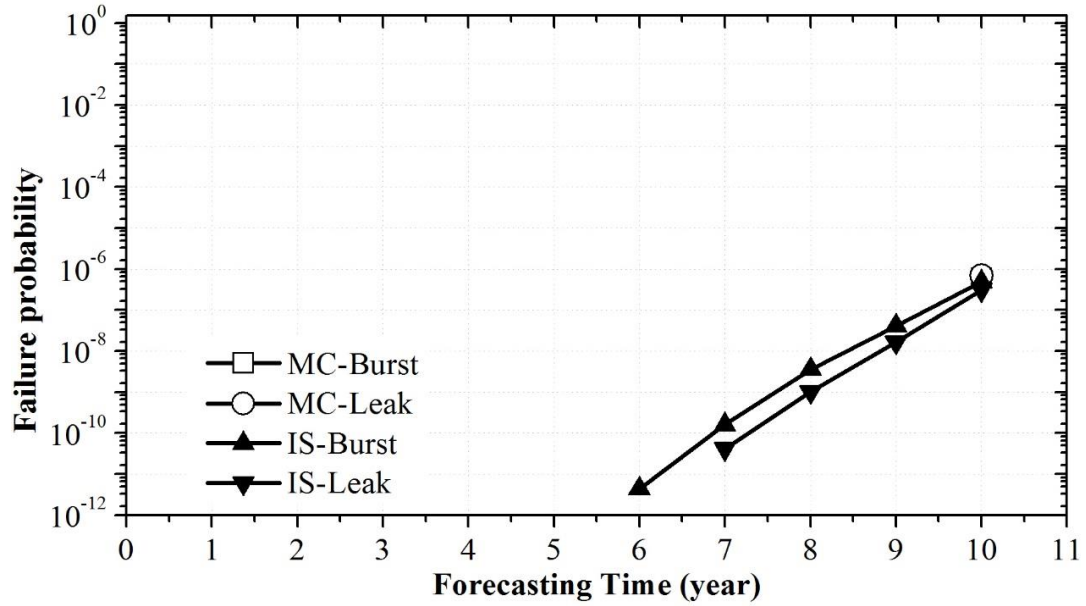
Figure 5.4 Failure probabilities of Example 1 considering ten corrosion defects and linear depth growth model with different values of ρ_1



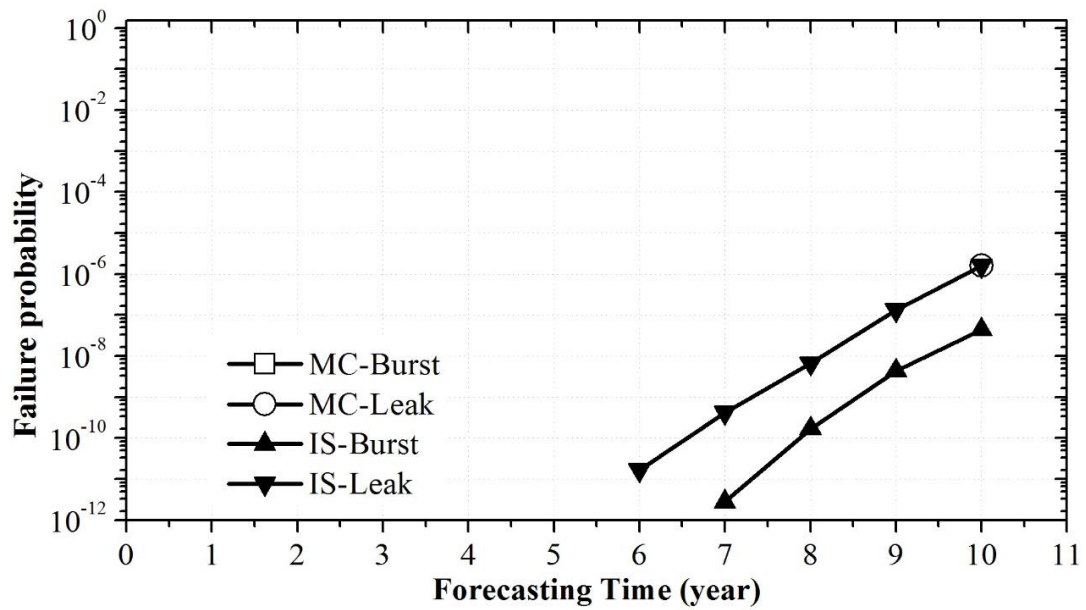
(a) Example 1



(b) Example 2

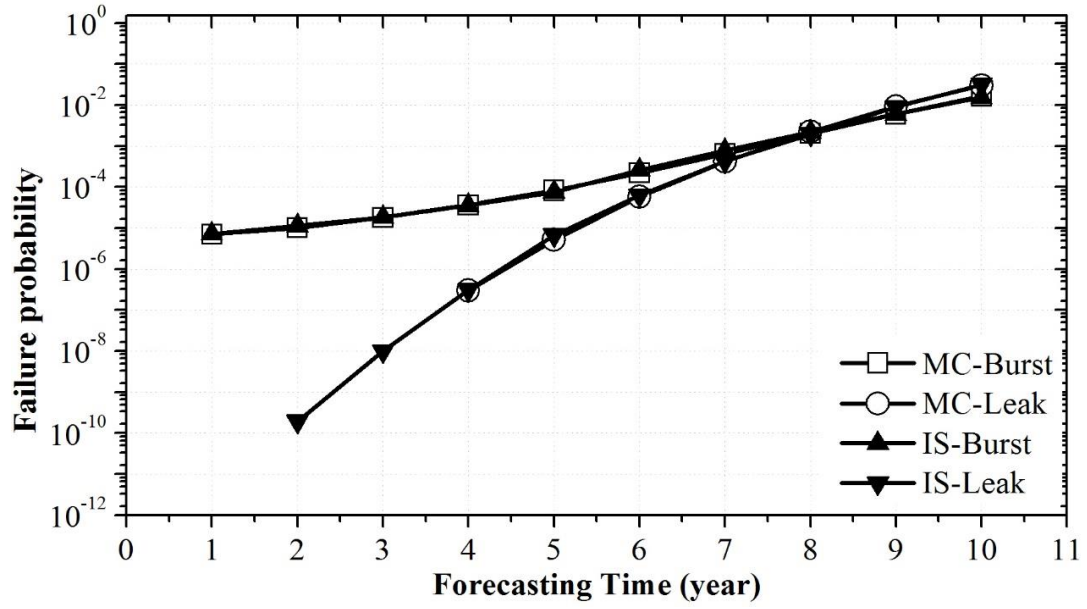


(c) Example 3

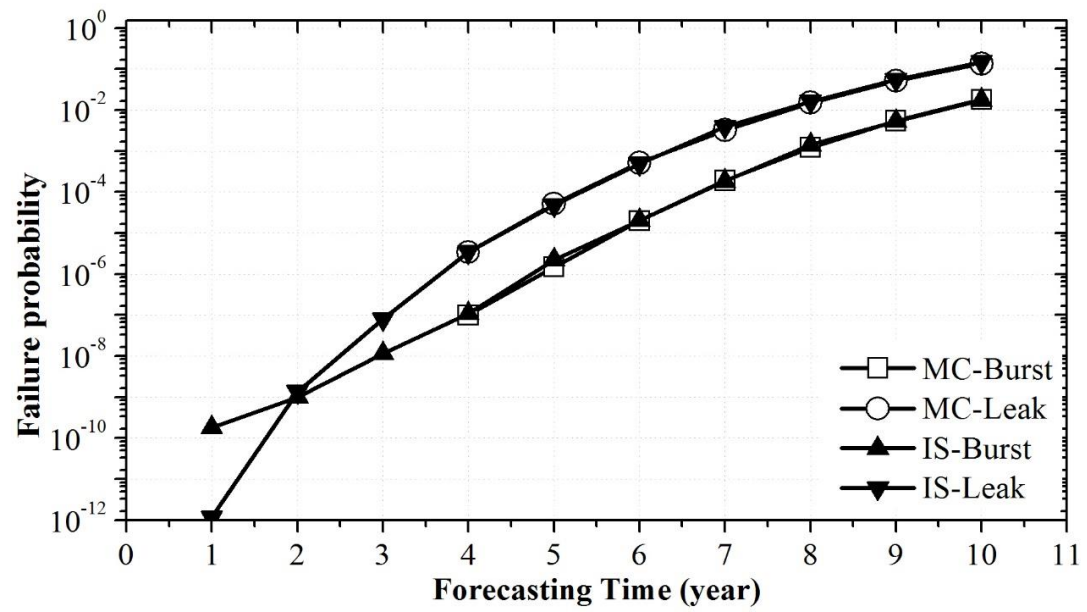


(d) Example 4

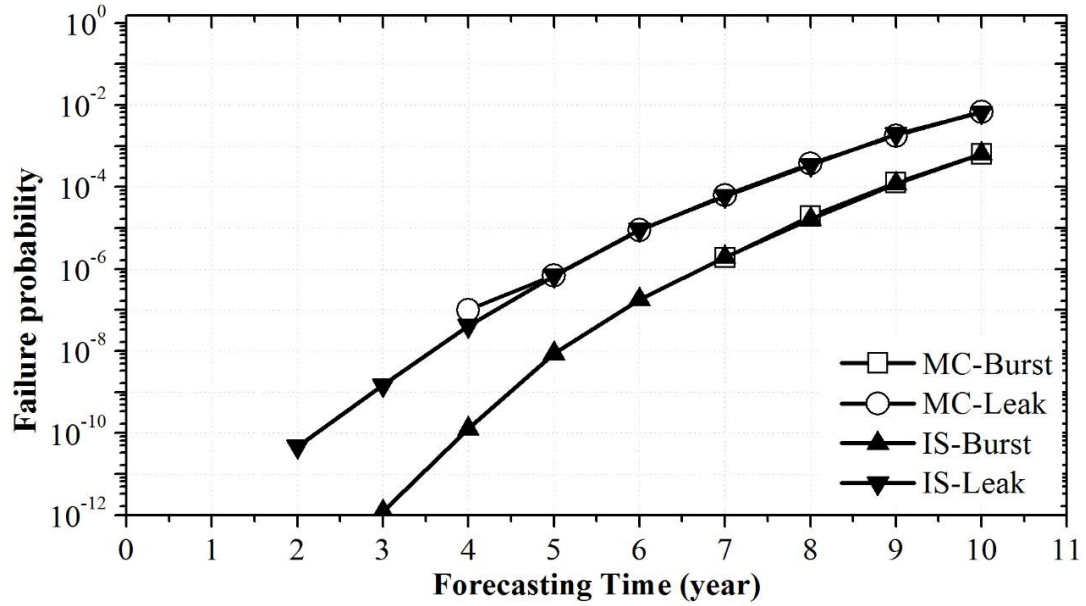
Figure 5.5 Failure probabilities of four pipeline examples considering a single corrosion defect and gamma process-based depth growth model



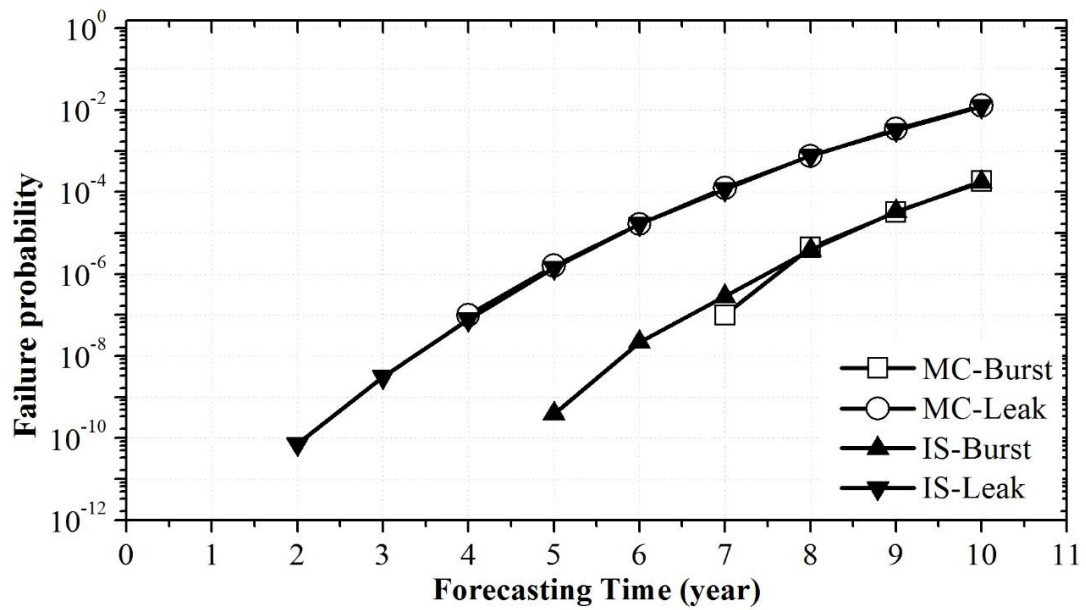
(a) Example 1



(b) Example 2

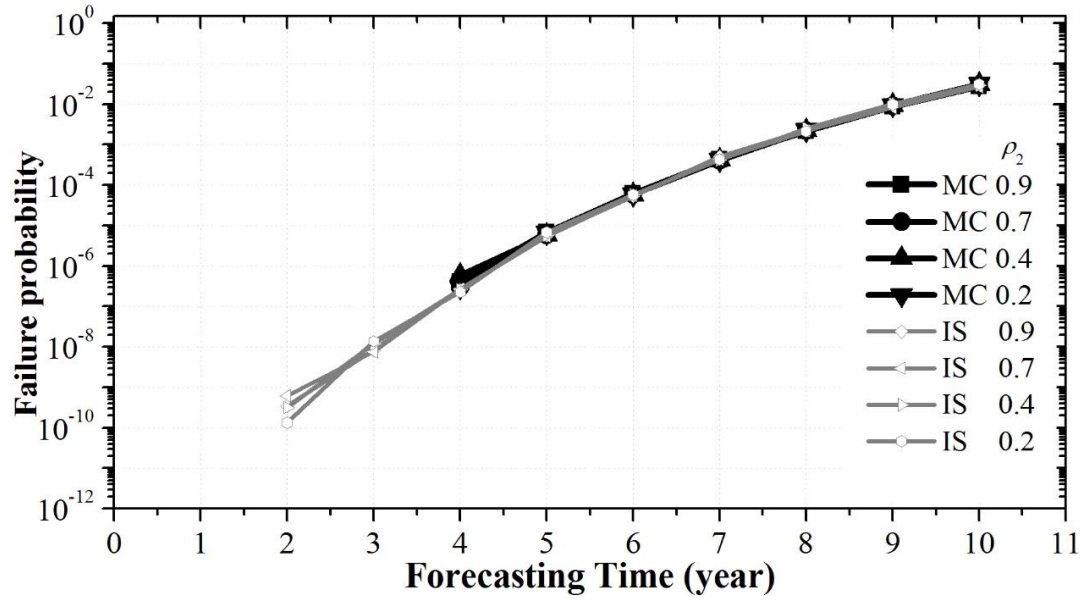


(c) Example 3

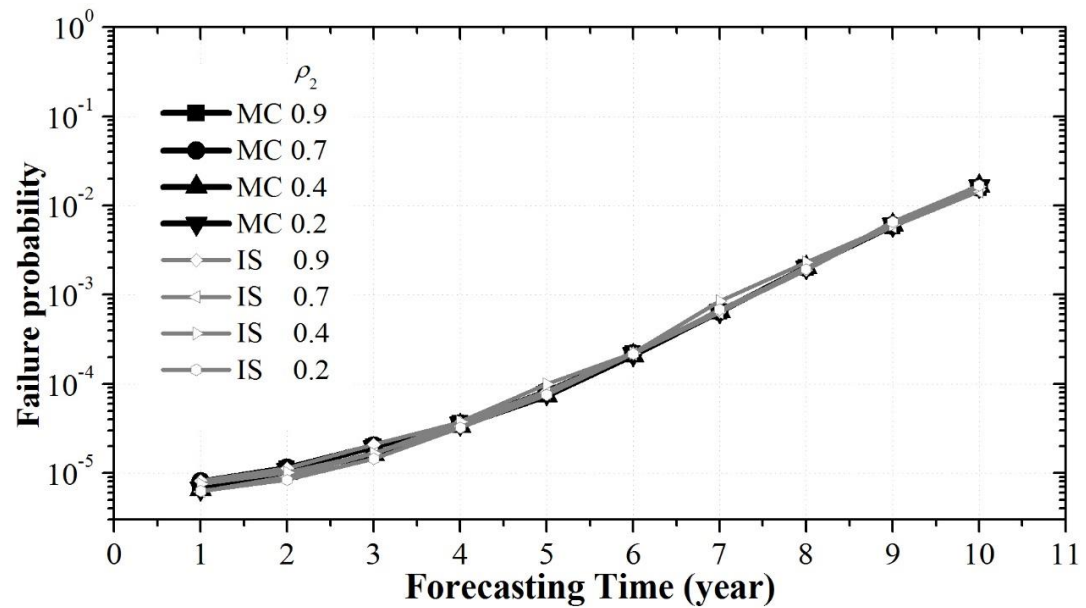


(d) Example 4

Figure 5.6 Failure probabilities of four pipeline examples considering ten corrosion defects and gamma process-based depth growth model



(a) Small leak



(b) Burst

Figure 5.7 Failure probabilities of Example 1 considering ten corrosion defects and gamma process-based depth growth model with different values of ρ_2

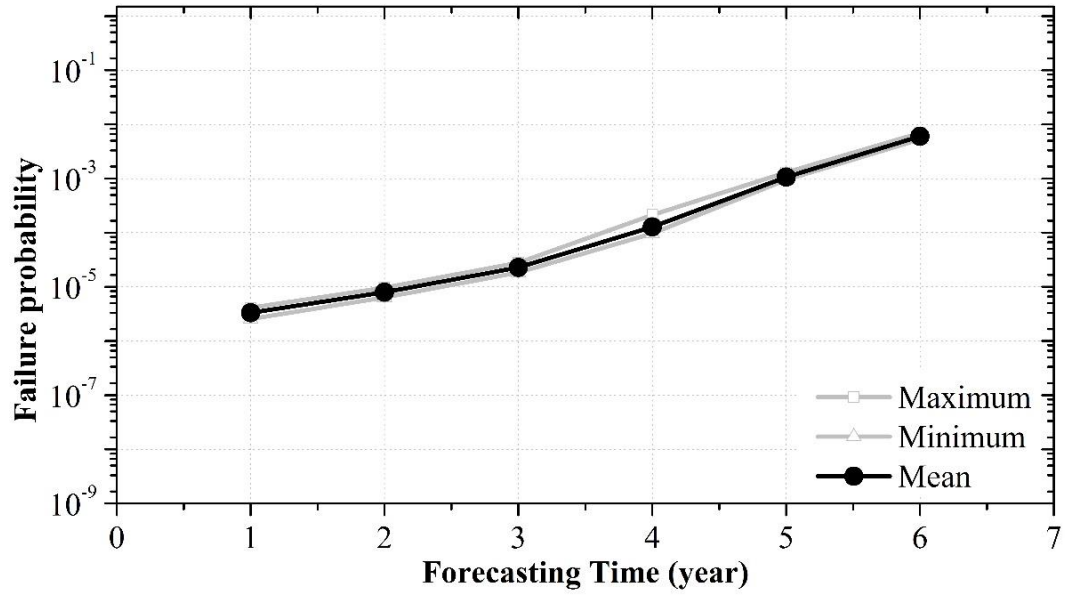


Figure 5.8 Range of probabilities of burst obtained from 30 repeated IS-based analyses for Example 1 with ten corrosion defects and linear defect depth growth model

6 Multi-objective Maintenance Strategy for In-service Corroding Pipeline Using Evolutionary Strategy

6.1 Introduction

The optimal maintenance strategies for corroding pipelines have been investigated in the past. Hong (1999) explored the optimal inspection and repair interval by considering the annual failure probability of the pipeline as the constraint. This method essentially formulates the maintenance plan investigation as a constrained single-objective optimization analysis. Gomes et al. (2013), and Gomes and Beck (2014) employed the minimum expected life-cycle cost criterion to investigate the optimal ILI (inline inspection) interval by assuming a single defect on a pipeline segment. Zhang and Zhou (2014) also employed the minimum expected life-cycle cost criterion to investigate the optimal ILI interval, albeit considering joint-based (as opposed to defect-based) defect mitigation actions. There are basically two conflicting objectives in finding the optimal maintenance strategy for corroding pipelines, i.e. maximizing the reliability of the pipeline and minimizing the maintenance cost. The minimum expected life-cycle cost criterion thus combines the two objectives into a single objective, which facilitates the search for the optimal maintenance strategy. However, the drawback of the single-objective solution is that it does not provide pipeline engineers with the flexibility to evaluate how other alternative maintenance strategies perform in terms of the objective functions. In real-life decision-making processes, decision makers typically need to consider multiple objectives in the optimization, and they may wish to select a maintenance strategy from a group of candidate solutions with diverse characteristics in terms of different merit measures. This option is particularly desirable considering that decision-makers may not treat the two objectives, i.e. reliability and cost, with equal importance: the former is generally deemed more important than the latter. To this end, the multi-objective optimization technique can be employed to find a distribution of solutions that achieve tradeoff between the two objectives in a Pareto optimal sense (Deb et al. 2002).

The application of the multi-objective optimization techniques to the maintenance of engineered structures has been extensively reported in the literature (Liu and Frangopol, 2005; Okasha and Frangopol, 2009; Ayoobian and Mohsendokht 2016; Yu et al. 2015). Liu

and Frangopol (2005) investigated the optimal bridge maintenance planning considering the cost, safety index and condition index as conflicting objectives. Okasha and Frangopol (2009) developed a multi-objective optimization framework for structural maintenance by incorporating the life cycle cost, redundancy and system reliability as the objectives. Ayoobian and Mohsendokht (2016) formulated the optimization of the maintenance of nuclear power plants considering three objectives: the cost, system unavailability and radioactive exposure. Yu et al. (2015) performed the multi-objective optimization of asphalt pavement maintenance plans by considering the pavement performance, environment impact and cost as the objectives. All of the above-cited investigations employed the genetic algorithm (GA)-based evolutionary computation (Deb et al. 2002) to search for a group of optimized tradeoff solutions with respect to conflicting objectives, i.e. the so-called Pareto optimal front.

The objective of the present chapter is to investigate the optimal maintenance planning for corroding pipelines by employing the genetic algorithm (GA)-based multi-objective optimization technique. The rest of the chapter is organized as follows. Section 6.2 describes the objective functions considered in the optimization of maintenance of corroding pipelines. Section 6.3 presents the formulations for the system reliability analyses of corroding pipelines considering two potential failure modes, i.e. small leak and burst. Section 6.4 describes the genetic algorithm for solving the mentioned multi-objective optimization problem, followed by an illustrative example in Section 6.5 and conclusions in Section 6.6.

6.2 Multi-objective Optimization of Maintenance of Corroding Pipelines

6.2.1 Practical Aspects

Consider that a recently-conducted ILI has identified a total of n_p corroding pipe joints in a buried pipeline. The pipeline operator is now faced with the task of determining which corroding pipe joints should be repaired as well as corresponding times of repair such that an optimal balance between the reliable operation of the pipeline and repair cost is achieved. The maintenance decision should take into account the growth of corrosion defects over time and potential constraints such as the minimum acceptable reliability level and annual

budget allocated for corrosion mitigation. Since the next ILI will provide updated corrosion information, the reference time period or time horizon for scheduling the defect repair is generally the time to the next ILI, denoted by T (years). It is noted that the number of joints to be repaired within the time horizon, denoted by m_p , does not necessarily equal the total number of corroding joints (n_p) identified by ILI, i.e. $m_p \leq n_p$. Note also that n_p does not necessarily equal the total number of joints in the entire pipeline as there may exist corrosion-free joints.

The maintenance decision for corroding pipelines is influenced by uncertainties from various sources. The ILI-reported sizes of corrosion defects are associated with measurement errors (Nessim et al. 2009; Zhang and Zhou 2014). The growth of the defect over time is random (Caleyo et al. 2009; Zhang et al. 2013; Al-Amin et al. 2014). The actual pipe wall thickness, yield strength and tensile strength differ from the corresponding nominal values by uncertain amounts (Nessim et al. 2009). The pipe internal pressure fluctuates randomly about the nominal operating pressure (Nessim et al. 2009; Zhang and Zhou 2013). Finally, models used to evaluate the remaining capacity of the corroded pipe for containing the internal pressure are imperfect and have model errors (Zhou and Huang 2012).

6.2.2 Merit Measures

The quantitative measure for the economic merit of a given maintenance decision is defined as the total present-value cost, denoted by C , of repairing m_p pipe joints over the time horizon T . The failure probability of the pipeline is selected as the measure for the safety merit of the maintenance decision, because the various uncertainties described in the previous section can be effectively accounted for in the evaluation of the failure probability. Consistent with the joint-based corrosion mitigation practice, the failure probability is evaluated on a joint-by-joint basis in this chapter. Note that an individual pipe joint can contain multiple active corrosion defects whereby failure may take place at any of the defects. It follows that the failure probability of the pipe joint is the time-dependent failure probability of a series system. Furthermore, a corroding pipe joint may fail by either small leak or burst; therefore, both the time-dependent probabilities of small leak and burst of the pipe joint are evaluated. In the pipeline industry, the annual (as opposed to cumulative)

failure probability is commonly used (Nessim et al. 2009; Kariyawasam and Peterson 2008). Given this, the annual probabilities of small leak and burst conditional on no failure in the past are evaluated. Let $P_{sa,q}(t)$ and $P_{ba,q}(t)$ ($t = 1, 2, \dots, T$) denote, respectively, the probabilities of small leak and burst of the q -th corroding pipe joint ($q = 1, 2, \dots, n_p$) between years $(t - 1)$ and t , conditional on no failure up to year $(t - 1)$. Then $P_{sa,q}(t)$ and $P_{ba,q}(t)$ are given by

$$P_{sa,q}(t) = \frac{P_{s,q}(t) - P_{s,q}(t-1)}{1 - P_{f,q}(t-1)} \quad (6.1a)$$

$$P_{ba,q}(t) = \frac{P_{b,q}(t) - P_{b,q}(t-1)}{1 - P_{f,q}(t-1)} \quad (6.1b)$$

where $P_{s,q}(t)$ and $P_{b,q}(t)$ ($0 \leq t \leq T$) are the cumulative probabilities of small leak and burst, respectively, of the q -th joint up to t , with $t = 0$ indicating the start of the time horizon T , i.e. immediately after the most recent ILI; $P_{f,q}(t)$ is the cumulative failure probability of the q -th joint due to either small leak or burst up to t . Methodologies for evaluating $P_{s,q}(t)$, $P_{b,q}(t)$ and $P_{f,q}(t)$ are described in Section 6.3. Let P_{sa} denote the maximum value of $P_{sa,q}(t)$ for $q = 1, 2, \dots, n_p$ and $t = 1, 2, \dots, T$, i.e. $P_{sa} = \max_{q=1,2,\dots,n_p} \{P_{sa,q}(t)\}_{t=1,2,\dots,T}$. Similarly define

$$P_{ba} = \max_{q=1,2,\dots,n_p} \{P_{ba,q}(t)\}_{t=1,2,\dots,T}. P_{sa} \text{ and } P_{ba} \text{ are considered as quantitative measures for the}$$

reliability of the entire set of n_p corroding pipe joints within the time horizon T .

6.2.3 Formulation for Multi-objective Optimization

Let $t_{r,q}$ denote the time of repair for the q -th ($q = 1, 2, \dots, m_p$) pipe joint that is subjected to repair within T (years). In this chapter, $t_{r,q}$ is treated as a discrete variable that equals 0, 1, 2, ..., or $(T - 1)$. A repair time $t_{r,q} = 0$ means that the q -th pipe joint is repaired immediately after the recently-run ILI. The upper bound for $t_{r,q}$ is $(T - 1)$ as opposed to T in that repairing any pipe joint at year T has no effect on P_{sa} or P_{ba} . Since a repaired pipe joint is considered as good as new, it is assumed that $P_{sa,q}(t) = P_{ba,q}(t) = 0$ for $t > t_{r,q}$ by considering the failure probability of a defect-free pipe joint under internal pressure to be negligible. The multi-objective optimization problem for the corrosion maintenance can then be stated as follows.

- Objective: To minimize P_{sa} , P_{ba} and C by selecting m_p ($m_p \leq n_p$) corroding pipe joints for repair and determining corresponding times of repair, $t_{r,q} = 0, 1, 2, \dots$, or $(T-1)$, for $q = 1, 2, \dots, m_p$.
- Subject to: $P_{sa} \leq P_1$, $P_{ba} \leq P_2$ and $C_{r,t} \leq C_{a,t}$ ($t = 0, 1, 2, \dots, (T-1)$), where P_1 and P_2 are the allowable annual probabilities of small leak and burst, respectively, of a single pipe joint; $C_{r,t}$ is the present-value cost of repairs conducted at time t , and $C_{a,t}$ is the annual budget in terms of present value allocated for corrosion repair at time t .

The value of $C_{r,t}$ is evaluated by

$$C_{r,t} = \frac{n_{r,t}C_s + I_r(n_{r,t})C_0}{(1+v_r)^t} \quad (6.2)$$

where $n_{r,t}$ is the number of joints repaired at time t ($t = 0, 1, 2, \dots, (T-1)$) with $\sum_{t=0}^{T-1} n_{r,t} = m_p$ (note that $n_{r,t} = 0$ means that no repair is carried out at time t); C_s is the cost of repairing a single joint, and v_r is the discount rate; C_0 is the mobilization cost, i.e. cost of bringing the repair crew and equipment to the pipeline right of way; $I_r(n_{r,t})$ is an indicator function that equals unity for $n_{r,t} > 0$ and zero for $n_{r,t} = 0$. It follows that the total present-value cost of repair, C , over the time horizon T is given by

$$C = \sum_{t=0}^{T-1} C_{r,t} \quad (6.3)$$

6.3 Reliability Analyses of Corroding Pipelines

For a given pip joint containing m_p ($m_p = 1, 2, \dots$) active corrosion defects, the limit state function corresponding to the j -th defect ($j = 1, 2, \dots, m_p$) penetrating the pipe wall at time t ($t=0$ corresponding to the time of the recent ILI), $g_j^s(t)$, is given by

$$g_j^s(t) = 0.8wt_j - d_j(t) \quad (6.4)$$

where wt_j is the wall thickness of pipe joint at the location of the j -th defect; $d_j(t)$ is the depth of the j -th defect at time t , and the coefficient 0.8 accounts for the fact that the remaining ligament of the pipe wall at a deep corrosion defect is prone to developing cracks

that cause a leak (Al-Amin and Zhou 2014). The limit state function for plastic collapse of the remaining ligament at the j -th defect at time t , $g_j^b(t)$, is given by

$$g_j^b(t) = p_{bj}(t) - p \quad (6.5)$$

where $p_{bj}(t)$ is the burst pressure capacity of the joint at the j -th defect at time t , and p denotes the pipe internal pressure, which is characterized by a time-independent random variable (as opposed to time-dependent random process) in this chapter. The following semi-empirical burst capacity model developed by Leis and Stephens (1997) is employed to calculate p_{bj} in this study:

$$p_{bj} = \xi_j \frac{2wt_j\sigma_{uj}}{D} \left[1 - \frac{d_j}{wt_j} \left(1 - \exp \left(\frac{-0.157l_j}{\sqrt{\frac{D(wt_j - d_j)}{2}}} \right) \right) \right] \quad (6.6)$$

where ξ is the model error associated with Leis and Stephens's model; D is the outside diameter of the pipe joint; σ_u is the ultimate tensile strength of the pipe steel; l is the defect length, and the subscript j in the above-described variables indicates the value of the variable corresponding to the j -th defect ($j = 1, 2, \dots, m$). For brevity, $p_{bj}(t)$, $d_j(t)$ and $l_j(t)$ are simply written as p_{bj} , d_j and l_j , respectively, in Eq. (6.6).

The defect depth $d_j(t)$ and length $l_j(t)$ can be further expressed as

$$d_j(t) = d_{0j} + \Delta d_j(t) \quad (6.7a)$$

$$l_j(t) = l_{0j} + \Delta l_j(t) \quad (6.7b)$$

where d_{0j} and l_{0j} are the depth and length, respectively, of the j -th defect at the time of the most recent ILI, and $\Delta d_j(t)$ and $\Delta l_j(t)$ denote the growths of the depth and length, respectively, by time t . Extensive research has been reported in the literature on the development of probabilistic models for characterizing $\Delta d_j(t)$ based on information obtained from successive ILI runs conducted on the same pipeline (Achterbosch and

Grzelak 2006; Zhang et al. 2013; Al-Amin et al. 2014). On the other hand, the development of probabilistic models for $\Delta l_j(t)$ is scarcely reported in the literature.

Based on the above-defined limit state functions, the cumulative probabilities of small leak and burst, $P_s(t)$ and $P_b(t)$ ($0 \leq t \leq T$), of the pipe joint are defined as

$$P_s(t) = \text{Prob} \left[\left(0 \leq \min_j \{t_j^s\} \leq t \right) \cap \left(\min_j \{t_j^s\} < \min_j \{t_j^b\} \right) \right] \quad (6.8a)$$

$$P_b(t) = \text{Prob} \left[\left(0 \leq \min_j \{t_j^b\} \leq t \right) \cap \left(\min_j \{t_j^b\} \leq \min_j \{t_j^s\} \right) \right] \quad (6.8b)$$

where t_j^s denotes the time at which the j -th ($j = 1, 2, \dots, m$) defect just penetrates the pipe wall (i.e. $g_j^s(t) = 0$); t_j^b denotes the time at which the j -th defect is just large enough to cause plastic collapse (i.e. $g_j^b(t) = 0$), and \cap denotes the intersection of two events. Implicit in Eq. (6.8) is that the small leak and burst are considered as two competing failure modes; that is, the occurrence of one failure mode eliminates the potential occurrence of the other failure mode. This is because in practice a failed pipe joint, either by small leak or burst, is typically repaired within a short timeframe such as within several days. It follows that the probability of no failure of the q -th pipe joint up to time t equals $P_{f,q}(t) = \text{Prob} \left[\left(0 \leq \min_j \{t_j^s, t_j^b\} \leq t \right) \right]$, which can be approximated as the sum of $P_{s,q}(t)$ and $P_{b,q}(t)$ (Gong and Zhou 2016).

An importance sampling-based methodology developed by Gong and Zhou (2016) is employed in this chapter to evaluate $P_s(t)$ and $P_b(t)$. This methodology can deal with potential correlations among different random variables associated with the same defect and different defects and has been demonstrated to be computationally efficient and accurate.

6.4 Genetic Algorithm for Multi-objective Optimization

6.4.1 Overview of Genetic Algorithm

Mimicking the natural biological evolution, the evolutionary GA is a stochastic search and optimization engine for global solutions. GA works on populations consisting of a series

of possible solutions, known as chromosomes (Deb et al. 2002). A given chromosome is made of discrete units called genes. The population of GA is initialized randomly and updated iteratively through the stochastic tournament mating selection, chromosome crossover and mutation operations (Deb et al. 2002). In the stochastic tournament selection, two chromosomes are randomly selected and the one with better fitness measures is added to the mating pool (Deb et al. 2002). The selection is continued until the mating pool is filled. The crossover operation recombines chromosomes randomly selected from the mating pool to form new chromosomes known as offspring by exchanging, with a prescribed crossover probability, the values of randomly selected genes in the parent chromosomes; the mutation operation changes, with a prescribed mutation probability, the values of one or more randomly selected genes in an offspring chromosome. In single-objective optimizations, the fitness of a given solution is measured in terms of the value of the objective function: the better objective value, the better fitness. The multi-objective optimization involves optimizing multiple conflicting objectives simultaneously, and the final solutions represent various tradeoffs. The fitness of a given solution in the multi-objective optimization can be measured using the Pareto front ranking and crowding distance approaches (explained briefly below) as proposed by Deb et al. (2002).

The Pareto front in the multi-objective optimization is defined as a tradeoff front where a series of solutions are non-dominated with respect to each other in terms of the objectives. A solution is dominated by another solution if the latter is better than the former in at least one objective and no worse than the former in all the other objectives. The Pareto front ranking involves first assigning the non-dominated solutions in the population as a rank of one (i.e. the first front) and then removes such solutions from the population; the non-dominated solutions in the remaining population are subsequently identified and assigned to the second Pareto front, and such a process is repeated until all solutions in the population are assigned appropriate ranks. Fitness values are then assigned to different solutions. The solutions with lower-numbered ranks are given higher fitness values than those with higher-numbered ranks. For solutions with the same rank, the corresponding fitness values can be assigned based on the crowding distance, which is a measure of the density of the solutions surrounding a given solution in the population (Deb et al. 2002). A solution with a larger crowding distance is more desirable and assigned a higher fitness

value in that it is more “dissimilar” than the other solutions and enhances the diversity of the population, which is important for searching for globally optimal solutions.

It should be noted that GA is a computationally intensive method, especially for large scale optimization problems. It may take a large number of generations of the solution population to reach the approximate Pareto front. Moreover, the convergence to the Pareto front is not guaranteed.

6.4.2 GA Used in this Chapter

For a pipeline segment consisting of n_p corroding pipe joints, the maintenance solution encoded in the GA used in the present chapter is schematically illustrated in Fig. 6.1. A given solution (chromosome) consists of n_p genes, each gene corresponding to one of n_p corroding joints. The value of the q -th gene equals 0, 1, 2, ..., or T (years) representing the time of repair of the q -th pipe joint, where T is the time horizon (i.e. the interval between the recently-run and next-scheduled ILIs, see Section 6.2.3) considered in the GA. A value of zero means that the pipe joint is repaired immediately after the recently-run ILI, whereas a value of T indicates that the joint is not repaired (see Section 6.2.3) prior to the next ILI.

To improve the robustness and efficiency of the GA, the initial solutions are not randomly generated in this chapter but selected using the approach as described in the following. Consider the constrained optimization problem of minimizing the present-value repair cost (C) subjected to $P_{sa} \leq P_1$. As illustrated in Fig. 6.2, the times corresponding to the intersection points of the horizontal line representing $P_{sa} = P_1$ and n_p curves respectively representing the time-dependent probabilities of small leak of n_p pipe joints are the optimal times of repair; the collection of these repair times, rounded off to the nearest smaller integers, is then considered as one initial solution to the multi-objective maintenance optimization problem. By varying the value of P_1 , i.e. the position of the horizontal line in Fig. 6.2, a set of initial solutions are then generated. This technique can be equally applied to generate another set of initial solutions by considering minimizing C subjected to $P_{ba} \leq P_2$. Finally, the union of the two sets of initial solutions forms the initial solution population to start the evolutionary process for the multi-objective optimization.

6.4.3 Constraint Handling

As described in the problem statement in Section 6.2.3, three constraints are considered in the optimization process: $P_{sa} \leq P_1$, $P_{ba} \leq P_2$ and $C_{r,t} \leq C_{a,t}$ ($t = 0, 1, 2, \dots, (T - 1)$). In this chapter, the first two constraints, i.e. $P_{sa} \leq P_1$ and $P_{ba} \leq P_2$, are not enforced until at the end of the optimization; that is, those solutions violating the two constraints are simply removed from the final converged Pareto front. On the other hand, the annual budget constraint $C_{r,t} \leq C_{a,t}$ is handled by adding penalty to the cost objective (Deb 2001). To this end, the maintenance cost is expressed as:

$$C = \sum_{t=0}^{T-1} C_{r,t} + \lambda \sum_{t=0}^{T-1} \max\{0, C_{r,t} - C_{a,t}\} \quad (6.9)$$

where the second term of the right hand side of Eq. (6.9) is the penalty term, and λ is the penalty factor modulating the relative amplitude of violation to $C_{r,t}$. A trial-and-error process can be conducted to determine λ . It is found in this study that $\lambda = 1$ results in fast convergence of the Pareto front.

6.5 An Illustrative Example

A numerical example representing an onshore underground natural gas pipeline is employed to illustrate the application of the above-described GA-based multi-objective optimization framework for determining the optimal corrosion maintenance strategy. The pipeline has a nominal operating pressure (P_0) of 5.7 MPa, a nominal outside diameter (D) of 508 mm and a nominal wall thickness (wt_n) of 5.56 mm. The specified minimum yield and tensile strengths (SMYS and SMTS) of the pipe steel equal 414 MPa and 517 MPa, respectively. For illustrative purpose, a total of 90 corroding pipeline joints, i.e. $n_p = 90$, are considered in the optimization analysis. It is assumed that the number and sizes of corrosion defects on the 90 pipe joints have been reported by a recently-run ILI. The ILI-reported defect information is summarized in Fig. 6.3: the number of defects per pipe joint ranges from 1 to 5; the defect depth ranges from 10 to 30% wt_n , and the defect length ranges from 30 to 70 mm. It is further assumed that the next ILI is scheduled in five years, i.e. $T = 5$ years. The cost of repairing a single corroding pipe joint is assumed to be \$125,000, which is representative of the typical practice in the Canadian pipeline industry (Zhang and

Zhou 2014), and the mobilization cost is assumed to be \$200,000. The allowable annual probabilities of small leak and burst, i.e. P_1 and P_2 , are assumed to be 10^{-2} and 10^{-4} , respectively. It is further assumed that there is no budget constraint for the defect repair at year zero, which is reasonable considering that in practice defects mitigated at year zero are typically critical and near-critical defects and great flexibility in the budget is therefore expected to accommodate the mitigation of such defects. Three scenarios regarding the budget constraints in years 1 through 4 are considered: 1) a constant annual budget constraint of \$3 million in each of years 1 through 4; 2) variable annual budget constraints with \$3m, \$2m, \$1.5m and \$1m in years 1 through 4, respectively, and 3) no annual budget constraint. Finally, the discount rate is assumed to be 5%.

For simplicity, the depth and length of a given defect are assumed to grow linearly over time, with the constant (but uncertain) depth and length growth rates denoted by g_d and g_l , respectively. The statistical information of the random variables relevant to the reliability analysis is summarized in Table 6.1. Note that the uncertainties associated with the initial defect depth and length (i.e. d_0 and l_0) are intended to reflect the measurement errors associated with the ILI-reported defect depth and length, respectively. All the random variables summarized in Table 6.1 are assumed to be mutually independent; random variables representing the same physical parameter associated with different defects on different pipe joints are also assumed to be mutually independent, and random variables representing the same physical parameters associated with different defects on the same pipe joints are assumed to be fully correlated except for g_d and g_l . The depth (length) growth rates for different defects on the same pipe joint are assumed to be statistically dependent, and the dependence is characterized by the Gaussian copula (Nelson 2006) with a correlation coefficient of 0.5.

The time-dependent failure probabilities of the 90 corroding pipe joints are evaluated using the IS method (Gong and Zhou 2016) with the number of IS trials equal to 3000 at each time step (equal to one year) for each pipe joint. The GA-based multi-objective optimization is conducted using the Matlab Optimization tool. The number of solutions in the population at a given generation is set at 500. The analysis is terminated if the number of generations reaches 300 or the average change of the Pareto front is 10^{-3} .

The annual conditional probabilities of small leak and burst for each of the 90 pipe joints are displayed in Fig. 6.4 as a function of time elapsed since the recent ILI. In general, the probability of small leak of a given pipe joint is markedly lower than the corresponding probability of burst at time zero, but the former increases more rapidly with time than the latter. Without any maintenance intervention, P_{sa} and P_{ba} increase to 1.2×10^{-1} and 4.0×10^{-2} , respectively, at the end of the time horizon ($T = 5$ years).

Figure 6.5 depicts the converged Pareto front obtained from GA for the considered example with the constant annual budget constraint of \$3m in each of years 1 through 4. The Pareto front is just below the allowable annual probability of burst of 10^{-4} , whereas the Pareto front is almost two orders of magnitude below the allowable annual probability of small leak of 10^{-2} . This implies that the constraint $P_{sa} \leq P_1$ is automatically satisfied once the constraint $P_{ba} \leq P_2$ is handled for this particular example. To gain further insights into the Pareto front, three solutions denoted by SC1, SC2 and SC3, respectively, are selected from the Pareto front and examined in detail. Table 6.2 presents the details of these three solutions with the corresponding locations of the to-be-repaired joints plotted in Fig. 6.6. The maximum annual conditional probabilities of small leak and burst of all 90 pipe joints corresponding to these three solutions are depicted in Figs. 6.7(a) and 6.7(b), respectively, as a function of time. The solution SC1 is at the upper extreme end of the Pareto front, i.e. the solution closest to the allowable annual failure probability boundaries and associated with the minimum cost. This solution can in fact be obtained from a single-objective constrained optimization analysis, i.e. minimizing the overall repair cost subjected to the allowable failure probability and annual budget constraints. The advantage of the multi-objective optimization is reflected in Fig. 6.5: the Pareto front, obtained from a single GA run, contains a diverse set of solutions corresponding to extended ranges of values of the three objective functions. Compared with SC1, solution SC2 leads to a 19% increase in C , but 99% and 95% decreases in P_{sa} and P_{ba} , respectively. If the decision maker prefers a significantly high safety level, solution SC3 could be a possible candidate. Compared with SC1, SC3 leads to a 51% increase in C , but more than two orders of magnitude decrease in P_{sa} and P_{ba} .

The impact of the annual budget constraint on the Pareto front is shown in Fig. 6.8, which depicts the projections of the Pareto fronts in the $C - P_{sa}$ and $C - P_{ba}$ spaces, respectively, corresponding to the three scenarios of budget constraints in years 1 through 4, i.e. constant constraint, variable constraint and no constraint. As expected, Fig. 6.8 shows that the Pareto front obtained by assuming no budget constraint includes more viable solutions than those corresponding to the other two scenarios. Details of two solutions (SV1 and SV2) selected from the Pareto front corresponding to the variable budget constraint, and two solutions (SN1 and SN2) from that corresponding to no budget constraint are shown in Table 6.3. The solutions SV1 and SC1 lead to the same value of P_{sa} and similar values of P_{ba} , but have markedly different repair schedules: SV1 involves repairing 15 joints in year 1 whereas no repair is needed in year 1 according to SC1. The solutions SV2 and SC2 lead to the same values of P_{sa} and P_{ba} , respectively, but the former involves repairing a large number of pipe joints (22) in year 1 and no joints need repairing the same time. It should be noted that although solution SN1 is included in the Pareto front corresponding to the scenario of no budget constraint, it in fact satisfies the constant annual budget constraint of \$3m from years 1 to 4. The fact that SN1 is not included in the Pareto front corresponding to the latter scenario as it should have been suggests that GA results in an approximation of the true Pareto front. On the other hand, the closeness between solutions SN1 and SC1 suggests that the Pareto front obtained from the GA is a good approximation of the true Pareto front. Note further that the solutions corresponding to the scenario of no budget constraint can provide the decision maker with insights into the appropriate distribution of the corrosion maintenance budget to achieve desired safety levels. For example, solution SN2 provides a possible budget allocation for maintaining P_{sa} and P_{ba} in the order of 10^{-6} .

Figure 6.9 compares the Pareto fronts associated with the scenario of constant annual budget constraint from years 1 through 4 obtained by using two different approaches for generating the initial solutions for the GA process: the pre-training approach as described in Section 6.4.2 and randomly generated initial solutions. Note that the total number of generations of the solution population remains the same (300). Figure 6.9 indicates that most of solutions in the Pareto front corresponding to randomly generated initial solutions are dominated by those corresponding to the pre-trained initial solutions. This suggests

that for a given total number of generations, the latter approach leads to more robust and faster convergence to the true Pareto front.

6.6 Conclusion

A multi-objective optimization based maintenance framework for in-service corroding pipelines is developed in the present chapter. Three objectives are considered in the optimization, namely, minimizing the annual conditional probabilities of small leak and burst over the time horizon, as well as the total present-value cost of corrosion repair. Consistent with the industry practice, the basic unit in the calculation of the failure probability and repair cost is the individual pipe joint. The design variables for the optimization are locations of to-be-repaired individual pipe joints along the pipeline and corresponding repair times elapsed from the most recent inline inspection. Three constraints are included in the optimization: the allowable annual probabilities of small leak and burst as well as the annual budget for corrosion repair. The genetic algorithm is employed to search for the Pareto front in which the solutions are non-dominated against each other with respect to the three objectives. A hypothetical natural gas pipeline consisting of 90 corroding pipe joints is used to illustrate the application of the developed maintenance framework. The analysis results indicate that the obtained Pareto front includes a diverse set of solutions that allow the decision maker to balance the tradeoff between the failure probabilities and cost of repair. The annual budget constraint can have a marked impact on the converged Pareto front and detailed repair schedules associated with individual solutions. Furthermore, it is observed that for the same number of iterations using the pre-trained initial solutions leads to more robust and faster convergence to the true Pareto front than using the randomly generated initial solutions. The proposed framework can be the basis of a decision-support tool for the optimal maintenance planning of corroding pipelines subjected to safety and resource constraints.

6.7 Reference

Achterbosch, G. G., and Grzelak, L. A. (2006,). Determination of the Corrosion Rate of a MIC Influenced Pipeline Using Four Consecutive Pig Runs. In 2006 International Pipeline Conference (pp. 209-217). American Society of Mechanical Engineers.

Al-Amin, M., Zhou, W., Zhang, S., Kariyawasam, S. and Wang, H. (2014). Hierarchical Bayesian corrosion growth model based on in-line inspection data. *Journal of Pressure Vessel Technology*, 136(4), p.041401.

Ayoobian, N., and Mohsendokht, M. (2016). Multi-objective optimization of maintenance programs in nuclear power plants using Genetic Algorithm and Sensitivity Index decision making. *Annals of Nuclear Energy*, 88, 95-99.

Caleyo, F., Velázquez, J. C., Valor, A., and Hallen, J. M. (2009). Probability distribution of pitting corrosion depth and rate in underground pipelines: A Monte Carlo study. *Corrosion Science*, 51(9), 1925-1934.

Deb, Kalyanmoy (2001). *Multi-objective optimization using evolutionary algorithms*. Chichester, UK: Wiley

Deb, K., Pratap, A., Agarwal, S., and Meyarivan, T. A. M. T. (2002). A fast and elitist multiobjective genetic algorithm: NSGA-II. *IEEE transactions on evolutionary computation*, 6(2), 182-197.

Gomes, W. J., Beck, A. T., and Haukaas, T. (2013). Optimal inspection planning for onshore pipelines subject to external corrosion. *Reliability Engineering and System Safety*, 118, 18-27.

Gomes, W. J., and Beck, A. T. (2014). Optimal inspection and design of onshore pipelines under external corrosion process. *Structural Safety*, 47, 48-58.

Gong, C. Q., and Zhou, W. X. (2016). Importance sampling-based system reliability analysis of corroding pipelines considering multiple failure modes. Submitted to *Reliability Engineering and System Safety*

Hong, H. P. (1999). Inspection and maintenance planning of pipeline under external corrosion considering generation of new defects. *Structural safety*, 21(3), 203-222.

Kariyawasam, S., and Peterson, W. (2008). Revised corrosion management with reliability based excavation criteria. In 2008 7th International Pipeline Conference (pp. 489-500). American Society of Mechanical Engineers.

Leis, B. N., and Stephens, D. R. (1997). An alternative approach to assess the integrity of corroded line pipe-part II: Alternative criterion. In the Seventh International Offshore and Polar Engineering Conference. International Society of Offshore and Polar Engineers.

Liu, M., and Frangopol, D. M. (2005). Multiobjective maintenance planning optimization for deteriorating bridges considering condition, safety, and life-cycle cost. *Journal of Structural Engineering*, 131(5), 833-842.

Nelsen, R.B., (2006). *An Introduction to Copulas*. Springer, New York.

Nessim, M., Zhou, W., Zhou, J., and Rothwell, B. (2009). Target reliability levels for design and assessment of onshore natural gas pipelines. *Journal of Pressure Vessel Technology*, 131(6), 061701.

Okasha, N. M., and Frangopol, D. M. (2009). Lifetime-oriented multi-objective optimization of structural maintenance considering system reliability, redundancy and life-cycle cost using GA. *Structural Safety*, 31(6), 460-474.

Yu, B., Gu, X., Ni, F., and Guo, R. (2015). Multi-objective optimization for asphalt pavement maintenance plans at project level: Integrating performance, cost and environment. *Transportation Research Part D: Transport and Environment*, 41, 64-74.

Zhou, W., and Huang, G. X. (2012). Model error assessments of burst capacity models for corroded pipelines. *International Journal of Pressure Vessels and Piping*, 99, 1-8.

Zhang, S., and Zhou, W. (2013). System reliability of corroding pipelines considering stochastic process-based models for defect growth and internal pressure. *International Journal of Pressure Vessels and Piping*, 111, 120-130.

Zhang, S., and Zhou, W. (2014). Cost-based optimal maintenance decisions for corroding natural gas pipelines based on stochastic degradation models. *Engineering Structures*, 74, 74-85.

Zhang, S., Zhou, W., and Qin, H. (2013). Inverse Gaussian process-based corrosion growth model for energy pipelines considering the sizing error in inspection data. *Corrosion Science*, 73, 309-320.

Table 6.1 The probabilistic characteristics of parameters involved in the reliability analysis

Variable	Distribution	Mean	COV (%)
D/D_n	Deterministic	1.0	-
wt/wt_n	Normal	1.0	1.5
$\sigma_u/SMTS$	Lognormal	1.09	3.0
p/p_0	Gumbel	1.0	3.0
d_0/wt_n	Normal	ILI-reported depth	20
l_0	Normal	ILI-reported length	20
gd	Weibull	0.1/0.2/0.3 ^a (mm/year)	50
gl	Lognormal	5.0 (mm/year)	50
ξ	Lognormal	1.0	10.0

^a The mean value of the defect depth growth rate is assumed to be 0.1 mm/yr for pipe joints #1-30, 0.2 mm/yr for pipe joints #31-60, and 0.3 mm/year for pipe joints #61-90.

Table 6.2 Details of solutions SC1, SC2 and SC3

	SC1	SC2	SC3
Number of joints repaired at each year	(0,0,9,24,15) ¹	(0,0,24,25,8)	(0,17,24,18,12)
Total number of repaired joints	48	67	71
$C_{r,t}$ ($k = 0, 1, \dots, 4$) (m\$)	(0,0,1.2,2.8,1.7) ²	(0,0,2.9,2.9,1.0)	(0,2.2,2.9,2.1, 1.4)
C (m\$)	5.7	6.8	8.6
P_{sa}	8.1×10^{-4}	7.1×10^{-6}	5.1×10^{-6}
P_{ba}	7.3×10^{-5}	3.8×10^{-6}	1.3×10^{-7}

Note: 1. The numbers of pipe joints to be repaired in years 0, 1, 2, 3 and 4, respectively.
2. The present costs of repair in year 0, 1, 2, 3 and 4, respectively.

Table 6.3 Details of solutions SV1, SV2, SN1 and SN2

	SV1	SV2	SN1	SN2
Number of joints repaired at each year	(0,15,14,11,8) ¹	(0,22,16,12,7)	(0,0,7,23,18)	(0,4,27,21,6)
Total number of repaired joints	48	57	48	58
$C_{r,k}$ ($k = 0, 1, \dots, 4$) (m\$)	(0,2,0,1.8,1.4,1.0) ²	(0,2,8,2,0,1.5,0.9)	(0,0,1,0,2.7, 2.0)	(0,0.7,3.2,2.4,0.8)
C (m\$)	6.1	7.2	5.6	7.1
P_{sa}	8.1×10^{-4}	7.1×10^{-6}	1.2×10^{-3}	2.5×10^{-6}
P_{ba}	6.6×10^{-5}	3.8×10^{-6}	9.0×10^{-5}	4.3×10^{-6}

Note: 1. The numbers of pipe joints to be repaired in years 0, 1, 2, 3 and 4, respectively.
 2. The present costs of repair in year 0, 1, 2, 3 and 4, respectively.

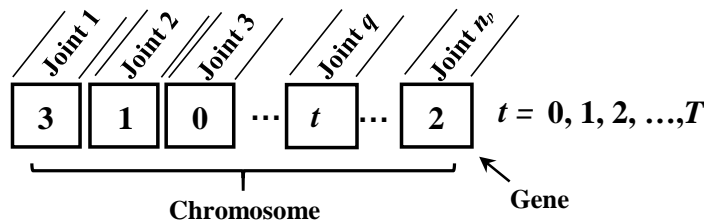


Figure 6.1 Illustration of one maintenance solution coded in GA

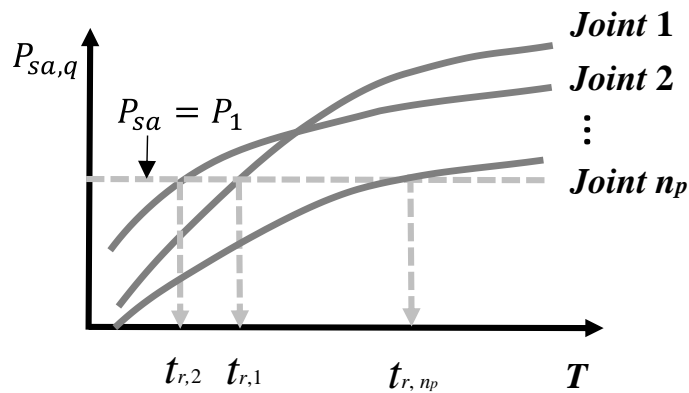
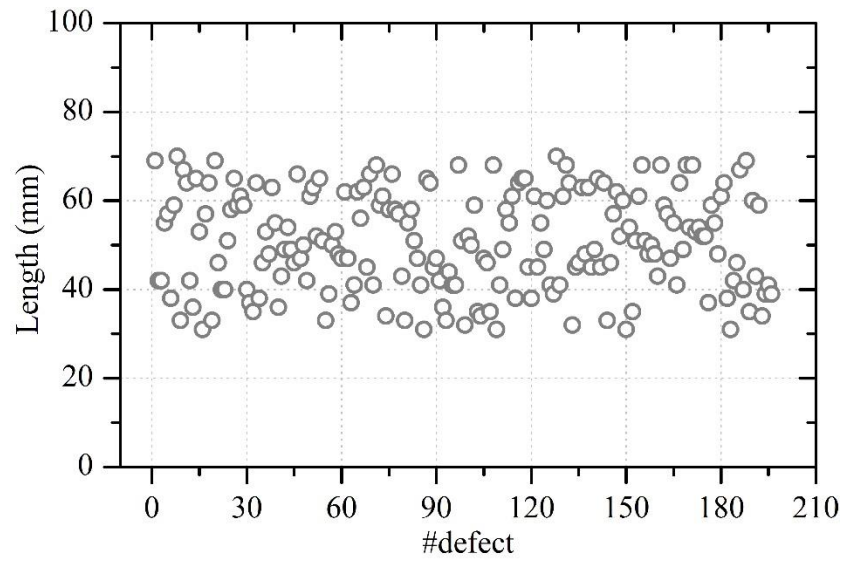
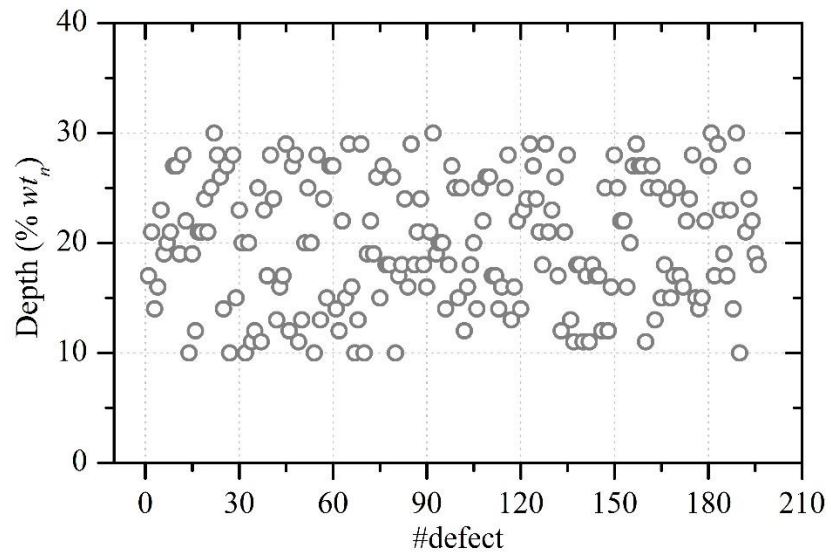


Figure 6.2 Illustration of the initial solution generation by minimizing C subjected to

$$P_{sa} \leq P_1$$



(a) Defect length



(b) Defect depth

Figure 6.3 The ILI-reported defect information

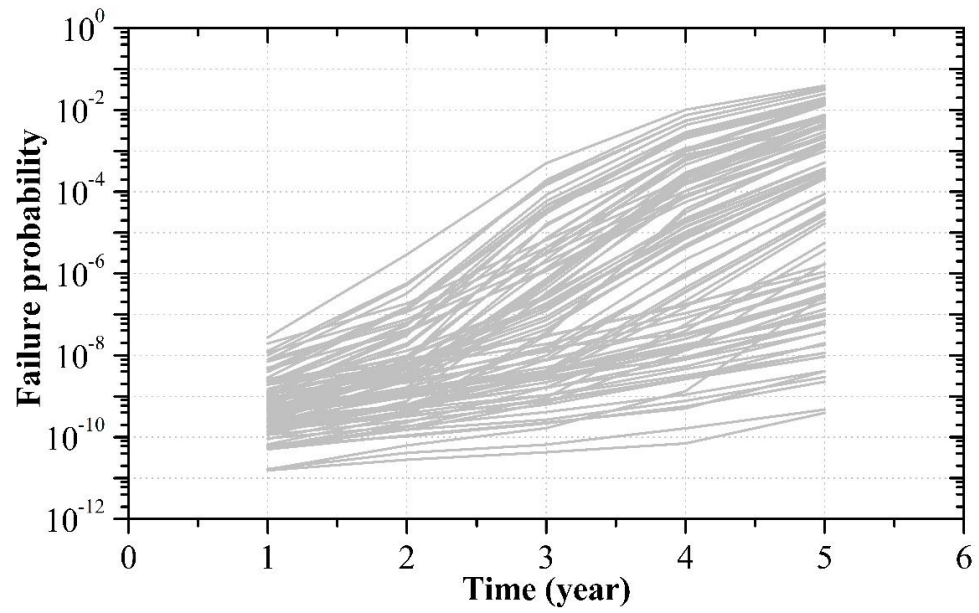
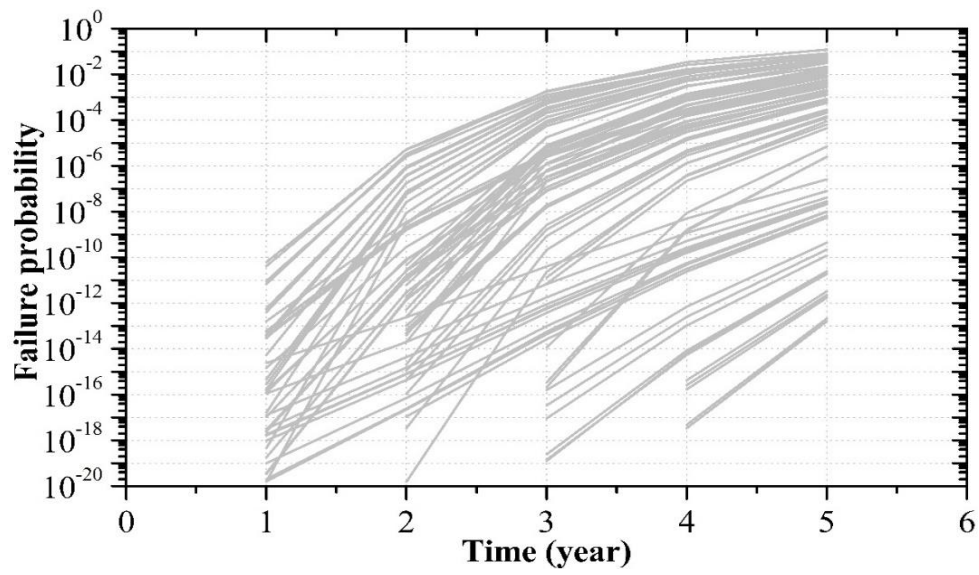
(a) $P_{ba,q}$ ($q=1, 2, \dots, 90$)(b) $P_{sa,q}$ ($q=1, 2, \dots, 90$)

Figure 6.4 Annual conditional failure probability for the considered pipe joints

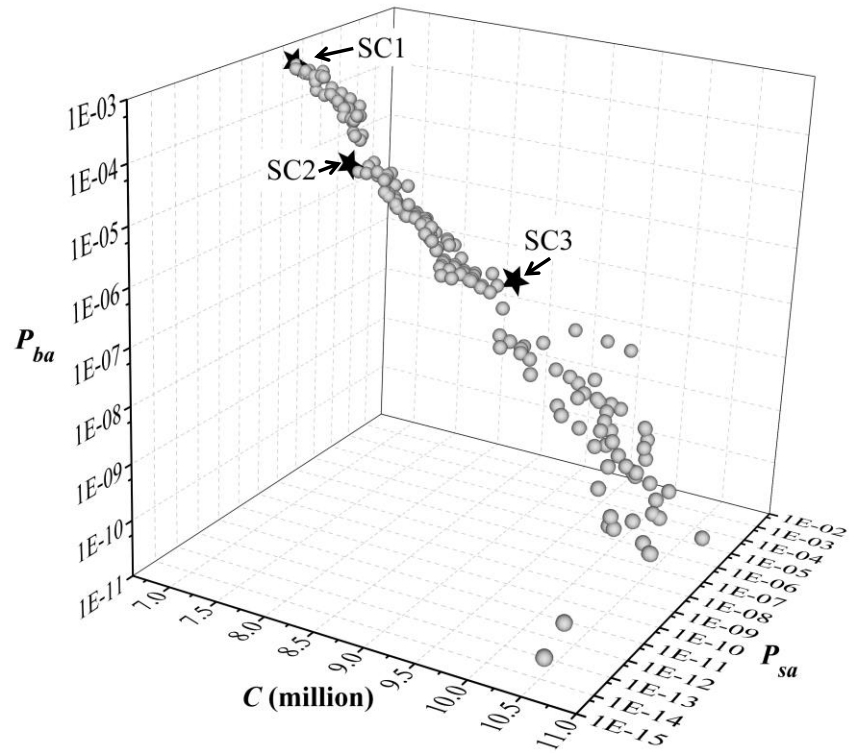
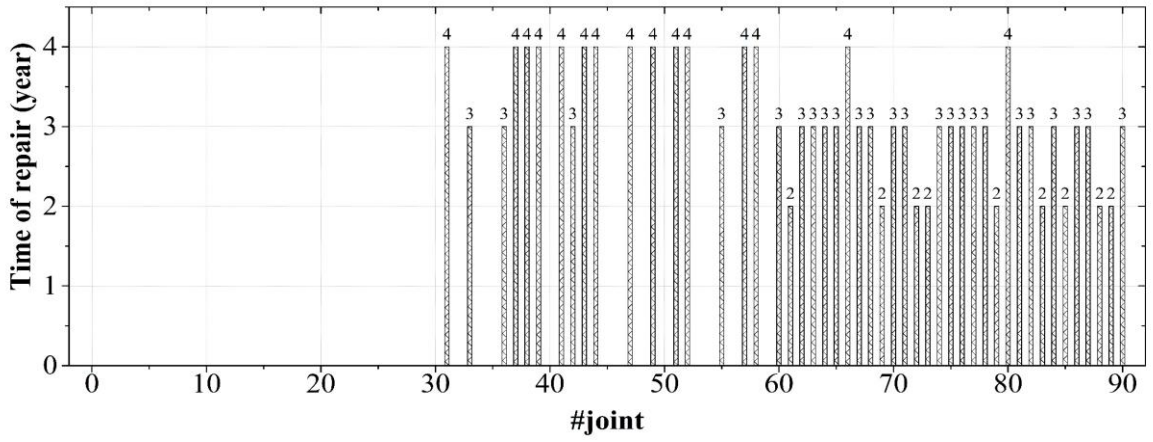
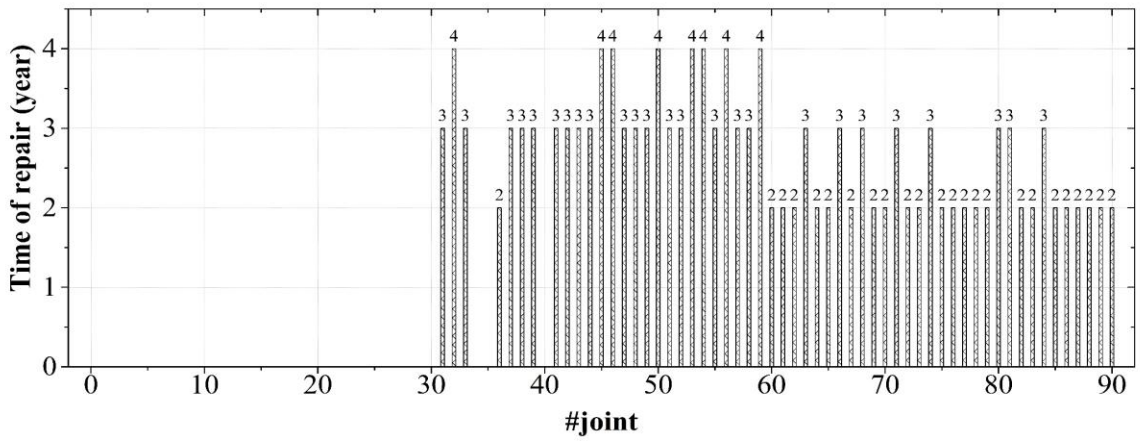


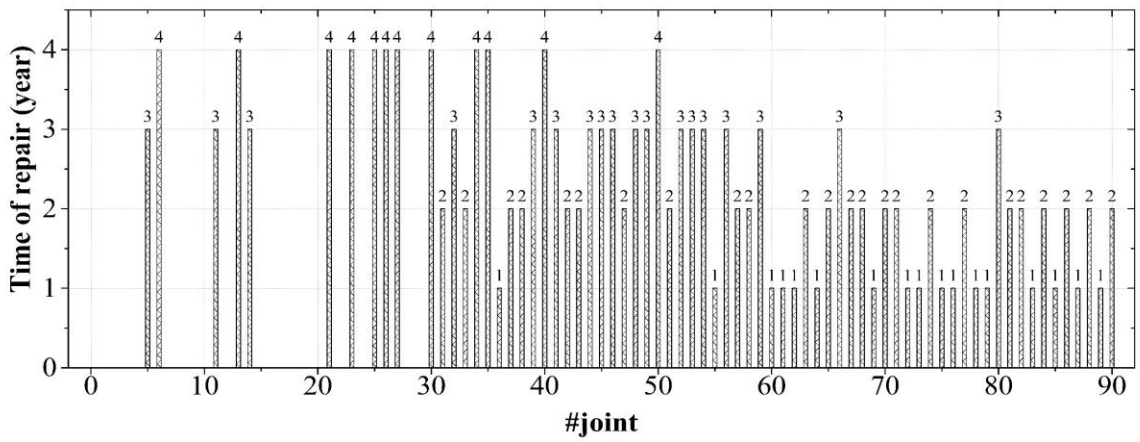
Figure 6.5 Pareto front of optimal solutions in terms of C , P_{sa} , and P_{ba} considering the constant budget constraint in years 1 through 4



(a) SC1



(b) SC2



(c) SC3

Figure 6.6 The locations of the to-be-repaired pipe joints associated with SC1, SC2 and SC3, respectively

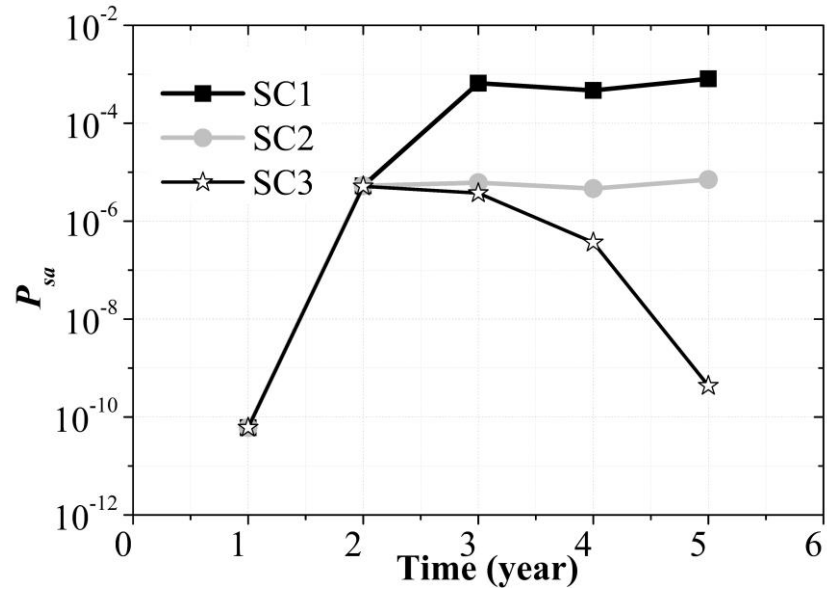
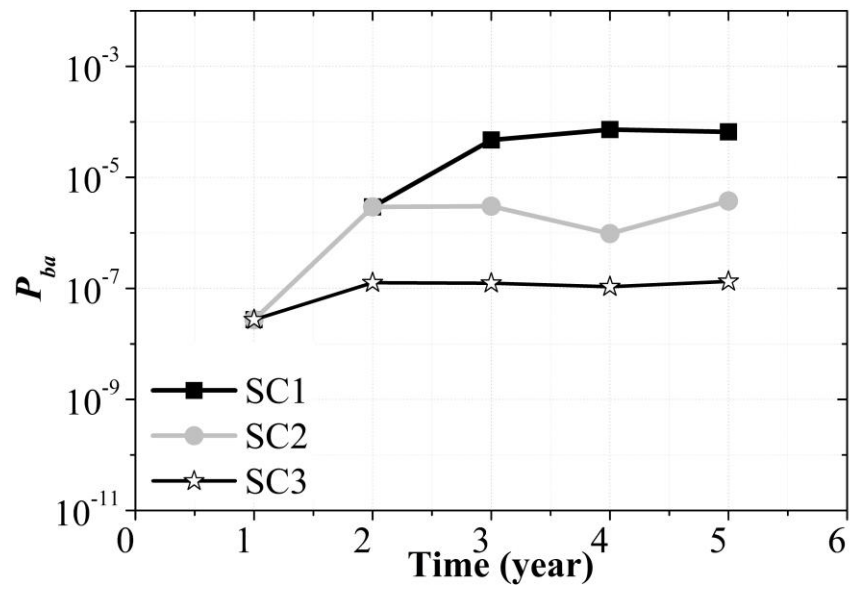
(a) P_{sa} (b) P_{ba}

Figure 6.7 The maximum annual conditional probabilities of small leak and burst of all 90 pipe joints corresponding to solutions SC1, SC2 and SC3

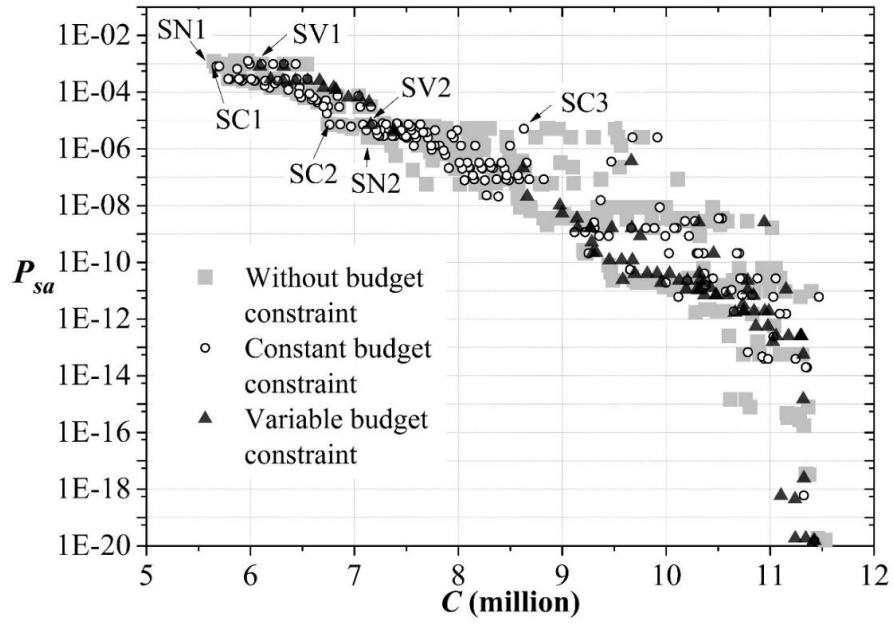
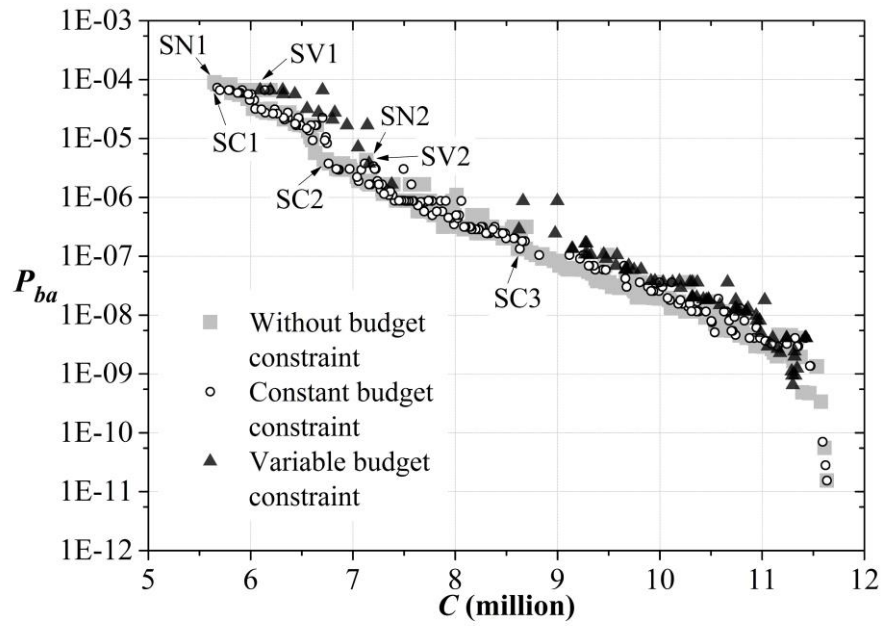
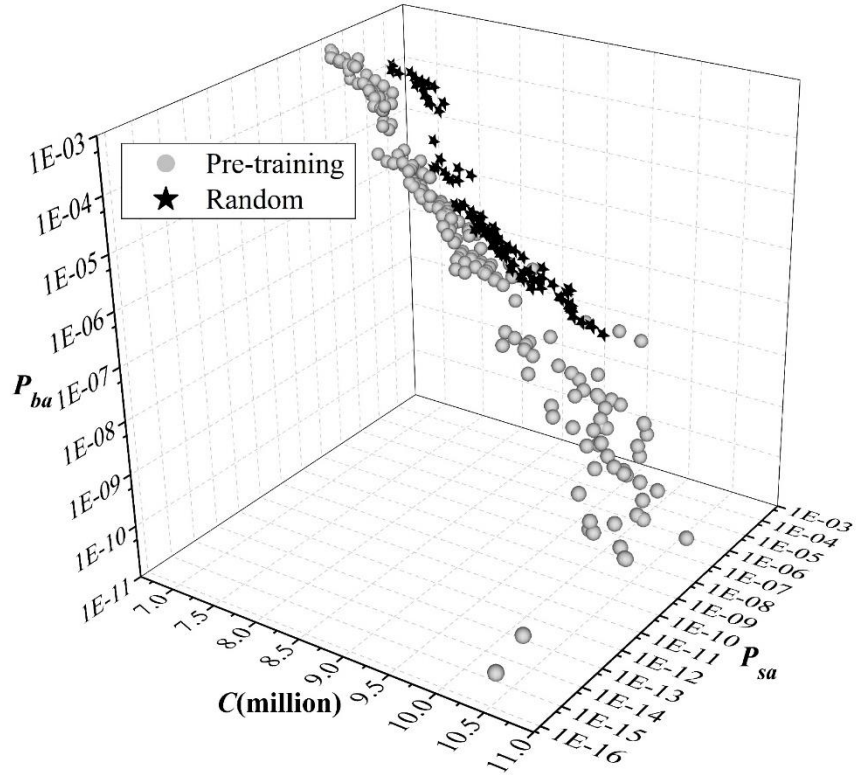
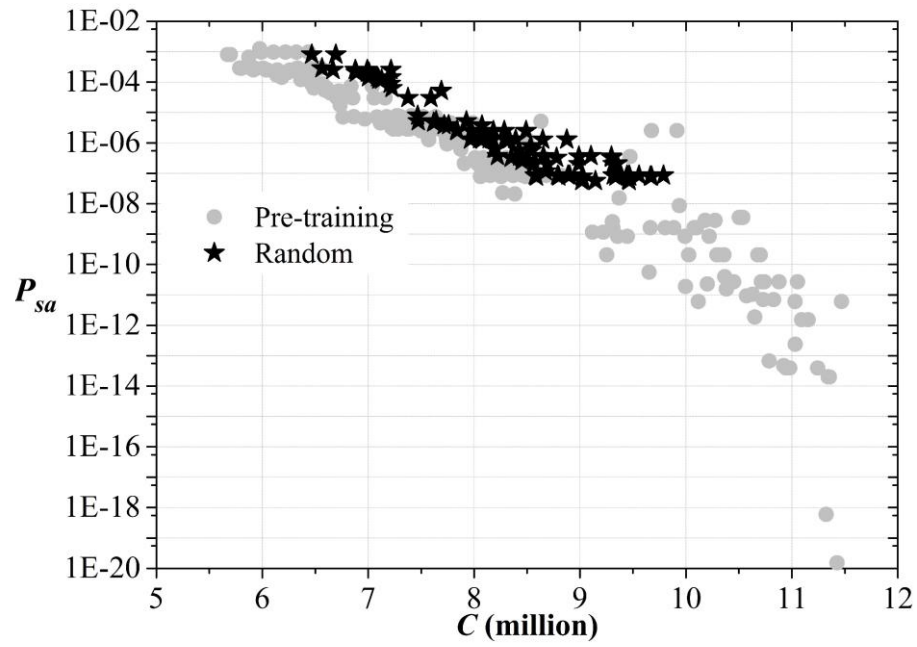
(a) $C - P_{sa}$ (b) $C - P_{ba}$

Figure 6.8 Pareto fronts corresponding to three scenarios of annual budget constraint

(a) C - P_{sa} - P_{ba} (b) C - P_{sa}

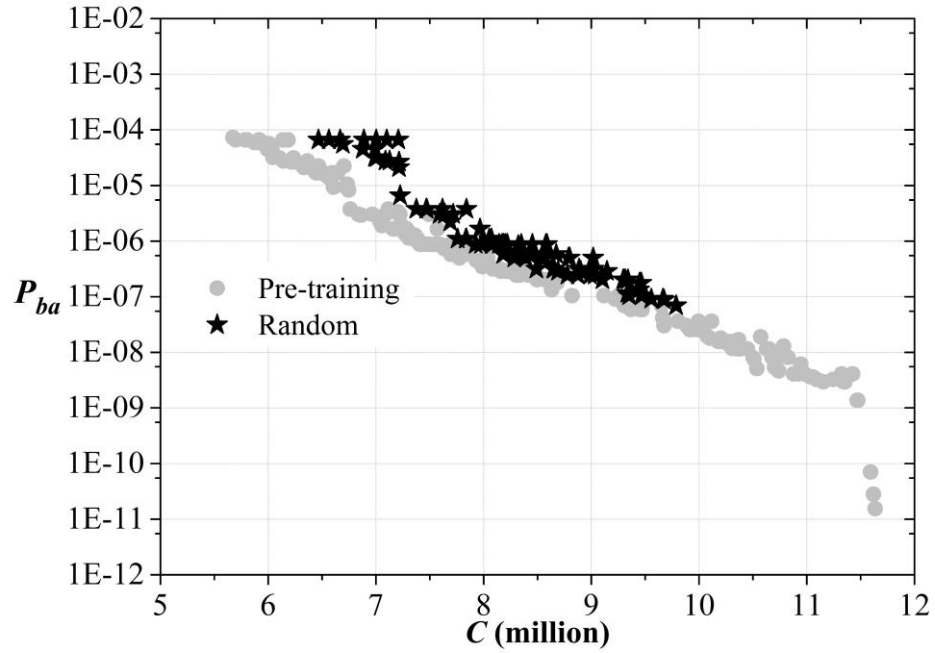
(c) C - P_{ba}

Figure 6.9 Comparison of Pareto fronts of optimal solutions corresponding to the scenario of constant annual budget constraint, obtained from pre-trained and random initial populations, respectively

7 Chapter 7 Summary, Conclusions and Recommendations for Future Study

7.1 General

The research described in this thesis primarily concentrates on the development of efficient system reliability methods for corroding pipeline systems considering multiple correlated corrosion defects, and the optimal corroding pipeline maintenance framework that balances safety and cost. The conclusions drawn from this thesis and recommendations for the future study are given as follows.

7.2 A New Perspective on the Application of the First-order Reliability Method

The FORM for system reliability analysis involves computing correlation coefficients between linearized limit state functions, which requires the optimization for each limit state function in a dimension where all random variables of the system are involved. To improve the efficiency of the FORM, a novel method is developed in Chapter 2. The method firstly conducts the FORM analyses to locate the design point through the optimization for an individual limit state function only considering the random variables that need to be defined in the limit state function itself instead of the entire system. Then, the identified design point is extended to a dimension where all random variables in a system are involved. The latter is employed as the basis to calculate the correlation coefficients among the linearized limit state functions at the design points for the system reliability assessment. By this procedure, the optimization variable dimension is reduced from total number of system variables to that of a given limit state function itself and thereby the computational cost can be reduced. It is further showed that correlation coefficients can be readily calculated in the correlated normal space as opposed to the standard normal space, whereby Cholesky decomposition is avoided.

The application of the developed procedure is demonstrated through three numerical examples: a pipeline joint with two corrosion defects; a parallel system with five components subjected to time variant dependent stochastic degradation; a transmission system with 11 individual towers subjected to spatially correlated wind loads.

7.3 Development of Improved Equivalent Component Approach for Reliability Analyses of Series Systems

In Chapter 3, an improved equivalent component approach is presented to efficiently compute the multi-normal integral within the context of the FORM. The improvement is established on two parts. The first one is the developed analytical expression relying on chain rule for the evaluation of equivalent unit normal vectors in the context of the FORM. The expression facilitates the assessment of correlation coefficients between the equivalent components and system component in the standard normal space. Second, an adaptive component combining order is proposed, where the two components with the highest correlation coefficient are combined at each combining step.

The effectiveness of the improved equivalent component method was illustrated on systems with equally correlated components and unequally correlated components, respectively. Four cases are investigated in terms of component reliability index 3, 4, 5 and 6, respectively. It is showed that the maximum absolute error for the system with 250 equally correlated components is slightly over 20% and the maximum absolute error is less than or equal to 20% for the system with unequally correlated components ranging from 30 to 250.

An investigation is conducted to compare the performance of the improved equivalent component method and state of art equivalent component methods, i.e. sequential combining method (SCM) and equivalent plane method (EPM). The comparison is performed on a series system of 250 components with the component reliability index of 6. Both equally and unequally correlated components are considered. Improved equivalent component method shows efficiency merits and comparable accuracy in comparison to SCM and EPM. Finally, the improved equivalent component method is applied to a pressurized steel pipeline joint containing ten active corrosion defects to demonstrate the application for series system reliability analyses.

7.4 First Order Reliability Method-based System Reliability Analyses of Corroding Pipelines Considering Multiple Defects and Failure Modes

In Chapter 4, a FORM based methodology was proposed to assess the time-dependent system reliability of pressurised corroding pipeline joints containing multiple active corrosion defects. Small leak and burst failure modes are considered and the spatial correlation among random variables associated with each defect is accounted for. At each given time, the FORM is applied to limit state functions regarding the pipe wall penetration and plastic collapse at each individual corrosion defects, respectively. Two linearized equivalent limit state functions representing burst and wall penetration failures of the joint are established, respectively, in the standard normal space. Each equivalent limit state function is described by equivalent reliability index and equivalent unit normal vector. The equivalent reliability index is computed as the reliability of system cumulative probabilities. The unit normal vector of the equivalent limit state is calculated as the product of the gradient of the equivalent reliability index relative to component reliability index, and the unit normal vector at individual defects. Then failure probabilities of burst and small leak are evaluated incrementally over time using a proposed procedure. The proposed methodology is applied on three pipeline examples representative of small-, medium and large diameter joints. Each joint contains ten active corrosion defects. Linear-, nonlinear and homogeneous gamma process-based corrosion depth growth models are investigated, respectively. Comparison of the failure probabilities from the proposed methodology and the simple Monte Carlo (MC) with 10^6 trials is carried out to assess the performance of proposed methodology. The results show that the obtained failure probabilities are in close agreement with those given by simulation for all three examples.

7.5 Important Sampling-based System Reliability Analyses of Corroding Pipelines Considering Multiple Failure Modes

In Chapter 5, the Importance Sampling (IS) technique is utilized to assess the time-dependent system reliability of corroding pipeline joints with multiple active corrosion defects. Competing failure modes, small leak and burst, are considered. Failure probabilities of small leak and burst of the pipe joint, respectively, are evaluated by

recursively summing up the corresponding incremental failure probabilities in a short time interval, where the IS probability density functions for incremental probabilities are computed as the weighted averages of the IS density functions for small leak and burst, respectively, at individual corrosion defects. Density functions are located at design points associated with individual defects for small leak and burst, respectively. The optimization constrained by three limit state functions defining the incremental domain at individual defects is conducted to obtain design points. An empirical expression is proposed to estimate the weighting factors that determine the contribution of incremental failure of each defect to that of the entire joint.

Four representative examples of onshore gas transmission pipelines in four different location classes in the US are used to demonstrate the application of the proposed methodology. Linear based- and Gamma process based-growth model for the defect depth are investigated, respectively. Two scenarios are considered: 1) single defect, and 2) ten correlated corrosion defects. Linear length growth is assumed for all the analyzed cases. The probabilities for small leak and burst are evaluated up to ten years with the IS simulation trials of 2000. Benchmark results for comparison are obtained from simple MC with 10^7 trials. It is revealed results from the IS agree very well with those by MC for all four examples, and the IS brings a significant reduction of calls to limit state functions.

7.6 Multi-objective Optimization Based Maintenance Strategy for In-service Corroding Pipelines Using Genetic Algorithm

In Chapter 6, a multi-objective optimization based maintenance framework for in-service corroding pipeline systems consisting of many joints is introduced, subjected to the constraints of annual failure probabilities and annual budget. The developed method is aimed at addressing the question regarding where and when to optimally perform joints excavation and defects mitigation after an in-line inspection, so that the pipeline safe operation is guaranteed before next inspection. Three objectives function are defined, i.e. conditioned annual small leak probability and burst probability, respectively, and maintenance cost. Those objectives are optimized simultaneously using genetic algorithm (GA). Important sampling based method developed in Chapter 5 is employed to evaluate

the time-dependent joint system failure probabilities of small leak and burst, respectively. The objective values of probabilities for small leak and burst, respectively, are calculated as the maximum in the entire system throughout the service time before next inspection. The maintenance cost is composed of the cost induced by excavation, repair and the spending for mobilizing activities. The constraint of failure probabilities is dealt with by directly removing the infeasible solutions from the obtained ultimate trade-offs, whereas annual budget constraint is considered by penalizing the cost objective whenever violated. Instead of randomly producing the initial population, it is proposed that GA starts up from a pre-training set of solutions to speed up the convergence. The maintenance framework is applied to a hypothetical pipeline system with 90 corroded joints. Results show that genetic algorithm with the pre-training population obtains a better Pareto front with better diversity and wider spectrum

Compared with the single optimization method that only gives one solution, the developed multi-objective optimization based framework provides decision makers with capability of investigating a series of solutions associated with various safety levels and repair cost. Decision makers can compare the cost benefits of solutions and finally select one based on their own preference and weight of importance of each objective.

7.7 Recommendations for Future Study

The recommendations for the future study are summarized as follows:

1. More advanced burst pressure prediction models should be investigated by conducting finite element analysis and experiments. Empirical experience shows that the current available model typically involves a large model uncertainty. This uncertainty leads to a very disperse distribution of predicted burst pressure, which propagates into the evaluated burst failure probability and results in over-conservative estimates.
2. For the small diameter corroding pipeline that is difficult to inspect using inline inspection, methodologies should be investigated to infer the condition of underground corroded pipeline joint from the corrosive soil properties, which is thereby based on to determine the optimum repairing schedules. Specifically, data driven technique can be

employed to establish the relationship between soil property and the condition of aging pipeline joints. Optimization is then formulated to identify the most cost effective solutions.

3. Third party damage, as one of the primary causes of pipeline failure, should also be investigated and quantified using the structural reliability method. The preventative measures against third party damage should be incorporated into the multi-objective optimization based maintenance framework.

4. Automatic aerial pipeline monitoring devices using machine learning techniques should be developed. In industry, aerial pipeline patrolling is performed through helicopter or fixed wing aircraft to detect right-of-way encroachments, excavation activities, and gas leaks. Those inspections are very costly and only conducted at regular intervals. Drones and satellites are economical tools for inspecting thousands of miles of pipelines but requires human intelligence to evaluate the pipeline conditions and still involves significant amount of human labor. Automatic detection methods using drones or satellites should be explored to replace human labor.

Appendix A Dimension Reduction Method

The unit normal vector for the equivalent component obtained by applying Eq. (3.7) is n -dimensional, i.e. the same dimension as that of all the random variables involved in the system. This dimension can be reduced to m (i.e. the total number of components in the system) in the equivalent component approach, if $m < n$. Note that the linearized limit state function at the j -th ($j = 1, 2, \dots, m$) component can be written as

$$g_j(y_j) = \beta_j - y_j \quad (\text{A.1})$$

where y_j is the value of a standard normal variate Y_j , and $g_j(y_j)$ is the limit state function in terms of y_j . It follows that $\mathbf{Y} = [Y_1, Y_2, \dots, Y_m]^T$ is an m -dimensional correlated standard normal variates with the correlation matrix \mathbf{R} . Furthermore, $\mathbf{V} = \mathbf{L}_Y^{-1}\mathbf{Y}$ is an m -dimensional vector in the independent standard normal space, where \mathbf{L}_Y is the lower-triangular matrix obtained from the Cholesky decomposition of \mathbf{R} . Note that the design point for $g_j(y_j)$, y_j^* , equals β_j .

The one-dimensional design point y_j^* can be mapped to the m -dimensional design point, $\mathbf{y}_D^*(j)$, corresponding to all m components by using the methodology proposed by Zhou et al. (2017); that is,

$$\mathbf{y}_D^*(j) = \begin{pmatrix} y_j^* \\ \mathbf{y}_{cj}^* \end{pmatrix} = \begin{pmatrix} \beta_j \\ \rho_{jk}\beta_j \end{pmatrix}, (k = 1, 2, \dots, m; k \neq j) \quad (\text{A.2})$$

where \mathbf{y}_{cj}^* denotes the values of Y_k ($k = 1, 2, \dots, m; k \neq j$) at the design point $\mathbf{y}^*(j)$ for the j -th component. By re-ordering the elements in $\mathbf{y}_D^*(j)$ based on the order of m components in the \mathbf{Y} space, $\mathbf{y}_D^*(j)$ is mapped to $\mathbf{y}^*(j)$, which is subsequently mapped to the design point in the \mathbf{V} space, $\mathbf{v}^*(j)$, where $\mathbf{v}^*(j) = \mathbf{L}_Y^{-1}\mathbf{y}^*(j)$. This allows the evaluation of the m -dimensional unit normal vector for the j -th component, $\boldsymbol{\alpha}'(j) = \mathbf{v}^*(j)/\beta_j$

Curriculum Vitae

Name: Changqing Gong

Post-secondary Education and Degrees: Yantai University
Yantai, Shandong, China
2006-2010 B.E.

Tongji University
Shanghai, Shanghai, China
2010-2013 M.E.Sc.

The University of Western Ontario
London, Ontario, Canada
2013-2017 Ph.D.

Honours and Awards: Research and Teaching Assistant Scholarship
The University of Western Ontario
2013-2017

Publications:

Gong, C., and Zhou, W. (2017). Improvement of equivalent component approach for reliability analyses of series systems. *Structural Safety*, 68, 65-72.

Gong, C., and Zhou, W. (2017). First-order reliability method-based system reliability analyses of corroding pipelines considering multiple defects and failure modes. *Structure and Infrastructure Engineering*, 1-11.

Zhou, W., Gong, C., and Hong, H. P. (2017). New perspective on application of first-order reliability method for estimating system reliability. *Journal of Engineering Mechanics-ASCE*, 143(9), 04017074.

Zhou, W., Gong, C., and Kariyawasam, S. (2016). Failure pressure ratios and implied reliability levels for corrosion anomalies on gas transmission pipelines. 2016 11th International Pipeline Conference. American Society of Mechanical Engineers.

Zhou, W., Siraj, T., and Gong, C. (2015). Reliability consistent mitigation criteria for corrosion defects on natural gas transmission pipelines. *Canadian Journal of Civil Engineering*, 42(12), 1032-1039.